Mathematical methods and terminology in geology 2022 : proceedings of reviewed papers / 4th Croatian scientific congress [on] geomathematics and terminology in geology

Edited book / Urednička knjiga

Publication status / Verzija rada: **Published version / Objavljena verzija rada (izdavačev PDF)**

Publication year / Godina izdavanja: **2022**

Permanent link / Trajna poveznica: https://urn.nsk.hr/urn:nbn:hr:169:805756

Rights / Prava: Attribution 4.0 International/Imenovanje 4.0 međunarodna

Download date / Datum preuzimanja: **2025-03-30**

DIGITALNI AKADEMSKI ARHIVI I REPOZITORIJI

Conference proceedings

RGNF

"Mathematical methods and terminology in geology 2022"

4th Croatian scientific congress about geomathematics and

terminology in geology

Matematičke metode i nazivlje u geologiji 2022

IV. hrvatski znanstveni skup iz geomatematike i nazivlja

u geologiji

održan na Rudarsko-geološko-naftnom fakultetu
Sveučilišta u Zagrebu

listopad 2022. godine

Skup su priredili:

Rudarsko-geološko-naftni fakultet
Sveučilišta u Zagrebu

Geomatematički odsjek
Hrvatskoga geološkog društva

Mathematical methods and terminology in geology 2022

4th Croatian scientific congress from geomathematics and terminology in geology
held on Faculty of Mining, Geology and Petroleum Engineering, University of Zagreb

October 2022

Organised by:

Facuty of Mining, Geology and
Petroleum Engineering of the
University of Zagreb

Geomathematical Section
of the
Croatian Geological Society

Matematičke metode i nazivlje u geologiji 2022

ZBORNIK RECENZIRANIH RADOVA

IZDAVAČ:

Sveučilište u Zagrebu

RGNF

Rudarsko-geološko-naftni fakultet

Zagreb, 2022.

Mathematical methods and terminology in geology 2022

PROCEEDINGS OF REVIEWED
PAPERS

SADRŽAJ / CONTENT

Sample size and application of the bootstrap method - case study Western Part of the Sava Depression

Josip Ivšinović[1]

[1] The 1st Catholic elementary school in the City of Zagreb, Zagreb, Croatia; ORCID: 0000-0002-7451-1677

Abstract

Bootstrap is a statistical method that allows you to retrieve a new set of data that is normally distributed from an existing set of input data that is not normally distributed. This method provides a set of data on which various statistical analyses can be applied. Deep geological data (petrophysical data) in many cases are not normally distributed. The application of the bootstrap method on small and large input data sets of porosity in the reservoirs of the western part of the Sava Depression was analysed. With 95% confidence level, the estimated porosity value for reservoir "L" is 0.1875 to 0.2144, while for reservoir "K" it is 0.2187 to 0.2493.

Keywords: sample size, bootstrap method, porosity, Sava Depression

1. Introduction

The bootstrap method (BM) is a nonparametric statistical method that has wide application in various fields of research (**Zientek and Thompson, 2007; Picheny et al., 2010; Matsuyama, 2018; Chibo and Aboko, 2021**). Depth geological data obtained from logging or laboratory measurements are heterogeneous and not normally distributed. In order to determine the individual petrophysical value at one point in space, when determining this value, the value obtained from the laboratory or read from the logging curves or a combination of both methods is taken. Due to heterogeneity in depth relationships, reservoir data are not normally distributed, which precludes classical statistical analysis.

In this paper, two reservoirs "L" and "K" located in the western part of the Sava Depression is analyzed. In these reservoirs, porosity was analyzed and the bootstrap method was applied. The porosity values of the reservoirs "L" and "K" were estimated after the application of BM.

2. Geological settings of the investigated area

Reservoirs "L" (field A) and "K" (field B) are located within the Croatian part of the Pannonian Basin System (CPBS), i.e. in the western part of the Sava Depression (**Figure 1**).
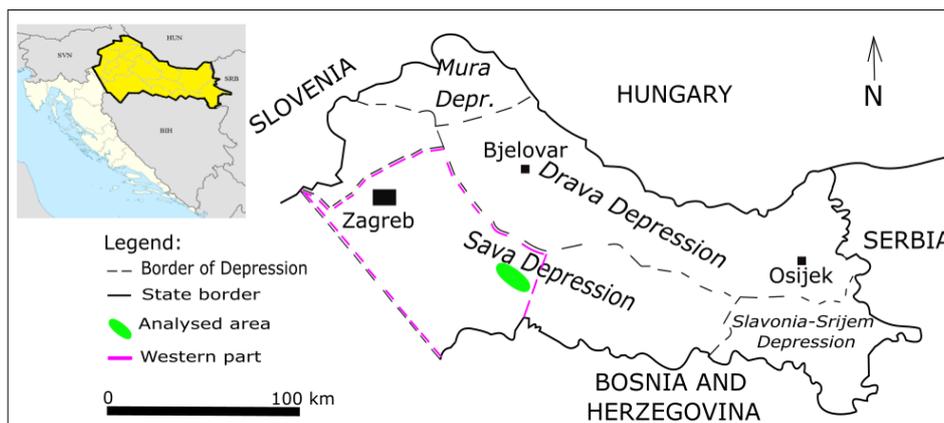
Figure 1: Fields A and B within the western part of the Sava Depression (green). (**Ivšinović et al., 2020**)

Corresponding author: Josip Ivšinović
josip.ivsinovic@skole.hr

In the western part of the Sava Depression, oil and gas exploration began in the second half of the 20th century. The largest reserves and realized hydrocarbon production are from the Upper Pannonian and Lower Pontian reservoirs (**Figure 2**). The "L" and "K" reservoirs belong to the Klostar Ivanic formation.
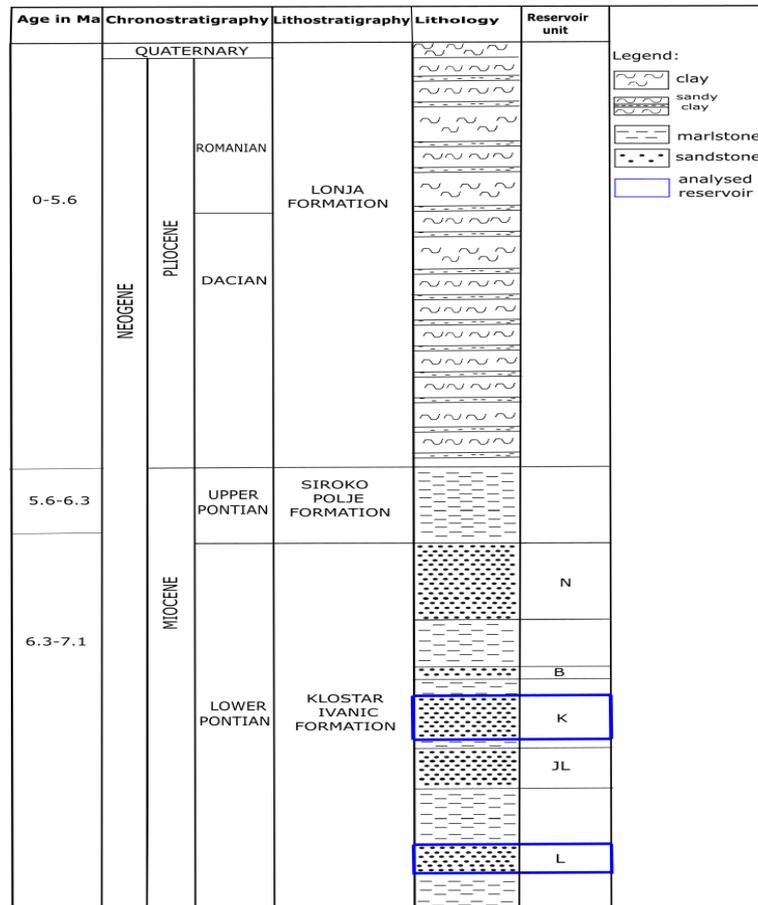
Figure 2: Geological column of fields A and B. (**Malvić et al., 2019)**

The analyzed petrophysical parameter in this paper is porosity, which was obtained from laboratory measurements of well cores or as a value obtained from logging measurements. Due to the pronounced tectonics, field B is divided into more hydrodynamic units than field A, which resulted in a smaller number of input data on individual reservoirs.

2.1. Mathematical set up of BM

In the bootstrap method, new number sets containing the same values of the initial set and the same sample size are obtained from the same input set of numbers. Each time a new set of numbers is created, the mean value that will be contained in the bootstrap function is calculated. The procedure is repeated iteratively, therefore, until a normal distribution of the analyzed data is obtained in bootstrap function. The smooth bootstrap method is applied in this paper.

From the obtained bootstrap function, it calculates the standard deviation of bootstrap (**Ivšinović et al., 2021; Ivšinović and Litvić, 2021**):

$$S_m = \sqrt{\frac{1}{m}\sum_{i=1}^{m}\left(\overline{X_i} - \overline{X_m}\right)^2}$$

(1)

Where are:

S_m - standard deviation of bootstrap,
$\bar{X}_m$ - arithmetic bootstrap mean,
$\bar{X}_i$ - mean sample value after resampling,
m - number of the resampling data set.

By calculating the standard deviation of the bootstrap function, an interval estimate of the expectations of the analyzed data according to the equation can be calculated (**Ivšinović et al., 2021; Ivšinović and Litvić, 2021**):

$$< \overline{X_m} - z \frac{S_m}{\sqrt{m}} , \overline{X_m} + z \frac{S_m}{\sqrt{m}} > \tag{2}$$

Where are:
S_m - standard deviation of bootstrap,
$\bar{X}_m$ - arithmetic bootstrap mean,
z - value from the normal distribution,
m - number of the resampling data set.

3. Results and discussion

Two cases of reservoirs were analysed in this case study: "L" representing a large data set (n = 25) and "K" representing a small data set (n = 19). Data on the porosity of the reservoirs were taken from **Ivšinović 2019**. Data of reservoir porosity used for BM calculation are shown in **Table 1**. The interval estimation of the porosity expectations of reservoirs "L" and "K" after BM application is shown in **Table 2**.

Table 1: Basic statistical data on porosity of reservoirs "L" and "K" (**Ivšinović, 2019**)

	Reservoir	n	Min	Max	$\overline{\overline{X}}$
Porosity	L	25	0.145	0.239	0.202
	K	19	0.217	0.315	0.232

Table 2: Interval estimation porosity of reservoirs "L" and "K" (after BM) (**Ivšinović et al., 2021; Ivšinović and Litvić, 2021**)

	Reservoir	m	Confidence interval (95%)
Porosity	L	1100	<0.1875 , 0.2144>
	L	1250	<0.1877 , 0.2144>
	K	500	<0.2187 , 0.2493>
	K	1000	<0.2182 , 0.2475>

For reservoir "K" the confidence interval is obtained already at 500 number of repeated resampling's, while for reservoir "L" is obtained at 1100 (**Table 2**). The number of repeated resampling's depends on the nature of the input data set (**Table 1**), sample size, and reservoir heterogeneity. A smaller input data set also requires a smaller number of repeated resampling's. The division into small and large sample described by **Malvić et al. (2019)** in the case of BM application is applicable, which is evident from the results in **Table 2**. The boundary between the large and small set is set to 20 which is seen by the required number of repeated resampling's. Also, the authors **Ivšinović et al. (2021)** by analyzing a small set of numbers and applying BM to the cost of disposal formation water whose input set of seven data yielded a result characteristic of a small data set, which is to obtain normality at 500 number of repeated resampling's. More estimated equal values in the input set of values may, due to the application of BM, obtain intervals of estimated values that include repetition of values, although new data sets are formed by random selection. Thus, when analyzing sets of numbers on which the BM is applied, data representativeness should be taken into account. In the porosity interval

estimated in **Table 2**, it can be seen that the change with resampling's increase after the normality of the set of numbers is reached, the change in value is in the fourth decimal place for reservoir "L", while for the "K" reservoir in the third decimal place.

4. Conclusions

BM can be applied to small and large data sets, while data analysis requires data representation. A small data set is considered to be an input data set less than 20.

For a large sample, a normal data distribution after BM application is obtained after 1100 number of resampling's, while for a small sample it is 500.

With 95% confidence level, the estimated porosity value for reservoir "L" is 0.1875 to 0.2144, while for reservoir "K" it is 0.2187 to 0.2493.

As can be seen from the results on reservoirs "L" and "K", BM is applicable to the entire area of the western part of the Sava Depression, regardless of sample size.

5. References

Chibo O. and Aboko, S. I. (2021): Bootstrapping - An Introduction And Its Applications In Statistics. International Journal of Innovative Mathematics, Statistics & Energy Policies 9(3), 22-28.

Ivšinović, J. (2019): Odabir i geomatematička obradba varijabli za skupove manje od 50 podataka pri kreiranju poboljšanoga dubinskogeološkoga modela na primjeru iz zapadnoga dijela Savske depresije (*Selection and geomathematical calculation of variables for sets with less than 50 data regarding the creation of an improved subsurface model, case study from the western part of the Sava Depression*). PhD, Rudarsko-geološko-naftni fakultet, Zagreb, 129 p. (*in Croatian – Abstract in English).*

Ivšinović, J. and Litvić, N. (2021): Application of the bootstrap method on a large input data set - case study western part of the Sava Depression. Rudarsko-geološko-naftni zbornik, 36 (5), 13-19 doi:10.17794/rgn.2021.5.2.

Ivšinović, J., Malvić, T., Velić, J. and Sremac, J. (2020): Geological Probability of Success (POS), case study in the Late Miocene structures of the western part of the Sava Depression, Croatia. Arabian Journal of Geosciences, 13 (714), 1-12 doi:10.1007/s12517-020-05640-z.

Ivšinović, J., Pimenta Dinis, M., Malvić, T. and Pleše, D. (2021): Application of the bootstrap method in low-sampled Upper Miocene sandstone hydrocarbon reservoirs: a case study. Energy sources part A-recovery utilization and environmental effects, 43, doi:10.1080/15567036.2021.1883773.

Malvić, T., Ivšinović, J., Velić, J. and Rajić, R. (2019): Interpolation of Small Datasets in the Sandstone Hydrocarbon Reservoirs, Case Study of the Sava Depression, Croatia. Geosciences, 9 (5), 201, 11, doi:10.3390/geosciences9050201.

Matsuyama, T. (2018): An application of bootstrap method for analysis of particle size distribution. Advanced Powder Technology, 29, 1404-408, https://doi.org/10.1016/j.apt.2018.03.002.

Picheny, V., Kim, N.H. and Haftka, R.T. (2010): Application of bootstrap method in conservative estimation of reliability with limited samples. Structural and Multidisciplinary Optimization 41, 205-217, https://doi.org/10.1007/s00158-009-0419-8.

Zientek, L.R. and Thompson, B. (2007): Applying the bootstrap to the multivariate case: Bootstrap component/factor analysis. Behavior Research Methods, 39, 318–325, https://doi.org/10.3758/BF03193163.

SAŽETAK

Veličina uzorka i primjena samonadopunjujuće metode – primjena na zapadnom dijelu Savske depresije

Samonadopunjujuća metoda je statistička metoda koja omogućuje dobivanje novog skupa ulaznih podataka koji je normalno distribuiran iz postojećeg skupa podataka koji nije normalno distribuiran. Ova metoda omogućava skup podataka na kojem se mogu primijeniti različite statističke analize. Dubinskogeološki podatci (petrofizikalni podatci) u mnogim slučajevima ne postoji normalna distribuiranost ulaznog skupa podataka. Analizirana je primjena samonadopunjujuće metode na malom i velikom ulaznom skupu podataka šupljikavosti u ležištima zapadnog dijela Savske depresije.

Ključne riječi: veličina skupa podataka, Samonadopunjavanje; šupljikavost; Savska depresija

Author's contribution

Josip Ivšinović (1) (PhD, research associate): completed the entire research and publishing process.

Computational skills in geosciences higher education system for the 21st century

Gordana Medunić[1]; Sanchita Chakravarty[2]; Rajen Kundu[2]

[1]University of Zagreb, Faculty of Science, Department of Geology, Horvatovac 95, Zagreb, Croatia, ORCID: 0000-0001-5261-3771

[2]CSIR-National Metallurgical Laboratory, P.O., Jamshedpur 831007, Jharkhand, India.

Abstract

There has been a lot of research worldwide on what the education of the future will look like. We are witnessing a growing number of indicators of the slow collapse of education as we know it. It is likely that higher education is approaching a major turning point. Thereafter, the speed and flexibility of adapting to global change will be the main determinants. Ubiquitous digitalisation, new trends, and sustainability will be the key concepts of business models in the future. Alongside computer skills, the new generations will need programming skills as well. The higher education system must take this task as seriously and urgently as possible. Without the mentioned knowledge and skills, it will be difficult for future employees to compete in the labour market and/or further professional career advancement. This article addresses the question of what the future directions of the geoscience education ought to be as the technology is evolving while datasets become richer. Hence, machine learning will have more success in the field. The application of computer and mathematical methods in geosciences, incorporated in the concept of computational geosciences, will determine the future of geology and related disciplines.

Keywords: geoscience, higher education, skills, job, computational science

1. Introduction

Times are challenging and completely unpredictable, but one thing is certain – human capital is the most valuable asset now more than ever. Another certainty relates to technological advances, specifically the ones that support digital and green transformation. Today's world teems with interesting new and innovative technologies and ways of working, with a direct contribution to the development of society. The three key concepts are reshaping the business world: recognizing new trends, reacting quickly, and applying digital thinking at all levels. Thanks to competition, the driving force behind the existing businesses should be a basic principle – always be one step ahead, think outside the box and set trends. But what about scientists? Students? Robots? Does it make sense to ask questions (respectively): how do you measure success? Does your teacher bring the surprise by classroom discussion and activity? All three categories (or entities) have something in common, and it is investment. Countries with large government spending on science and education programs have leading roles on the global stage. Chances are that you've probably heard of this mantra. However, many of us have no idea how long, difficult and tough journey it is. Even in affluent societies, there is still a long way to go. They have so many new potential projects, initiatives and partnerships in their plate, and it's been a real struggle to keep pace with such giants in terms of know-how, know-what, and know-why. Long ago, their citizens have realized the importance of focus on lifelong learning and openness to change.

Scientists bring their personal purpose into their work; science is their raison d'être. They understand very well the practical meaning of investments. One example is attending the conferences that have hefty prices. More and more, such events bring together science and business for dialogue on innovative ways to enhance productivity in the respective field, and investment as well. In fact, this is composed of the following: 1. investing in the science, 2. inventing the products (patents, publications, concrete products, etc.), 3. rising the scientometric indicators of success, 4. rising the investments, 5. developing the entire science and education system, 6. improving the entire physical landscape that makes people appreciative, and so on. Therefore, it deserves to say plain and simple: science is business.

Corresponding author:GordanaMedunić
gordana.medunic@geol.pmf.hr

It is everywhere, in everything, for everyone. The biggest challenge is finding a way to stay competitive in the conditions of generally underpaid science, let alone schools and universities. Students should strive for excellence which should be the way of their daily work and thinking, yet many of them struggle financially. Both, scientists and students, operate in the global labour market where trends and needs are the same. Systematic monitoring of the scientific advancements should be one of their priorities, but that is hardly possible without investments in the development of technologies of the future. One of them is computers, mother of a hot topic discipline called computational science. Computational science is a discipline concerned with the design, implementation and use of mathematical models to analyse and solve scientific problems. Typically, the term refers to the use of computers to perform simulations or numerical analysis of a scientific system or process (**URL 1**).

When we talk about the geoscience, or earth science (i.e. the study of Earth), many things have changed in the discipline since 17th or 18th century, when it became its own entity in the world of natural science. It was the first science in human history, and almost everything we use comes directly or indirectly from Earth. Nowadays, climate change, the petroleum industry and mineral resources are perceived as the top priority fields in applied geosciences. In spite of the fact that nearly everything around us – from the mountains out our window to the cell phone in our hand to the water from our tap – is connected to geoscience (**URL 2**), geology is one of the most underrated and underappreciated sciences out there (**URL 3**). Many people find rocks boring, but geology is much more than studying rocks; earth scientists are at the forefront of addressing complex problems such as climate change, natural resource use, environmental degradation, and energy sustainability (**Medunić et al., 2016**; **URL 2**). Geologists are people who study earthquakes and break down this knowledge for everyone, and not only that, but they're some of the people who are doing research to find a solution (**URL 3**).

Orion (**2019**) elaborated the gap between the importance and relevance of the earth science to society and its low status in schools worldwide. According to the author, significant research efforts should be invested among the university geoscience researchers and professors to undertake a deep change at all levels of the university geoscience education programs by applying a new, holistic research agenda. The proposed change should include the integration of the following three subjects within the traditional university geoscience disciplinary courses: the earth systems approach, geo-ethics education, and the development of communication skills. The truth is that geoscience study programs in Europe face a serious challenge to attract students. **Mileusnić** (**2020**) presents an innovative teaching method that has become more recognized by US geoscience teachers compared with their European counterparts. It is called service learning with real science and engineering at its centre. It has the potential to raise the awareness of the study program and interest in geosciences in the wider society. The author described the service learning (or community-based learning) features; it is an educational approach that combines learning objectives with community service in order to provide a pragmatic, progressive learning experience while meeting societal needs. Student teams apply the structured knowledge and skills acquired in the academic course while developing a project that deals with a specific social problem. For example, risk management of earth-quake hazard has important social aspects. Helping in clearing rubble or supplying groceries after an earthquake is service, while measuring active faults in the field is learning. A review paper by **King** (**2008**) indicated that geoscience education would progress most effectively through the following aspects: 1/ extending geoscience learning to all children; 2/ educating teachers in effective implementation of new curriculum initiatives; 3/ evaluating the progress of the initiatives and using the results to refine them; and 4/ researching the whole process to demonstrate its effectiveness and to ensure wide dissemination on the basis of well-founded research findings.

By all means, geoscience education should adapt to the radically and rapidly changing world. We are facing energy transition, economic slowdown (degrowth), the rise of artificial intelligence and large data sets (big data). Western geoscience universities have already embraced "outside-the-box" thinking by creating new avenues for students in the geoscience workforce. Specifically, their programs offer non-geoscience majors supported by enough technical geoscience skills and adequate soft skills. With this in mind, the aim of this paper is to present some of the geoscience workforce skills, particularly computational ones that will remain in high demand in the decades to come.

2. Employment prospects in the geosciences

Geoscientists study the physical aspects of the Earth, such as its composition, structure, and processes, to learn about its past, present, and future. Their employment opportunities are expanding as natural hazards are more frequent and intense, coastal infrastructure is threatened from rising sea levels, food and water supplies are affected by warming

climate, while global energy and resource needs should be met in a sustainable and environmentally responsible way. According to **Mosher and Keane** (**2021**), students who conduct quantitative analysis easily, apply critical thinking and problem-solving skills, manage and analyse large data sets, communicate effectively in a variety of formats, and work well in teams will likely succeed in the future work environment. The authors emphasize that students need to be prepared for changing workforce needs, including new careers and jobs that require the use of new technologies, strong quantitative and computational skills, data analytics and machine learning, interdisciplinary teamwork and problem solving. However, there are opponents who call it 'Nintendo' geology, an over-reliance on 3D mapping and visualization techniques; they complain that today's workforce lacks a knowledge base in four areas in particular – stratigraphy, structural geology, sedimentology and field geology (**Gewin, 2016**). The author concluded that despite financial shortages of all kinds, geoscience skills remain in great demand, even during difficult times (e.g. the low price of oil). According to **Geological Society of America** (**2016**), the interdisciplinary geosciences require the next generation of skilled geoscience workers to not only tackle the serious challenges in natural resource development and management, natural hazards mitigation, environmental protection, and ecosystem restoration, but also to apply integrative geoscience skills and knowledge to a host of related (civil and environmental engineering, environmental studies, agricultural sciences, atmospheric and ocean sciences, and life sciences) and seemingly unrelated (materials research, homeland security and emergency services, medicine, law, public administration, public health, and economics) fields. In a very optimistic tone, **Mosher et al.** (**2014**) point out that a large segment of the current workforce begins to retire, and geoscience jobs increase in number; hence, we will face a shortage of geoscientists for the future workforce. Therefore, the authors suggest a roadmap for the future undergraduate geoscience education by combining efforts of departments and programs, led by administrators, individual faculty innovators, geoscience professional societies, and industry (investment!). It shouldn't be difficult in educational settings (in affluent countries mostly) where technology is being used in new ways, including virtual experiences, flipped classrooms, blended learning, massive open online courses, and crowdsourcing of open education resources. Major advances have taken place in visualization and geospatial tools, generation and use of massive amounts of quantitative information (big data), and computational modelling, and simulation for both predictive capabilities and insight into processes and global-scale events. The authors conclude that undergraduate students must be prepared to use rapidly advancing technologies and big data in the future (**Mosher et al., 2014**).

3. Quantitative geosciences skills in the 21st century

Geosciences used to be largely descriptive back in the past. This is no longer true as they have become rather quantitative in the 21st century. As modern geosciences use equations, models, and numbers in conjunction with observations, maps, and words as fundamental tools for investigating the Earth, the geoscience workforce of tomorrow need to be prepared to meet the quantitative demands of industry, research, and education. However, building quantitative information into any geoscience course can be challenging (**Manduca et al., 2008**). The authors list specific skills that are important for geoscience students as follows: basic arithmetic, algebra, and statistics; the ability to use equations and models to describe natural processes; estimation and back-of-the-envelope calculations; and modelling and understanding uncertainty.

Macdonald and McNeill Bailey (**2000**) described the departmental context and their approach (known as the matrix approach) to developing skills across the departmental curriculum (**Table 1**). The quantitative components they identified as most important included estimating, measuring, and determining rates of earth processes, modeling earth processes, doing geochronological calculations, and statistically analysing data. Examples included using real data to estimate and measure ground-water-flow velocities, erosion rates, weathering rates, and tectonic plate velocities. They noted how some students had been quite hostile to quantitative work (based on student comments), whereas at the time of writing their paper (2000) such work was simply accepted. Briefly, following the identification of critical quantitative skills and applications (the matrix approach), faculty members in the department systematically incorporated quantitative activities in geoscience courses throughout the curriculum. Of course, faculty members had to be willing to discuss their courses in detail and change course content and activities as necessary.

Quantitative component	Physical Geology, Geography	Historical geology	Mineralogy	Petrology	Sed/Strat	Surficial processes	Paleontology	Structural geology
Estimating	M	L	L	L	M	M	L	M
Measuring	L	M	M	M	M	M	H	H
Determining rates	H	M	L	L	M	H	M	M
Graphing	M	L	M	H	L	M	M	H
Modelling	L	L	M	M	L	H	L	M
Geochronology	M	M	L	L	M	H	L	H
Statistics	L	L	L	M	M	M	H	M

Table 1: Matrix of quantitative components versus core curriculum courses with light (L), medium (M), and heavy (H) reflecting the emphasis of a particular component in a specific course (**Macdonald and McNeill Bailey, 2000**)

Ma (**2019**) points out how Earth science, like other scientific disciplines, is increasingly becoming quantitative because of the digital revolution. At the modern workplace, quantitative analysis is equivalent to numeracy a century ago and literacy before that. The author highlights the importance of the quantification of scientific and technical problems as the core of the ongoing 4th industrial revolution that includes digitalization and artificial intelligence. The author remarks that quantitative analyses of geosciences are not to replace their descriptive counterparts but to complement and enhance them. According to the author, the large potential of big data and quantitative methods is not yet universally recognized in the geoscience community, due, in part, to a lack of familiarity. Essentially, quantitative analysis and modelling are foundations for testing the geological concepts and hypotheses in a quantitative manner. Hereby, probabilistic analytics is used to resolve inconsistency in various data and integrate them coherently. Furthermore, 3D reservoir modelling of heterogeneous subsurface formations has become increasingly important. The essence of modelling lies in using all the relevant data to build an accurate reservoir model that is fit-for-purpose to the business and/or research needs. **Ma** (**2019**) points out that heterogeneities in subsurface formations are complex, and effective application of statistics to subsurface geoscience problems requires immersion in the underlying subject matter. One respective example was elaborated by **Maniar et al.** (**2018**) by using the potential of machine learning to address complex geoscientific problems such as seismic fault interpretation and well log correlation. Their work is based on deep neural networks with modern constructs. These models, together with large datasets, extract relevant features from the data and predict the response variables reliably and precisely with minimal or no human interaction. For example, the authors showed qualitatively how well the model predicts faults on the test crossline sections of seismic datasets.

4. Big data and machine learning in geosciences

Geoscience students should be familiar with concepts such as big data, cloud, and the Internet of Things (IoT). Briefly, computers are searching for trends in enormous collections of information, a task that would be impossible to humans. Within the past 10-15 years, improvements in data processing have made a comprehensive analysis of enormously huge amounts of data possible. In other words, big data is about finding data needles in data haystacks, and each step in a complex manufacturing process can generate tremendous amounts of data (**URL 4**).

Since scientific research has resulted in the accumulation of a large amount of data and conventional methods cannot handle such a massive amount of data, alternatives such as big data, cloud computing, artificial intelligence, and block chain have emerged. Scientific big data is characterized by its non-reproducibility, high degree of uncertainty, high dimensionality, and high complexity. Therefore, big data is a new challenge for conventional data processing techniques and methods (**Qi and Xuelong, 2019**). The authors explain how big data research progresses via the determination of correlations among data and is characterized by decision-making based on high probability. Combined with the advantages of using machine learning algorithms for data processing, methods of data analysis facilitated advancements of the geoscience into new realms of quantitative research. For example, **Ma** (**2019**) gives an excellent remark that data cannot speak for itself unless data analytics is employed. The author emphasizes the importance of in-depth data analytics, as many exotic modelling methods do not generate good reservoir models, because they tend to have too many assumptions, either explicit or implicit, and work well only for synthetic data. To tell a story with geoscience data, numerous hurdles need to be solved. Not only that, but science career stories usually unfold with all

their unexpected twists and turns. For example, skills used to be broad, then specialized, and now broad is stellar again. From the book by **Ma** (**2019**), the revolution brought by the geological and reservoir modeling is that it requires a geoscientist who has a broad knowledge in many disciplines (e.g., structural geology, sequence stratigraphy, siliciclastic geology, carbonate geology, sedimentary geology, etc.). Big data have made multidisciplinary skills even more desirable, especially for geosciences applied to resource characterization and modeling. Therefore, integrated modeling using geology, geophysics, petrophysics, reservoir engineering, data science, and geostatistics becomes increasingly important. Prospective geoscience students should learn this along the way and imagine how it may play out for them in their future dream job.

More and more, we read how data is our most valuable asset. According to an article (**URL 5**) in the leading financial magazine (The Economist), the world's most valuable resource is no longer oil, but data. Alphabet (Google's parent company), Amazon, Apple, Facebook and Microsoft, they are the five most valuable listed firms in the world. Without any doubt, we live in the era of the data economy. Economists, professors and even CEOs are touting that data is the new oil in today's economy (**URL 6**). But oil is finite, and it will become harder to extract as less is available. Also, oil is just oil, used in many products. Data, on the other hand, is growing rapidly, it can become any number of things, and data mining has a much less detrimental impact on the environment. Hence, data should be compared with renewables (the sun, water, and wind) since there is an abundance of those. So, the proponents and opponents agree on the one thing, which is the power that comes from the resource, while treating data like oil only contributes to the imbalance of power; those who have the resources and those who don't (**URL 6**).

In 2021, a Thematic Section of Geoscience Frontiers (journal) was devoted to insights into the latest developments and challenges in applying big data and machine learning (ML) to geoscience and geoengineering. Editorial section (**Zhang et al., 2021**) points out that the nature of scientific geoscience and geoengineering data, and the processes used to retrieve and analyse them, may differ substantially from those in other fields. Therefore, geoscience and geoengineering professionals should pay increased attention to big data research, create the environment to utilize data to add value to the geoscience, and promote collaboration with data analysts from other disciplines. The authors explain ML as the scientific study of algorithms and statistical models that allows computers to learn from existing data to improve their performance on specific tasks without being explicitly programmed. Thanks to peculiar features of geological materials, the geoscience and geo-engineering disciplines face more significant uncertainties than other fields of civil and mechanical engineering. Based on considerable monitoring and site investigation data in geotechnical engineering, ML can be a suitable and effective alternative for the purpose of solving various geotechnical engineering problems. In doing so, the combination of big data and ML may create unexpected solutions to the conventional geotechnical problems. Hereby, **Wang et al.** (**2020**) used a large volume of landslide data compiled in Hong Kong over the past few decades and introduced a novel ML and deep learning method to identify natural terrain landslides. Different types of landslide-related data were compiled, including topographic data, geological data and rainfall-related data. Three integrated geodatabases were also established, represented by Recent Landslide Database, Relict Landslide Database and Joint Landslide Database. Promising results were achieved by ML and deep learning methods, particularly the convolutional neural networks (CNN) method, owing to its strengths in feature extraction and multi-layer two-dimensional data processing, which are important for landslide identification problems.

Karpatne et al. (**2017**) discussed some of the emerging research themes in ML that are applicable across all problems in the geosciences, and the importance of a deep collaboration between ML and geosciences for synergistic advancements in both disciplines. They emphasize that the analysis of geoscience data has several unique aspects that are strikingly different from standard data science problems encountered in commercial domains. Noteworthy, geoscience phenomena are governed by physical laws and principles and involve objects and relationships that often have amorphous boundaries and complex latent variables. Furthermore, spatio-temporal structure of geoscience phenomena should be considered, also the facts that they are highly multi-variate, that they follow non-linear relationships (e.g., chaotic), that they show non-stationary characteristics, and commonly involve rare but interesting events. Moreover, the procedures used for collecting geoscience observations (or samples) introduce more challenges for ML, such as the presence of data at multiple resolutions of space and time, with varying degrees of noise, incompleteness, and uncertainties. Additional difficulties refer on the small sample size (e.g., small number of historical years with adequate records) and lack of gold-standard ground truth in geoscience applications. So, the article by **Karpatne et al.** (**2017**) addresses challenges, problems, and promising ML directions, and demonstrates the great emerging possibilities of future ML research in the important geoscience area of research.

Due to a large and complex nature of geological research objects, traditional geological research is often coupled with problems related to complex data sources and low precision. Lately, a huge number of emerging technologies (artificial intelligence, AI) are improving the precision of geological data and expand the data volume. Nevertheless, big

data and AI-based geoscience applications are still in their infancy, and the methods and objectives are still scattered, lacking a unified theoretical and application framework (**Chen et al., 2020**). By comparing with traditional geological research methods, big data and AI can take advantage of the vast amounts of geological data to summarize geological characteristics; explore the rules of geological activity; analyse geological phenomena objectively, impartially, and quickly; and provide more scientific results for geological work. The authors give an optimistic message that geological big data technology research will inject new vitality into the development of geology.

Two computer scientists, Thul D. and Blevins K. (**URL 7**) delivered a virtual meeting on new computer approaches (data analysis, machine learning, and big data) to data science in geology (petroleum systems). The authors nicely said that the principal skill of geoscientists is applying domain expertise to sparse data. Something computers, no matter how sophisticated, can't do. In fact, geoscientists recognize patterns and find trends, mostly visually. Hence, the two explored how geologists might leverage new technology to augment their capability and shift cognitive load to computer systems to greatly change information flow and decision making.

Nativi et al. (**2015**) discussed the impact of big data dimensionalities (commonly known as 'V' axes: volume, variety, velocity, veracity, visualization) on the Global Earth Observation System of Systems (GEOSS) and particularly its common digital infrastructure (the GEOSS Common Infrastructure). GEOSS is a global and flexible network of content providers allowing decision makers to access an extraordinary range of data and information. GEOSS is a pioneering framework for global and multidisciplinary data sharing in the EO realm. The authors introduced and discussed the general GEOSS strategies to address big data challenges, focusing on the cloud-based discovery and access solutions.

5. Geoscientists need coding and programming

Once we've established awareness of the quantitative nature of the contemporary geosciences, the next step is to grow the business. Coding makes computers work. Coders are always looking for a way to do something better. Coding is the business literacy of the future. Coding skills are in high demand across a broad range of careers. Coding skills provide an avenue to high-income jobs (**URL 8**). And so on… Essentially, coding is assigning a computer a task to do based on some logic. Highly complex tasks are a collection of smaller operations once they are broken down. This methodical and logic-heavy approach to problem solving can be a boon for figuring out problems beyond a coding challenge (**URL 9**).

Programming skills are commonly perceived as a tool just for modelers or quantitative scientists, but **Valle and Berdanier** (**2012**) dispute this view and argue that programming skills are extremely useful for almost any scientist, particularly with the advent of scripted analysis programs (e.g., Matlab and R). For example, these programming skills enable us to query, pre-process, visualize, and analyse data sets in a much less error-prone way than spreadsheets. Furthermore, these scripting languages allow for a natural documentation of the judgment calls that are often needed when pre-processing the data, being a critical step toward reproducible research. The authors point out that programming skills are critical for data pre-processing, allowing data to be combined, queried, and summarized. These skills are particularly relevant when using data collected by multiple researchers, which is becoming more frequent as we strive to understand environmental (or geological) phenomena across larger regions and over longer time scales. They conclude that these languages (e.g. Python, R, Matlab, etc.) should become part of the formal training of scientists so as to facilitate data sharing, reproducible research, and statistical fluency.

Much of contemporary geoscience evolves around novel analyses of large data sets that require custom tools – computer programs – to minimize the drudgery of manual data handling. **Grapenthin** (**2011**) emphasizes that current curricula do not recognize the gap between user and machine. Therefore, students require specialized courses teaching them the skills they need to make tools that operate on particular data sets and solve their specific problems.

On **URL 10**, a computational scientist shares his insights on the best practices to make scientific software better. He notes that while there are still interesting analytical studies to be made, and important data to be gathered, it is increasingly common that PhD students in geodynamics are expected to work exclusively on data interpretation, computational models, and in particular the accompanying development of geodynamic software packages. For example, one of them is GPlates (**Müller et al., 2018**), a virtual globe software that provides the capability to reconstruct geodata attached to tectonic plates to develop and modify models that describe how the plates and their boundaries have evolved through time. It allows users to deform plates and to visualize surface tectonics in the context of convecting mantle structure and evolution by importing seismic tomography models or outputs from geodynamic models. GPlates applications include tectonics, geodynamics, basin evolution, orogenesis, deep Earth resource

exploration, paleobiology, paleoceanography, and paleoclimate. The software is enabling end-users in universities, government organizations, industry, and schools to explore the evolution of planet Earth on their desktop.

6. Conclusions

With the advent of new technologies, such as augmented and virtual reality, or the emergence of web 3.0 and promises of a metaverse, the question arises as to what will happen to the labour market in the near and distant future. This paper suggests that it is imperative to start discussing these topics throughout the education system. More and more universities in the world are implementing transformations of curricula because they are realizing that without greater quantitative knowledge and programming skills, students will not be able to compete in any labour market or business domain. All this is taking place in the context of a green and digital transition in which investments are progressively growing, and such sustainable business should result in climate neutrality and greater competitiveness. This paper shows that the wave of newly expected skills has already swept the labour market, and that all higher geoscience education institutions must learn to swim among all these new trends. In today's dynamic business environment, geoscience students are best equipped if they possess both hard (job duties) and soft (personal qualities) skills, aided by quantitative and computing ones. The crises that humanity is going through are new opportunities in new markets, for the improvement of business and educational processes, restructuring, but above all for greater investment. Ambitious and talented geoscience students need to start preparing for better starting positions in their future careers as early as possible through their educational journey. If we all evolve this part of the business, our prospects of better future are clearly in capable hands.

7. References

Chen, L., Wang, L., Miao, J., Gao, H., Zhang, Y., Yao, Y., Bai, M., Mei, L., He, J. (2020): Review of the Application of Big Data and Artificial Intelligence in Geology. Journal of Physics: Conference Series, 1684, 012007.

Geological Society of America (2016): Expanding and improving geoscience in higher education: GSA position statement. Geological Society of America, www.geosociety.org/gsa/positions/position18.aspx

Gewin, V. (2016): Geoscience: Ups and downs. Nature, 530, 371–372, doi:10.1038/nj7590-371a.

Grapenthin, R. (2011): Computer Programing for Geosciences: Teach Your Students How to Make Tools. Eos, 92, 469-470.

Karpatne, A., Ebert-Uphoff, I., Ravela, S., Ali Babaie, H., Kumar, V. (2017): Machine Learning for the Geosciences:Challenges and Opportunities. arXiv: 1711.04708v1 [cs.LG] 13 Nov 2017.

King, C. (2008): Geoscience education: an overview. Studies in ScienceEducation, 44:2, 187-222.

Ma, Y.Z. (2019): Quantitative Geosciences: Data Analytics, Geostatistics, Reservoir Characterization and Modelling. Springer Nature Switzerland AG, 640 p.

Macdonald, R.H. and McNeill Bailey, C. (2000): Integrating the Teaching of Quantitative Skills Across the Geology Curriculum in a Department. Journal of Geoscience Education, 48, 482.

Manduca, C.A., Baer, E., Hancock, G., Macdonald, R.H., Patterson, S., Savina, M., Wenner, J. (2008): Making Undergraduate Geoscience Quantitative. Eos, 89, 16, https://doi.org/10.1029/2008EO160001

Maniar, H., Ryali, S., Kulkarni, M.S., Abubakar, A. (2018): Machine learning methods in Geoscience. SEG International Exposition and 88th Annual Meeting, 4638-4642, https://doi.org/10.1190/segam2018-2997218.1

Medunić, G., Ahel, M., BožičevićMihalić, I., GaurinaSrček, V., Kopjar, N., Fiket, Ž., Bituh, T., Mikac, I. (2016): Toxic airborne S, PAH, and trace element legacy of the superhigh-organic-sulphur Raša coal combustion: Cytotoxicity and genotoxicity assessment of soil and ash. Science of the Total Environment, 566, 306-319.

Mileusnić, M. (2020): Service learning in geoscience education. European Geologist Journal, 50, https://doi.org/10.5281/zenodo.4311367

Mosher, S., Bralower, T., Huntoon, J., Lea, P., McConnell, D., Miller, K., Ryan, J.G., Summa, L., Villalobos, J., White, L. (2014): Future of Undergraduate Geoscience Education: Summary Report for Summit on Future of Undergraduate Geoscience Education. School of Geosciences Faculty and Staff Publications. 1127, https://scholarcommons.usf.edu/geo_facpub/1127

Mosher, S. and Keane, C. (2021): Vision and Change in the Geosciences: The Future of Undergraduate Geoscience Education. Published by the American Geosciences Institute., 176 p.

Müller, R.D., Cannon, J., Qin, X., Watson,R.J., Gurnis, M., Williams, S.,Pfaffelmoser, T., Seton, M., Russell, S.H.J., Zahirović, S. (2018): GPlates: Building a virtual Earth throughdeeptime.Geochemistry, Geophysics,Geosystems,19, 2243–2261.

Nativi, S., Mazzetti, P., Santoro, M., Papeschi, F., Craglia, M., Ochiai, O. (2015): Big Data challenges in building the Global Earth Observation System ofSystems. Environmental Modelling & Software, 68, 1-26.

Orion, N. (2019): The future challenge of Earth science education research. Disciplinary and Interdisciplinary Science Education Research, 1:3, https://doi.org/10.1186/s43031-019-0003-z

Qi, Z. and Xuelong, L. (2019): Big data: new methods and ideas in geological scientific research. Big Earth Data, 3:1, 1-7, doi: 10.1080/20964471.2018.1564478

Valle, D. and Berdanier, A. (2012): Computer Programming Skills for Environmental Sciences. Bulletin of the Ecological Society of America, 373-389.

Wang, H.J., Zhang, L.M., Xiao, T., Zhang, L.L., Li, J.H., 2020. Landslide identification using machine learning. Geoscience Frontiers, https://doi.org/10.1016/j.gsf.2020.02.012

Zhang, W., Ching, J., Goh, A.T.C., Leung, A.Y.F. (2021): Big data and machine learning in geoscience and geoengineering: Introduction. Geoscience Frontiers, 12, 327–329.

Internet sources (URLs):

1: https://www.nature.com/subjects/computational-science(accessed on April 13, 2022)
2: https://www.egi.utah.edu/why-geoscience-matters (accessed on April 13, 2022)
3: https://www.theodysseyonline.com/geology-underrated-science (accessed on April 13, 2022)
4:https://arstechnica.com/information-technology/2015/02/the-big-deal-about-big-data-your-guide-to-what-the-heck-it-actually-means/
5: https://www.economist.com/leaders/2017/05/06/the-worlds-most-valuable-resource-is-no-longer-oil-but-data
6: https://www.f5.com/company/blog/oil-vs-data-which-is-more-valuable
7: https://archives.datapages.com/data/HGS/vol63/063007/pdfs/9.pdf
8: https://www.burning-glass.com/wp-content/uploads/Beyond_Point_Click_final.pdf
9: https://www.rasmussen.edu/degrees/technology/blog/why-learn-to-code/
10: https://blogs.egu.eu/divisions/gd/2018/10/09/its-just-coding-scientific-software-development-in-geodynamics/

Sažetak

Značaj računalnih vještina u visokoobrazovnom sustavu geoznanosti za 21. stoljeće

U svijetu se provode brojna istraživanja o tome kako će izgledati obrazovanje u budućnosti. Svjedoci smo rastućeg broja pokazatelja sporog urušavanja obrazovnog sustava kakvog poznajemo. Izgledno je da se visoko obrazovanje približava velikoj prekretnici nakon koje će ono biti diktirano brzinom i fleksibilnošću prilagodbi globalnim promjenama. Sveprisutna digitalizacija, novi trendovi i održivost bit će ključni koncepti poslovnih modela u budućnosti. Uz poznavanje rada na računalu, novim će generacijama trebati i vještine programiranja. Visokoškolski sustav mora što ozbiljnije i hitnije shvatiti ovaj zadatak. Bez navedenih znanja i vještina budućim će zaposlenicima biti teško konkurirati na tržištu rada i/ili dalje napredovati u karijeri. Ovaj članak bavi se pitanjem budućih smjernica glede visokoobrazovnog sustava geoznanosti s obzirom na ubrzan razvoj tehnologija te eksponencijalan rast skupova podataka. Stoga je potrebno imati na umu da će strojno učenje imati sve više uspjeha na tom polju. Primjena računalnih i matematičkih metoda u geoznanostima, uklopljenih u koncept računalnih geoznanosti, odredit će budućnost geologije i srodnih disciplina.

Ključne riječi: geoznanosti, visoko obrazovanje, vještine, zaposlenje, računalne znanosti

Acknowledgement

Author's contributions

Gordana Medunić, **Sanchita Chakravarty** and **Rajen Kundu** equally contributed to all aspects of paper.

Meteorite impacts on Mars

Željko Andreić[1] and Indramani Sharma[2]

[1] University of Zagreb, Faculty of Mining, Geology and Petroleum Engineering,
Pierottijeva 6, 10000 Zagreb, Croatia, ORCID 0000-0003-0175-8174

[2] University of Zagreb, Faculty of Mining, Geology and Petroleum Engineering,
Pierottijeva 6, 10000 Zagreb, Croatia, ORCID 0000-0002-0577-5855

Abstract

The consequences of impact of a meteorite (less than 10 kg in mass) on Mars surface are investigated. The atmospheric braking is found to be important only for smaller objects with a strong dependence on density, impact angle and velocity of the meteorite. The limits for efficient atmospheric braking of incoming meteorites are determined, depending on initial mass, velocity and impact angle, but also on the surface atmospheric pressure at the moment of impact.

Keywords: Mars, meteorite flight, atmosphere stopping power

1. Introduction

Mars is in the research focus in the last decade. Several probes are currently in orbit and on the surface of the planet conducting various scientific missions with the common goal of gathering more data on Mars and its history. Space agencies are preparing for more advanced (possibly human) missions in the future. Most of the research is geological in nature, but other aspects of Martian environment are under consideration as well. In this context we tried to model meteorite impacts on the Martian surface and the ability (if any) of the Martian atmosphere to stop or slow down the impactors. Combined with knowledge of mean meteorite flux on Mars, the results obtained can be used to estimate the possible danger for robotic or human missions on the planet surface. To simplify the text we ignored the common astronomical terminology that makes distinction between a body in deep space, a body in the atmosphere and the one on the surface, and we simply used term meteorite for all these cases. Before we start our modelling, we need to know basic facts about the planet Mars, its atmosphere and the impacting bodies. Data we used in our modelling are summarized in the **Table 1** and **Table 2**.

Equatorial diameter (km)	6780
Surface gravity (m/s^2)	3.71
Atmosphere composition	96 % CO_2; 1.9 % Ar; 1.9 % N_2
Surface atmospheric pressure (Pa)	636
Expected variations of surface pressure (Pa)	400-870
Mean surface temperature (K)	210
Expected variations of surface temperature (K)	130-308
Mean orbital speed (km/s)	24
First cosmic speed (km/s)	3.57
Second cosmic speed (km/s)	5.03
Third cosmic speed (km/s)	34.1

Table 1: Physical characteristics of the planet Mars.

Corresponding author: Željko Andreić
zandreic@rgn.hr

The **Table 1** gives basic physical characteristics of the planet Mars, starting with its diameter and surface gravity. Note that, although Mars is about half the size of the Earth, its surface acceleration is only about one third of the surface acceleration of the Earth. Martian atmosphere is very rare; surface pressure varies widely depending on the location and the time of the Martian year. Mars is farther from Sun than Earth and is accordingly slower in its orbit. Also, the third cosmic velocity for Mars (the velocity needed for a body to leave the Solar System) is about three quarters of the corresponding velocity for Earth. Combined with a weaker Martian gravity, this results in lower impact velocities for Martian meteorites, compared to the Earth. Thus, meteorites will strike Mars with velocities between about 5 and 58 km/s, compared to 11 to 72 km/s for Earth.

The **Table 2** summarizes meteorite properties used in our calculations. In addition to common meteorite types found on Earth, we added ice as the lowest density meteorite group. Ice meteorites do not survive travel through the dense Earth's atmosphere so from the Earth's perspective, they simply do not exist. However, the Martian atmosphere is much less dense than the Earth's, and smaller incoming velocities increase the possibility of icy bodies reaching the planet's surface. The percent abundances of various meteorite types are taken from the fall statistics, i.e. the number of meteorites of a certain type found on the Earth. With no accurate statistics for Mars, we can only assume that the abundances are similar, with the argument that the origin of meteorites in both cases is the same, i.e. mostly the asteroid belt. Ice cannot survive the interplanetary environment unprotected so we can also conclude that ice meteorites will be rare, if any (larger chunks with surfaces covered by dust particles).

Meteorite types	Ice ? Chondrites 95 % Iron 5 %
Meteorite densities (kg/m^3)	Ice 917 Chondrites 3300 Iron 8000
Meteorite mass (kg)	0.001 - 28
Meteorite impact angle (towards horizontal, deg)	10 – 90
Meteorite incoming velocity (km/s)	10 - 50

Table 2: Physical characteristics of meteorites as used in our calculations.

2. Methods
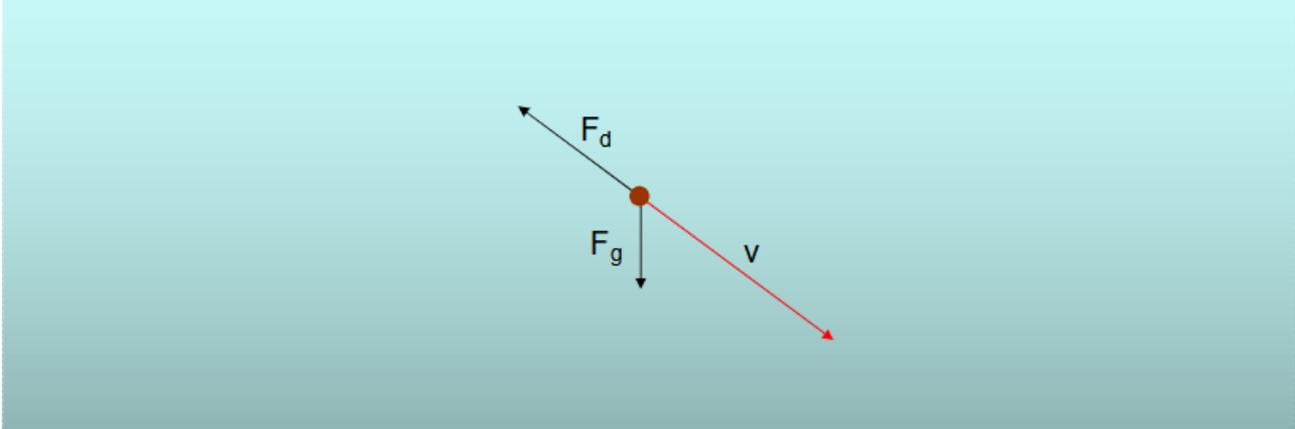
Figure 1: Forces acting on an incoming body in a planetary atmosphere. The incoming body is travelling with the velocity v, which is usually specified by its magnitude and the angle between the direction of the flight and the horizontal. The body is attracted towards the surface by the gravitational force F_g and is slowed down by the drag force F_d, which is always in opposite direction to the velocity.

The trajectory of the incoming body is determined by the forces acting on it. In this case the dominant force is the gravitational force of the planet Mars which, to a very good approximation, can be described by the Newton's **Equation 1**:

$$\overrightarrow{F_g} = G \frac{Mm}{r^2} \frac{\vec{r}}{r} \tag{1}$$

Where:
$\overrightarrow{F_g}$ *is the gravitational force,*
G is the universal gravitational constant,
M is the mass of the planet,
m is the mass of the incoming body,
$\vec{r}$ *is the distance between centres of these two bodies.*

It is common to rewrite this formula using the surface acceleration $\overrightarrow{a_g}$ as (**Equation 2**):

$$\overrightarrow{F_g} = \overrightarrow{a_g} m \frac{r^2}{r_o^2} \tag{2}$$

Where are:
$\overrightarrow{a_g}$ *standing for surface gravitational acceleration,*
r as before for the distance between the two bodies and
r_o *the diameter of the planet.*

The formula is valid for $r > r_o$. For small heights above the surface, the weakening of the gravitational acceleration with height is usually neglected, thus simplifying **Equation 2** to **Equation 3**:

$$\overrightarrow{F_g} = \overrightarrow{a_g} m \tag{3}$$

When the impactor enters the Martian atmosphere the drag force arises and Newton's drag law is used to describe it (**Equation 4**):

$$\overrightarrow{F_d} = -\frac{1}{2}c\rho Av^2 \frac{\vec{v}}{v} \qquad (4)$$

Which simplifies to **Equation 5**:

$$\overrightarrow{F_d} = -\frac{1}{2}c\rho Av\vec{v} \qquad (5)$$

Where:
c is the drag coefficient,
ρ is the density of the surrounding medium (Martian atmosphere in this case),
A is the cross-sectional area of the meteorite and
$\vec{v}$ is the relative velocity between the atmosphere and the meteorite.

The constant c depends on the meteorite shape and varies with the speed to a certain extent. For its values we used data from (**Carter at al., 2009**) for a spherical meteorite. As we are not interested in the exact location of the meteorite fall, we neglected wind in our calculations (in other case, wind would be included in the relative velocity term $\vec{v}$ in the drag equation). Similar argument applies to the planetary rotation which we also did not take into account.

In such a simplified situation, the model can be reduced to a two dimensional case by performing calculations in the plane of the meteorite trajectory. Here, x axis is horizontal, +x pointing in the direction of the flight, and y axis is vertical, pointing up. In this coordinate system the equation of motion of the meteorite can be written as **Equation 6**:

$$m\vec{a} = m\overrightarrow{a_g} - \frac{1}{2}c\rho Av\vec{v} \qquad (6)$$

or, by the components (**Equations 7** and **8**):

$$a_x = -\frac{c\rho A}{2m}vv_x \qquad (7)$$

$$a_y = -g - \frac{c\rho A}{2m}vv_y \qquad (8)$$

These two equations are then solved numerically, starting with a meteorite at a large distance from the planet and ending with the collision with the surface.

3. Results

The parameter most interesting to us in this study is the ability of the Martian atmosphere to slow down the incoming meteorite. For this, we required, somewhat arbitrarily, that the meteorite should be slowed down by the atmosphere to below 1 km/s before it hits the ground. Although this is quite a large remaining velocity, it is much smaller than the initial meteorite velocity, so such a projectile would be much easier to slow down with some protective measure (shielding or sim.) than the meteorite with its initial velocity. We found that the dependence of the maximal mass of a meteorite that can be slowed down to our criterium is strongly dependent on the impact angle and the initial velocity. The results of our model for the most common stony meteorites passing through a "standard" Martian atmosphere are shown on the **Figure 2**.
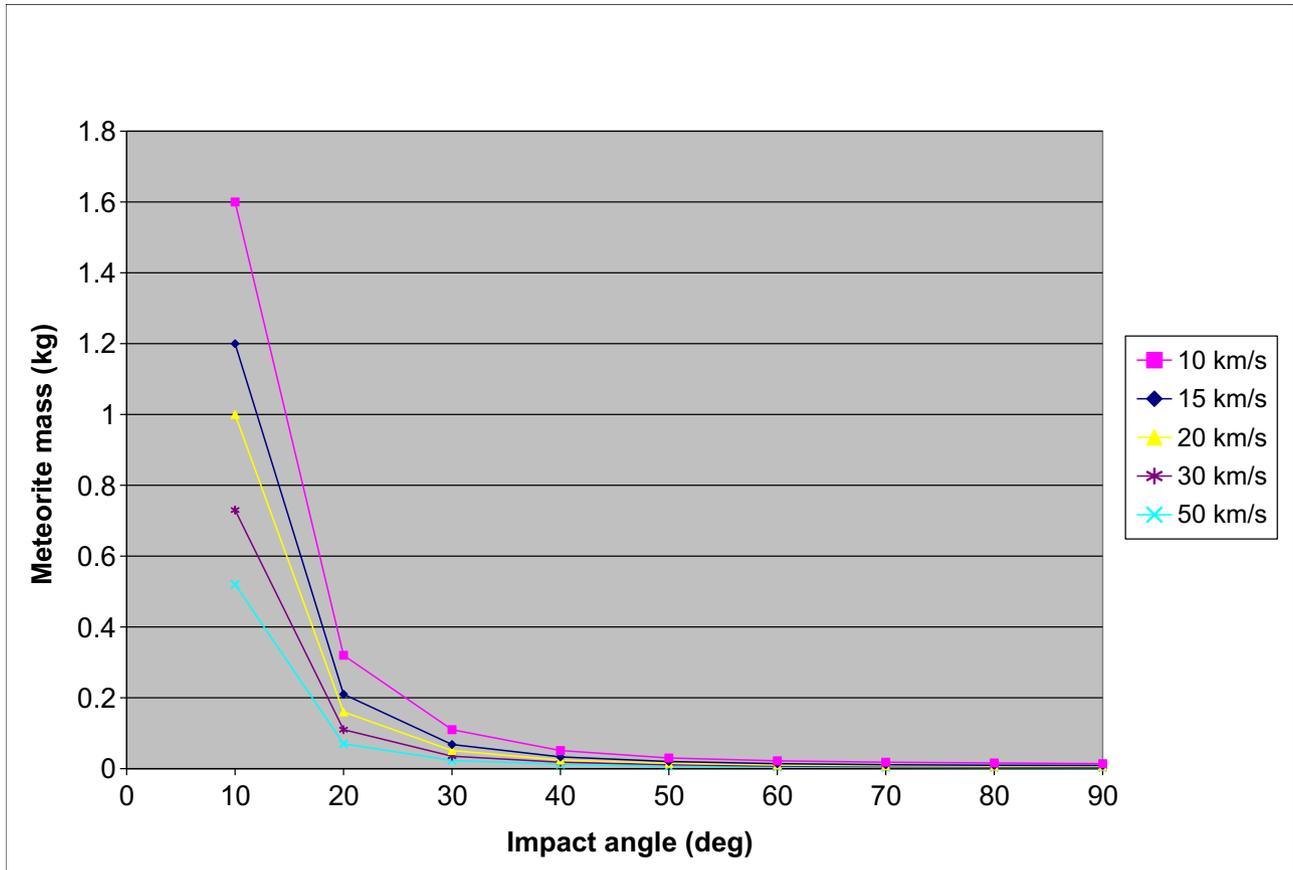
Figure 2: The dependence of the maximal mass of a meteorite that will be slowed down to 1 km/s before impacting the surface on the impact angle for various initial velocities. The graph is produced for the most common stony meteorite passing through a "standard" Martian atmosphere with a surface pressure of 636 Pa.

From the **Figure 2** it is obvious that the stopping power of the Martian atmosphere is extremely week indeed. The masses of meteorites that can be slowed down below 1 km/s are very small for all impact angles except the angles close to the horizontal. That means that any objects on the Martian surface (including people in protective suits) would be exposed to a large part of the incoming meteorite flux without any significant protection by the atmosphere. Moreover, the stopping power is strongly dependent on the surface atmospheric density at the moment of impact, as is illustrated by the **Figure 3.** At elevated places that naturally have lower surface pressure the protection by the atmosphere is minimal.
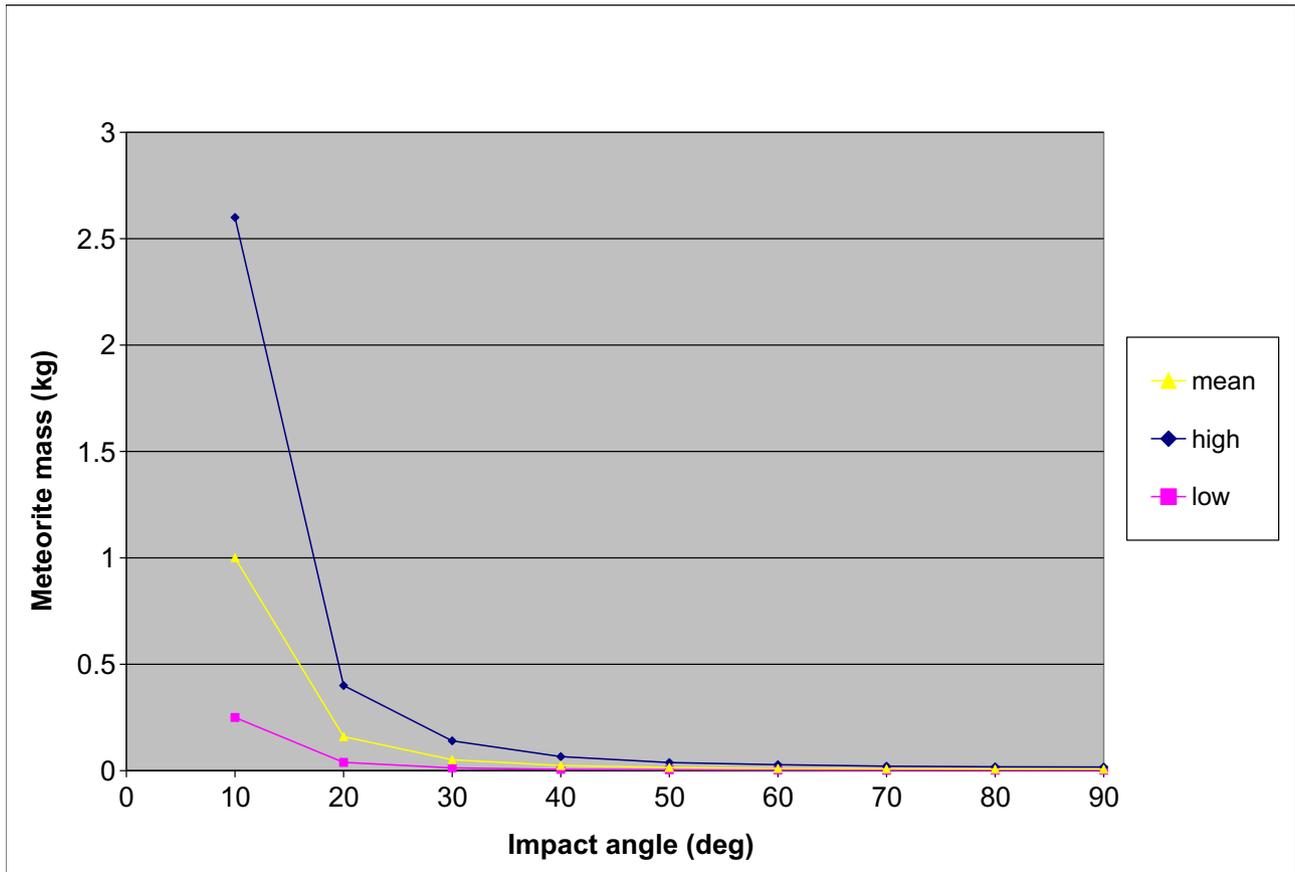
Figure 3: The dependence of the maximal mass of a meteorite that will be slowed down to 1 km/s before the impact on the impact angle for various atmospheric pressures. "mean" is the average pressure of the Martian atmosphere (636 Pa), "high" is the maximal expected pressure of 870 Pa and "low" is the minimal expected pressure of 400 Pa. The graph is produced for a stony meteorite with an initial velocity of 20 km/s.

The density of the meteorite (i.e., the material and consistence of the meteorite body) has a large influence on the ability of the Martian atmosphere to slow it down. Less dense meteorites have larger cross-section than more dense meteorites with the same mass and thus are exposed to a larger drag force. This fact is illustrated in the **Figure 4**.
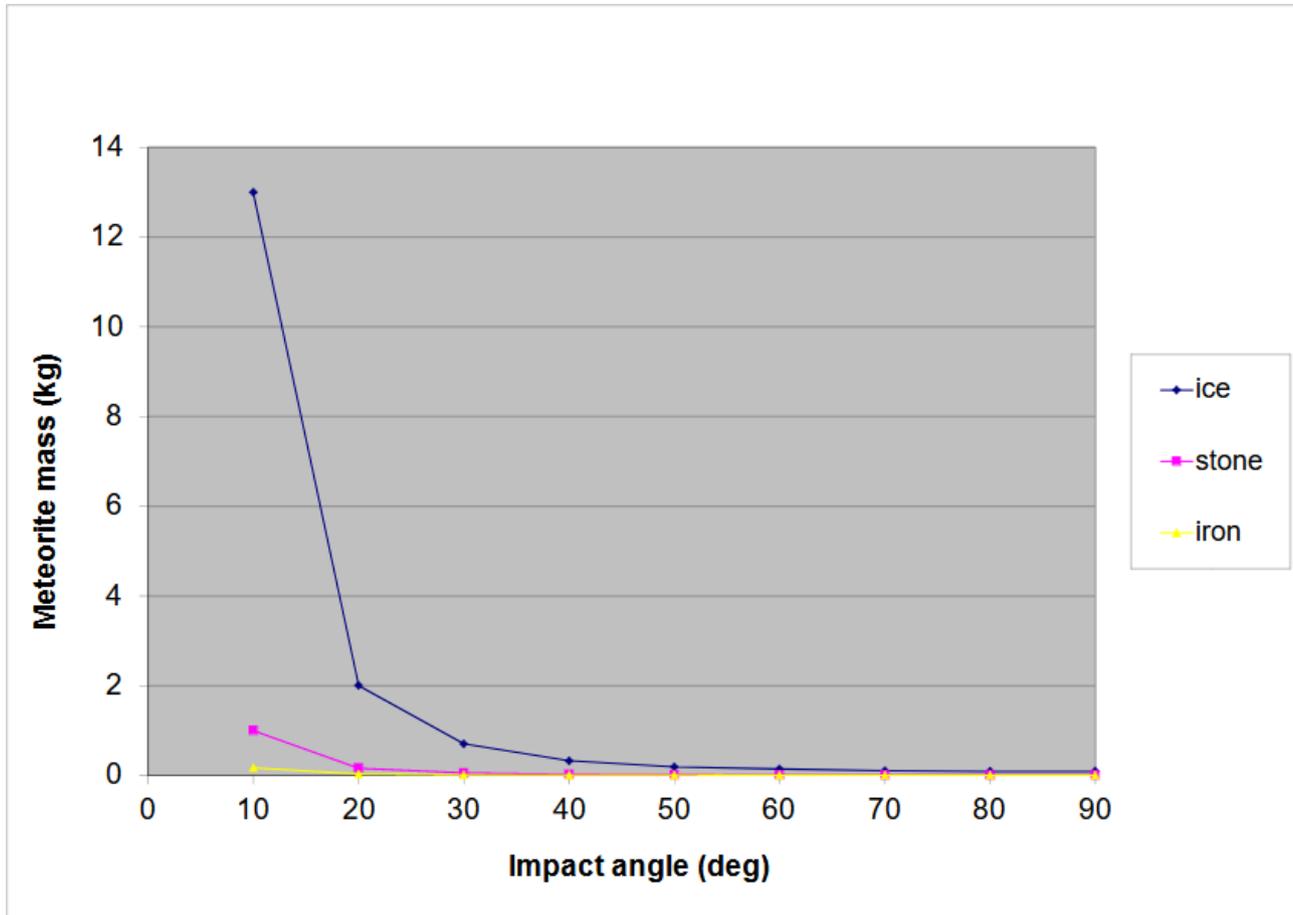
Figure 4: The dependence of the maximal mass of a meteorite that will be slowed down to 1 km/s before the impact on the impact angle, for three meteorite types (densities). The graph is produced for a meteorite with an initial velocity of 20 km/s

4. Discussion

The results show that the limiting size (defined as the maximal mass of the meteorite that will be slowed down to 1 km/s or less before the impact) strongly depends on four parameters: the incoming velocity, the incoming angle, the density of the meteorite and the surface atmospheric density at the time and place of the impact. In such circumstances it is hard to define a single "limiting" size of a meteorite that will be slowed down enough, but we can resort to taking the most unfavourable conditions. In such a case, the maximal mass of a meteorite that can be slowed down below 1 km/s is about 1g for the most common stony meteorites, about 50g for icy ones and less than 100 mg for the iron ones.

Some information about Martian meteor showers can be found in (**Jenniskens, 2006**) but estimated shower fluxes are missing. The average flux of the meteorites larger than these limits is about 10^{-14} m^{-2}s^{-1} (**Grün et all, 2002**) at the Earth's orbit, and only slightly less at the orbit of Mars. The meaning of this is that any square meter of the Martian surface will be hit by a meteorite larger than the limit size once in 10^{14} seconds (about 3 million years). Thus our concern for the safety of unprotected objects/people on the Martian surface seems to be exaggerated. However, due to many simplifications made in this short study, further work is necessary to support this conclusion.

5. Conclusions

The results of the modelling of meteorite flight through the Martian atmosphere show that only small meteorites will be significantly slowed down. This is a consequence of the low density of the Martian atmosphere. Thus, for stony meteorites which are the most common type with the abundance of about 95 %, the limiting mass is about 1 g, for ice

about 50 g and for iron less than 100 mg. A strong dependence on the local atmospheric density is shown. Also noticed is a less pronounced dependence on the impact parameters (impact angle and velocity). A rough estimate of the meteorite impact rate per square meter of Martian surface is one hit in 3 million years.

6. References

Papers:

Carter, R.T., Jandir, P.S. and Kress, M. E., Estimating the Drag Coefficients of Meteorites for All Mach Number Regimes, 40th Lunar and Planetary Science Conference, (Lunar and Planetary Science XL), held March 23-27, 2009 in The Woodlands, Texas, id.2059

Chapters in books or proceedings with editor(s):

Grün, E., Dikarev, V, Kruger, H. and Landgraf, M. (2002): Space dust measurements, p. 56, In: Murad, E. and Williams, I.P.(eds.): Meteors in the Earth's Atmosphere. - Cambridge University Press, 35-75, 322 p.

Jenniskens, P. (2006): Meteor showers on other planets, p. 752-758, in Meteor showers and their parent comets - Cambridge University Press.

Sažetak

Udari meteorita u Mars

Istraživane su posljedice udara meteorita (s manje od 10 kg mase) o Marsovu površinu. Atmosfersko usporavanje bitno je samo za manje meteorite uz snažnu ovisnost o gustoći, upadnom kutu i brzini meteorita. Određene su granice efikasnog atmosferskog usporavanja u ovisnosti o početnoj masi, brzini i upadnom kutu, ali i o površinskom atmosferskom tlaku u trenutku udara.

Ključne riječi: Mars, Let meteorita, Atmosfersko usporavanje

Acknowledgment

Author's contributions

Ž.A. made the numerical flight model and carried out the calculations, I.S. analysed the results and prepared graphs.

Numerical models of the deep geological repository for the spent nuclear fuel

Želimir Veinović[1]; Helena Vučenović[2]; Galla Uroić[3]; Andrea Rapić[4]

[1] University of Zagreb, Faculty of mining, geology and petroleum engineering, Pierottijeva 6, 10000 Zagreb, Croatia, 0000-0002-1572-2191

[2] University of Zagreb, Faculty of mining, geology and petroleum engineering, Pierottijeva 6, 10000 Zagreb, Croatia, 0000-0001-6512-0669

[3] Fund for financing the decommissioning of the Krško Nuclear Power Plant and the disposal of Krško NPP radioactive waste and spent nuclear fuel, Ulica Vjekoslava Heinzela 70A, 10000 Zagreb, Croatia, 0000-0003-4114-5225

[4] Fund for financing the decommissioning of the Krško Nuclear Power Plant and the disposal of Krško NPP radioactive waste and spent nuclear fuel, Ulica Vjekoslava Heinzela 70A, 10000 Zagreb, Croatia

Abstract

Numerical analysis of the deep geological repository (DGR) for the spent nuclear fuel (SNF) and/or high-level radioactive waste (HLW) is crucial part of safety case for every SNF/HLW disposal program. Before any activity concerning the disposal starts it is necessary to prove functionality of the future disposal concept applied to the specific host rock. Apart from laboratory work, including underground research laboratories (URLs), which should also prove applicability of the disposal concept and appropriateness of the host rock and buffer material, numerical model of the future DGR should be designed and tested in order to check the adequacy of the solution, to identify possible errors and problems, and to adjust future works, the dimensions of individual elements of the repository and the choice of materials. Numerical models presented in this paper are developed for the KBS-3V concept for the disposal of the SNF and/or HLW, in Plaxis and GeoStudio software. Granodiorite was selected as a host rock, and sodium bentonite as buffer material. Comparison of respected models created in these two software packages, as well as their verification according to required safety parameters for the repository, are discussed and compared to state-of-the-art research of running programs (i.e., Finnish and Swedish SNF disposal program). Outcomes of the research show that both software give alike results, comparable and with an equal stress distribution with respect to the shape of the underground spaces. Both numerical models show that the excavated spaces will remain stable even without the support system, and that maximal displacement will not affect the disposal tunnel and borehole. It is evident that the presented numerical models correspond to the results of other similar research and that they may possibly be used for the development of safety case and testing the design of future repository of SNF or HLW.

Keywords: numerical model; deep geological repository; spent nuclear fuel; bentonite; granodiorite

1. Introduction

Deep geological repository (DGR) for the spent nuclear fuel (SNF) and/or high-level radioactive waste (HLW) might be the most challenging engineering problem, considering that the lifetime of DGR corresponds to the half-life of radionuclides contained in the material to be disposed of. Therefore, DGR is designed to stay safe and maintain functionality for a period of 10 000 up to 100 000 years (depending on national regulations) (**Veinović et al., 2015**).

Materials in which DGRs are constructed can vary from sedimentary (clay, salt domes…) to magmatic rocks (granite, granodiorite…) but there are several conditions that have to be fulfilled considering the geology of the host rock during the site selection process (simplified acc. to (**DOE, 1984; GD 736/2008; IAEA, 1994; IAEA, 2011; JPN, 2000; STUK, 2015)**):

- Low ambient host rock temperature
- Slow groundwater movement (0,1 – 1 mm/y)
- Minimal rock deformations
- Neither low nor high groundwater pH
- Reductive groundwater conditions

Corresponding author: Želimir Veinović
zelimir.veinovic@rgn.hr

- Small amounts of dissolved inorganic carbon in groundwater
- Glaciation is not expected at the site during the (next) ice age
- No tectonic shifts are expected at the site during the required period of operation of the DGR
- There were no active tectonic processes over a period of preferably more than ten million years (it is undesirable if the change was within a million years)
- Areas with the maximum possible earthquake intensity in the range of I-IV degrees of the MCS scale.
- There is no likelihood of a volcano within a radius of 10 km
- There is no diapirism and salt tectonics in the region
- The default distance from the active fault is 1/100 of the length of the active fault, taking into account all its segments. The area has no recently active faults (Quaternary)
- Areas where with a geothermal gradient up to 6 ° C per 100 m at a disposal depth of 500 m does not exceed 30 ° C
- There are no specific paleo hydrological phenomena
- Rock type has been identified directly or indirectly empirically as poorly permeable to impermeable even under tectonic or technological stresses
- The host rock is not and does not have soluble interlayers
- There are no significant fossil fluid inclusions
- The floor of the host rock will not be made of soluble rock
- There are no liquid or gaseous hydrocarbons in the bottom of the host rock
- The host rock will maintain low permeability even under dynamic stresses
- The cracks are closed completely due to the ductile behavior of the material while compensating for surface roughness
- The cracks are closed by geochemical processes with renewed activation of atomic bonds in the crack area
- No boundary tendency to form groundwater pathways
- There is no significant aquifer of any type in the area
- No particularly pronounced erosion (erosion rate less than 100 m / 100,000 years)
- No creep
- No flooding
- Excluding existing and planned flood protection areas for high water evacuation
- Areas outside 1000 annual flood lines.

DGR is supposed to be constructed at the depth of 500 up to 1 000 m, which will guarantee safety from biological intrusion (including anthropogenic), and the choice of the disposal concept will depend upon geological properties of the site (**Umeki, 2007; Baldwin et al., 2008**). The technology of the construction of the DGR (underground spaces) must be chosen and adjusted according to the host rock properties and the repository design. Concept of the DGR and the rock excavation technology must be selected in a way that it minimizes disturbance of and damage to the host rock (**Uroić et al., 2022**). If simplified, most of the applicable disposal concepts include either the disposal into boreholes vertical to the disposal tunnels or axially in the disposal tunnels (**Figure 1**). In this paper KBS-3V concept of disposal into short boreholes from the disposal tunnel (**Umeki, 2007; Baldwin et al., 2008; Ikonen, 2003**) will be analyzed.
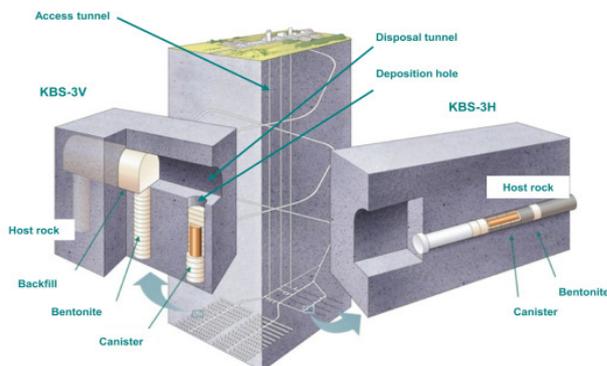
Figure 1: Simplified schematic (disposal depth 500-1 000 m) KBS-3V and KBS-3H disposal concepts of repositories for SNF and/or HLW (**Sinnathamby et al., 2014**)

Before the DGR is constructed, apart from the thorough geological survey of the location during the site selection process, it is necessary to develop the underground research facility (URF) in order to test the disposal technologies, as well as the excavation methods (**Veinović et al., 2012a, Veinović et al., 2012b**). Results from tests and experiments performed in URF, as well as the results obtained from testing samples from exploratory boreholes and geophysical exploration of the site, are the basis for the numerical analysis of the future DGR (**Åkesson et al., 2010; Chen et al., 2012; Kwon et al., 2013; Rutqvist et al., 2005; Saanio et al., 2013; Schäfers et al., 2019; Toprak et al., 2012; Toprak et al., 2013; Zhao et al., 2014**). However, numerical model will incorporate parameter of the engineering barriers: cannister and buffer material (**Figure 2**).
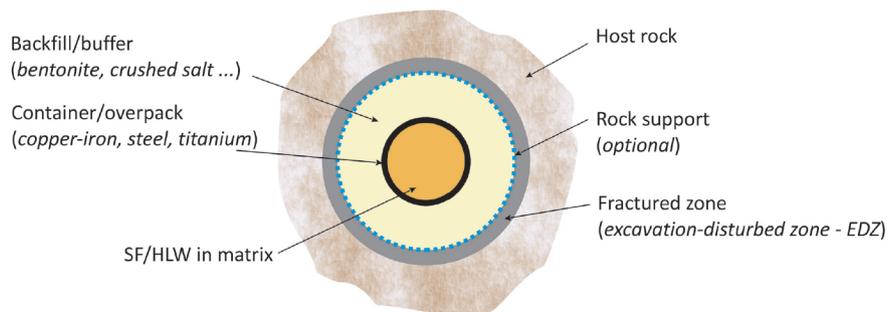
Figure 2: Conceptual solution for the disposal (isolation) of the SNF and/or HLW (**Veinović et al, 2015**). Scale would depend on the concept and the program, diameter of the container/overpack can vary from 0,6 up to 1,2 m.

Characteristics of the cannister for the disposal of the SNF or HLW, used for the development of DGR's numerical model, mainly refers to mechanical properties and the heat transfer properties of the cannister material. However, the properties of buffer material needed for the numerical model of the disposal concept (**Domitrović et al., 2012**) will include much more parameters. Since the topic of this paper is mainly consideration of the mechanical behavior of the host rock after the excavation and installation of the cannister, and the comparison of the analysis performed in two software (Plaxis and Geostudio), only mechanical characteristics of the buffer material and the host rock will be considered. More detailed research considering the Thermo-Hydro-Mechanical Effects on Host Rock for SNF DGR is presented in Veinović, et al. (**2020**). As the host rock, the granodiorite is selected, being the most likely geologic material in which the future Croatian/Slovenian DGR for the SNF will be constructed in (**Veinović et al., 2020**). The disposal depth will probably be 500 m, the location cannot be defined because the site selection process has not been carried out, the geology of Croatia and Slovenia does not offer any other type of host rock other than igneous rocks, and after a preliminary analysis it was assumed that host rock would be granodiorite.

Most of the numerical modelling and analysis of the thermal-hydro-mechanical effects (HME) of SNF or HLW on host rock and the buffer material is done by Abaqus (**Åkesson et al., 2010**), Code_Bright (**Åkesson et al., 2010; Toprak et al. 2012; Toprak et al., 2013**) and Tough-Flac 3D (**Blanco-Martin et al., 2017; Rutquist, 2011**). However, fairly good results, which correspond to the results of research conducted in other software, were obtained using the GeoStudio software package (**Veinović et al., 2020**). GeoStudio and Plaxis are two software packages available at the Faculty of Mining, Geology and Petroleum Engineering, University of Zagreb, and they are readily used for lectures and research. Both software packages offer several types of numerical analysis, including:
- slope stability
- groundwater flow (saturated and non-saturated conditions)
- stress and strain analyses
- earthquake-induced liquefaction and dynamic load
- heat transfer
- transport of liquids and gasses trough a porous medium.

In order to perform numerical analysis of stress/strain effects of repository's disposal tunnels excavation, certain the starting parameters had to be set:
1. KBS-3V disposal concept was selected as the most probable variant of repository design, considering that it will be the first concept applied for the disposal of SNF in Finland.

2. Sodium bentonite was selected as a buffer material, since it is probably the most considered and researched buffer material, whether the disposal is to be in crystalline or argillaceous host rock.
3. Disposal cannister is selected according to Croatian/Slovenian generic model – copper lined cannister containing 4 SNF assemblies.
4. As the most probable host rock granodiorite was selected.
5. The numerical model is to be a 2d model of cross section trough the disposal tunnel and the disposal borehole.
6. Support systems will not be necessary since the disposal is planned to be done at the depth of 500 m in monolithic solid rock with a minimum number of fissures.

2. Numerical model of DGR concept in Geostudio

Material parameters chosen for the model design are given in **Table 1** and were selected according to the literature related to the selected concept and the proposed generic location (**ARAO & Fond NEK, 2019; Korkiala-Tanttu, 2009; Keto et al., 2012; Juvankoski, 2010**). Same parameters were used for earlier research (**Veinović et al., 2020**).

Table 1: Parameters selected for numerical analysis in GeoStudio (from: **Veinović et al., 2020**, acc. to: **ARAO & Fond NEK, 2019; Korkiala-Tanttu, 2009; Keto et al., 2012; Juvankoski, 2010; Nguyen et al., 2017; Jacinto and Ledesma, 2016**)

Material	Model used	Young's elasticity modulus [kPa]	Cohesion [kPa]	Weight density [kN/m³]	Poisson's coefficient
Granodiorite in situ	Elasto-plastic	40 000 000	10 000	27.00	0.23
Granodiorite disturbed		2 000 000	6 000	26.00	0.28
Bentonite	Linear elastic	10 000 000	20	20.59	0.30
Copper		1.17×10^8	-	87.57	0.36

In order to better explain the selection of granodiorite as host rock, it is necessary to clarify part of the geology of Croatia. The Creating of the the Croatian part of the Pannonian Basin System (CPPBS) space (e.g. **Malvić´, 1998, 2003, 2004, 2012**) began at the edge of the Pannonian Basin system (e.g., **Royden, 1988; Rögl, 1996, 1998; Steininger et al., 1978**) resulting in certain sedimentary and tectonic specificities. The entire CPPBS area opened up and formed along a series of transcurrent fault systems, and the first lake environments were created in the Lower Miocene. In the Lower Baden (16.4-15.0 m.g.), the first marine transgression covered Northern Croatia with the environments of Central Paratethys with the dominance of alluvial environments and the amount of descent greater than deposition. This marked the beginning of the first tension phase. Sources of material were Siliciclasts of the Paleozoic and Mesozoic subsoil as well as numerous coralinacea reefs. In the middle and upper Baden (15.0-13.0 m.g.) there is a calming of tectonics and the dominance of the deposition of fine-grained and carbonate detritus, and another flooding of the Central Paratethys at the end of the upper Baden. After that, the first transpression phase begins, which lasted from the Sarmatians to the end of the Lower Pannonian (13.0-9.3 m.g.) when the marine environment gradually disappears, creating a large, closed Pannonian Lake, initially brackish and later freshwater. The second transtension phase followed, which lasted during the upper Pannonian (9.3-7.1 m.g.) and the lower pontoon (7.1-6.3 m.g.). This is precisely the time of deposition of thick, monotonous sequences of sandstone and marl in the lake environment of Lake Pannonia, and at the end of local lakes such as the Sava and Drava lakes. The sandstones were transported by turbidite currents from their origin in the Eastern Alps and were deposited several times on tectonic ramps. In contrast, marls are lake, pelitic sediments. Finally, the shaping of the CPPBS area ends with the second transpression phase, which began in the Upper Pontus (6.3-5.6 m.g.), completed the process of lake reduction by creating and then degrading Slavonian Lake, and the Pliocene terrestrial environments (5.6 -2.6 m.g.) and especially the Quaternary (2.6-0.0 m.g.). During all this time, especially during the transpression periods, older mountains such as Medvednica, Papuk and Psunj rose, and during the last 2.5 m.g. and Bilogora (**Prelogović, 1975**). The result of all these events is a significant thickness of Neogene-Quaternary sediments in all our depressions and subdepressions, with more than 7000 m in the deepest part of the Drava Depression, and 3000+ m in the deepest parts of the Bjelovar subdepression. Sediment development and lithological units in CPPBS are best seen on regional lithostratigraphic columns. The one for the Drava Depression is shown in **Figure 3**.

It has to be noted that the regional lithostratigraphic column shown in **Figure 3** does not present potential disposal site! It was only taken as a typical example.
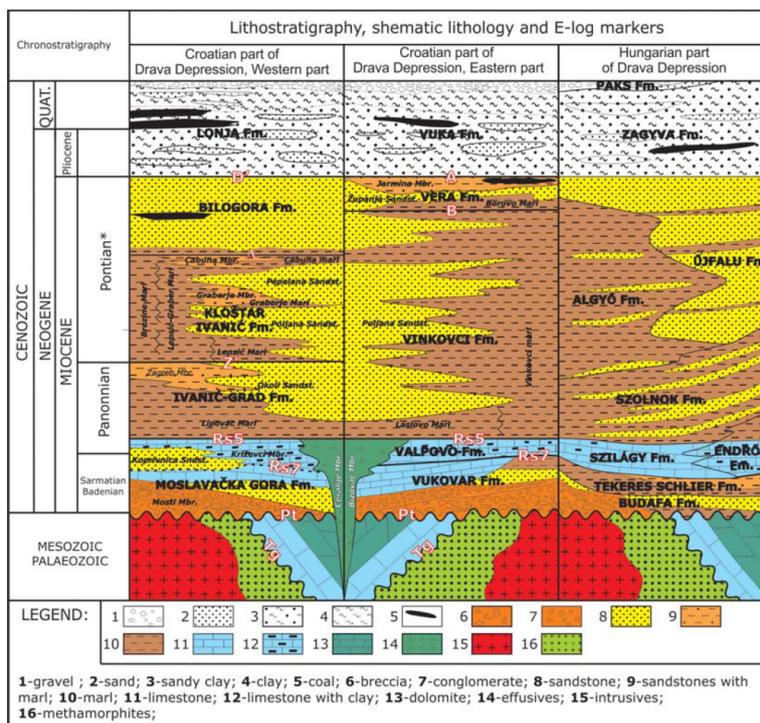
Figure 3: Schematic representation of the lithological composition and correlation of the units of the Croatian and Hungarian parts of the Drava Depression - thicknesses are not in scale (**Malvić & Cvetković, 2013**)

The basic model with finite element mesh was defined by stages:

1. Excavation
2. Cannister emplacement
3. Filling/closing the disposal tunnel with bentonite.

The regions of material in model were defined as:

- Intact host rock
- Excavation damaged/disturbed zone
- Copper cannister
- Bentonite buffer / filling material.

Starting model according to stages is shown at **Figure 4**.
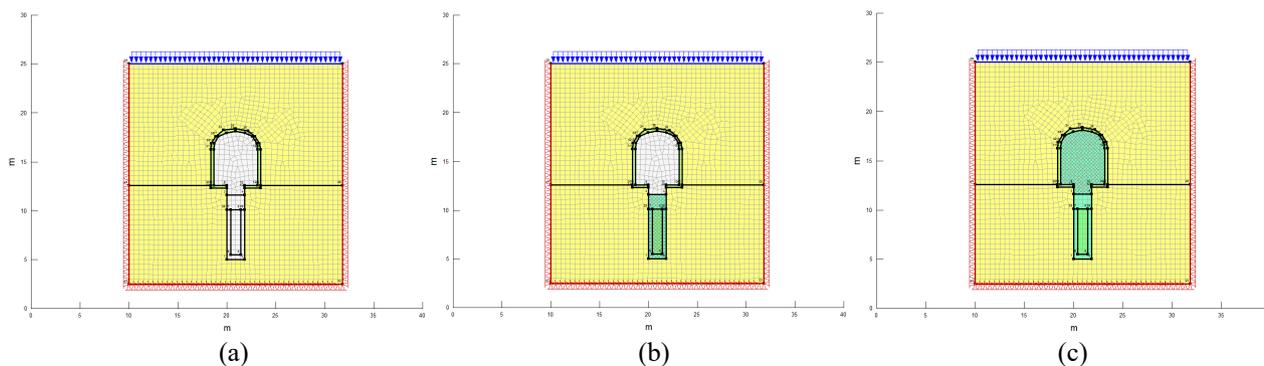
Figure 4: Stages of the basic model: (a) after the excavation, (b) after installation of disposal canister and buffer material; (c) after closing the disposal tunnel (**Veinović et al. 2020**)

The analysis performed in GeoStudio show that the critical stress areas are appearing at the calotte – top (ceiling) of the disposal tunnel and at the edges at the bottom of the disposal tunnel. Critical stresses also appear at the bottom of the disposal borehole. **Figure 5** shows resulting stresses by phases. In order to show total stresses at the critical points, software allows "click and show" mode with the corresponding Mohr's circles (**Figure 6**).

Figure 5: Mode [...] nstallation of disposal canister a [...] l version of the
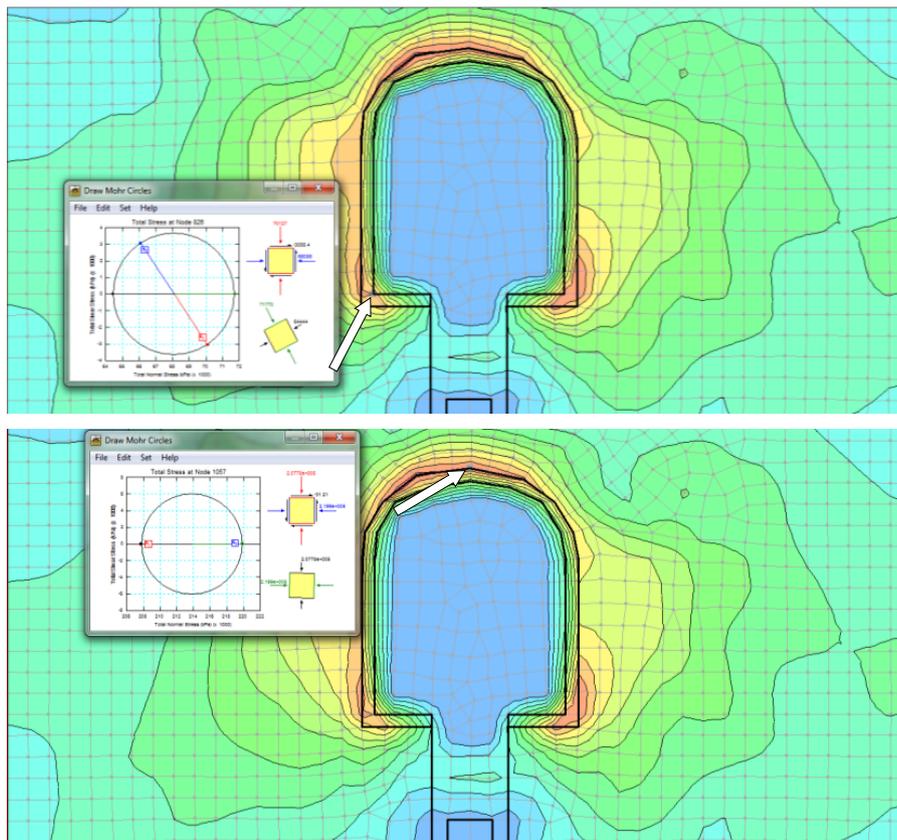
Figure 6: Mohr's circles of total stress at critical points of the model

Stresses in the presented numerical model did not exceed shear or normal strength of the host rock, and there were no signs of failure of rock mass during the analysis.

Analysis of the strain/displacement of the host rock has shown that the maximal displacement can be found during the phase of filling of the disposal tunnel (latest phase in the model) and is shown at **Figure 7**.
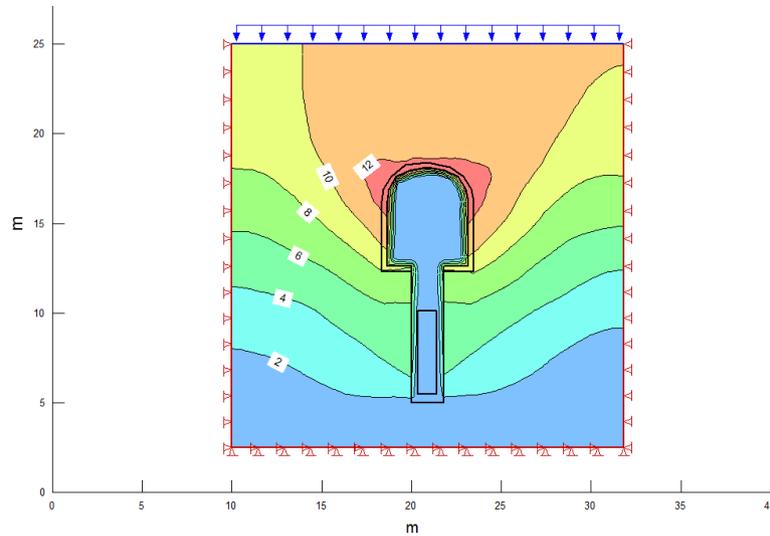
Figure 7: Host rock strain/displacement for the last phase (filling the disposal tunnel). Displacement is shown in [mm] (**Veinović et al., 2020**)

3. Numerical model of DGR concept in Plaxis

Plaxis is a software package in which numerical models simulate soil/rock behavior. It evolved from a program aimed at analyzing embankments on soft soil in the Netherlands. The software is based on the finite element method and is intended for 2D and 3D geotechnical analysis of soil deformation and stability, groundwater flow and heat. Plaxis contains a wide range of models to describe soil/rock behavior. The basic models are in fact mathematical equations that describe the relationships between stresses and strains for a particular material, taking into account the properties that are expressed as scalar parameters. In geotechnical engineering, Plaxis is most commonly used for modelling excavations, foundations, embankments and tunnels. Numerical methods often used to predict soil and rock behavior, are also used to predict the interaction between tunnels and soil and rock structures (**Fasihnikoutalab et al., 2012**)

The basic model is defined as a plane model (plane strain) 120 m long and 120 m high. The generated network of elements is medium density. Since the tunnel is to be excavated at a depth of 500 m, the total vertical stress above the tunnel was simulated by a continuous surface load of 11 880 kN/m², and the Morh-Coulomb model of soil/rock was used. Copper cannister was defined by the Linear elastic model. The calculation with the initial phase contains three phases, initial conditions, excavation and filling of the tunnel (**Figure 8**).

(a)   (b)   (c)
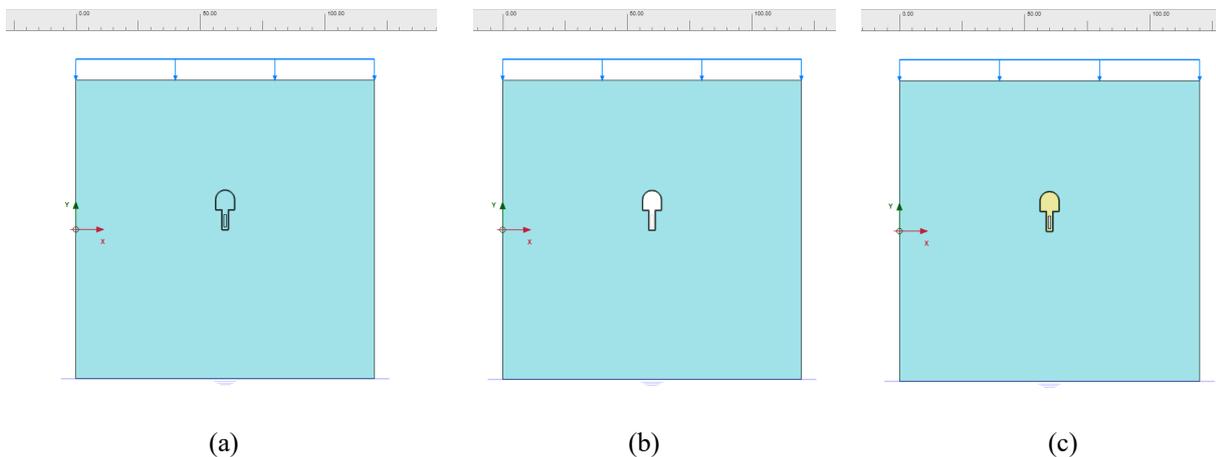
Figure 8: Calculation stages of the basic model: (a) after the excavation, (b) after installation of disposal canister and buffer material; (c) after closing the disposal tunnel

The results of the numerical analysis conducted in the Plaxis program show the displacements and the state of stress through the phases of excavation and filling of boreholes and tunnels. The stresses change significantly after excavation and the maximum stresses in the last phase of the calculation are 68 030 kN/m² at the calotte of the tunnel and below the borehole (**Figure 9**) marked red. The largest total displacements (**Figure 10**) are 0.0039 m in the excavation phase.
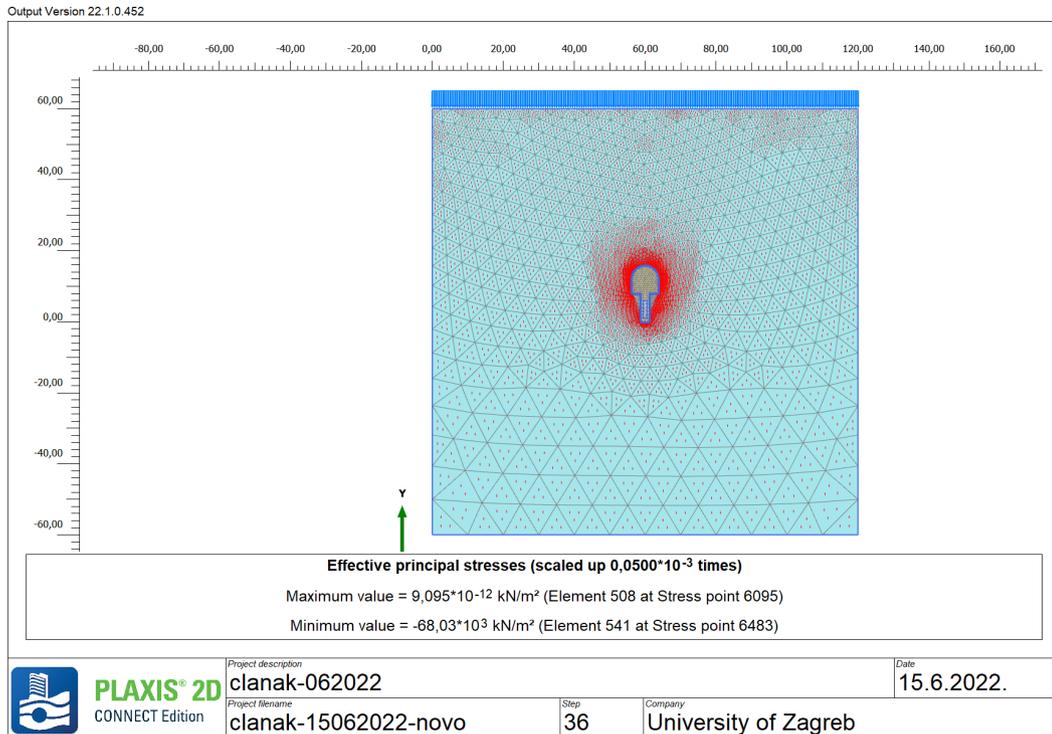
Figure 9: Effective stress after closing the disposal tunnel
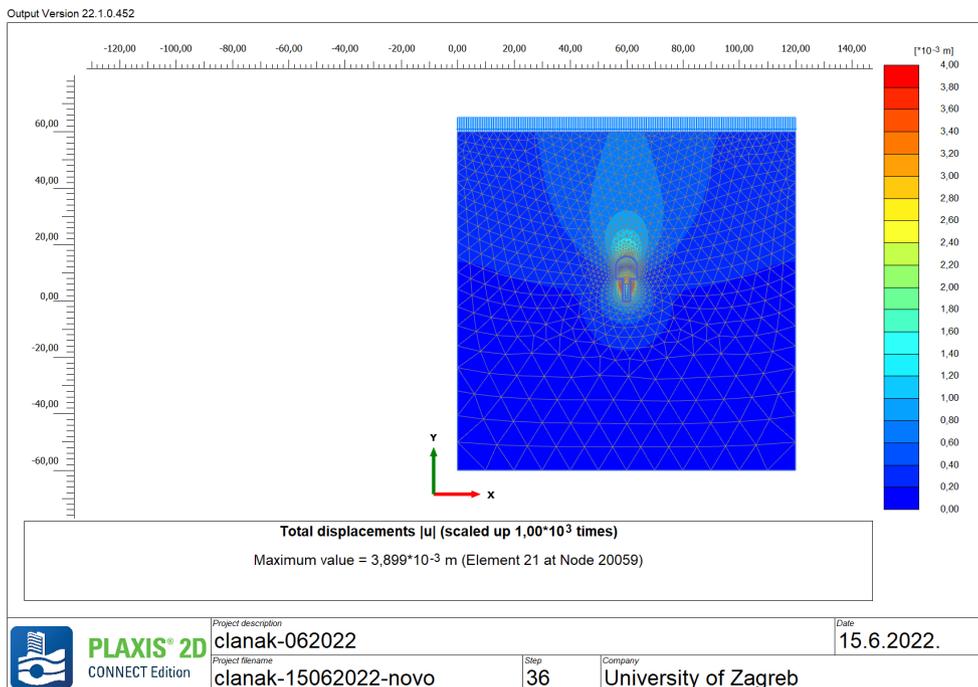
Figure 10: Total displacement after closing the disposal tunnel

4. Discussion

The research of the disposal of SNF and/or HLW in Croatia is at its starting phase. So far, the initial research is based upon the KBS-3V disposal model as it was suggested by ARAO & Fond NEK (**2019**) in a generic project of the SNF repository. Development of the numerical model was not the part of the generic project and was developed as the research project of the Faculty of Mining, Geology and Petroleum engineering. Initially the GeoStudio software was applied for the numerical analysis, and this paper presents the continued research using Plaxis software to compare results with the previous research.

Both software packages, GeoStudio and Plaxis, have some advantages and disadvantages, and it is planned to acquire newer versions of software to continue research. One of the ideas of continuation of the research is to acquire the CodeBright program, which is used in similar analysis around the world. This would provide comparable results and facilitate modelling.

The reasons for the differences in the results of numerical modelling of SNF repository in GeoStudio and Plaxis are mainly related to different approaches and utilization of the finite elements method. The difference in maximal displacement, although in millimetres, is still significant being four times larger for the model designed in GeoStudio. More detailed model will certainly be more accurate, and it would be a greater match between the results obtained by the two software.

The comparison of stresses in both models are shown at **Figure 11**.

(a)   (b)
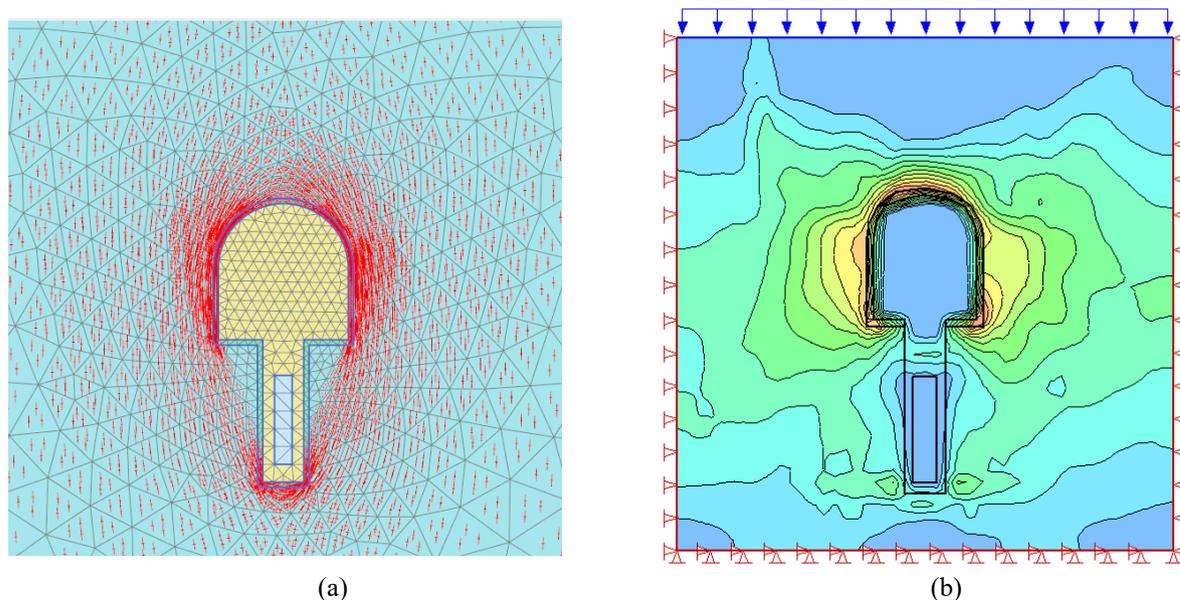
Figure 11: Details of the stress distribution at the disposal tunnel during the last phase – installation of bufferand closing the disposal tunnel in Plaxis (a) and GeoStudio (b).

The stresses distribution shown at **Figure 11** do correspond to one another, however, more detailed results would be needed for the in the case of specific research for a future repository. In that case, the more specific parameters of the host rock would be included, as well as the more detailed model. Also, the future research will include software developed and adapted to repository modelling, CodeBright.

There are many issues concerning presented research, mainly considering using the generic model of the repository and assumption that the granodiorite would be the probable host rock for the repository. Without proper research during the site selection, it is not possible to acquire more detailed and accurate host rock parameters. However, this research is necessary in order to acquire the necessary experience and routine in research of this kind and educate workforce who will one day engage in site specific research.

There are several issues that should be addressed in the future:
1. Specific software which is readily used in the running disposal programs in other countries should be used.
2. The disposal concept, since it is not yet defined which concept will be applied, should be selected in a manner to suite the site and its geological properties.

3. After the preliminary site selection properties of the potential host rocks from preferred sites should be known and used for the numerical analysis.
4. Although it is probable that sodium bentonite is to be used as a buffer and filling material, detailed data on properties of the bentonite cay as well as the manner of bentonite emplacement is needed for the proper numerical model.
5. Apart from the stress/strain numerical analysis it is necessary to model groundwater flow, thermal effects on host rock and buffer material and a radionuclide spread.
6. In stead of 2D model it would be advisable to create 3D model of the repository.

5. Conclusions

This paper presents initial research of the stress/strain model of the generic repository for the spent nuclear fuel designed in GeoStudio and Plaxis software. The model presented in the paper is developed for the KBS-3V concept of the deep geological disposal facility with granodiorite as the generic host rock and sodium bentonite as the buffer and filling material.

Results of the numerical analysis show that KBS-3V concept of the deep geological repository developed in granodiorite as the host rock, at the depth of 500 m and with the sodium bentonite as the buffer material, is potentially stable construction with acceptable values of stress and displacement. Both software – GeoStudio and Plaxis, give analogous results. The stresses change significantly after excavation and the maximum stresses, according to Plaxis, in the last phase of the calculation are 68 030 kN/m^2 at the calotte of the tunnel and below the borehole, the largest total displacements are 0,0039 m in the excavation phase. GeoStudio analysis resulted in maximum stresses of 70 127 kN/m^2 at the same places of the crossection (the calotte of the tunnel and below the borehole) and the maximal displacement of 0,012 m in the excavation phase.

The results of the analysis made with the assumed values for this generic case show that the construction of a deep geological repository in the given geological conditions would be feasible. As a continuation of the research, it is proposed to include the impact of groundwater as well as the thermal impact of spent fuel cannisters. It is also planned to create a model in the CodeBright software, which would provide data comparable to the research of other programs for the spent fuel disposal.

The development of the model presented in the article is important for the education of new workforce and gaining experience in numerical analysis of this problem. In this manner needed knowledge is acquired and transferred, which will help education of the workforce that will participate in the development of Croatian-Slovenian program when it starts.

6. References

6.1. Published works

1) Blanco-Martin, L., Rutqvist, J. Birkholzer, J.T. (2017): Extension of TOUGH-FLAC to the finite strain framework. Computers & Geosciences. Elsevier, UK, 64-71, 108 p. doi:10.1016/j.cageo.2016.10.015.

2) Chen, L., Wang, J., Liu, Y., Collin, F., Xie1, J. (2012): Numerical thermo-hydro-mechanical modeling of compacted bentonite in China-mock-up test for deep geological disposal. Journal of Rock Mechanics and Geotechnical Engineering, 4, 2, 183–192.

3) Domitrović, D., Vučenović, H., Kovačević Zelić, B. (2012): Ispitivanje svojstava bentonita kao inženjerske barijere u odlagalištima radioaktivnog otpada (*Characterization of bentonite for engineered barrier systems in radioactive waste disposal sites*). Rudarsko-geološko-naftni zbornik, 24, 19-27. (*in Croatian*)

4) Fasihnikoutalab, M., Bujang, H., Afshin, A., Saman, D. (2012): Numerical stability analysis of tunnel by PLAXIS. EJGE. Vol. 17, Bund. D, PP 451-461.

5) Jacinto, A.C., Ledesma, A. (2016): Thermo-hydro-mechanical analysis of a full-scale heating test. Environmental Geotechnics, 4, 2, 123-134.

6) Kwon, S., Cho, W.J., Lee, J.O. (2013): An analysis of the thermal and mechanical behavior of engineered barriers in a high-level radioactive waste repository. Nuclear engineering and technology, 45, 1, 41-52.

7) Keto, P., Karttunen, P., Kumpulainen, S., Kiviranta, L., Korkiala-Tanttu, L., Koskinen, V. & Koho, P. (2012): Design, production and initial state of the deposition tunnel backfill. Clays in natural and engineered barriers for radioactive waste confinement - 5 International meeting Book of abstracts, p. 923. France.

8) Malvić, T. (1998): Structural and tectonic relations and characteristics of hydrocarbons in the wider area of the Galovac-Pavljani oil field. MSc. thesis, University of Zagreb, Faculty of Mining, Geology and Petroleum Engineering, p. 112, Zagreb. (*in Croatian*)

9) Malvić, T. (2003): Oil-Geological Relations and Probability of Discovering New Hydrocarbon Reserves in the Bjelovar Sag, PhD Thesis, University of Zagreb, Faculty of Mining, Geology and Petroleum Engineering.

10) Malvić, T. (2004): Regional geological settings and hydrocarbon potential of Bjelovar sag (subdepression), R. Croatia, Nafta, 55, 273–288. (*in Croatian*)

11) Malvić, T. (2012): Review of Miocene shallow marine and lacustrine depositional environments in Northern Croatia. Geological quarterly, 56, 493-504.

12) Malvić, T., Cvetković, M. (2013): Korelacija litostratigrafskih jedinica u Dravskoj depresiji (hrvatski i mađarski dio (*Lithostratigraphic units in the Drava Depression (Croatian and Hungarian parts) – a correlation*). Nafta: exploration, production, processing, petrochemistry, 64, 1, 27-33. (*in Croatian*)

13) Nguyen, T.S., Li, Z., Garitte, B., Barnichon, J.D. (2017): Modelling a heater experiment for radioactive waste disposal. Environmental Geotechnics, 6, 2, 87–100.

14) Prelogovic, E. (1975): Neotektonska karta SR Hrvatske (*Neotectonic map of SR Croatia*), Geološki vjesnik, 28, 97–108 (*in Croatian*)

15) Royden, L. (1988): Late Cenozoic Tectonics of the Pannonian Basin System, In ROY- DEN, L. H. and HORVÁTH, F., (eds.) The Pannonian Basin (Memoir 45), American Association of Petroleum Geologists, pp. 27–48.

16) Rögl, F. (1996): Stratigraphic Correlation of the Paratethys Oligocene and Miocene, Mitteilungen Ges. Geol. Bergbaustudenten Österreich, 41, 65–73.

17) Rögl, F. (1998): Palaeographic Consideration for Mediterranean and Paratethys Sea- ways (Oligocene to Miocene), Ann. Naturhist. Mus. Wien, 99A, 279–310.

18) Rutqvist, J. (2011): Status of the TOUGH-FLAC simulator and recent applications related to coupled fluid flow and crustal deformations. Computers & Geosciences, 37, 6, 739-750.

19) Rutqvist, J., Chijimatsu, M., Jing, L., Millard, A., Nguyen, T.S., Rejeb, A., Sugita, Y., Tsang, C.F. (2005): A numerical study of THM effects on the near-field safety of a hypothetical nuclear waste repository-BMT1 of the DECOVALEX III project. Part 3: Effects of THM coupling in sparsely fractured rocks. International Journal of Rock Mechanics & Mining Sciences, 42, 745–755.

20) Schäfers, A., Gens, A., Rodriguez-Dono, A., Baxter, S., Tsitsopoulos, V., Holton, D., Malmberg, D., Sawada, M., Yafei, Q., Ferrari, A., Laloui, L., Sjöland, A. 2019. Increasing understanding and confidence in THM simulations of Engineered Barrier Systems. Environmental Geotechnics, 172. 2, 155–173.

21) Sinnathamby, G., Korkiala-Tanttu, L., Forés, J.G. (2014): Interface shear behaviour of tunnel backfill materials in a deep-rock nuclear waste repository in Finland, Soils and Foundations, Volume 54, Issue 4, p. 777-788, ISSN 0038-0806.

22) Steininger, F., Rögl, F. and Müller, C. (1978) Chronostratigraphie und Neo- stratotypen Miozän der Zentralen Paratethy, chap. Geodynamik und paläogeograph- ische Entwicklung des Badenien, Verlag der Slowak. Akad. der Wissenschaften, p. 110-127.

23) Toprak, E., Olivella, S., Mokni, N., Pintado, X. 2012. Modelling of the THM-evolution of Olkiluoto nuclear waste repository. 5. international meeting on clays in natural and engineered barriers for radioactive waste confinement; Montpellier. p. 923. France.

24) Umeki, H. (2007): Repository design. Ch 5 in W.R.Alexander and L.E.McKinley (eds): Deep geological disposal of radioactive wastes – Elsevier Publ. Co., 112-143, 273 p.

25) Uroić, G., Veinović, Ž. & Alexander, W. (2022): KBS-3V And Axial Canister Emplacement Of SNF - Comparison Of Disposal Concepts. In: Proceedings of 13th International Conference of the Croatian Nuclear Society. Zadar, Croatia. 115-1-115-16.

26) Veinović, Ž., Kovačević Zelić, B., Domitrović, D. (2015): Deep geological disposal of spent nuclear fuel and high-level waste: current state and future challenges. Handbook of research on advancements in environmental engineering. Gaurina-Međimurec, N. (ed.). Hershey: IGI Global, 367-399, 660 p.

27) Veinović, Ž., Kovačević Zelić, B., Gradiški, K. (2012a): Potreba za osnivanjem podzemnog istraživačkog laboratorija u Hrvatskoj (*Necessity for underground research laboratory in Croatia*). Rudarsko-geološko-naftni zbornik, 19, 99-110. (*in Croatian*)

28) Veinović, Ž., Kovačević Zelić, B. & Končić, A. (2012b): The Role of Underground Research Laboratories within National Repository Development Programmes. U: Kolić, D. (ur.). Proceedings of UNDER CITY Colloquium on Using Underground Space in Urban Areas in South-East Europe.

29) Veinović, Ž., Uroić, G., Domitrović, D. & Kegel, L. (2020): Thermo-Hydro-Mechanical Effects on Host Rock for a Generic Spent Nuclear Fuel Repository. *Rudarsko-geološko-naftni zbornik*, 35, 1, 65-80 doi:10.17794/rgn.2020.1.6.

30) Zhao, H.G., Shao, H., Kunz, H., Wang, J., Su, R., Liu, Y.M. (2014): Numerical analysis of thermal process in the near field around vertical disposal of high-level radioactive waste. Journal of Rock Mechanics and Geotechnical Engineering, 6, 55–60.

6.3. Sources from professional archives

1) Åkesson, A., Kristensson, O. Börgesson, L., Dueck, A. (2010): THM modelling of buffer, backfill and other system components. Critical processes and scenarios. (SKB-TR--10-11) Stockholm, 368 p.

2) ARAO & Fond NEK (2019): Revised referenced scenario for geological disposal facility in hard rock with cost estimation for its implemetation - Spent nuclear fuel and high-level waste disposal in Slovenia or Croatia. IBE Consulting Engineers. Ljubljana, 172 p.

3) Baldwin, T., Chapman, N., Neall, F. (2008): Geological disposal options for high-level waste and spent fuel. Report for the UK Nuclear Decommissioning Authority, 117 p.

4) DOE (1984): Sitting guidelines. Department of Energy, USA.

5) GD (736/2008): Government Decree on the safety of disposal of nuclear waste. Issued in Helsinki 27 November 2008.

6) IAEA (1994): Siting of Geological Disposal Facilities. A Safety Guide, A PUBLICATION WITHIN THE RADWASS PROGRAMME. SAFETY SERIES No 111-G-4 1, Vienna.

7) IAEA (2011): Geological disposal facilities for radioactive waste. SPECIFIC SAFETY GUIDE, IAEA SAFETY STANDARDS SERIES No. SSG-14, Vienna.

8) Ikonen, K. (2003): Thermal Analyses of Spent Nuclear Fuel Repository. POSIVA 2003-04. Olkiluoto. 61 p.

9) Juvankoski, M. (2010): Description of Basic Design for Buffer. Posiva. Working Report 2009-131. Eurajoki, 58 p.

10) JPN (2000): Designated Radioactive Waste Final Disposal Act. (In Japanese).

11) Korkiala-Tanttu. L., (2009): Finite Element Modelling of Deformation of Unsaturated Backfill Due to Swelling of the Buffer. Posiva. Working Report 2009-88, Helsinki, 35 p.

12) Saanio, T., Ikonen, A., Keto, P., Kirkkomäki, T., Kukkola, T., Nieminen, J., Raiko, H. (2013): Design of the Disposal Facility 2012. Posiva Working Report 2013-17. Finland, 196 p.

13) STUK (2015): STUK's review on the construction license stage post closure safety case of the spent nuclear fuel disposal in Olkiluoto. Säteilyturvakeskus Strålsäkerhetscentralen, Radiation and Nuclear Safety Authority, STUK-B 197 / NOVEMBER 2015.

14) Toprak, E., Mokni, N., Ollvella, S. (2013): Thermo-Hydro-Mechanical Modelling of Buffer. Synthesis Report. Posiva 2012-47, 120 p.

SAŽETAK

Numerički modeli dubokog geološkog odlagališta za iskorišteno nuklearno gorivo

Numerička analiza dubokog geološkog odlagališta (DGO) za istrošeno nuklearno gorivo (ING) i/ili visokoradioaktivni otpad (VRAO) ključni je dio studije sigurnosti za svaki program zbrinjavanja ING/VRAO. Prije početka bilo kakve aktivnosti u vezi odlaganja potrebno je dokazati funkcionalnost budućeg koncepta zbrinjavanja primijenjenog na određenu stijenu. Osim laboratorijskih istraživanja, uključujući podzemne istraživačke laboratorije (PIL), koji bi također trebali dokazati primjenjivost koncepta odlaganja te prikladnost stijene i materijala za popunjavanje, potrebno je osmisliti i testirati numerički model budućeg DGO-a kako bi se provjerila adekvatnost rješenje, identificirati moguće pogreške i probleme, te prilagoditi buduće radove, dimenzije pojedinih elemenata odlagališta i izbor materijala. Numerički modeli prikazani u ovom radu razvijeni su za koncept KBS-3V za zbrinjavanje ING-a i/ili VRAO-a, u softveru Plaxis i GeoStudio. Granodiorit je odabran kao matična stijena, a natrijev bentonit kao materijal ispune. Usporedba pojedinih modela izrađenih u ovim dvama softverskim paketima, kao i njihova verifikacija prema potrebnim sigurnosnim parametrima za spremište, raspravlja se i uspoređuje s najsuvremenijim istraživanjem pokrenutih programa (tj. finski i švedski program zbrinjavanja SNF). Evidentno je da prikazani numerički modeli odgovaraju rezultatima drugih sličnih istraživanja i da bi se eventualno mogli koristiti za razvoj studije sigurnosti i testiranje dizajna budućeg odlagališta ING-a ili VRAO-a.

Ključne riječi: numerički model; duboko geološko odlagalište; istrošeno nuklearno gorivo; bentonit; granodiorit.

Acknowledgment

Author's contribution

Želimir Veinović (Associated Professor, radioactive waste management, spent nuclear fuel disposal, waste management, soil mechanics, geotechnics, earthquake engineering, ionizing radiation protection, numerical analysis) provided the data on the disposal concept, spent fuel management, host rock and engineering barriers and developed numerical models of the deep geological repository. **Helena Vučenović** (Assistant Professor, radioactive waste management, spent nuclear fuel disposal, soil mechanics, soil dynamics, numerical analysis) developed numerical models of the deep geological repository in Plaxis and carried out numerical analysis of the deep geological repository. **Galla Uroić** (mag.ing.min., Senior Associate - Department for preparation of the Program for Decommissioning and Disposal of Radioactive Waste and Spent Nuclear Fuel from the Krško Nuclear Power Plant; geotechnics, radioactive waste management, spent nuclear fuel disposal, NORM and residues management, ionizing radiation protection, numerical analysis) developed numerical models in GeoStudio and carried out numerical analysis of the deep geological repository. **Andrea Rapić** (B.Sc. Biology, Head of the Department for preparation of the Program for Decommissioning and Disposal of Radioactive Waste and Spent Nuclear Fuel from the Krško Nuclear Power Plant, Fund for financing the decommissioning of the Krško Nuclear Power Plant and the disposal of Krško NPP radioactive waste and spent nuclear fuel) safety case, spent nuclear fuel management and disposal, radioactive waste disposal), provided data for generic project of the deep geological disposal facility concerning disposal concept and host rock parameters.

Possibilities of energy storage in geological structures in Poland

**Marek L. Solecki[1]; Paweł Wojnarowski[1]; Gordon Wasilewski[2];
Grzegorz Machowski[3], Jerzy M. Stopa[1]**

[1]AGH University of Science and Technology, Faculty of Drilling, Oil & Gas,
Mickiewicza 30, 30-059 Kraków, Poland

[2]Astronika, Bartycka 18/33, 00-716 Warszawa, Poland

[3]AGH University of Science and Technology, Faculty of Geology, Geophysics &
Environmental Protection, Mickiewicza 30, 30-059 Kraków, Poland

Abstract

The paper describes the possibilities of energy storage in geological structures in Poland. Three types of subsurface storages are considered: salt caverns, exploited gas reservoirs and aquifers. Salt caverns in Poland are already fully operational methane and oil storages. Hydrocarbon reservoirs are found in southern Poland (Carpathians and the Carpathian Foredeep) in the Devonian, Mesozoic, and Cenozoic strata, in north-western Poland in the Zechstein Basin and in the Rotliegendes (Polish Lowlands), and in eastern Poland in the Lublin Basin (Devonian) and in the Baltic Sea (Cambrian strata). Some of the depleted reservoirs are also used as methane storages. Aquifers exist in the Mid-Polish Mesozoic Basin (Polish Lowlands) in the Lower Triassic, Lower Jurassic, and Lower Cretaceous strata. All these structures, after a detailed selection and meeting the appropriate criteria, are perspective to store the energy, e.g., hydrogen, which can be used as a fuel of the future.

Keywords: energy storage, hydrogen, salt caverns, depleted reservoirs, aquifers, Poland

1. Introduction

Hydrogen as an ecological source of energy begins to be recognized as one of the main elements of the decarbonisation of European economies. It can be mixed with natural gas, or can be burned as a pure hydrogen (used for emission-free car propulsion). Poland is one of the largest producers of hydrogen in Europe. It is mainly produced by the nitrogen industry as well as by coking plants. An alternative is to use renewable energy to produce energy, and then production of hydrogen by electrolysis. Renewable energy sources can be installed, for example, right next to the underground storages, which eliminates the problem of hydrogen transport. Hydrogen from nitrogen plants or coking plants should be sent via hydrogen pipelines.

In March 2022, Astronika and the AGH University of Science and Technology in Krakow (Department of Petroleum Engineering, Faculty of Drilling, Oil and Gas) started a project called GeoStorage, which analyses the feasibility of the use of geological formation for energy storage in terrestrial and planetary conditions. The European Space Agency (ESA) selected GeoStorage in an open tender focused on the use of space resources. The project is developed by a consortium led by Astronika in cooperation with the AGH. The project analyses the technical and economic feasibility of utilization of formations such as salt caverns, and depleted hydrocarbon reservoirs as energy storage facilities – a key element of the Polish energy transition. The main objective of this project is to calculate the potential of geologic energy storage in the context of broader utilization of renewable energy in the national energy system for its increased resilience and adaptability.

2. Geological setting of analyzed formations

2.1. Salt domes

Salt-bearing formations occur in Poland in the Upper Permian (Zechstein) and in the Neogene strata. Due to their geological properties, only Zechstein salts are considered as potential reserves in Poland. They occur as salt beds or structures (pillows, walls, domes, crests) and occupy about 65% of the territory of Poland (see **Figure 1**) (**Czapowski et**

Corresponding author: Marek L. Solecki
marek.solecki@agh.edu.pl

al., 2017; Tarkowski and Czapowski, 2018). Salt domes have great thickness of rock salt body (about several kilometers high), with small surface area of horizontal cross-section. These properties, along with the existence of leaching caverns, make salt domes the best choice for storage of hydrogen, methane and other gases, or petroleum and fuels (in Poland exists one underground storage of liquid petroleum fuels).

The Zechstein salts in Poland are situated in the eastern part of the large Permian salt basin of central Europe (extending from England, through Germany and Denmark to Poland). Salts were deposited in this basin because of evaporation of a marine basin **(Wagner, 1994; Wagner and Peryt, 1997)**. Zechstein strata are a part of Zechstein-Mesozoic structural stage which forms a large complex (up to 6 km thick) in Polish Lowlands (see **Figure 2**). Within the Zechstein succession, four cyclothemes were distinguished, comprising salts as one of the main components **(Wagner, 1994; Wagner and Peryt, 1997; Czapowski and Bukowski, 2015)**.
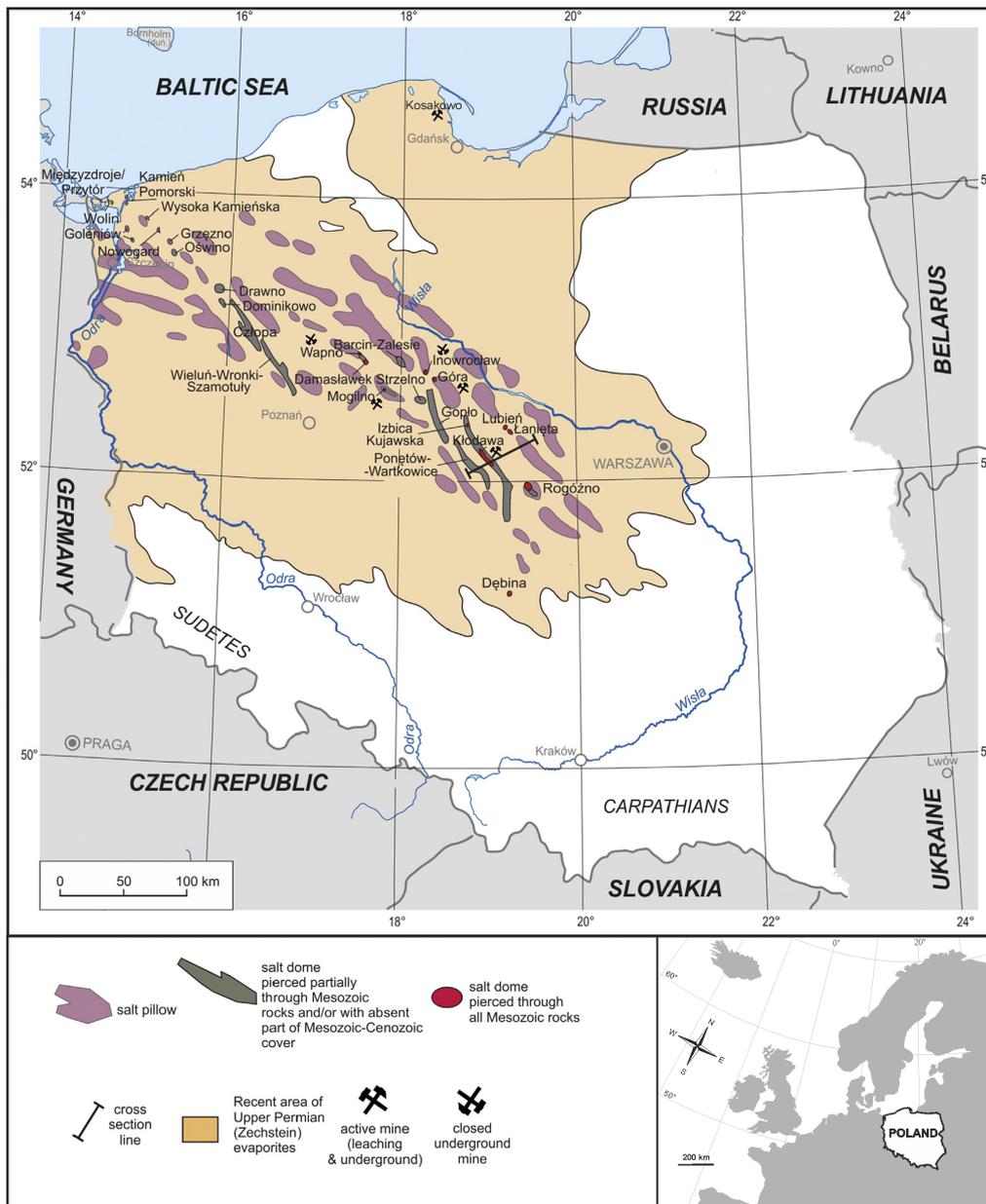
Figure 1: Salt structures in the Upper Permian (Zechstein) deposits in Poland
(after **Czapowski et al., 2017; Tarkowski and Czapowski, 2018**, modified)
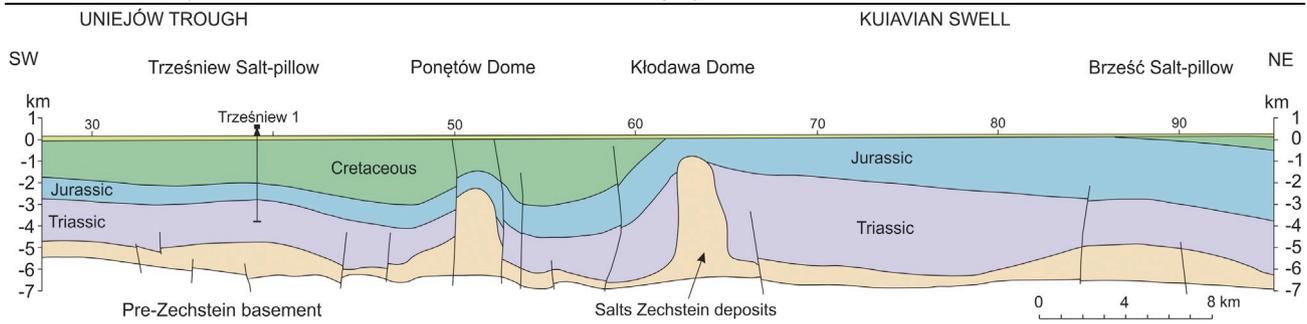
Figure 2: Simplified geological cross-section (SW-NE) of the Polish Lowlands presenting salt structures
(after **Dadlez, 2001; Tarkowski and Czapowski, 2018**)

2.2. Hydrocarbon reservoirs

According to **Czapigo-Czapla and Brzeziński (2021a)**, in Poland there are 87 oil fields: 29 in the Carpathians, 12 in Carpathian Foredeep, 44 in the Polish Lowlands, and 2 in the Polish Exclusive Economic Zone of the Baltic Sea. The Carpathian oil reservoirs occur in the region of the world's oldest oil mining (middle of the 19th century), but their resources are small and mostly depleted. Oil fields discovered in the Polish Lowlands are of the greatest economic importance.

Based on **Czapigo-Czapla and Brzeziński (2021b)**, Poland has 306 natural gas reservoirs including 200 developed: 26 in the Carpathians, 83 in the Carpathian Foredeep, 89 in the Polish Lowlands, and 2 in the Polish Exclusive Economic Zone of the Baltic Sea. About 75% of the gas resources have been discovered in the Neogene (Miocene) and Permian (Rotliegendes) formations, and the rest in the Cambrian, Devonian, Carboniferous, Permian (Zechstein), Jurassic and Cretaceous. Location of oil and gas fields together with underground gas storages in Poland is presented in **Figure 3**. The exploration of oil and gas in Poland began in the 19th century, only in the Outer Carpathian flysch belt in southern Poland. Since that time, many oil and gas reservoirs have been discovered in the Carpathian Foredeep and Polish Lowland (**Karnkowski, 1999; Wójcik et al., 2022**). Four petroleum provinces have been described by **Wójcik et al. (2022)** - Northern and Eastern Petroleum Provinces for the East European Platform areas, Western Petroleum Province for the West European (Variscan) Platform, and Southern Petroleum Province for the Carpathian units and its basement (see **Table 1**).

Table 1: Principal geological horizons and units of crude oil and natural gas occurrences in Poland with several fields and documented resources (based on **Wójcik et al. 2022**, modified)

Petroleum Province	Geological Horizon/Unit	Number of Documented Gas Fields	Documented Resources of Gas [MCM]	Number of Documented Oil Fields	Documented Resources of Oil [kTOE]
Northern and Eastern	Carboniferous	2	50.08	1	29.62
	Devonian	3	1154.99	1	6.36
	Middle Cambrian	9	5189.44	6	6215.27
Western	Zechstein – Main Dolomite	59	52,559.32	38	14,381.59
	Zechstein Limestone	21	22,365.79	-	-
	Permian Rotliegendes	61	26,763.87	-	-
	Carboniferous	7	2762.01	-	-
Southern	Outer Carpathians	34	1320.71	29	676.7
	Carpathian Foredeep	99	29,985.34	-	-
	Paleozoic-Mesozoic basement	11	1768.96	12	815.17
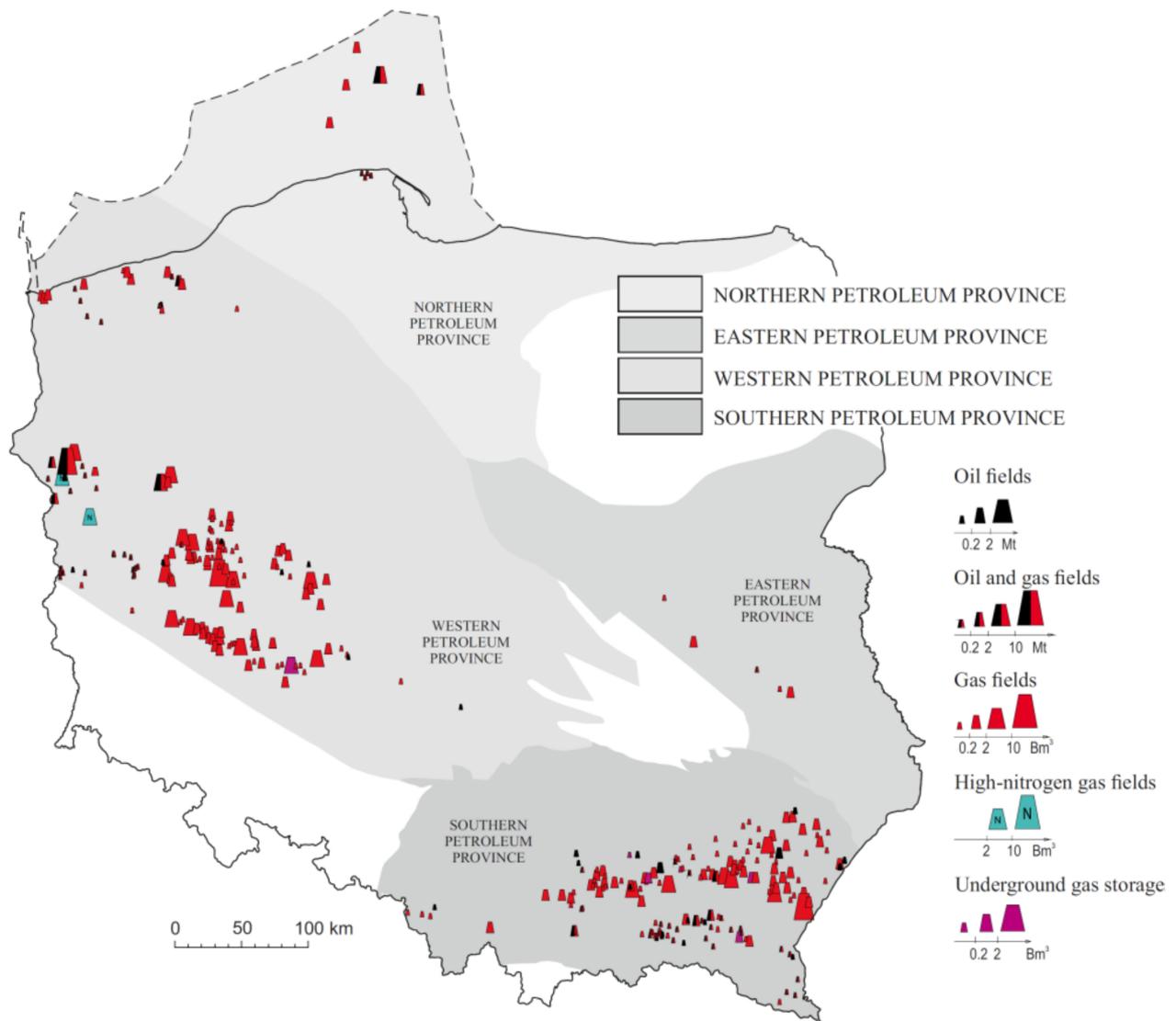
Figure 3: Location of oil and gas fields and underground gas storages in Poland in relation to petroleum provinces (after **Wójcik et al., 2022**)

2.3. Aquifers

According to **Lemieux et al. (2020)**, an aquifer is a sedimentary rock, which is saturated with water. The water can be replaced with injected fluids. Aquifers are porous and permeable strata (only water-bearing), which could be used for gas storage, if there is a reservoir with proper parameters (porosity, permeability, caprock, trapping structure). The only difference between aquifers and hydrocarbon reservoirs is filling – in aquifers oil and gas cannot be found.

In Poland, one of the largest sedimentary basins of Europe exists, it is called Mid-Polish Trough. It consists of the large deep aquifers with Lower Triassic, Lower Jurassic, and Lower Cretaceous strata. **Górecki et al. (2006)** proved the existence of thick reservoirs rocks, lack of contact with potable waters, position at a large depth and a good geological recognition level of these structures. Cretaceous reservoir consists mainly of sandstones, sandy and carbonate-sandy deposits of the Barremian-Middle Albian age. They are overlain by the Upper Cretaceous limestones, marls, opokas and chalk with low permeability **(Tarkowski, 2010; Tarkowski et al., 2014; Wójcicki et al., 2014)**. The total thickness of the Lower Cretaceous strata varies from several meters at the peripheral zones of the basin to several hundred meters in the center. The effective porosity is around 20-40% and pore water salinity reaches 100 g/l **(Górecki et al., 2006)**. Lower Jurassic reservoir horizons are composed predominantly of sandstones of the Hettangian, Sinemurian, Pliensbachian, and the Late Toarcian age. The total thickness of the Lower Jurassic succession ranges from several meters at the basin edge, up to 1200 m in the central part **(Górecki et al., 2006)**.

3. Possibilities of geological energy storage in analyzed formations

3.1. Salt domes

The key element to select a proper salt dome to build a cavern is the appropriate thickness of a salt massif, its width and homogeneity. These parameters and the internal structure of a salt dome should be analyzed **(Tarkowski and Czapowski, 2018; Lankof and Tarkowski, 2020; Lankof et al., 2022)**. At this moment, there is no active underground hydrogen storage in salt structures in Poland, but **Tarkowski and Czapowski (2018)** typed 27 structures suitable for hydrogen storage. Nevertheless, salt caverns are used for storing natural gas (Mogilno and Kosakowo) and fuels (Góra near Inowrocław) (see **Figure 1**). The next underground gas storage is to be built in the Damasławek salt dome.

3.2. Hydrocarbon reservoirs

Several oil and gas reservoirs are taken into account. The criteria for underground hydrogen storage are as follows **(Tarkowski, 2017; Lewandowska-Śmierzchalska et al., 2018)**:
- the depth to the top of the reservoir should not exceed 2000m,
- the reservoir should be listed in the current balance of mineral resources,
- 15-25% of depletion of geological resources or 50% for recoverable resources for crude oil,
- 75% of depletion of recoverable resources for gas.

With such criteria, 3 oil reservoirs (Carpathian Foredeep) and 16 gas reservoirs (6 in the Polish Lowlands and 10 in the Carpathian Foredeep) are proposed for underground storage in Poland. Authors of this paper added additional criteria, limiting the original ranking list made by **Tarkowski (2017) and Lewandowska-Śmierzchalska et al. (2018)**:
- distance from potential hydrogen sources (offshore wind farms),
- structural homogeneity of the reservoir – structural traps with very good sealing (e.g., with evaporites),
- availability of geological and geophysical data,
- location near the existing gas pipelines.

Based on the improved criteria, the list was narrowed. Only 4 gas reservoirs in the Polish Lowlands fulfil the extended criteria. These are reservoirs in the Rotliegend sandstones, sealed with the thick series of the Zechstein evaporites. All oil and gas reservoirs existing in the Carpathian Foredeep were withdrawn because of their position far away from the desired wind and offshore development regions. Furthermore, 10 gas reservoirs in the Polish Lowlands (also Rotliegend sandstones) were listed as perspective, because of the possibility of their depletion in the near future. Nevertheless, in the next 20-30 years, more hydrocarbon reservoirs in Poland will be depleted, which will increase the potential volume for underground storage.

3.3. Aquifers

Tarkowski (2017) and Lewandowska-Śmierzchalska et al. (2018) analyzed geological and economic data used in the ranking of geological structures for CO_2 storage in the Mesozoic aquifers of the Polish Lowlands in order to perform a preliminary selection of the most suitable structures for hydrogen underground storage. Only the structures not exceeding 2000 m in depth (measured from the top of reservoir) have been chosen. The next important variables were reservoir parameters (thickness, porosity, and permeability of the reservoir horizon), storage security, and the degree of exploration advancement. Under these criteria, the best parameters are found for 8 geological structures in Lower Cretaceous strata and 6 geological structures in the Lower Jurassic strata.

As was done in the case of hydrocarbon reservoirs, additional criteria that limited the original ranking, were made. After the limitation, only 3 aquifers (Lower Jurassic) localized in the northwestern Poland, have been listed. All existing aquifers in the Lower Cretaceous deposits were rejected, because of the geothermal use and drinking water intakes. Some of the Lower Jurassic strata are also perspective for geothermal energy – deeper parts are not well recognized yet.

4. Conclusions

Based on the available data and analysis done, it can be concluded, that Poland has a potential for hydrogen storage in the following underground structures:

a) Salt caverns are the best structures for hydrogen storage because of the geological setting, good sealing, and the technology availability. Efficiencies of injection/production of hydrogen are very high due to the non-porous structure. Due to a small distance of salt caverns from the sea in Poland (max 250km), where offshore wind farms can be built, it makes them the cheapest way to create such installations.

b) Depleted gas reservoirs are the second possibility. Their main advantage is the limited need to build a surface installation (which is needed in case of salt caverns and aquifers). On the other hand, pore space in natural gas reservoirs may result in lowered flexibility in the amount of gas injection and uptake. What is more, the problem of sealing can exist – gas reservoir was hermetic for methane, but hydrogen may require lower permeabilities – the verification needs to be done. Finally, hydrogen can react with some minerals – there is a need study its effect on the pore space.

c) The last possibility is aquifers. Here we have to analyze all available archival data. If the study unveils potential geological structures, the set of prospecting should be made (seismic, drilling, well-logging, core analysis etc.). Also, there is a need to analyze the interaction of hydrogen with rocks, and build a numerical geological and dynamical model, which should identify the working and active volumes, as well as gas injection and uptake efficiencies. The last stage is to construct a surface infrastructure. Unfortunately, during the process verification, the structure may be deemed unsuitable for storage (leakages, gas reaction etc.). To sum up, it is the most expensive solution – even with a positive test result.

5. References

Czapigo-Czapla, M., Brzeziński, D. (2021a): Natural gas. In The Balance of Mineral Resources Deposits in Poland as 31-12-2020. In: Szuflicki, M., Malon, A., Tymiński, M. (eds.): Polish Geological Institute—National Research Institute: Warsaw, Poland, pp. 11–22. (in Polish).

Czapigo-Czapla, M., Brzeziński, D. (2021b) - Crude oil. In The Balance of Mineral Resources Deposits in Poland as 31-12-2020. In: Szuflicki, M., Malon, A., Tymiński, M. (eds.): Polish Geological Institute—National Research Institute: Warsaw, Poland, pp. 29–34. (in Polish).

Czapowski, G., Bukowski, K. (2015): Mapy wystąpień zasobów perspektywicznych soli w Polsce jako narzędzie w projektowaniu przyszłego zagospodarowania złóż kopalin. Przegląd Solny, 11, 5-31. (in Polish).

Czapowski, G., Aleksandrowski, P., Jarosiński, M. (2017): Struktury solne, 1:5000. In: Nawrocki, J., Becker, A. (eds.): Atlas Geologiczny Polski. Warszawa: PIG-PIB; pp. 1-170. (in Polish).

Dadlez, R. (2001): Przekroje geologiczne przez bruzdę śródpolską 1:200 000. Warszawa: Państwowy Instytut Geologiczny. (in Polish).

Górecki W., (Ed.), Hajto M., Papiernik B., Szczepański A., Kuźniak T., Kozdra T., Soboń J., Szewczyk J., Strzetelski W., Haładus A., Banaś J. (2006): Atlas of Geothermal Resources of Mesozoic Formations in the Polish Lowlands. AGH University of Science and Technology in Krakow, Krakow, Poland; Ministry of Environment, Warsaw; NFEP&WM, Warsaw. ISBN 978-83-88927-13-3, p. 484.

Karnkowski, P. (1999): Oil and gas deposits in Poland. The Geosynoptics Society GEOS – University of Mining and Metallurgy, Cracow, 380 pp.

Lankof L., Tarkowski R. (2020): Assessment of the potential for underground hydrogen storage in bedded salt formation. International Journal of Hydrogen Energy, 45 (38), pp. 19479–19492. https://doi.org/10.1016/j.ijhydene.2020.05.024

Lankof L., Urbańczyk K., Tarkowski R. (2022): Assessment of the potential for underground hydrogen storage in salt domes. Renewable and Sustainable Energy Reviews, 160, 112309. https://doi.org/10.1016/j.rser.2022.112309

Lemieux A., Shkarupin A., Sharp K. (2020): Geologic feasibility of underground hydrogen storage in Canada. International Journal of Hydrogen Energy, 45, 56, pp. 32243-32259. https://doi.org/10.1016/j.ijhydene.2020.08.244

Lewandowska-Śmierzchalska J., Tarkowski R., Uliasz-Misiak B., 2018 - Screening and ranking framework for underground hydrogen storage site selection in Poland. International Journal of Hydrogen Energy, 43, pp. 4401–14. https://doi.org/10.1016/j.ijhydene.2018.01.089.

Tarkowski R. (2010): - Potencjalne struktury geologiczne do składowania CO2 w utworach mezozoiku Niżu Polskiego (charakterystyka oraz ranking). IGSMiE PAN. Studia. Rozprawy. Monografie 164, pp. 1-138 (in Polish).

Tarkowski R., Dziewińska L., Marek S. (2014): The characteristics of selected potential geological structures for CO2 underground storage in Mesozoic deposits of the Szczecin–Mogilno–Uniejów Trough. Studia, Rozprawy, Monografie 185. Kraków: MEERI PAS, 105 pp. (in Polish).

Tarkowski, R., Czapowski, G. (2018): Salt domes in Poland – Potential sites for hydrogen storage in caverns. International Journal of Hydrogen Energy, 43, 21414-21427. https://doi.org/10.1016/j.ijhydene.2018.09.212

Wagner, R. (1994): Stratygrafia osadów i rozwój basenu cechsztyńskiego na Niżu Polskim, vol. 146. Wydawnictwo PIG. (in Polish).

Wagner, R., Peryt, T.M. (1997): Possibility of sequence stratigraphic subdivision of the Zechstein in the Polish basin. Geological Quarterly, 41, 4, 57-74.

Wójcicki A., Nagy S., Lubaś J., Chećko J., Tarkowski, R. (2014): Assessment of Formations and Structures Suitable for Safe CO2 Geological Storage (in Poland) Including the Monitoring Plans (Summary). Warszawa.

Wójcik, K., Zacharski, J., Łojek, M., Wróblewska, S., Kiersnowski, H., Waśkiewicz, K., Wójcicki, A., Laskowicz, R., Sobień, K., Peryt, T., Chylińska-Macios, A., Sienkiewicz, J. (2022): New Opportunities for Oil and Gas Exploration in Poland - A Review. Energies, 15, 1739. https://doi.org/10.3390/ en15051739

Sažetak

Mogućnosti skladištenja energije u geološkim strukturama u Poljskoj

Analizirane su mogućnosti skladištenja energenata u podzemnim geološkim strukturama u prostoru Poljske. Zaključeno je da postoje tri glavne mogućnosti skladištenja: solne kaverne, iskorištena plinska ležišta i vodonosnici. Solne kaverne su potpuno operativna skladišta metana i nafte u Poljskoj. Ležišta ugljikovodika otkrivena u južnoj Poljskoj (Karpatima i karpatskom predgorju) su devonske, mezozojske i kenozojske starosti. U sjeverozapadnoj Poljskoj ona su u bazenima Zechstein i Rotliegendes (Poljska nizina), a u istočnoj Poljskoj u bazenu Lublin (devon) i Baltičkom moru (kambrij). Neka iscrpljena ležišta se već koriste za skladištenje metana. Vodonosnici su otkriveni u mezozojskom bazenu središnje Poljske (Poljska nizina) u slojevima donjega trijasa, donje jure i donje krede. Sve opisane strukture, analizirane pravilnim kriterijima, su potencijalna skladišta energije, npr. u obliku vodika, koja se može naknadno koristiti kao energent.

Ključne riječi: skladištenje, vodik, solne kaverne, iscrpljena ležišta, vodonosnici, Poljska

Acknowledgment

Author's contribution

Marek L. Solecki (M. Sc. in Petroleum Geology and Ph.D. Candidate in Geology) and **Grzegorz Machowski** (Ph. D. in Geology) described the geological setting of analyzed structures. **Paweł Wojnarowski** (Assoc. Prof. in Reservoir Engineering) developed criteria for the selection of geological structures. **Gordon Wasilewski** (PhD in Geophysics) provided the analysis of the availability of structures. **Jerzy M. Stopa** (Full. Prof. in Reservoir Engineering) participated in writing the introduction and conclusions.

Small asteroid impact and cratering on Mars

Indramani Sharma[1]; Željko Andreić[2]; Tomislav Malvić[3] and Uroš Barudžija[4];

University of Zagreb, Faculty of Mining, Geology and Petroleum Engineering,
    Pierottijeva 6, 10000 Zagreb, Croatia

[1] ORCID 0000-0002-0577-5855

[2] ORCID 0000-0003-0175-8174

[3] ORCID 0000-0003-2072-9539

[4] ORCID 0000-0002-1617-9362

Abstract

The consequences of impact of small stony asteroids (with masses less than 100 t) on Mars surface are investigated. The atmospheric braking is found to be negligible as is the maximal dynamic pressure exerted on the impacting body. In other words, the impactor remains unfragmented until the impact. The resulting crater size depends on the kinetic energy of the impactor and the lithological properties of the Martian surface and shallow crust as well as later atmospheric erosion.

Keywords: Mars, cratering on Mars, meteorite flight

1. Introduction

Mathematical model of a small asteroid dynamics during a flight through the Martian atmosphere determines the final remaining kinetic energy of the impacting body. By calculating the deceleration and the dynamic pressure exerted on the incoming body over the course of its trajectory through the atmosphere, the height at which the largest dynamic pressure is reached, and incoming body's final velocity are determined. Input parameters are the mass of the incoming body, initial velocity vector's magnitude and the angle of entry. Initial height above the ground level (z coordinate in a Cartesian coordinate system fixed at the Mars surface) is set at 100 km, for all simulated cases.

In all flight calculations we used the usual approach: the drag force is calculated through the Newton's drag law, with variable, velocity dependent drag coefficient. Here, we assumed a spherical body and used the coefficient from **(Carter at al., 2009).** For the atmosphere, exponential model with data for the Mars atmosphere was used. All initial calculation parameters are summed up in the **Table 1** and **Table 2**.

However, the bombardment of planetary surface is casual process, nowadays on declining frequency in the whole Solar system, therefore on the Mars as well. This in contrast to the beginning of Solar system's existence when such processes were very frequent and widely varied in numbers and sizes of falling bodies. Back then, Mars played significant role in creation of still existing asteroid belt. In the very beginning, the early bombardment phase took place until 0.5 Ga after creation of the system. Perhaps the most prominent result of this bombardment is the creation of the Moon, after inclined collision of the proto-Earth and Theia. Some calculations (**Petit & Morbidelli, 2001; Kominami & Ida, 2001**) indicated that in this phase of it's development the Solar system included 50-100 planetary bodies with sizes more or less equivalent to the size of Mars. Most of them collided in the first 0.1 Ga and were merged or destroyed (**Lin, 2008**), and the Solar system was left with four present-day terrestrial planets.

The early bombardment period was followed by late bombardment phase, which lasted approx. 0.5-1.0 Ga after the creation of the Solar system. There was no merging or destroying of planets and planetoids, and this phase was characterised by large scale bodies impacts on the existing four planets and the Moon. The most objects, but not all, had their origin in the asteroid belt. Although such impacts were extraordinarily energetic, and often affected the planets' crusts, their impact craters are later eroded and lost. The erosion took place on all terrestrial planets due to early volcanism as well as atmospheric and oceanic processes (Earth, Venus, Mars). The asteroid belt, today located between 2 and 4 a.

Corresponding author: Indramani Sharma
indramani.sharma@rgn.hr

u., played the main role in the late bombardment phase. In the beginning this belt included mass of about 2-3 Earth masses, probably in the form of 20-30 planetoids, ranging in sizes from Moon's to Mars' (**Bottke et al., 2005**). However, the Jupiter, even the Saturn, gravitationally prevented the accretion of planetoids into larger planet(s), assisted with later approaching of the Jupiter to the Sun, which increased the orbital velocities of the belt bodies and pushed them toward inner Solar system (**Bottke et al., 2005**; **Raymond et al., 2007**). When the gravitational balance had been established again, only 1 % of the Earth mass remained in the asteroid belt, still occasionaly ejecting asteroids across the Solar system until today, when the remaining mass is the 0.05 % of the Earth. Many of the asteroids brought water on the planets, and larger planets, like the Earth and Venus, kept it in their oceans. Among the terrestrial planets, only the Earth has one additional process that's changing its shape and is responsible for the destruction of the older surface structures. It is plate's tectonic.

Equatorial diameter (km)	6780
Surface gravity (m/s^2)	3.71
Atmosphere composition (%)	96 CO_2 1.9 Ar 1.9 N_2
Surface atmospheric pressure (Pa)	636
Expected variations of surface pressure (Pa)	400-870
Mean surface temperature (K)	210
Expected variations of surface temperature (K)	130-308
Mean orbital speed (km/s)	24
First cosmic speed (km/s)	3.57
Second cosmic speed (km/s)	5.03
Third cosmic speed (km/s)	34.1

Table 1: Physical characteristics of the Mars

The **Table 1** gives basic physical characteristics of the planet Mars, starting with its diameter and surface gravity. Note that, although Mars is about half the size of the Earth, its surface acceleration is only about one third of the surface acceleration of the Earth. Martian atmosphere is very rare. The surface pressure varies widely depending on the location and the time of the Martian year. Mars is farther from Sun than Earth and is accordingly slower in its orbit. Also, the third cosmic velocity for Mars (the velocity needed for a body to leave the Solar System) is about three quarters of the corresponding velocity for Earth. Combined with a weaker Martian gravity, this results in lower impact velocities for impacting bodies, compared to the Earth. Thus, incoming objects will strike Mars with velocities between about 5 and 58 km/s, compared to 11 to 72 km/s for the Earth.

Asteroid type	Chondritic (stony)
Asteroid density (kg/m^3)	3300
Asteroid mass (kg)	10 - 81920
Angle of entry (towards horizontal, deg)	10 - 90
Incoming velocity (km/s)	10 - 50

Table 2: Physical characteristics of asteroids as used in our calculations.

As stony asteroids are the most common type, the calculations were done for this type of asteroids only, with their physical properties summarized in the **Table 2**. The Martian atmosphere is significantly less dense than the Earth's, thus the resulting drag forces and dynamic pressures are much smaller as well (**Figure 1**). This means that fragmenting of the incoming body is less probable, as also suggested by the results of the calculations.

2. Methods
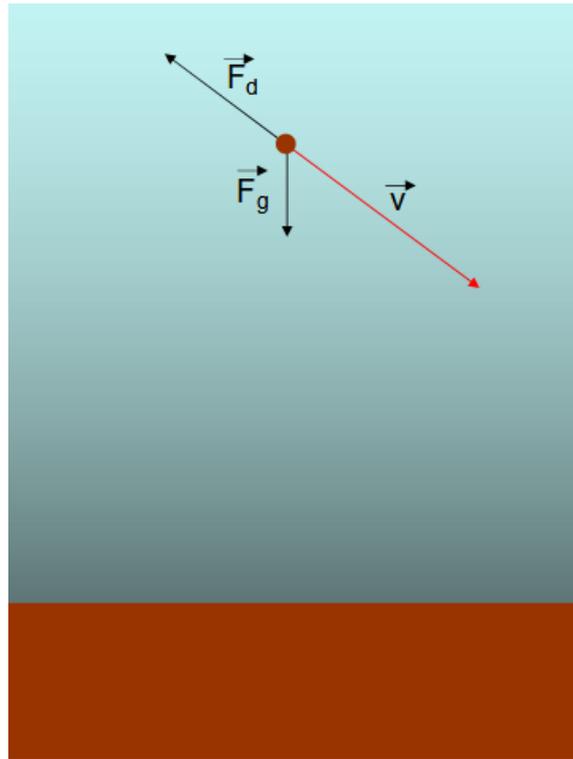
Figure 1: Forces acting on an incoming body in a planetary atmosphere (blue). The asteroid velocity is $\vec{v}$, and is usually specified by its magnitude and the angle of entry (usually measured between the direction of the flight and the horizontal). The body is simultaneously influenced by the gravitational force of the planet, $\overrightarrow{F_g}$ and the drag force $\overrightarrow{F_d}$.

The gravitational force is, to a very good approximation, described by the well known Newton's **Equation 1**:

$$\overrightarrow{F_g} = G\frac{Mm\,\vec{r}}{r^2}\frac{\vec{r}}{r}$$

(1)

Where are:
$\overrightarrow{F_g}$ *is the gravitational force,*
G is the universal gravitational constant,
M is the mass of the planet,
m is the mass of the asteroid,
$\vec{r}$ *is the distance between these two bodies.*

Usually, this formula is rewritten using the surface acceleration $\overrightarrow{a_g}$ as **Equation 2**:

$$\overrightarrow{F_g} = \overrightarrow{a_g}m\frac{r^2}{r_o^2}$$

(2)

Where are:
$\overrightarrow{a_g}$ *stands for the surface gravitational acceleration,*
r for the distance between the two bodies and
r_o *is the diameter of the planet.*

The decrease of the gravitational acceleration with distance is often neglected for small distances (compared to the planet's diameter), resulting in a simpler **Equation 3**:

$$\vec{F_g} = \vec{a_g}m \tag{3}$$

The drag force imparted on the asteroid inside the Martian atmosphere is given by the Newton's drag law (**Equation 4**):

$$\vec{F_d} = -\frac{1}{2}c\rho Av\vec{v} \tag{4}$$

Where are:
c is the drag coefficient,
ρ is the density of the surrounding medium (e.g. Martian atmosphere),
A is the cross-sectional area of the incoming body and
$\vec{v}$ is the velocity of the body relative to the atmosphere.

The drag coefficient depends on the shape of the body and varies with the speed to a certain extent. We used data from (**Carter at al., 2009**) for a spherical asteroid. The dynamic pressure is, to a first approximation, equal to the drag force divided by the cross-sectional area of the body moving through the fluid (i.e., atmosphere). Wind is neglected in our calculations as is the planetary rotation.

Under these approximations the model can be reduced to a two-dimensional problem. Calculations are performed in the plane of the meteorite trajectory. The cartesian coordinate system is set up with the x axis horizontal, +x pointing into the direction of the flight. The y axis is vertical, +y pointing up. The equation of motion of the asteroid is now (**Equation 5**):

$$m\vec{a} = m\vec{a_g} - \frac{1}{2}c\rho Av\vec{v} \tag{5}$$

or, separated into the components (**Equations 6** and **7**):

$$a_x = -\frac{c\rho A}{2m}vv_x \tag{6}$$

$$a_y = -g - \frac{c\rho A}{2m}vv_y \tag{7}$$

These equations are solved numerically, with initially the asteroid being at a large distance from Mars, ending in the collision with the surface.

3. Results

The parameter most interesting to us in this study is the remaining kinetic energy of the asteroid in the moment of impact, as this determines how the cratering process will evolve. The ability of the Martian atmosphere to slow down the incoming body is very small due to low density of the atmosphere. Modelling shows it is insignificant for asteroid masses larger than about 100 kg. The maximal dynamic pressure for stony asteroids passing through a "standard" Martian atmosphere is shown in **Figures 2** to **6**.

Maximal dynamic pressure vs angle @ 10 km/s
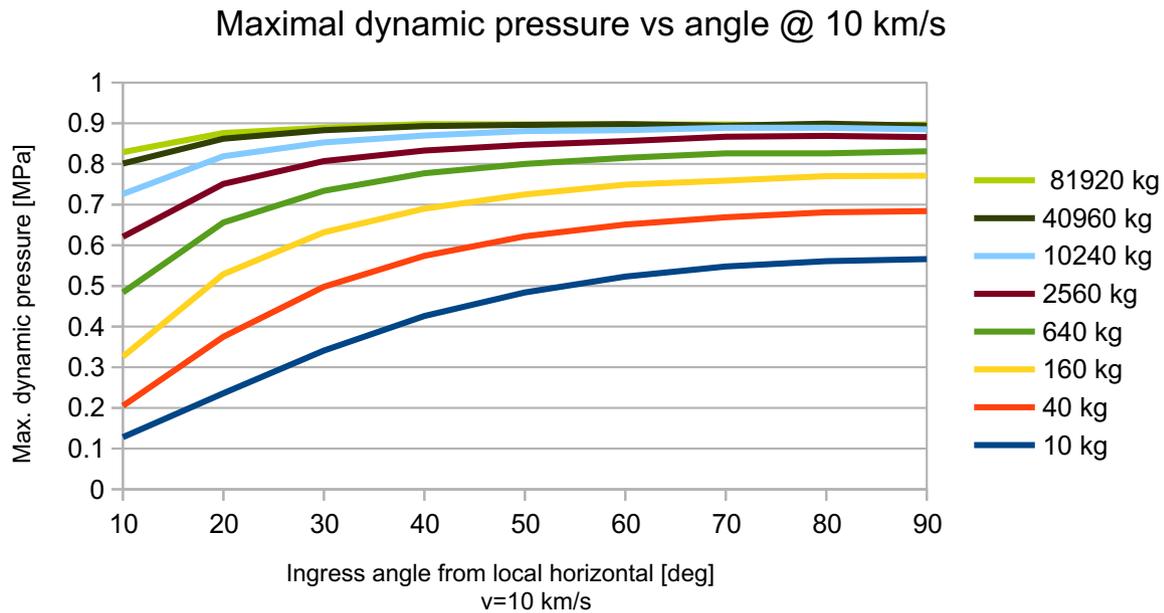
Figure 2: Maximal dynamic pressure as a function of angle of entry (measured from the local horizontal) for asteroids of varying mass and initial velocity of 10 km/s

Maximal dynamic pressure vs angle @ 20 km/s
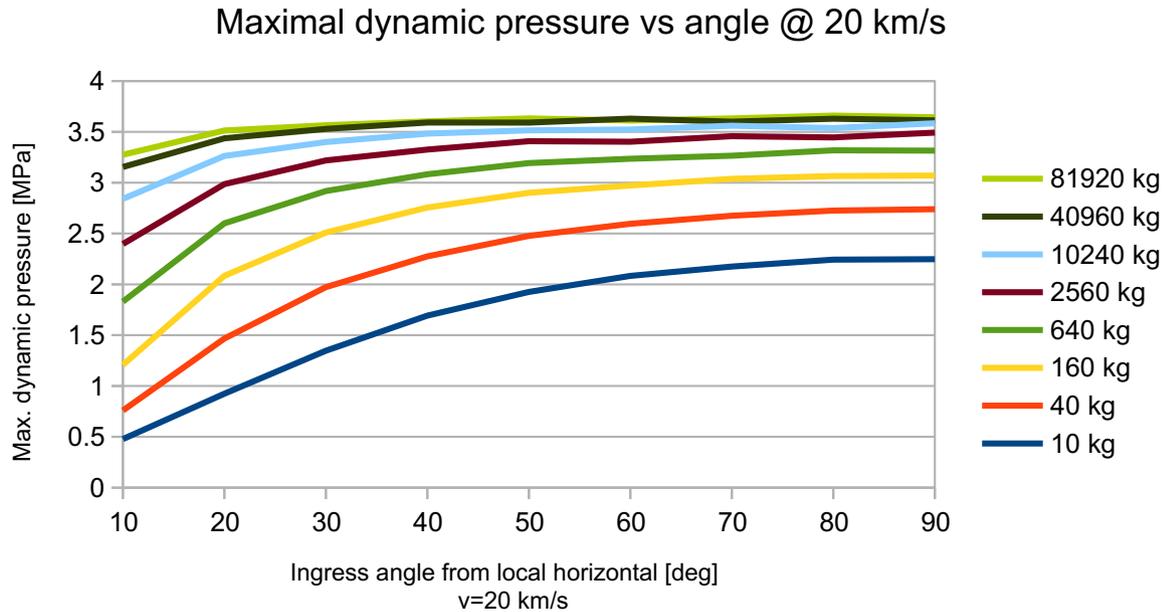
Figure 3: Maximal dynamic pressure as a function of angle of entry (measured from the local horizontal) for asteroids of varying mass and initial velocity of 20 km/s
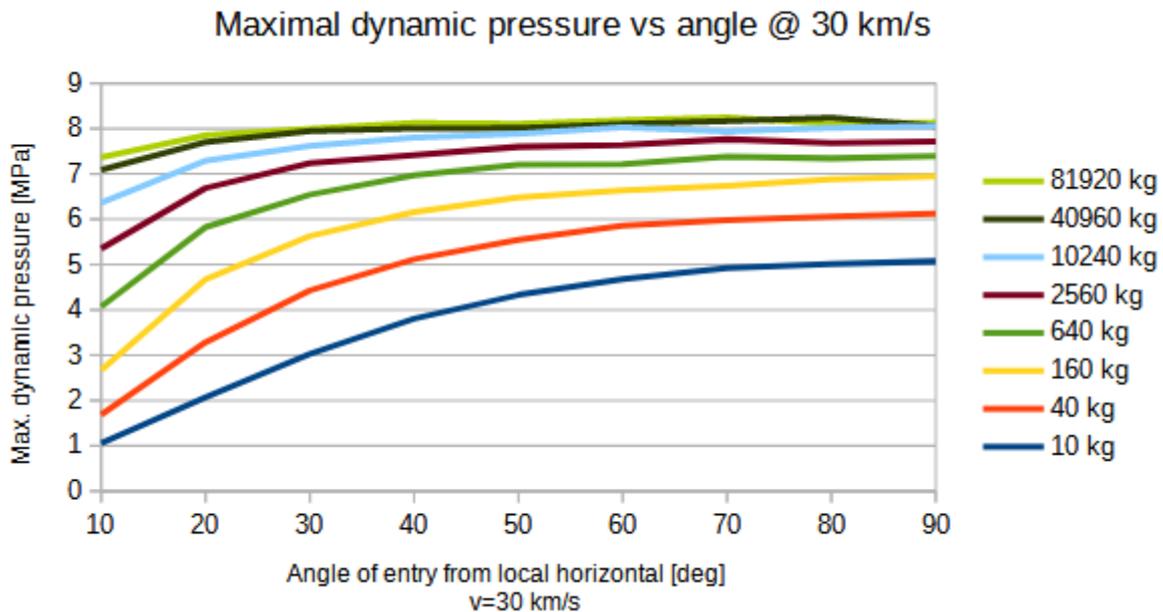
Figure 4: Maximal dynamic pressure as a function of angle of entry (measured from the local horizontal) for asteroids of varying mass and initial velocity of 30 km/s
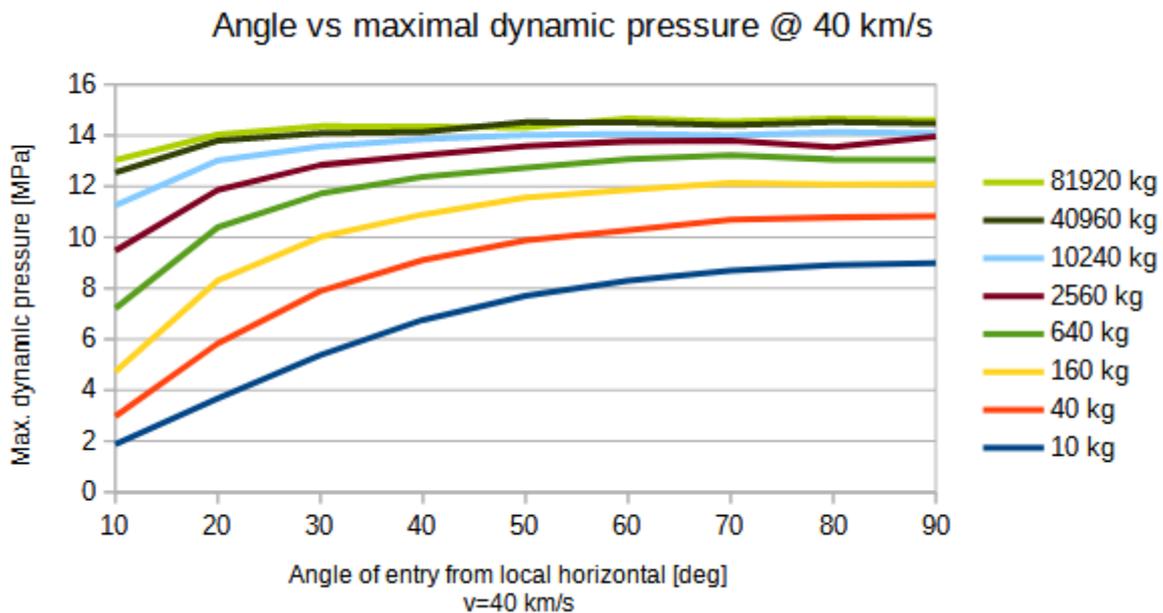
Figure 5: Maximal dynamic pressure as a function of angle of entry (measured from the local horizontal) for asteroids of varying mass and initial velocity of 40 km/s
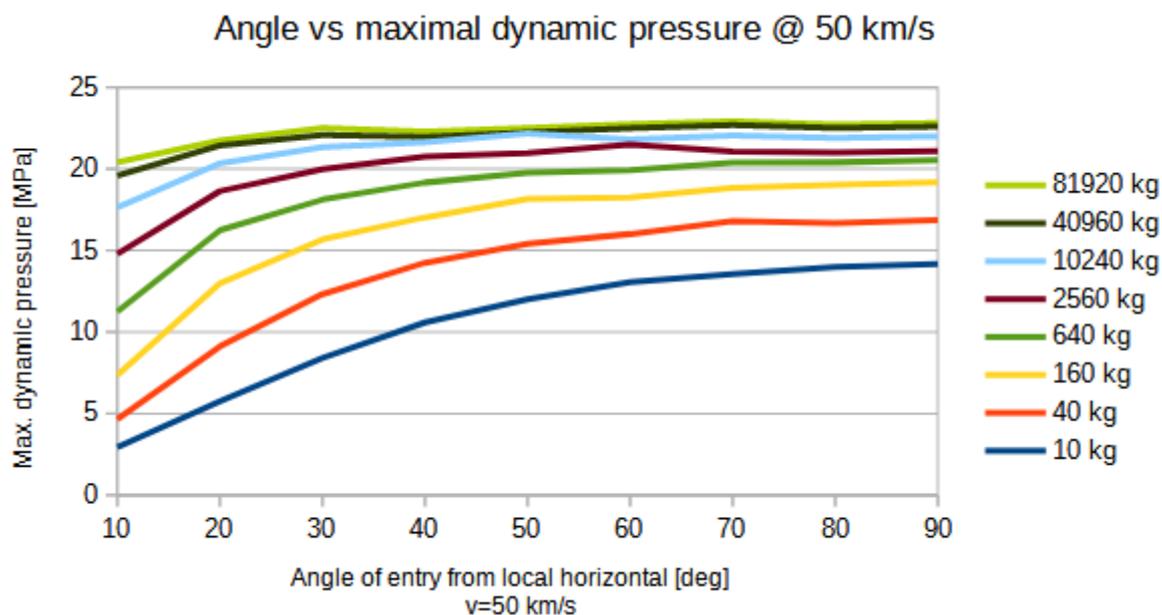
Figure 6. Maximal dynamic pressure as a function of angle of entry (measured from the local horizontal) for asteroids of varying mass and initial velocity of 50 km/s

Maximal dynamic pressure exerted on an asteroid at a given velocity increases with the mass. Also, as initial velocity (taken as a parameter) increases, so does the maximal dynamic pressure. If both velocity and mass are at fixed values, maximal dynamic pressure increases with increasing angle of entry from horizontal. The graphs on Figures 2-6 allow us to judge the maximal dynamic pressure for any combination of initial parameters. Generally, we can conclude that the maximal dynamic pressure is more influenced by the angle of entry for low mass meteorites, less for high mass ones. The maximal dynamic pressure generally increases with the initial velocity. At low velocities (~10 km/s) maximal dynamic pressure is spread in the range from 0.1 MPa to 1 MPa. At midrange velocities (30-40) maximal dynamic pressure values are distributed over the interval from 2 - 15 MPa. For large velocities in 40-50 km/s range, maximal dynamic pressure lies in 3 - 25 MPa interval.

The remaining kinetic energy in the moment of the impact is the most important factor that determines if, and how, the cratering process will evolve. The results of the model are shown on the **Figures 7** to **15**. As the remaining kinetic energy depends on three parameters, assuming a "standard" atmosphere with a constant surface pressure, different combinations of parameters are used to produce easy-to-read two-dimensional graphical representations. Obviously, the remaining kinetic energy grows with the mass and is roughly proportional to the square of the velocity, at least for more massive asteroids. The incoming angle dependence is more pronounced for less massive asteroids, as atmospheric drag influences them more than the more massive ones. Altogether, **Figures 7** to **15**. allow assessing the remaining kinetic energy at impact for any combination of these parameters.
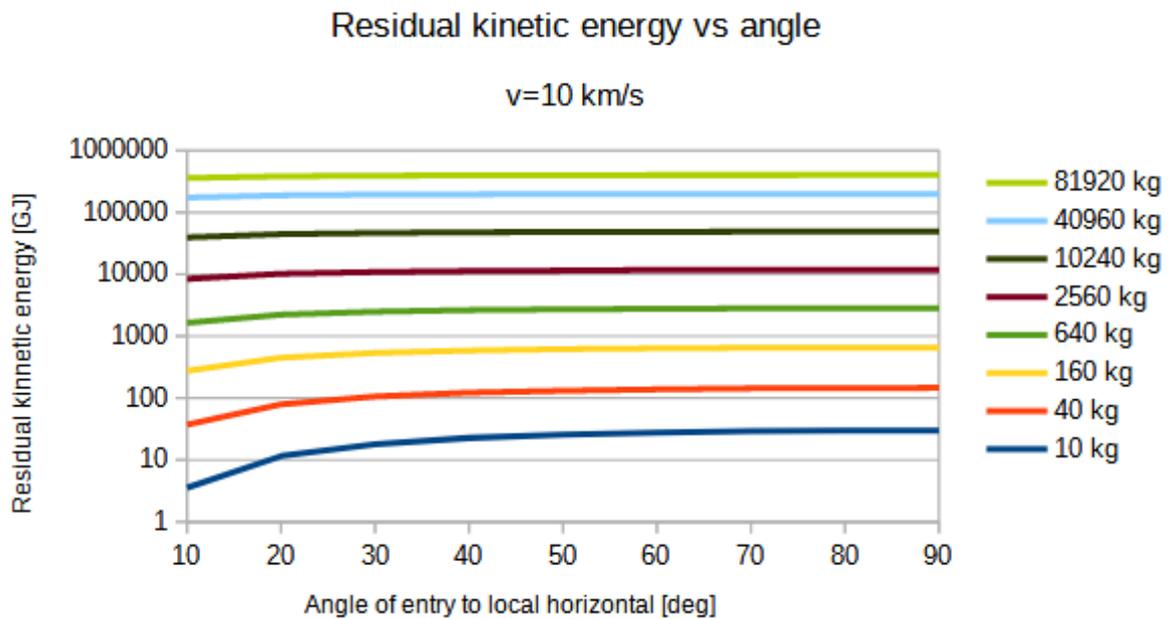
Figure 7: Dependence of residual kinetic energy on angle of entry for various asteroid masses, for initial velocity of 10 km/s.
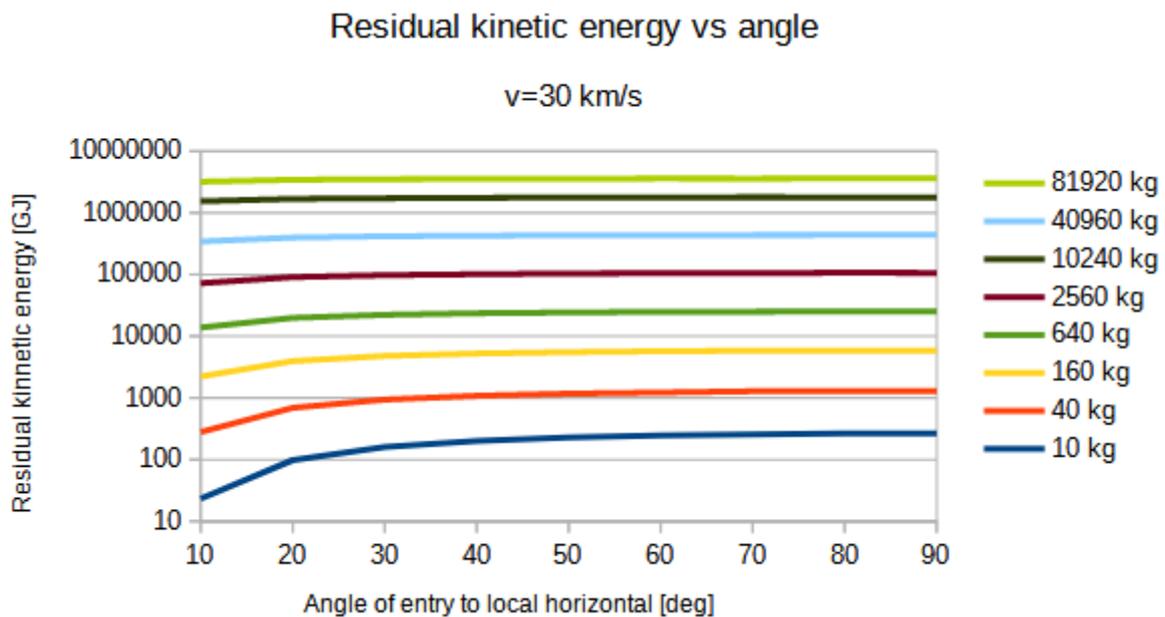
Figure 8: Dependence of residual kinetic energy on angle of entry for various asteroid masses, for initial velocity of 30 km/s
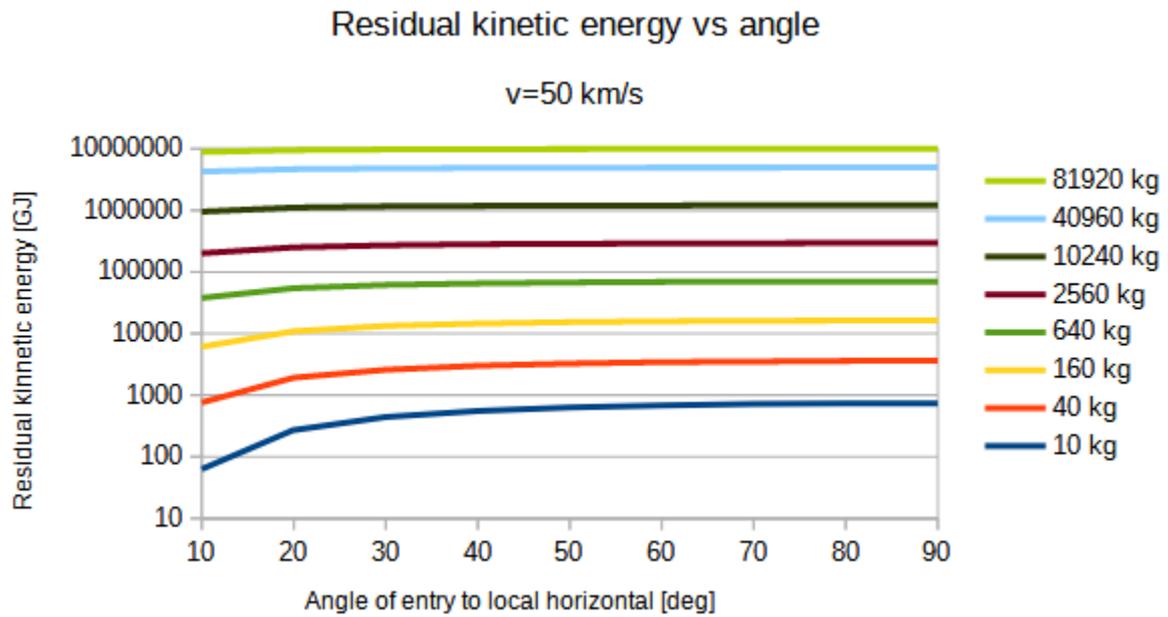
Figure 9: Dependence of residual kinetic energy on angle of entry for various asteroid masses, for initial velocity of 50 km/s
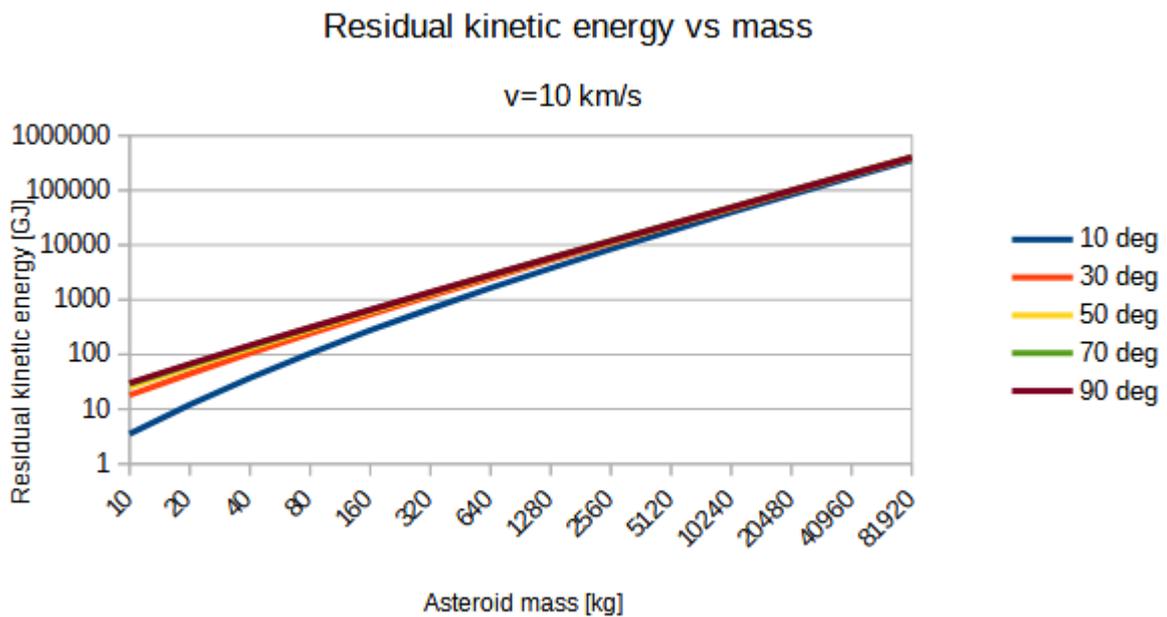
Figure 10: Residual kinetic energy as a function of the asteroid mass, at fixed velocity of 10km/s
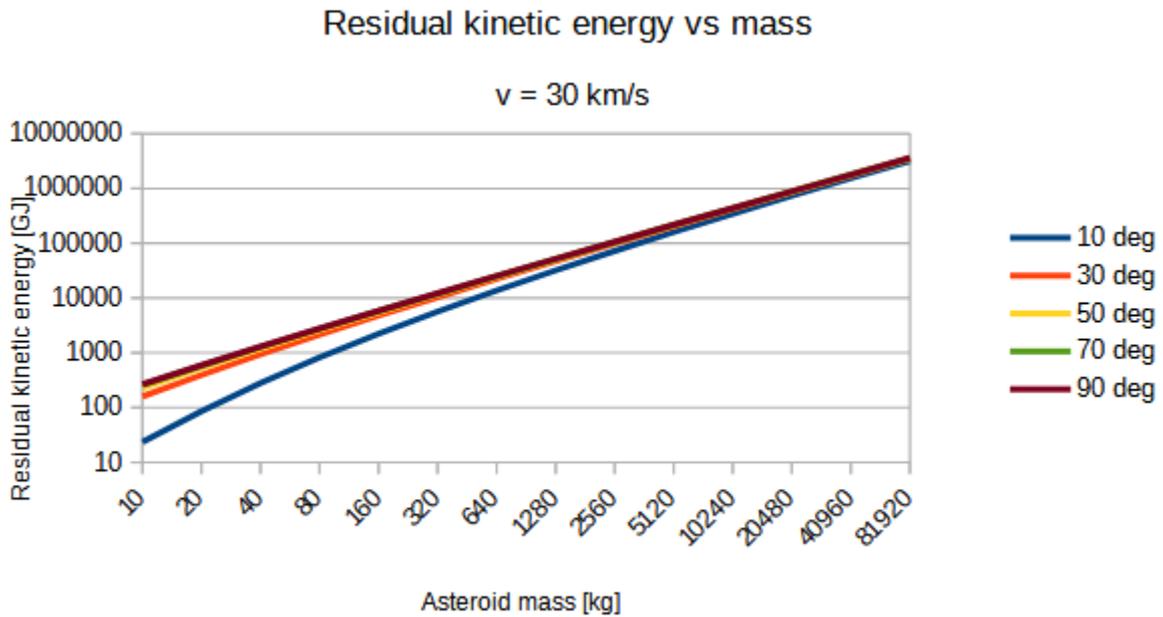
Figure 11: Residual kinetic energy as a function of the asteroid mass, at fixed velocity of 30km/s
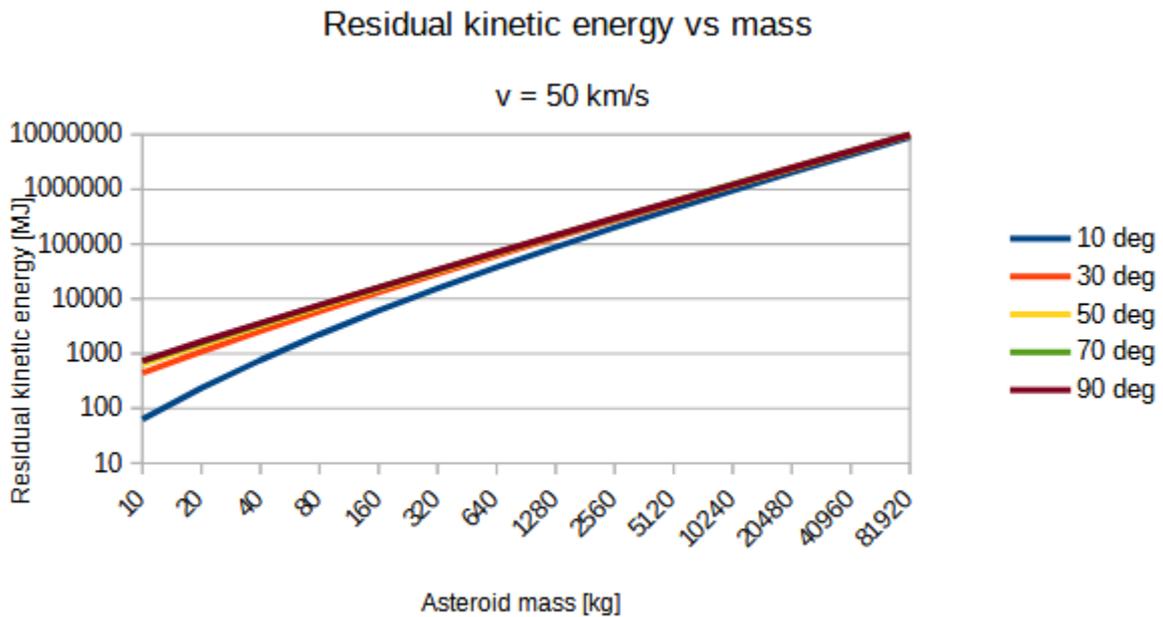
Figure 12. Residual kinetic energy as a function of the asteroid mass, at fixed velocity of 50km/s
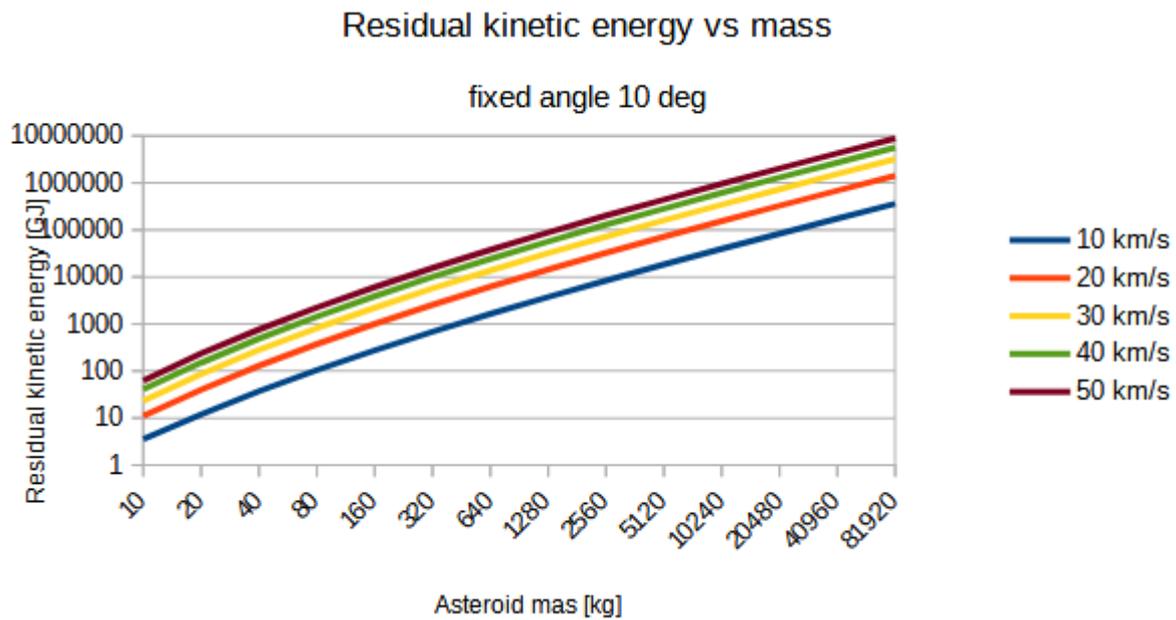
Figure 13: Residual kinetic energy as a function of the asteroid mass, at fixed angle of entry of 10 deg
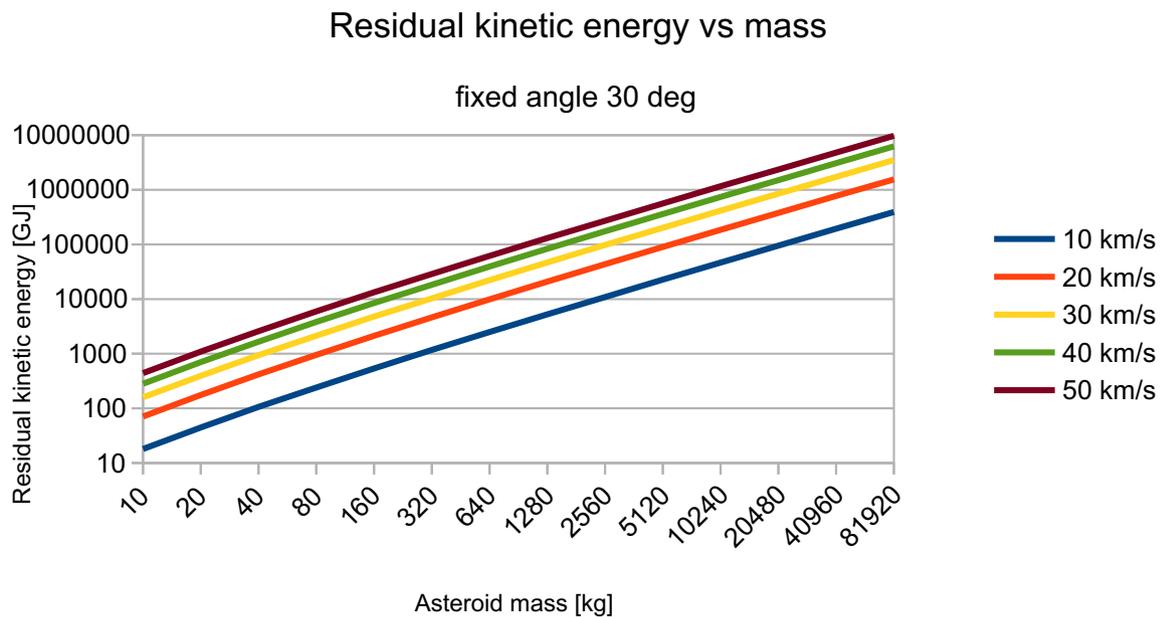
Figure 14: Residual kinetic energy as a function of the asteroid mass, at fixed angle of entry of 30 deg

Residual kinetic energy vs mass
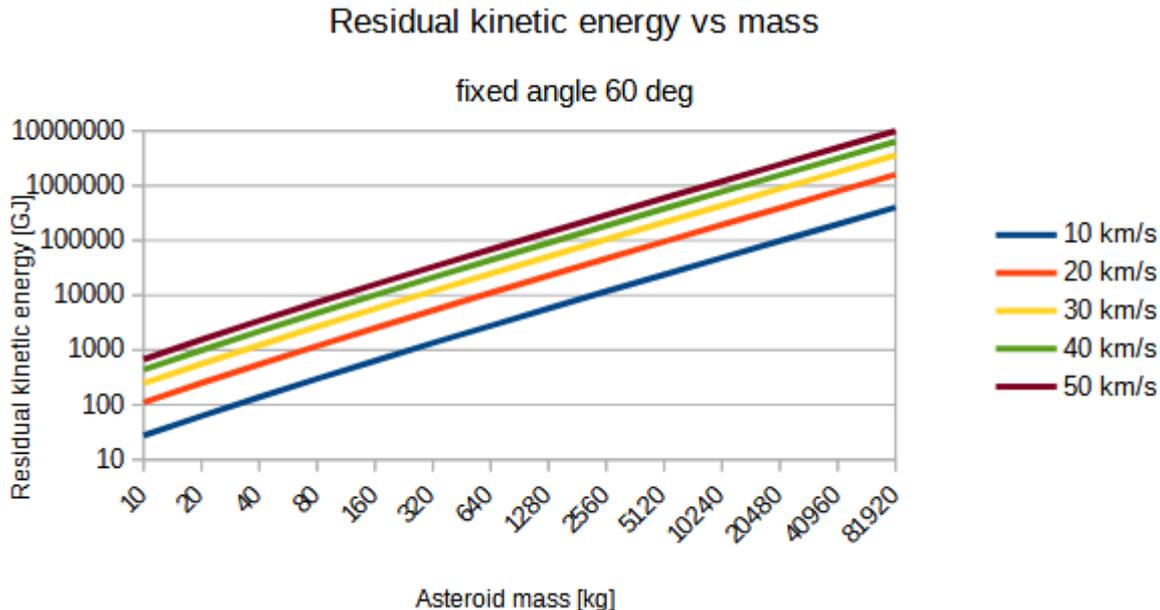
fixed angle 60 deg

Figure 15: Residual kinetic energy as a function of the asteroid mass, at fixed angle of entry of 60 deg

4. Discussion

Dynamic pressure can be used to distinguish between bodies that reach the ground intact (assuming no thermal ablation) and those that break up due to aerodynamic forces acting on the incoming body. Those reaching the ground are considered impactors and are crater forming candidates. Incoming bodies that do break up in the atmosphere won't be treated as potential impactors. Rather low dynamic pressures are due to the rare Martian atmosphere, so we assume that the breakup happens mainly to bodies composed of loosely bound material. We did not treat such cases in our study.

In-flight breakup of the incoming asteroid due to forces originating from interaction with the planet's atmosphere happens when dynamic pressure becomes larger than asteroid's critical or break-up pressure. Calculations show that for the most part, velocity at the zero height is only slightly reduced compared to the in-flight velocity of the asteroid. This, in turn, means that in most cases, neither terminal velocity nor the maximal dynamic pressure is reached before the impact. Therefore, the rarity of Martian atmosphere along with presumed compactness of stony asteroids suggest relatively small dynamic pressure to critical pressure ratio, reducing the probability of a breakup.

The results of Martian impacts are directly linked to the Martian geology and stratigraphy. It could be compared with the Earth's geology, where the oldest geological units, eons, are time periods characterised with the planet forming and developing of the main structures of core, asthenosphere, and lithosphere. Most impacts on the Earth, as well as other terrestrial planets, happened during the first eon called Hadean (4-5-4.0 Ga), when the Earth's structure differentiated and the Moon had formed after collision with another planet (**Portegies Zwart, 2009**; **Kaib & Quinn, 2008**; **Greaves, 2005**). The Hadean had been followed by the Archean (3.9-2.5 Ga), the Proterozoic (2.4-0.55 Ga) and the Phanerozoic (0.54 Ga-rec.). The Martian geological history is also divided into chronostratigraphic units of lower ranks – periods. They are pre-Noachian (4.5-4.1 Ga), Noachian (4.0-3.8 Ga), Hesperian (3.7-3.0 Ga) and Amazonian (2.9 Ga-rec.), defined by studies of impact crater density on planet surface (**Tanaka, 1986**; **Caplinger, 2007**).

All impacts on the Mars are greatly influenced by low surface gravity (38 % of the Earth's) and surface lithology. The planet diameter is 6790 km (half of the Earth's) and general density is 3.9 g/cm^3 (primary silicate with small metal core). The result of impact is mostly determined with interplanetary object's speed and the lithology of the Martian surface (**Figure 16**) at the impact site.

Generalised Geological Map of Mars
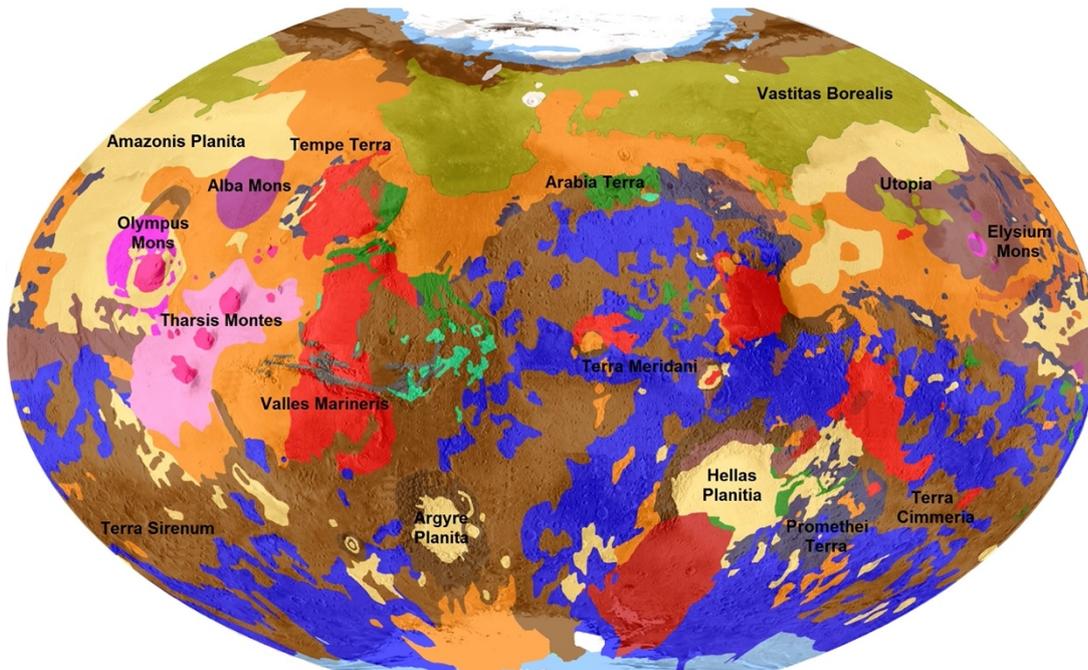
Based on Scott & Carr (1978) and MOLA-data from NASA

☐ Polar ice		Bedded plain material of eolian deposits	
	Volcanic plains	Canyon floor material of the Valles Marineris: made of fluvial and eolian sediments, as well as of landslide material (possibly with partial exposed bedrock)	
	Smooth plains made of eolian deposits	Basalt (200-800 Ma)	
	Volcanic material with a moderated relief, made of basalt and pyroclastic material	Fluvial and eolian deposits	
	Crater plains made of lava, coated by loess	Breccia material, due to subsurface collapse of ground ice melting	
	Fissured lava plains	Aureole material: lava flows from fissures	
	Marginal lifted volcanic material, potentially made of ancient volcanic shields	Belted plains with lava channels	
	Plains with lava-channels	Mottled lava plains	
	Lavaplateaus covered by breccia-like ejecta	Knobs: orogen relics, relief inversion and subsurface collapse (contains ejecta)	
	Eroded edges and pyroclastic basin rim material with a knobby texture	Hilly lava plains	

© P. Zasada

Figure 16: Generalised Geological Map of Mars, 1:140.000.000 (**Zasada, 2013**)

The size of craters, regarding surface lithology, is directly linked to the rock density on the bottom of the crater. The magmatic rocks, especially uplifted intrusive rocks, will be more resistant impacts than sedimentary ones. Weathering decreases the resistance to impacts and the role of Martian soil, regolith, especially one of aeolian origin and can diminish the consequences of the impact. Generally (***), the Martian craters are shallower and smoother than the Lunar ones, due to significantly stronger erosional and depositional geological history. However, the Martian impacts are also result of hypervelocity impacts and are more morphologically complex when larger (***). They can be classified as: (a) simple craters with the diameter <7 km; (b) more complex craters (>7 km), having central peak(s) and (c) extremely large multi ring basins (>100 km) where central peak is replaced with concentric rings of hills.

5. Conclusions

Dynamic pressure was found to be insufficient to affect breakup of stony asteroids, meaning that they will reach the surface in one piece. Rather low dynamic pressures are a natural consequence of the rarity of the Martian atmosphere.

The surface effects of Martian impacts are linked to the Martian geology and stratigraphy. Most impacts on the Earth and other terrestrial planets happened during the Hadean (4-5-4.0 Ga), when the Earth differentiated and the Moon had formed. The Martian geological history is also divided into chronostratigraphic units of lower ranks – periods. They are pre-Noachian (4.5-4.1 Ga), Noachian (4.0-3.8 Ga), Hesperian (3.7-3.0 Ga) and Amazonian (2.9 Ga-rec.), based on studies of impact crater density on planet surface.

Impacts on the Mars are shaped by low surface gravity (38 % of the Earth's) and Martian surface lithology. The planet diameter is half of the Earth's and mean density is much lower, roughly 3.9 g/cm^3. The final result of an impact is determined by the impactor's size, speed and impact angle, combined with the lithology of the Martian surface at the impact site.

The size of craters is determined by the rock density on the bottom of the crater. The magmatic rocks, especially uplifted intrusive rocks, will be more resistant to impacts than sedimentary ones. Martian regolith, especially one of aeolian origin can diminish the consequences of the impact. Generally, Martian craters are shallower and smoother than the Lunar ones, due to significantly stronger erosional and depositional geological history. However, they can be clasified in the same way as lunar ones, namely: simple craters with the diameter smaller than about 7 km, more complex larger craters, having central peak(s) and extremely large multi ring basins with sizes greater than about 100 km.

6. References

Bottke, W. F., Durda, D. D., Nesvorny D., Jedicke, R., Morbidelli, A., Vokrouhlický, D. & Levison, H. F. (2005): Linking the collisional history of the main asteroid belt to its dynamical excitation and depletion. Icarus, 179, 1, 63–94.

Caplinger, M. (2007): Determining the age of surfaces on Mars. Archived from the original on February 19, 2007. Accessed 20th June 2022 - https://web.archive.org/web/20070219192450/http://www.msss.com/http/ps/age2.html

Carter, R.T., Jandir, P.S. and Kress, M. E., Estimating the Drag Coefficients of Meteorites for All Mach Number Regimes, 40th Lunar and Planetary Science Conference, (Lunar and Planetary Science XL), held March 23-27, 2009 in The Woodlands, Texas, id.2059

Greaves, J. S. (2005): Disks Around Stars and the Growth of Planetary Systems. Science, 307 (5706), 68–71. DOI: 10.1126/science.1101979.

Kaib, N. A. & Quinn, T. (2008): The formation of the Oort cloud in open cluster environments. Icarus, 197, 1, 221–238. DOI: 10.1016/j.icarus.2008.03.020.

Kominami, J. & Ida, S. (2001): The Effect of Tidal Interaction with a Gas Disk on Formation of Terrestrial Planets. Icarus, 157, 1, 43–56. DOI:10.1006/icar.2001.6811.

Lin, N. C. D. (2008). The Genesis of Planets. Scientific American, 298, 5, 50–59. DOI:10.1038/scientificamerican0508-50.

Petit, J.-M. & Morbidelli A. (2001): The Primordial Excitation and Clearing of the Asteroid Belt. Icarus, 153, 2, 338–347. DOI:10.1006/icar.2001.6702.

Portegies Zwart, S. F. (2009): The Lost Siblings of the Sun. Astrophysical Journal, 696, L13–L16. DOI 10.1088/0004-637X/696/1/L13.

Raymond, S. N., Quinn, T. & Lunine, J. I. (2007): High-resolution simulations of the final assembly of Earth-like planets 2: water delivery and planetary habitability. Astrobiology, 7, 1, 66–84. DOI: 10.1089/ast.2006.06-0126.

Tanaka, K.L. (1986): The Stratigraphy of Mars. Journal of Geophysical Research, Seventeenth Lunar and Planetary Science Conference Part 1, 91(B13), E139–E158.

Zasada, P. (2013): Generalised Geological Map of Mars, 1:140.000.000. https://astronomynow.com/2015/02/01/4billion-year-old-meteorite-reveals-mars-darker-side/ . Accessed on 21th June 2022

*** (2022): Geology of Mars. National Aeronautics and Space Administration Wiki. https://nasa.fandom.com/wiki/Geology_of_Mars#Impact_craters . Accessed on 21th June 2022

Acknowledgment

Sažetak

Udari malih asteroida i nastanak kratera na Marsu

Istraživane su posljedice udara malog asteroida (manje od 100 T mase) u površinu Marsa. Ustanovljeno je da ni atmosfersko kočenje ni maksimalni dinamički tlak ne utječu bitno na padajuće tijelo. Drugim riječima, asteroid ostaje cjelovit sve do samog udara u tlo. Veličina nastalog kratera ovisi o kinetičkoj energiji asteroida i litološkim svojstvima marsove površine i plitke kore, kao i o kasnijoj atmosferskoj eroziji.

Ključne riječi: Mars, krateri na Marsu, let meteorita

Author's contribution

I.S. analysed the results and prepared graphs. Ž.A. made the numerical flight model and carried out the calculations. T.M. and U.B. made the context of Martian geology on impacts and described impacts origins in the Solar system.

Spatial analytical set of methods applied in the cement raw material deposit, case study exploitation field "St. Juraj – St. Kajo"

Nikolina Bralić[1]; Tomislav Malvić[2]

[1] Cemex Hrvatska d.d, F. Tuđmana 45, HR 21212 Kaštel Sućurac, Croatia, ORCID: 0000-0001-6276-8283

[2] University of Zagreb, Faculty of Mining, Geology and Petroleum Engineering, Pierottijeva 6, HR 10000 Zagreb, Croatia ORCID: 0000-0003-2072-9539

Abstract

Presented research included testing of normal distribution of input data and creating interpolation maps of chemical components as well as cement modules and compared the two approaches for the volume calculation of cement raw material by geological sections and structural maps. The researched area was the exploitation field "St. Juraj – St. Kajo" of raw material for cement production in Southern Croatia. The deposit is situated in Eocene flysch where are seven different lithological units which had been divided technologically based on the proportions of chemical compounds. Based on input data number (from 7 to 36) in total 144 normality tests (Kolmogorov-Smirnov and Shapiro-Wilk) were applied for the chemical analyses (CaO, SiO_2, Al_2O_3, Fe_2O_3, MgO, SO_3, Na_2O, K_2O, $CaCO_3$) and cement modules (lime saturation factor (LSF), silicate module (SM), aluminate module (AM)) in the lithological units. The interpolation had been performed by the Kriging and Inverse Distance Weighting, mapping CaO (%), SiO_2(%) and LSF (-). The interpolation methods had been selected based on normality test passage and the amount of data. The analysed lithological unit for volume calculation was technologically homogeneous but contains interlayers (lenses) of different characteristics which affect the material's quality. Using geological sections for volume calculation is based on the block volume between two parallel vertical sections which is obtained as a product of the mean areas of adjacent sections multiplied by the distance between them. Structural maps represent the calculation of the volume of the observed object under a function $f(x, y)$ defined by a double definite integral. The results of the comparison of the two mentioned approaches for the calculation of the volume of cement raw material for exploitation showed that in this case both approaches are suitable for future use for the purpose of planning the future exploitation of the analysed raw material.

Keywords: cement raw material; flysch; interpolatin maps; geological section; structural maps

1. Introduction

Under spatial analytical set of methods there were three research objectives: (1) statistically test the normal distribution the chemical data (XRF analyses) of nine compounds (CaO, SiO_2, Al_2O_3, Fe_2O_3, MgO, SO_3, Na_2O, K_2O, $CaCO_3$ (%)) and three cement modules (lime saturation factor (LSF), silicate module (SM), aluminate module (AM)) in six different lithological units using Kolmogorov–Smirnov (K–S) and Shapiro–Wilk (S–W) tests; (2) creating interpolation mapps from collected values of CaO (%), SiO_2 (%) and cement module LSF (-) by using two methods: ordinary kriging (OK) and inverse distance weighting (IDW) in three different lithological units; (3) compared the geological section approach for volume calculation of the analysed lithological unit versus the volume estimated as a number of cells between two structural maps. i.e. maps interpolated at the top and bottom of the analysed lithological unit.

The research has been done in the exploitation field "St. Juraj – St. Kajo", owned by Cemex Hrvatska d.d., situated near the town of Split, in the region of Middle Dalmatia, Southern Croatia (**Figure 1**). Total area was 215.85 ha and it is the largest exploitation field of the raw material for cement production in Croatia. Cement production is a complex technological process started with the exploitation of the raw material which are particular lithological units in the deposit. In this research the Eocene flysch is dominant lithology. Dalmatian flysch can reach at outcrops of up to 700 m thickness (**Marinčić, 1981**). The exploitation field had been analysed according to significant lithological variation expressed as 7 different lithological units (after **Pencinger et. al, 2009**; **Bralić and Malvić, 2021**). Based on lithology, the units differ the most in their texture and clay and limestone content.

Corresponding author: Nikolina Bralić
nikolina.bralic@cemex.com
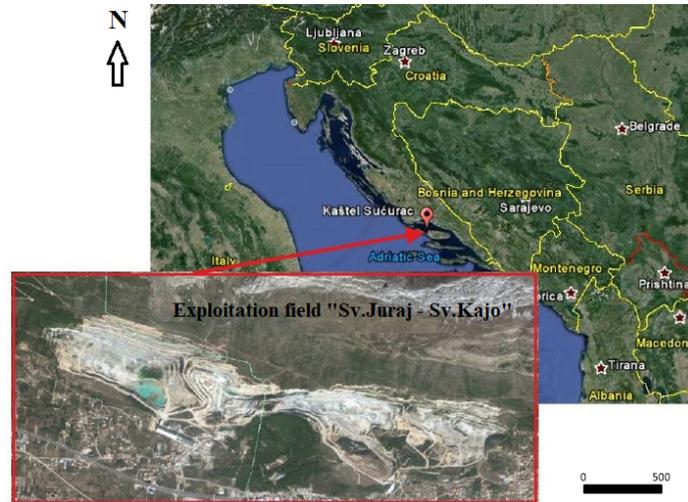
Figure 1: Geographic location of the exploited field "St. Juraj – St. Kajo". (from **Bralić and Malvić, 2021**)

The mentioned lithological units were (**Figure 2**): (1) change between marl, sandstone with alterations of conglomerates (2) limy (calcitic) marl; (3) calcsiltite (clayey limestone); (4) calcarenite; (5) nummulitic marl; (6) debrites and (7) clayey marl. The units (6) are divided into the western and eastern layer while all others into the northern and southern layer (after **Pencinger et. al, 2009**). Based on $CaCO_3$ (%) content lithological units were divided (after **Matijaca and Vujec, 1990**): nummulitic (micro) breccia (77–80); calcarenite and calcsiltite (80–95%); marly limestone (77–80%); limy marl (75–77%); marl and clayey marl (65–74%); marl with redeposited nummulite (highly variable $CaCO_3$); and alternations of marl, sandstone, and limestone (55–70%). In the exploited field the strata direction is NW–SE with a dip towards the N–NE of around 30°–40° (**Pencinger et. al, 2009**).
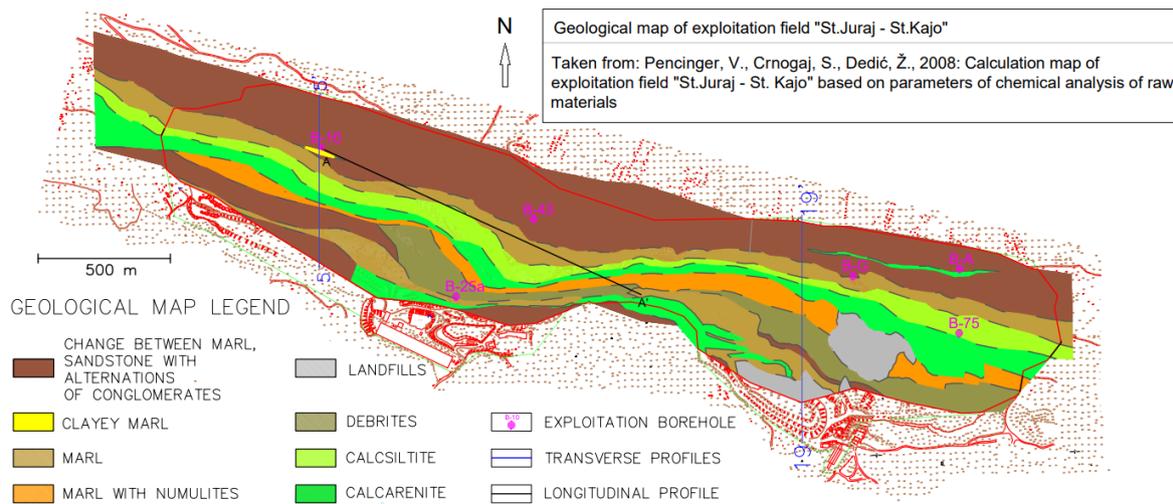
Figure 2: Geological map of the field of exploitation "St. Juraj – St. Kajo". (from **Bralić and Malvić, 2021**)

To meet the requirements of quality control of cement production all described lithological units had been divided technologically based on their chemical compounds taken from exploitation boreholes data (**Figure 3**). Chemical analyses were performed at each 2-meter depth borehole interval. Technologically, four main oxides (CaO, SiO$_2$, Al$_2$O$_3$, Fe$_2$O$_3$) were used as ranking parameters e. g. the weighting ratios of mentioned oxides define three cement modules: LSF (**Eq. 1**), SM (**Eq. 2**), AM (**Eq. 3**) (**Duda, 1985**):

$$LSF = [CaO / (2.8 * SiO_2 + 1.18\ Al_2O_3 + 0.65\ Fe_2O_3)] \tag{1}$$

$$SM = SiO_2 / (Al_2O_3 + Fe_2O_3) \tag{2}$$

$$AM = Al_2O_3 / Fe_2O_3 \tag{3}$$

Based on the LSF values, lithological units were divided into three raw material types on: (1) high raw material (LSF > 110): calcarenite, calcsiltite, nummulite marl, debrites; (2) normal raw material (LSF = 90 – 110): calcite marl, nummulite marl, debrites; (3) low raw material (LSF < 90): marl/sandstone with conglomerate alterations, marl, clayey marl, debrites.
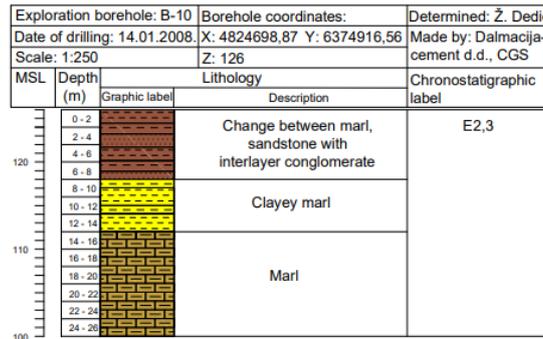
Figure 3: Exploitation borehole B-10. (from **Bralić and Malvić, 2021**)

2. Methods

The first objective in the research was statistical analyses of the chemical data (XRF analyses) of nine chemical compounds (CaO, SiO$_2$, Al$_2$O$_3$, Fe$_2$O$_3$, MgO, SO$_3$, Na$_2$O, K$_2$O, CaCO$_3$ (%)) and three cement modules (LSF, SM, AM (-)), collected in six different lithological units. The data were tested using Kolmogorov–Smirnov (K–S) and Shapiro–Wilk (S–W) tests. The total number of data was n = 214, with a single set including n=4 to n=36. The α value was 0.05. The sets with n < 30 were tested with K–S, and those with n > 30 were tested using the S–W test.

Interpolation maps were performed in three different lithological units and in all units were collected values of CaO (%), SiO2 (%) and cement module LSF (-). The mapping was carried out using two methods: ordinary kriging (OK) and inverse distance weighting (IDW) (**Table 1**). The selection was based on normality tests results. If data had normal distribution the mapping was carried out by OK and if they did not have normality, IDW was applied. The problem of small datasets (n < 15) was nonreliable testing. Consequently, in such a case IDW was (again) applied.

Lithological unit	Statistic		Mapping					
			CaO (%)		SiO2 (%)		LSF (-)	
	Data number (n)	Normality test	Test outcome	Interpolation method	Test outcome	Interpolation method	Test outcome	Interpolation method
Change between marl, sandstone with alternations of conglomerates - norther layer	36	SW	Pass	OK	Pass	OK	Pass	OK
Calcarenite - northern layer	18	KS	Pass	OK	Pass	OK	Pass	OK
Debrites - western layer	7	KS	Pass	IDW	Pass	IDW	Fail	IDW

Table 1. Input data, formality tests results, and interpolation methods for different units (from **Bralić and Malvić, 2021**)

Using geological sections for the volume calculation is based on the calculation of the block volume (V) between two parallel geological sections (P$_1$, P$_2$) which is obtained as a multiplication of the mean areas (Paverage) of adjacent sections

(P_1, P_2) multiplied by the distance between them (d). In case the areas between the adjacent sections differ by less than 50%, the volume of the block between these two sections is calculated according to **Krklec and Zidar, 1989**, i.e., **Eq.4** :

$$V = d/2 * (P_1 + P_2) \tag{4}$$

Where are:
V - block volume (m^3)
P_1, P_2 - section area (m^2)
d - distance between sections (m).

In case the area between sections differs by more than 50 % the volume of the block between the two sections is calculated according **Krklec and Zidar, 1989**, i.e., **Eq. 5**:

$$V = d/3 * (P_1 + P_2 + \sqrt{P_1 * P_2}) \tag{5}$$

The volume below some area expressed with a structural map can be calculated as the sum of finite volumes under the function *f (x, y)* defined by a double definite integral (**Eq. 6**):

$$\text{Volume} = \int_{x_{min}}^{x_{max}} \int_{y_{min}}^{y_{max}} f(x,y) dx\, dy \tag{6}$$

Rules for integrating a function *f (x, y)* between a lower limit (xmin; ymin) and an upper limit (xmax; ymax), over a particular number of intervals, are based on numerical formulas for equally spaced lags (h) (Figure 5). As the number of intervals increases, rules for polynomials of high order are used. The range interval range is denoted by a (xmin) and b (xmax). Approximation of definite integral is obtained using three numerical integration formulas: extended trapezoidal rule (**Eq. 7**), extended Simpson's rule (**Eq. 8**) and extended Simpson's 3/8 rule (**Eq. 9**):

$$\int_{x_1}^{x_N} f(x)\, dx = h \left[\frac{1}{2} f_1 + f_2 + f_3 + \cdots + f_{N-1} + \frac{1}{2} f_N \right] + O\left(\frac{(b-a)^3 f''}{N^2} \right) \tag{7}$$

$$\int_{x_1}^{x_N} f(x)\, dx = h \left[\frac{1}{3} f_1 + \frac{4}{3} f_2 + \frac{2}{3} f_3 + \frac{4}{3} f_4 + \cdots + \frac{2}{3} f_{N-2} + \frac{4}{3} f_{N-1} + \frac{1}{3} f_N) \right] + O\left(\frac{1}{N^4} \right) \tag{8}$$

$$\int_{x_1}^{x_N} f(x)\, dx = h \left[\frac{3}{3} f_1 + \frac{7}{6} f_2 + \frac{23}{24} f_3 + f_4 + f_5 + \cdots + f_{N-4} + f_{N-3} + \frac{23}{24} f_{N-2} + \frac{7}{6} f_{N-1} + \frac{3}{8} f_N \right] + O\left(\frac{1}{N^4} \right) \tag{9}$$

Where are:
N – number of points (-)
O – error for the trapezoidal rule (-)
a – (xmin)
b – (xmax).

The final volume of the observed object was reported as the average of the three values (**Golden Software, Inc.. Surfer 8 User's Guide**).

3. Results

In the research 144 normality tests were performed, 132 K–S and 12 S–W tests, of these 71% of tests passed. The lowest pass level is calculated for the oxides SO_3 (58%) and K_2O (33%) and the cement modules SM (42%) and AM (50%) while the highest pass is attributed to the oxides Al_2O_3, Fe_2O_3, and MgO (92%). If lithological units are considered, the lowest pass can be observed in the marl from the northern layer (25%) and the highest in debrites, from both the western and eastern layers (92%).

The total of 9 interpolation maps were created. The lithological unit – change between marl, sandstone with alterations of conglomerates, in its northern layer, was interpolated by OK, for variables CaO (%), SiO2 (%), and LSF (-). The layer

width was 200–300 m with 35 data. The experimental variogram was calculated using the nugget C = 0, sills CaO = 3, SiO2 = 5, LSF = 145, range a = 240 m, total calculation distance h = 1033 m, number of classes 15, and tolerance 45°. The approximation was carried out using the exponential model. Variograms defined searching ellipsoid with axes 240 × 50 m, directions -15° and 105°, and anisotropy factor 4.8. The maps of CaO (%), SiO2 (%), and LSF (-) for the lithological unit change between marl, sandstone with alterations of conglomerates in the northern layer are shown in **Figures 4–6**.
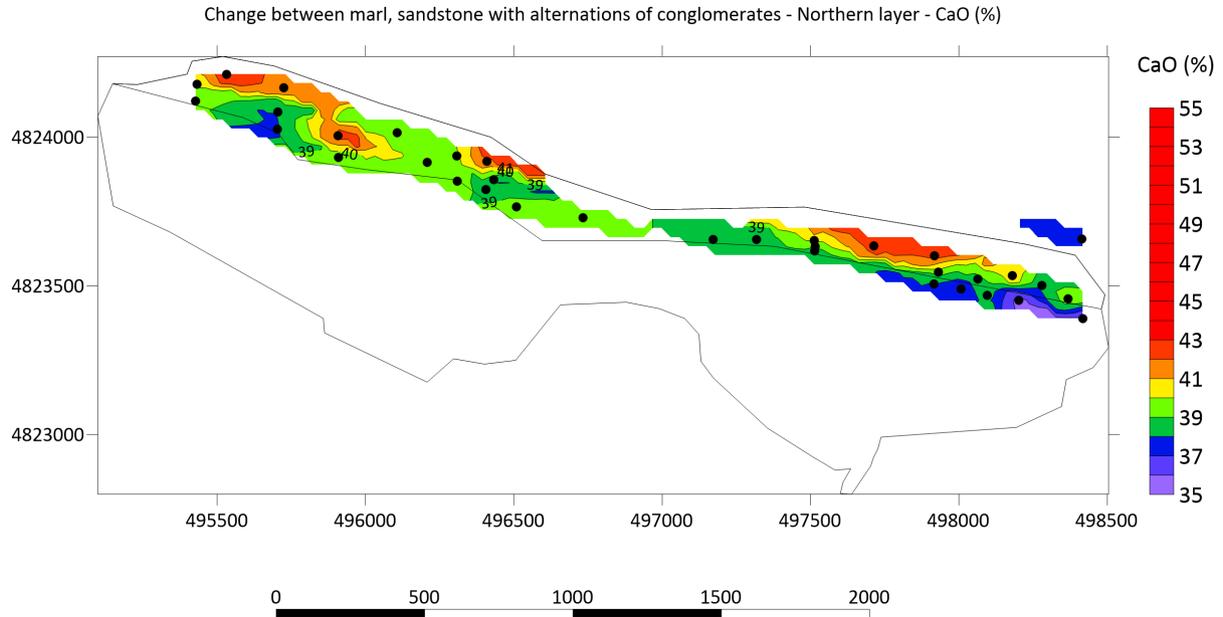
Figure 4: CaO (%) distribution in the lithological unit change between marl, sandstone with alterations of conglomerates, northern layer (boreholes are black dots). (from **Bralić and Malvić, 2021**)
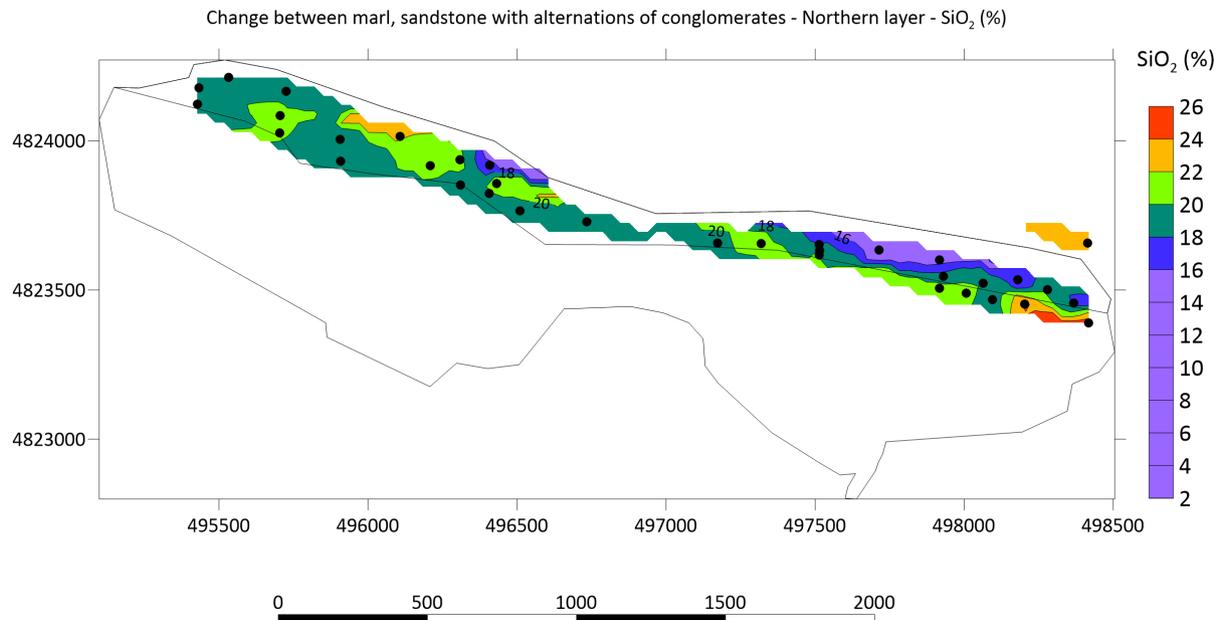
Figure 5: SiO2 (%) distribution in the lithological unit change between marl, sandstone with alterations of conglomerates, northern layer (boreholes are black dots). (from **Bralić and Malvić, 2021**)

Change between marl, sandstone with alternations of conglomerates - Northern layer - LSF (-)
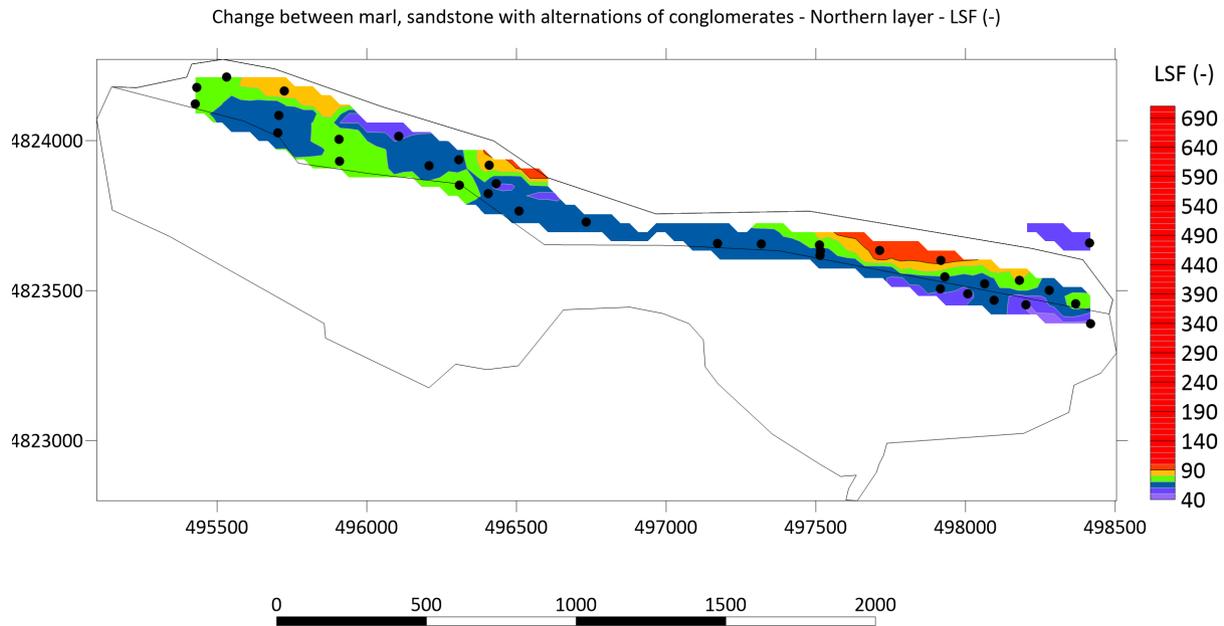
Figure 6: LSF (-) distribution in the lithological unit change between marl, sandstone with alterations of conglomerates, northern layer (boreholes are black dots). (from **Bralić and Malvić, 2021)**

The three maps in the lithological unit calcarenite, in the northern layer, showed values of CaO (%), SiO2 (%), and LSF (-). The layer width was 50–150 m with 18 data. All were interpolated by OK, using the nugget $C_0 = 0$, sill $C(CaO)$ = 1, $C(SiO_2)$ = 1, $C(LSF)$ = 15,000, range a = 320 m, total calculation distance h = 1033 m, number of classes 17, and tolerance 45°. The experimental variogram was approximated with the exponential model. The searching ellipsoid had axes of 320 × 50 m with strikes -15° and 105° and an anisotropy factor 6.4.

The last three maps were interpolated for the lithological unit debrites, in the western layer. The layer width was 30–200 m with 7 data. Interpolation for CaO (%), SiO$_2$ (%) and LSF (-) was carried out using IDW. Power exponent was 2, searching circle 335 m, and anisotropy = 1 (no anisotropy). The volume calculation procedure using the geological section for the lithological unit is shown in steps:

1. Prepare geological sections (example 5-5' and 19-19' at **Figure 1**)
2. Determine the area (m²) of the lithological unit as well as for interlayers from each geological section (P) on each geological section;
3. Determine the distance between the main and auxiliary sections (d) from the geological map (**Figure 1**);
4. Calculate the volume of the lithological unit (Vunit) according to Equations (4) and (5);
5. Calculate the volume of interlayers (Vinterlayers) according to Equations (4) and (5);
6. For each geological section where it is necessary subtract the value calculated in step 5 from the value calculated in step 4.

Steps in the procedure for the volume calculation by structural maps:

1. Prepare data from 35 exploration boreholes (**Pencinger et. al, 2009**) from which are determined coordinates (x, y, z) of the lithological unit top and bottom, as well as of interlayers (**Figure 3**);
2. Interpolated top and bottom structural maps using the OK with the following values (**Figure 7**):
2a. The experimental variogram for the top surface was calculated using the nugget $C = 0$, sills 400, range a = 240 m, total calculation distance h = 1033 m, number of classes 15, and tolerance 45°. Variogram defined searching ellipsoid with main axis 1550 m and anisotropy factor 2
2b. The experimental variogram for the bottom surface was calculated using the nugget $C = 0$, sills 520, range a = 240 m, total calculation distance h = 1033 m, number of classes 15, and tolerance 45°. Variogram defined searching ellipsoid with main axis 1550 m and anisotropy factor 4
3. Interpolate top and bottom for interlayers using (due to a low number of data) IDW. Power exponent was 2, searching circle 335 m, and anisotropy = 1
4. Calculate the volume of the lithological unit using top and bottom structural maps of the lithological unit and its interlayers.

5. Process the volumes with the **Equations 7, 8** and **9**;

6. Calculated averages for **Equations 7, 8** and **9**;

7. Subtract the volumes of interlayers from the volume of the lithological unit.
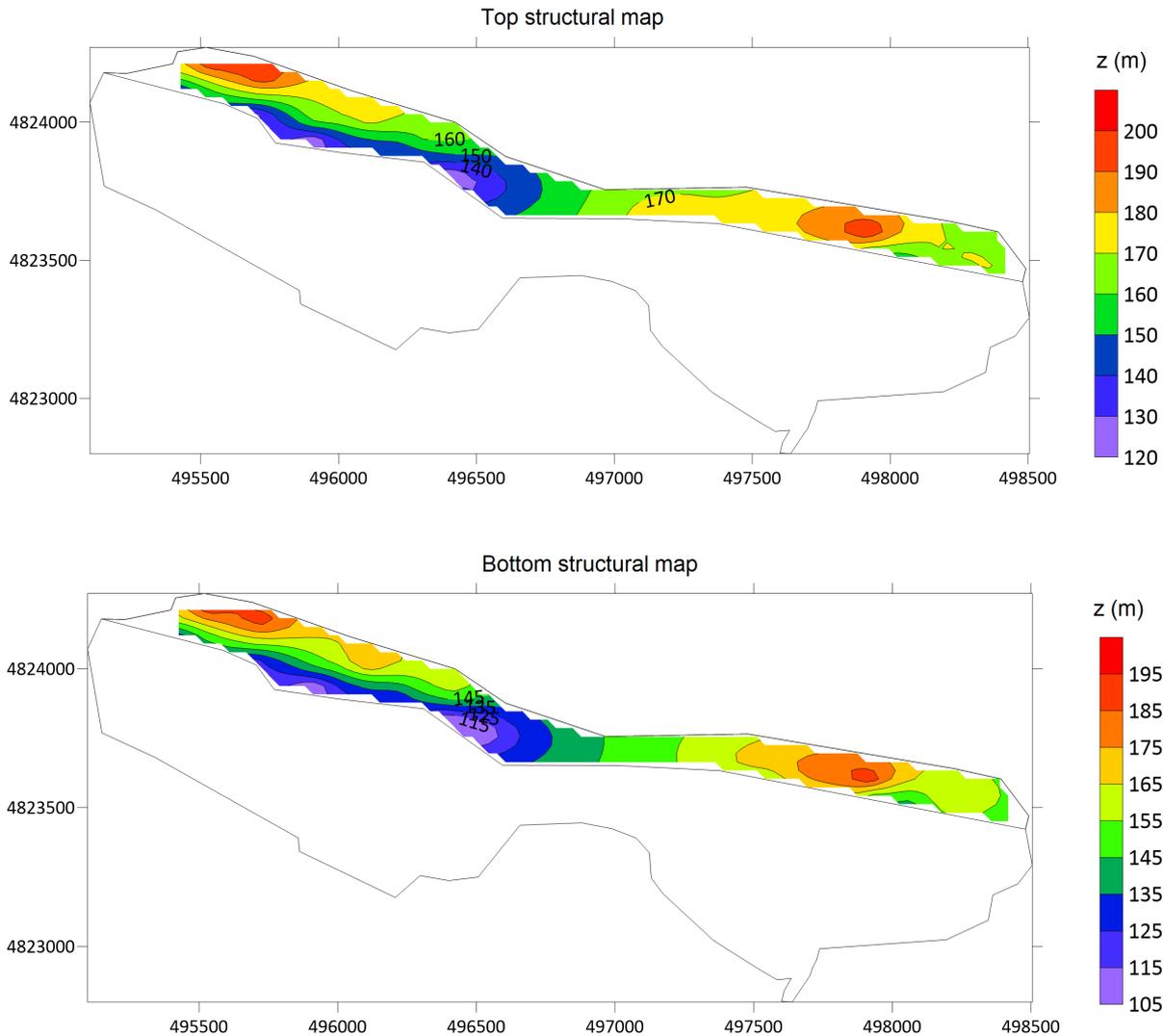
Figure 7: Top and bottom interpolation maps of the lithological unit change between marl, sandstone with alterations of conglomerates

The existing network of 35 properly distributed exploitation boreholes, by the geological situation, in the analysed lithological unit with both approaches, by geological sections and by structural maps, gave satisfactory results and an acceptable difference of 15 %.

The calculation of the volume of very small areas, such as the example of interlayers is extremely unreliable using the structural map due to the small number of input data. The differences in the input data are very small so their structural is hard clearly display on the same scale as values of the main units. The volume of interlayers, based on structural maps, was almost twice bigger than the same values obtained by the geological sections approach.

5. Conclusions

In this research three objectives were presented: (1) the normal distribution tests for the chemical data of nine compounds (CaO, SiO_2, Al_2O_3, Fe_2O_3, MgO, SO_3, Na_2O, K_2O, $CaCO_3$ (%)) and three cement modules (lime saturation factor (LSF), silicate module (SM), aluminate module (AM)) in six different lithological units using Kolmogorov–Smirnov (K–S) and Shapiro–Wilk (S–W) tests; (2) creating interpolation mapps from CaO (%), SiO_2 (%) and LSF (-) by

two methods: ordinary kriging (OK) and inverse distance weighting (IDW) in three different lithological units; (3) compared the geological section approach for volume calculation of the one analysed lithological unit versus the volume estimated as a number of cells between two structural maps.

The research area was the exploitation field for cement raw material "St. Juraj – St. Kajo" situated in the region of Middle Dalmatia, Southern Croatia. The exploitation of the cement raw material which are particular lithological units in the deposit represents the beginning of the cement production. The exploitation field is part of Eocene flysch and based on lithology had been divided on 7 different lithological units, which differ the most in their texture and clay and limestone content and consequently in $CaCO_3$ content. All lithological units were divided into the northern and southern layer except the lithological unit debrites divided into the western and eastern layer. Lithological units had been divided technologically based on their chemical compounds, e. g. chemical analyses at each 2-meter depth exploitation borehole interval. Technologically, the weighting ratios of four main oxides (CaO, SiO_2, Al_2O_3, Fe_2O_3) define three cement modules: LSF, SM and AM.

Chemical analyses of oxides and cement modules of all seven lithological units gave the 144 datasets which were analysed with formal normality tests, namely the Kolmogorov–Smirnov and Shapiro–Wilk tests. In total, 71% of datasets (n from 7 to 35) showed normal distribution.

Three lithological units were interpolated for distribution of CaO, SiO_2 (%) and LSF (-). The first one, lithological unit change between marl, sandstone with alterations of conglomerates (with a layer width of 200–300 m and 35 data) showed that CaO and LSF values slightly decreased toward the south, but values of SiO_2 varied by 18–20%. The second one, the lithological unit calcarenite (with a layer width of 50–150 m and 18 data) showed that CaO concentrations were slight, but SiO_2 was highly variable throughout the unit. However, the LSF values were gradual, but very variable which is crucial information for quality control. The last unit, the lithological unit debrites was the most irregular (with a width of 30–200 m and 7 datapoints), with the largest variations of all three variables.

In the lithological unit that covered the largest area in the field, change between marl and sandstone with alternations of conglomerate, two approaches for calculating its volume were applied; geological sections and structural maps. Although technologically it is a homogeneous unit locally contains interlayers or lenses of different lithological and thus technological characteristics. Importance of the present interlayers is that uniform material quality should not be expected at that location. The volume of interlayers was subtracted from the volume of the lithological unit in both approaches. The difference between calculated volumes obtained by the two presented approaches was 15 % which is acceptable in this case. With more depth data and more geological sections, the differences between these two approaches will be less. For this reason, in the case of a very small amount of input data, as is the case with the calculation of interlayers, the method of structural maps is unreliable. The obtained difference between approaches is deviation of structural map approach in comparison to traditionally used geological section approach. What makes the difference is the customer's need for precision. Drawing of geological sections still ranks very high among researchers even though anyone who has encountered it knows how exhaustive and time-consuming it is. But with a better understanding of the methods implemented in computer programs, one gains confidence in their reliability and one should not hesitate to use them.

The statistical results in this research are the most extensive statistical and mapping analysis of an exploited cement raw material in the research area in the last decade. It was possible to estimate chemical compounds and cement modules in any part of the field for the analysed lithological units. This is important because the final raw material, which is main input material for technological process of cement production, is obtained by mixing different raw materials exploited as different lithological units. With more detailed monitoring and knowledge of the adequate mixture, the production requirements set by the quality control are better met. One of the ways of monitoring is certainly the calculation of the amount of cement raw material for exploitation, which is very important for future use for the purpose of planning the future exploitation of the analysed raw material.

6. References

Bralić, N.; Malvić, T. (2022): Interpretation of Chemical Analyses and Cement Modules in Flysch by (Geo)Statistical Methods, Example from the Southern Croatia. Processes, 10, 813, doi:10.3390/pr10050813.

Duda, W.H. (1985): Cement-Data-Book: International Process Engineering in the Cement Industry; Bauverlag: Gütersloh, Germany.

Krklec, N.; Zidar, M. (1989): "Area" - Program for the estimation of the mineral reserves. Rudarsko-Geološko-Naftni Zbornik, 1, 35-39.

Marinčić, S. (1981): Eocene flysch of the Adriatic belt. Geološki Vjesnik, 34, 27–38. (In Croatian)

Matijaca, M.; Vujec, S. (1990): Statistical interpretation of raw materials for the cement industry in Split (in Croatian with English abstract). Rudarsko-Geološko-Naftni Zbornik, 2, 75–81.

Pencinger, V.; Ožanić, M.; Crnogaj, S.; Dedić, Ž.; Jurić, A. (2009): Study on the Reserves of Mineral Raw Materials for the Production of Cement in the Exploitation Field "St. Juraj—Sv. Kajo "- Restoration; Croatian Geological Survey: Zagreb, Croatia. (In Croatian, un published)

Internet sources:

Golden Software, Inc.. Surfer 8 User's Guide, Contouring and 3D Surface Mapping for Scientists and Engineers. 2002. URL: https://manualzz.com/doc/4237921/surfer-8-user-s-guide (accessed on 22 April 2022).)

Acknowledgment

Sažetak

Prostorno analitički skup metoda primijenjenih u ležištu mineralne sirovine za proizvodnju cementa, studija slučaja eksploatacijsko polje „Sv. Juraj – Sv. Kajo"

Istraživanje je uključivalo ispitivanje normalne razdiobe ulaznih podataka i interpolacijskih karata kemijskih komponenti kao i cementnih modula te usporedbu dvaju pristupa za proračun volumena mineralne sirovine za proizvodnju cementa prema geološkim presjecima i strukturnim kartama. Područje istraživanja bilo je eksploatacijsko polje mineralne sirovine za proizvodnju cementa "Sv. Juraj – Sv. Kajo" u Južnoj Hrvatskoj. Ležište se nalazi u eocenskom flišu u kojem se razlikuje sedam različitih litoloških jedinica koje su tehnološki podijeljene na temelju omjera kemijskih komponenti. Na temelju broja ulaznih podataka (od 7 do 36) primijenjena su ukupno 144 testa normalnosti (Kolmogorov-Smirnov i Shapiro-Wilk) na podatcima kemijskih komponenti (CaO, SiO_2, Al_2O_3, Fe_2O_3, MgO, SO_3, Na_2O, K_2O, $CaCO_3$) i cementnih modula (SZ, SM, AM) u litološkim jedinicama. Interpolacija je provedena krigiranjem i metodom inverzne udaljenosti za kartiranje vrijednosti CaO (%), SiO_2(%) i SZ (-). Metode interpolacije odabrane su na temelju prolaska na testu normalnosti i broja podataka. Promatrana jedinica za proračun volumena bila je tehnološki homogena, ali sadrži međuslojeve (leće) različitih karakteristika što utječe na kvalitetu materijala. Korištenje geoloških presjeka za izračun volumena temelji se na volumenu bloka između dvaju paralelnih vertikalnih presjeka koji se dobiva kao umnožak srednjih površina susjednih presjeka pomnoženih s razmakom između njih. Strukturne karte predstavljaju proračun volumena promatranog objekta pod funkcijom f (x, y) definiranom dvostrukim određenim integralom. Rezultati ovog istraživanja predstavljaju pouzdane buduće prognoze za eksploataciju mineralne sirovine.

Ključne riječi: mineralna sirovina za proizvodnju cementa; fliš; interpolacijske karte, metoda geoloških presjeka; strukturne karte

Author's contribution

Nikolina Bralić (quarry specialist; PhD student): provided the conceptualization, formal analysis, investigation, software, validation, visualization, writing—original draft, writing—review and editing for this research. **Tomislav Malvić** (full professor; a permanent scientific advisor) provided the conceptualization, formal analysis, supervision, validation, and editing for this research.

Ilmenite, the raw material of the future

Adam Jan Zwierzyński[1,2]; Albert Złotkowski[3]; Marek Leszek Solecki[4]; Rafał Balicki; Weronika Binkowska, Adam Janiak, Hanna Edelmüller, Aleksandra Gardynik, Magdalena Leśniowska

[1]AGH University of Science and Technology, 30 Mickiewicza Ave, 30-059 Krakow, Poland, zwierzyn@agh.edu.pl, ORCID: 0000-0002-2568-6446

[2]Solar System Resources Corporation Sp. z o. o., Szlak Street 77/222, 31-153 Krakow, Poland

[3]AGH University of Science and Technology, 30 Mickiewicza Ave, 30-059 Krakow, Poland, azlot@agh.edu.pl, ORCID: 0000-0002-7085-2693

[4]AGH University of Science and Technology, 30 Mickiewicza Ave, 30-059 Krakow, Poland, mlsoleck@agh.edu.pl, ORCID: 0000-0001-8637-8300

Abstract

The article is about the extraction of the helium-3 isotope from lunar deposits. The authors presented information about the presence of helium-3 deposits on the Moon, as well as the mechanism of their formation. The role of ilmenite in helium storage is presented. The use of helium-3 in fusion power and the reasons why it is considered a raw material of the future was also discussed.

Keywords: helium-3; fusion; ilmenite; moon; space mining

1. Introduction

The world is facing with huge climate crisis. The data of scientists **(climate.nasa.gov)** are highly disturbing and indicate a disturbance in the energy balance of our planet. There are high hopes for the development of revenable sources of energy and this is undoubtedly the right path, but it will not solve all of energy problems. Moreover, the daily production from these sources may fluctuate by up to 90%. The solution would be electricity storage. So far, mankind has not invented methods of cheap electricity storage on an industrial scale - the current solutions are still too expensive. Moreover, the weather conditions in February 2021 in Germany and in Texas showed that the supply chain of electricity from renewable sources of energy (solar and wind farms) could collapse.

If we really want to build green networks based on renewable sources of energy (in order to minimize the carbon footprint), we must make a quick breakthrough in electricity storage or supplement the energy mix with additional sources of electricity that will stabilize the power grid in times of decline in energy production. Nuclear energy can be such a stabilizer. This is one of the reasons why the Polish Government plans to build several nuclear power plants in Poland.

However, to meet the future needs of all mankind, whose energy needs are doubling every 25 years, and to prevent a climate catastrophe, we need to master fusion energy. For decades, research has been conducted in the world on controlled thermonuclear fusion. After all, in recent years there has been a major breakthrough, especially in materials and high temperature superconductor. The most famous project is ITER. It is an important international research project, but the price is estimated at $ 20 billion **(ScienceMag.Org)**. Start-up`s and companies such as Chevron, Microsoft, Amazon (Jeff Bezos), and Eni are working at this problem. They invest in fusion energy. General Fusion can be an example of a startup working on fusion. The company has signed a contract with the British Government and it is planned to open a pilot commercial **(General Fusion Webpage)** industrial plant by 2025. There are more examples of such companies. There is Helion Energy **(Helion Energy Website)** and there is also small American start-up MIFTI **(Bloomberg)**.

The first fusion reactors will probably use first generation fusion fuels, which will follow the reaction **(Harms et al. 2000)** described in **Equation 1**. This is the fusion reaction requiring the lowest ignition temperature. Unfortunately, tritium is difficult to produce and the price is much more higher than even the ultra-rare isotope helium-3 (^{3}He) on

Corresponding author: Adam Jan Zwierzyński
e-mail address: zwierzyn@agh.edu.pl

Earth. The half-life of tritium is 12.33 years, which means that this energy resource cannot be stored in the long term. Second generation fuels will follow the reaction of **Equation 2** and **Equation 3**.

$$^{2}H + \ ^{3}H \rightarrow n + \ ^{4}He + Energy \ (17.6 \ MeV) \tag{1}$$

$$^{2}H + \ ^{2}H - (50\%) \rightarrow n + \ ^{3}He + Energy \ (3.3 \ MeV) \tag{2}$$

$$^{2}H + \ ^{2}H - (50\%) \rightarrow \ ^{1}H + \ ^{3}H + Energy \ (4 \ MeV) \tag{3}$$

Where are:

n – neutron,
^{1}H – hydrogen (hydrogen isotope, proton),
^{2}H – deuter (hydrogen isotope),
^{3}H – tritium (hydrogen isotope),
^{3}He – helium-3 (helium isotope),
^{4}He – helium-4 (helium isotope),

The disadvantage of the first- and second-generation fuels is the production of neutrons. In classical nuclear energy using the nuclear fission reaction, the produced neutrons cause gradual degradation of the materials they react with (e.g. shielding materials). In the case of thermonuclear reactions, the neutron flux will be much higher, which will result in rapid degradation of the reactor shell materials and the need for repairs every few years. It will raise the cost of electricity production. Additionally, the neutrons reacting with the shielding material will induce secondary nuclear reactions, resulting in a trace of radioactivity. Therefore, it will not be a 100% ecological source of energy that humanity dreams of.

The solution to the described problem are third-generation fuels in which the reaction takes place according to the patterns (6) described in **Equation 4** and **Equation 5**. In both of these reactions, the fuel component is helium-3 (^{3}He). In such reactions, energy can be produced directly without the need for gas turbines and a thermodynamic medium circulation system, which increases the efficiency of the entire system. Fusion reactors based on He-3 as fuel can be small, compact and will be competitive with classical nuclear energy.

$$^{2}H + \ ^{3}He \rightarrow \ ^{1}H + \ ^{4}He + Energy \ (18.4 \ MeV) \tag{4}$$

$$^{3}He + \ ^{3}He \rightarrow \ ^{1}H + \ ^{1}H + \ ^{4}He + Energy \ (12.9 \ MeV) \tag{5}$$
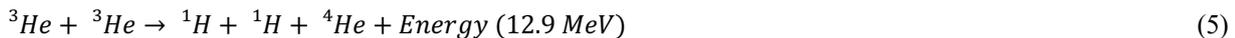
The first fusion reactors will not use third-generation fuels based on helium-3. The first reason is the ignition temperature, which is higher than that of the first generation fuels - a thermonuclear reaction is more difficult to obtain. The second reason is that helium-3 is an ultra-rare isotope on Earth.

The helium-3 isotope, however, is more abundant on the moon. There are other aneutronic fusion reactions that do not require the use of helium-3, as described in Equation 6, which uses the boron-11 isotope common on Earth. However, the ignition temperature for such a reaction is higher than for all of the aforementioned thermonuclear reactions, and obtaining such a reaction is a much higher technological challenge. However, there is a start-up called Marvel Fusion **(Marvel Fusion Website)** that claims to have discovered a quantum phenomenon that is independent of temperature and can be used to build fusion reactors based on this reaction.

$$^{1}H + \ ^{11}B \rightarrow 3 \ ^{4}He + Energy \ (8.7 \ MeV) \tag{6}$$

For these reasons, helium-3 will be probably a highly sought-after resource in the future. It is also needed in other industries (e.g., neutron detectors for the detection of radioactive substances at airports, border crossing points, etc.; medical imaging; cooling of quantum computers). There is already a shortage of this raw material on the market, and its price is 16.6 M\$/kg.

Zwierzyński, A. J.; Złotkowski, A.; Solecki, M. L.; Balicki, R.; Binkowska, W; Janiak A.; Edelmüller, H.; Gardynik, A; Leśniowska, M.

2. Helium-3 on the Moon

Helium is an element that occurs on Earth in small amounts, and its isotope helium-3 is an ultra-rare resource. Global production of He-3 comes mainly from the decay of tritium used in fusion weapons. The demand for this raw material increased significantly after the attacks of September 11, 2001 - it is used in the production of detectors detecting smuggling of radioactive materials.

There are studies showing that **(Niechciał et al., 2020)** volcanoes can emit helium-containing gases with a ^{3}He content of between 14 and 30 ppm (parts per million). A similar concentration of the helium-3 isotope can be found in young basalt rocks. However, these are not large deposits and are difficult to exploit. The ^{3}He isotope is also present in the Earth's atmosphere. At sea level, its concentration is 7.27 ± 0.20 parts per trillion volumes. In the 1940s and 1950s, research was conducted on the possibility of recovering ^{3}He from the Earth's atmosphere. They proved that this is an economically unprofitable process. Helium-3 can also **(Niechciał et al., 2020)** be obtained from natural gas containing natural helium. World helium production in 2014 from natural gas was 20,000 tons per year, which with an average ^{3}He concentration of 0.2 ppm would give about 2 kg of ^{3}He per year. In turn, the global production of helium-3 from the decay of tritium (an isotope of hydrogen) amounts to about 20 kg.

If not on Earth, then perhaps helium-3 should be searched for in space. The Moon is a promising place because of physical conditions. For billions of years, the sun has been sending the so-called solar wind, which is composed of electrically charged particles. It also includes helium atomic nuclei (both of the ^{4}He isotope and the ^{3}He isotope). The ^{3}He/^{4}He ratio is about 1: 10,000. The Earth has a magnetic field that deflects the solar wind and an atmosphere that additionally protects the Earth's surface from the solar wind. The situation is different for the Moon, which has a residual magnetic field and no atmosphere. Solar wind particles reach the surface of the Moon and are absorbed by the minerals that occur there, including regolith.

The mechanism of the formation of helium deposits on the Moon is described in publication **(O'Reilly, 2016)**, although the actual mechanism is more complex. In item **(Niechciał et al., 2020)**, the concentration of helium-3 in selected places on the Moon is presented, the average value of which is 20 ppb/m2 (particles per billion per square meter). With such a concentration, it is necessary to process 150 tons of regolith to obtain 1 gram of the helium-3 isotope. It is technically feasible, although ineffective and one should look for places with a higher concentration. The economy of the process is improved by the fact that by processing such large amounts of regolith, other substances are obtained in large amounts. An example of a device that was designed to obtain helium-3 from lunar regolith processing is the Mark IV device concept **(Olson 2013)**.

Scientists believe there may be regions with higher helium-3 concentrations on the Moon. The results of the Change-1 probe show that **(Fa and Jin 2010; Lunar Networks)** there are regions on the Moon with a concentration of ^{3}He of 80 ppb / m^2 and more. In turn, work **(O'Reilly 2016)** presents the relationship between helium (including the helium-3 isotope) and ilmenite. Due to its crystal structure, this mineral binds helium up to 100 times better than ordinary lunar regolith.

During a day on the Moon, its surface heats up to 120 degrees Celsius in equatorial regions. At this temperature, the regolith gives off part of the accumulated helium. Ilmenite, due to its crystal structure, binds helium more tightly and gives it back less. Therefore, it can be expected that higher helium-3 concentrations will occur in areas close to the poles. Helium (including helium-3) in concentrations profitable for exploitation should be expected on the Moon mainly in places where ilmenite is present. **Song et al. (2021)** present simulations of the thermal extraction of helium-3 from the lunar ilmenite. It is one of the first works of this type in the literature.

How much helium-3 is on the Moon? There are many estimates depending on the model adopted. In order to be able to answer this question precisely, in-situ research is needed. All other methods are just an estimate. What is certain is that the solar wind continues to deposit helium on the Moon's surfaces. This is the reason why some researchers refer to helium-3 deposits on the Moon as a renewable resource. When estimating resources, models of the changes in the Moon's magnetic field over time, and more specifically when the Moon's magnetic field have disappeared, are important. The latest research **(science.org)** indicates that it could have been much earlier than previously thought. This shows how little we know about the Moon's evolution, and how accurately estimating the Moon's helium-3 deposits without in-situ research can be highly biased.

3. Ilmenite

Chemical formulation - $FeTiO_3$. Theoretically, it contains 52,56% TiO_2 and 47,34% FeO. It can contain up to 14% of Mn. When roasted, it becomes magnetic. It is resistant to the HCl. A component of igneous rocks (gabbro, diabase, etc.) in which it accompanies magnetite or titanomagnetite. It occurs in significant amounts in some syenite pegmatites.

Zwierzyński, A. J.; Złotkowski, A.; Solecki, M. L.; Balicki, R.; Binkowska, W; Janiak A.; Edelmüller, H.; Gardynik, A; Leśniowska, M.

Resistant to weathering, it passes into the sands, sometimes creating concentrations containing up to 60% ilmenite (ilmenite sands) **(Bolewski, 1982)**.

Deposits of ilmenite sands are mined off the coast of Kerala (India), Ceylon, Florida (USA), Brazil, Russia and other countries. Ilmenite crystals were found in the Ilmenite Mountains in the Ural Mountains (Russia) **(Bolewski, 1982)**. In Poland, ilmenite occurs in alkaline and neutral igneous rocks near Nowa Ruda in Lower Silesia. It occurs in the pegmatites of Łomnica and Szklarska Poręba near Jelenia Góra. It was found in the gold-bearing sands near Złotoryja, in the sands of Dunajec near the Červený Kláštor in Pieniny Mountains (Slovakia) **(Bolewski, 1982)**.

4. Project X-GOMOON00

In order to develop an effective technology for the extraction of helium-3 from ilmenite, firstly it is necessary to test the ability of this mineral to absorb and release helium (which also includes the helium-3 isotope). It is also necessary to investigate the conditions under which these processes take place and what are the optimal conditions. The specificity of the lunar environment should be taken into account here, as well as the technological limitations of the devices used on the lunar surface. Such research is already carried out by several teams around the world, including computer simulations. However, it is still an innovative research area.

Student of Space Mining Assciation "COSMODRILL" at the Faculty of Drilling, Oil and Gas of the AGH in cooperation with Solar System Resources Corporation Sp. z o. o. has obtained a grant to conduct the research. The project "X-GOMOON00: Lunar ilmenite, a raw material of the future" is a response to contemporary civilization challenges related to searching for new energy resources in space, building industrial space infrastructure. The project will be implemented in cooperation with the industrial partner Solar System Resources Corporation Sp. z o. o. - a Polish spin-off from AGH dealing with space mining and energy transformation. If the results are industrially useful, the results will be commercialized by Solar System Resources Corporation Sp. z o. o. The project aims to:
1) study the properties of ilmenite as a material that is a valuable reservoir of the helium-3 isotope on the Moon
2) investigating the possibility of recovering helium-3 from ilmenite in lunar conditions,
3) investigating the possibility of recovering titanium and iron from ilmenite in lunar conditions,
4) investigating the possibility of recovering oxygen from ilmenite under Moon conditions.

5. Methods

The research will be carried out on Earth's ilmenite, which has a chemical composition comparable to that found on the Moon. The helium-3 isotope will not be used for research, as there is very little of it on Earth and it is extremely expensive at 16.6 M $ / kg. Natural helium will be used for this purpose. It is a mixture of helium-4 (the dominant isotope) and helium-3 (the trace isotope). This corresponds to the conditions on the Moon - ilmenite captures helium atoms from the solar wind, i.e. both helium-4 (dominant isotope) and helium-3 (trace isotope). The ^{3}He / ^{4}He ratio in the solar system is about 1: 10,000. It is not a constant isotopic ratio in the universe and it may differ in other planetary systems. The extraction of helium-3 from ilmenite (or even regolith) is thus actually extraction of natural helium followed by isotope separation. The project will use the laboratory infrastructure and equipment available at the Faculty of Drilling, Oil and Gas of the University of Science and Technology (AGH) and cooperating units (laboratories) of AGH.

Ilmenite samples will be subjected to thermal (annealing), physico-chemical processes (helium injection under pressure, recovery of helium from an annealed sample, reduction of oxides) depending on the purpose (among the above-mentioned objectives 1 - 4) of a specific study. Before each test, the sample will be prepared, weighed, examined under a microscope and examined in terms of chemical composition with specialized devices. An important element of sample preparation will also be the removal of moisture and its degassing to obtain conditions as close to space conditions as possible. The level of helium uptake and subsequent recovery will be measured using ultra-sensitive scales. Since, it is so important that the subsequent samples of the material are as pure ilmenite as possible, have a similar composition, and are not rocks (or powder) containing a large admixture of other minerals, which would reduce the accuracy of the analyses and make it impossible to compare them.

6. Conclusions

Humanity faces a historic climate and energy challenge. If it is resolved (or not), it will decide whether the next generations will experience a prosperous future and progressive enrichment, or a stagnation and a less optimistic future. The pressure of environmental groups will increase and the society is becoming more and more aware of the negative effects of climate change. The prices of high-carbon solutions will be more and more burdensome for societies, forcing

Zwierzyński, A. J.; Złotkowski, A.; Solecki, M. L.; Balicki, R.; Binkowska, W; Janiak A.; Edelmüller, H.; Gardynik, A; Leśniowska, M.

the acceleration of the energy transformation. The war in Ukraine will also force the search for alternative energy solutions to increase security. On the other hand, enormous technological progress is taking place in the energy, electromobility and space industries. All these factors mean that revolutionary changes in the energy sector should be expected in the near future. Many projects and initiatives that were previously not possible due to technological, economic and geopolitical reasons will receive the green light. Perhaps energy based on fusion reactors using helium-3 from lunar deposits may become a fact, and lunar ilmenite saturated with helium may become the strategic raw material of tomorrow.

7. References

Papers:

Fa, W.; Jin, Y. (2010) Global inventory of Helium-3 in lunar regoliths estimated by a multichannel microwave radiometer on the Chang-E 1 lunar satellite. Chinese Sci. Bull. 2010, 55, 4005–4009.

Niechciał, J.; Banat, P.; Kempiński, W.; Trybuła, Z.; Chorowski, M.; Poli´nski, J.; Chołast, K.; Kociemba, A. (2020): Operational Costs of He3 Separation Using the Superfluidity of He4. Energies 2020, 13, 6134.

Song, H.; Zhang, J.; Sun, Y.; Li, Y.; Zhang, X.; Ma, D.; Kou, J. (2021): Theoretical Study on Thermal Release of Helium-3 in Lunar Ilmenite. Minerals 2021, 11, 319.

Books/thesis:

Bolewski A. (1982). Mineralogia szczegółowa. Wydawnictwa Geologiczne, Warszawa, 542pp. (in Polish)

Harms, A.A.; Schoepf, K.F.; Miley, G.H.; Kingdon, D.R. (2000): Principles of Fusion Energy: An Introduction to Fusion Energy for Students of Science and Engineering. – World Scientific Publishing Co. Pte. Ltd.: Singapore, 8–11 p.

O'Reilly B. (2016): LUNAR EXPLORATION FOR HE-3 - The Ohio State University, URL: https://core.ac.uk/download/pdf/159567253.pdf (accessed 16th June 2014)

Internet sources:

URL: https://climate.nasa.gov/scientific-consensus/ (accessed 16th June 2014)

ScienceMag.Org—UPDATED: Panel Backs ITER Fusion Project's New Schedule, but Balks at Cost. URL: //www.sciencemag.org/news/2016/04/updated-panel-backs-iter-fusion-project-s-new-schedule-balks-cost/ (accessed 16th June 2022).

General Fusion Webpage. URL: https://generalfusion.com/2021/06/general-fusion-to-build-its-fusiondemonstration-plant-in-the-uk-at-the-ukaea-culham-campus/ (accessed 16th June 2022).

Helion Energy Website. Available online: https://www.helionenergy.com/ (accessed 16th June 2022).

Bloomberg: US Nuclear Corp.: Oil Companies Under Pressure by Activists, Investing in Fusion Energy: US Nuclear and MIFTI Ready with Fusion. URL: https://www.bloomberg.com/press-releases/2021-06-03/us-nuclear-corp-oil-companiesunder-pressure-by-activists-investing-in-fusion-energy-us-nuclear-and-mifti-ready-with-fusion (accessed 16th July 2021).

Marvel Fusion Website. URL: https://marvelfusion.com/ (accessed on 16th June 2022)

Olson, A. The Mark IV (2013): A Scalable Lunar Miner Prototype, Conference: 64th International Astronautical Congress, Beijing, China, URL: https://www.researchgate.net/publication/272744550_THe_Mark_IV_A_scalable_lunar_miner_prototype (accessed 16th June 2022).

Lunar Networks—Chang'e-1 Maps Moon's Helium-3 Inventory. URL: http://lunarnetworks.blogspot.com/2010/12/change-1-maps-moons-helium-3-inventory.html (accessed 16th June 2022)

URL: https://www.science.org/doi/10.1126/sciadv.abi7647 (accessed 16th June 2022)

Zwierzyński, A. J.; Złotkowski, A.; Solecki, M. L.; Balicki, R.; Binkowska, W; Janiak A.; Edelmüller, H.; Gardynik, A; Leśniowska, M.

Sažetak

Ilmenit, sirovina budućnosti

Članak opisuje ekstrakciju izotopa helija-3 na Mjesecu. Dani su podatci o postojanju ležišta toga izotopa na Mjesecu, njegovu postanku, ali i ulozi ilmenita kao mineralu u kojem je očuvan taj izotop. Uporaba helija-3 se očekuje kod fuzijskih reaktora, što ga svrstava u vrlo važne sirovine budućnosti.

Ključne riječi: helij-3; fuzija; ilmenit; Mjesec; rudarenje u svemiru

Author's contribution

Adam Jan Zwierzyński (Ph.D. Eng., associate professor) wrote the skeleton of the article and the main part of it. Space technology input for article. **Albert Złotkowski** (Ph.D. Eng., associate professor) edited and proofread the text of the article. **Marek Solecki** (M.Sc. Eng., assistant) geological and petrographic input for the article. **Rafał Balicki**; **Weronika Binkowska**, **Adam Janiak**, **Hanna Edelmüller**, **Aleksandra Gardynik**, **Magdalena Leśniowska** students involved in the project the article is related to, the main experimenters, technical and 'supporting scientific' assistance in the preparation of the article.

Coal-derived sulphur and selenium in marine sediment cores (Raša Bay, Croatia): recommended steps of analysing environmental earth data

Shuai Kang[1]; Tatjana Ivošević[2]; Gordana Medunić[3]; Shifeng Dai[1]

[1]College of Geoscience and Survey Engineering, China University of Mining and Technology (Beijing), Beijing 100083, China, ORCID 0000-0001-5249-7854 (S.K.), 0000-0002-9770-1369 (S.D.)

[2]Faculty of Maritime Studies, University of Rijeka, Studentska 2, Rijeka, Croatia, ORCID 0000-0001-5140-8354

[3]University of Zagreb, Faculty of Science, Department of Geology, Horvatovac 95, Zagreb, Croatia, ORCID0000-0001-5261-3771

Abstract

Coal may be the most complex geological material that is commonly enriched in sulphur (S) and selenium (Se). Coal combustion and related industries release the two elements into the environment. Considering the fact that both elements can have beneficial as well as detrimental effects on living systems, the knowledge of their fate in the ecosphere should be a matter of the utmost importance. Croatian superhigh-organic-sulphur (SHOS) Raša coal (Raša Bay, Croatia) is highly enriched in S and Se, the levels of which are usually as high as 9-11%, and 50 mg/kg, respectively. Several point sources of the two elements contaminate the Raša study area. The aim of this study was to explore depth profiles of S and Se by collecting seven sediment cores (down to 30-50 cm) from the Raša Bay, and by determining their levels with sulphur carbon analyser and ICP-MS, respectively. Data analysis showed that the both elements were elevated in two sediment cores located closest to a former Raša coal separation and washing facility, which was a source of wastewater disposed of directly in the bay during the period 1930s-1960s. Minimum to maximum S and Se levels in sediments were 0.22–2.6%, and 0.11–12 mg/kg, respectively. In the most contaminated sediment core the correlation S-Se was 0.87 (p = 3.3E-05). Differences among sites were statistically significant for both elements. This paper shows how to analyse environmental data by using nonparametric methods. Also, this paper should increase the public awareness of the marine Raša Bay environmental status.

Keywords: Raša coal; sulphur; selenium; sediment cores; nonparametric data analysis

1. Introduction

Coal may be the most complex geological material that is commonly enriched in sulphur (S) and selenium (Se), chemically similar elements that play vital roles in living systems (**Tang et al., 2021**). The largest percentage of global electricity production is accounted for by coal with as much as 40%, which is more than any other raw material. Due to its abundance and affordable costs, coal remains the key and most reliable source of electricity, mostly in China and India, but also in South Africa, some European countries (Poland, Greece, Serbia, Bosnia and Herzegovina, Croatia and Romania), some US states, Australia, and Indonesia. From an environmental point of view, it represents the most dangerous source of energy. Thanks to its complex composition (**Dai et al., 2021**), coal combustion commonly results in airborne fly ash which is partly synonymous for particulate matter, then gases SO_2, NOx, and CO_2, and hazardous trace elements, Hg, As, Cr, Ni, V, Se, Cd, etc. (**Saikia et al., 2018**). Their environmental fate is a matter of great concern with respect to human health (**Rajak et al., 2020**). Their adverse effects on humans and animals largely result from drinking contaminated water, and consuming crops grown on contaminated soil (**Habib and Khan, 2021**). Due to a variety of their sources and the steady input in the environment, there are still several knowledge gaps concerning their spatial distribution (**Espitia-Pérez et al., 2018**).

Croatian superhigh-organic-sulphur (SHOS) Raša coal (Raša Bay, Croatia) is highly enriched in S (especially organic form) and Se, the levels of which are usually as high as 9-11%, and 50 mg/kg, respectively. It was mined on the Istrian Peninsula (NW Croatia; Fig. 1) for nearly 400 years up to 1999 (**Medunić et al., 2016**). Similar coal can be

Corresponding author:GordanaMedunić
gordana.medunic@geol.pmf.hr

found in China. **Dai et al.** (**2020**) point out how understanding organic, mineral, and intimate organic associations of elements is important not only because non-mineral elements and, to a lesser extent, elements associated with fine-grained minerals, play a significant role in affecting the utilization of coal, but also such modes of occurrence of elements provide useful geochemical information on coal formation and coal-bearing basin evolution. Regarding this study, the sampling locality belongs to coastal karst of the northern Adriatic Sea. There, Raša coal has been continuously leached by groundwater (mix of freshwater and seawater) for decades. Also, abandoned Raša coal and ash waste dumps and coal mine drainage pose hazard for karstic coastal ecosystem (**Medunić et al., 2020b**). Namely, Se is essential to human health in trace amounts but is harmful in excess (**Prakash et al., 2010**). According to research, possible harmful effects of long-term, low-level exposure to selenium should be studied. Selenium deficiency, which is more common, is regarded as a major health problem for 0.5 to 1 billion people worldwide. Even more of them are consuming less Se than required for optimal protection against cancer, cardiovascular diseases, and severe viral infections. Its semiconducting properties make it of special value for industry. Selenium is a rare element on the planet, it is a non-renewable resource due to its non-efficient and difficult recycling, and there are no ores which could be mined for Se. Herewith, the world's scarce Se resources need to be managed carefully, monitored, and stockpiled for use by future generations (**Haug et al., 2007**).

The main objectives of this paper were as follows: 1/ to demonstrate how to analyse sparse environmental data on S and Se by using nonparametric methods, and 2/ to interpret data on sedimentary S and Se in the context of impact of Raša coal on its surroundings at the Raša Bay area. Its purpose is to increase the public awareness of the marine Raša Bay environmental status.

Figure 1: Map of the study area: a) the circle in blue marks the position of Istrian Peninsula, and the black dot marks the position of a Raša study locality; b) sediment core locations (RS1-RS7) with respect to the RCSW (former Raša coal separation and washing facility).

2. Methods

Comprehensive geological and hydrogeological characteristics of the study area are provided in **Medunić et al.** (**2020a, b**) and **Fiket et al.** (**2021**). Briefly, the karstic hydrogeological units are situated close to the Adriatic Sea coastline. The Liburnian Raša coal deposits are overlain and underlain by highly permeable carbonates, and chemically mixed groundwater is circulating through the system. The groundwater contamination derived from abandoned Raša

coal deposits as well as coal waste dumps is of a major concern due to seawater and freshwater mixing as well as the lack of a natural filtration system in the karst.

2.1. Sampling of bottom sediments

Sediment core samples were retrieved in November 2020, by means of a boat B Light Dufour 525 Grand Large (private ownership of Dr. Ivica Orlić), shown on **Figure 2**. A part of the Raša Bay along the mouth of the Raša River is a naturally very shallow area, up to 15 m deep. The eastern side of the bay is artificially deepened for the needs of a local Bršica port, and other activities such as mussel farming. The sampling locations were selected at a depth of 3 to 5 m, due to the dimensions of the sampler which was pushed into the sediment by a long metal pipe (mounted on the pipe shown on **Figure 3**), until the depth of the core was 50 to 80 cm long.

Figure 2: The vessel which was used for the sampling campaign carried out in November 2020.

For the sampling work, we used a hand core sampler, designed and constructed by Dr. Ivica Orlić. Its main elements were as follows (**Figure 3**): a plastic pipe with a diameter of 70 mm, and a one-way valve that prevents the loss of sediment when retrieving the pipe from the sea bottom. All sediment cores were divided into several subsamples. The upper 10-cm portion was sliced into 1-cm subsamples, and the rest of the material was sliced into 5-10 cm subsamples.

Figure 3: A hand core sampler (a) with one way valve (b) showing retrieved sediment (c).

2.2. Geochemical analysis of S and Se

Sediment core samples were analysed in the China University of Mining and Technology (Beijing). Sulphur was analysed by Sulphur carbon analyser (SC832 Series, LECO, USA), according to the Standard Test Methods for Sulphur in the Analysis Sample of Coal and Coke Using High Temperature Tube Furnace Combustion Methods: ASTM D4239 Sulphur (Method A). Inductively coupled plasma mass spectrometry (X series II ICP-MS, Thermo Fisher Scientific, Waltham, MA, USA) was used to determine Se concentrations. Prior to ICP-MS analysis, samples were digested using an UltraClave Microwave High Pressure Reactor (Milestone) (after **Dai et al., 2011**). Collision cell technology (CCT) was used to avoid disturbance of polyatomic ions (**Li et al., 2014**). Multi-element standards (Inorganic Ventures: CCS-1, CCS-4, CCS-5, and CCS-6; Chinese standard reference GBW07381 and GBW07980) were used for calibration.

2.3. Data analysis

Data analysis was conducted with the free PAST software (**Hammer et al., 2001**). It included calculations of basic statistical parameters, Shapiro Wilk test (variable distributions; level of significance was 0.10), and nonparametric Kendall's tau correlation coefficients, and Kruskal–Wallis test (level of significance was 0.05). Prior to the testing of null hypotheses (i.e. there is no difference among groups, and there are no relations among variables in the groups), we first checked variable distributions. This is a very important step in data analysis as parametric methods are commonly not suitable for environmental data (**Reimann and Filzmoser, 2000**) due to either a low number of samples or skewed (asymmetric) variable distributions. Parametric methods are based on mean and SD, but they can be severely inflated by only a few outliers (unusually high variable values); hence, nonparametric methods, based on Q_{50}, which is resistant to outliers, is recommended (**Helsel et al., 2020**). We chose the nonparametric methods because the two variables were not symmetrically distributed.

3. Results and discussion

Basic statistical parameters of sediment core S and Se are shown in **Tables 1** and **2**, respectively. Clearly, S is increased in the core RS5 which is closest to the former Raša coal separation and washing facility, RCSW (**Fig. 1**). During the period 1930s-1960s, huge quantities of wastewater were dumped directly into the bay (**Medunić et al.,**

2020b), and Raša coal particles ended up in the local estuarine sediment brought up by the Raša River. With time, the deposit has got perched above seawater level, and its surface has become covered in wild grasses and other vegetation. Similarly, maximum Se value was found in the core RS5. These results are in line with the fact that Raša coal is enriched in S (**Medunić et al., 2018**) and Se (**Medunić et al., 2018, 2020a**). Hence, the two fingerprint elements, elevated in the bottom Raša Bay sediment, are indicative of Raša coal legacy. According to **Ketris and Yudovich (2009)**, world coal Se level is 8.8 mg/kg, while it is up to 25 mg/kg in Raša coal (**Medunić et al., 2020a**). **Reimann and de Caritat (1998)** report natural S and Se levels in stream overbank sediments (neither element was reported in marine bottom sediments in the publication) are as follows: 0.01%, and 0.37 mg/kg, respectively. Therefore, Raša Bay sediment S and Se are increased up to 260 and 30 times, respectively. Sulphur and Se levels in Raša Bay sediments are also shown on **Figures 4** and **5** where the core RS5 stands out from the rest, and both figures show essentially identical pattern. Generally, sediment cores RS5, 6, and 7, being closest to the RCSW, have higher S and Se concentrations compared with the rest of the cores, situated further away from the RCSW. However, the most striking feature of sediment core S and Se levels (**Tables 1, 2**) is the fact that RSD values are exceptionally high regarding both elements, more so for Se. Anthropogenic processes usually result in high RSD values of trace elements in the environment, causing their skewed distributions (**Reimann and Filzmoser, 2000**). The RSD values of S and Se in Raša Bay sediments are certainly very interesting, thus warranting further detailed mineralogical, petrological, and geochemical analyses of collected samples. Although we noted above that the core RS3 belongs to an area of the bay less affected by the RCSW, the results in **Tables1** and **2** are indicative of the opposite, and therefore our ongoing work will try to reveal the possible reasons for that.

S	RS1	RS2	RS3	RS4	RS5	RS6	RS7
n	18	20	16	15	13	12	16
Min	0.22	0.26	0.21	0.30	0.84	0.70	0.29
Max	0.49	0.36	1.5	0.64	2.6	1.7	0.95
Mean	0.35	0.31	0.56	0.41	1.4	1.1	0.45
SD	0.07	0.04	0.4	0.09	0.6	0.3	0.2
Q_{50}	0.34	0.31	0.39	0.41	1.3	1.1	0.38
Q_{25}	0.31	0.29	0.27	0.32	0.92	0.85	0.34
Q_{75}	0.37	0.34	0.73	0.45	1.6	1.4	0.46
RSD	19	9.4	74	22	41	29	42

Table 1: Levels of S (%) in Raša Bay sediment cores (RS1-RS7). Q_{50} – median; Q_{25} and Q_{75} – quartiles

Se	RS1	RS2	RS3	RS4	RS5	RS6	RS7
n	18	20	16	15	13	12	16
Min	0	0	0.05	0	3.1	0.86	0.65
Max	1.2	1.5	5.4	1.2	12	9.7	4.0
Mean	0.58	0.46	1.6	0.33	5.4	4.5	1.7
SD	0.4	0.4	2	0.4	3	2	0.9
Q_{50}	0.60	0.41	1.0	0.22	5.0	4.6	1.3
Q_{25}	0.31	0.15	0.40	0	3.2	3.4	1.2
Q_{75}	0.91	0.67	2.2	0.52	6.4	5.3	1.8
RSD	64	83	99	120	49	46	57

Table 2: Levels of Se (mg/kg) in Raša Bay sediment cores (RS1-RS7). Q_{50} – median; Q_{25} and Q_{75} – quartiles

We tested variable distributions by applying Shapiro Wilk test (recommended level of significance is 0.10), and it showed for S the following p values: RS1 0.25, RS2 0.16, RS3 0.001, RS4 0.17, RS5 0.01, RS6 0.76, and RS7 0.0004. Sulphur values in cores supposedly less affected by the RCSW (RS1-4) should be symmetrically distributed (their p values should be >0.10), but that was not the case with the core RS3. In the case of Se, p values were as follows: RS1 0.59, RS2 0.08, RS3 0.01, RS40.005, RS5 0.008, RS6 0.15, and RS7 0.001. The results warrant further specific mineralogical, petrological, and geochemical analyses, to find out why the data have large spread (large SD and RSD) in almost all the cores, Se in particular.

By applying Kruskal-Wallis test, to explore if there is any difference among the seven groups (i.e. sediment cores), p values for S and Se were 7E-12, and 9.9E-14, respectively. Such low numbers are indicative of a very strong difference among the groups. By applying a multiple comparison Duncan test, we were able to see specifically among which groups the differences were statistically significant (at p<0.05), and the results are shown in **Tables 3** and **4**. The lowest p values for S and Se were found for the cores RS5 and RS6 with respect to other cores, and from these values it

seems that the cores RS2 and RS4 were the least affected by the RCSW. Regarding the core RS5, the most contaminated by the RCSW, the levels of S and Se showed peaks in the sediment depth 15-20 cm.

By using Kendal tau correlation, coefficients between S and Se were as follows (p values in parentheses): RS1 0.08 (p>0.05), RS2 -0.08 (p>0.05), RS3 0.54 (p = 0.003), RS4 -0.20 (p>0.05), RS5 0.87 (3.3E-05), RS6 0.67 (p = 0.002), and RS7 0.68 (p = 0.0002). Since S and Se were found to be positively correlated in Raša coal (**Medunić et al., 2018**), it was expected to find them related the same way here, at least in the cores RS5 and RS6. Thanks to statistically significant positive correlations between S and Se in the cores RS5, 6, and 7, closest to the RCSW, but also in the core RS3, we now know that the impact of the RCSW has been profound in terms of the element composition of the bottom sediment of the Raša Bay.

	RS1	RS2	RS3	RS4	RS5	RS6	RS7
RS1							
RS2	0.17						
RS3	0.16	*0.01*					
RS4	0.19	*0.01*	0.95				
RS5	*4.6E-07*	*1.4E-10*	*0.00*	*0.00*			
RS6	*3.4E-06*	*2.3E-09*	*0.00*	*0.00*	0.80		
RS7	0.19	*0.01*	0.94	0.99	*0.00*	*0.00*	

Table 3: Results of Duncan post-hoc test for S (bold italic underlined values are significant at p<0.05)

	RS1	RS2	RS3	RS4	RS5	RS6	RS7
RS1							
RS2	0.50						
RS3	0.08	*0.01*					
RS4	0.19	0.49	*0.00*				
RS5	*4.8E-07*	*8.8E-09*	*0.00*	*1.6E-09*			
RS6	*4.6E-06*	*1.4E-07*	*0.00*	*2.4E-08*	0.75		
RS7	*0.00*	*0.00*	0.25	*5.3E-05*	*0.02*	0.06	

Table 4: Results of Duncan post-hoc test for Se (bold italic underlined values are significant at p<0.05)
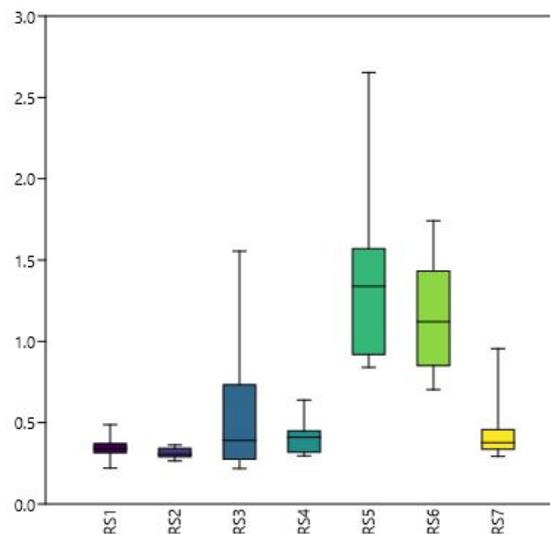
Figure 4: Box-plots of S (%) in sediment cores RS1-RS7.
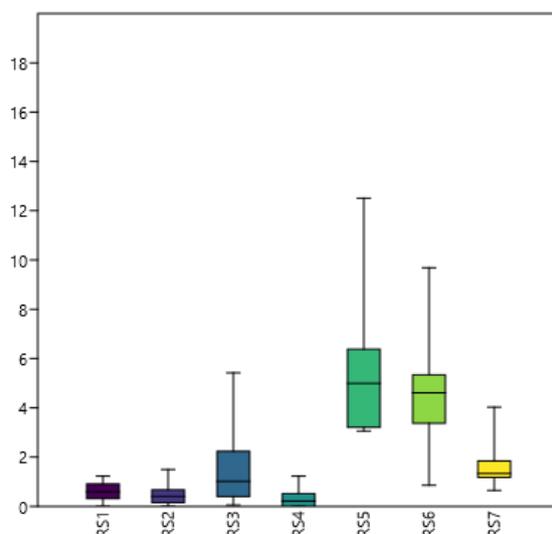
Figure 5: Box-plots of Se (mg/kg) in sediment cores RS1-RS7.

4. Conclusion

Data analysis (nonparametric methods) conducted on sediment core sulphur and selenium concentrations, the two fingerprint elements of Raša coal, confirms that the Raša Bay has been impacted by the former Raša coal separation and washing (RCSW) facility, which had disposed of wastewater directly in the bay during the period 1930s-1960s. The legacy of such an environmentally hazardous practice is reflected in the estuarine sediments' geochemistry, at least considering S and Se spatial distributions in bottom sediments. Both elements were found to be elevated in two sediment cores located closest to the RCSW, but other cores have been affected by the RCSW to a certain extent as well. Moreover, this paper should guide scholars, inexperienced in data analysis, that using nonparametric methods (testing differences among groups, and correlation analysis) is the safest strategy when the number of samples per group is less than 30, and variable distributions are skewed (large spread of data reflected in large RSD values). Finally, this paper shows interesting results that warrant further analytical work on the retrieved samples from the marine Raša Bay, that deserves environmental protection in terms of a bioaccumulative, potentially toxic trace element selenium.

5. References

Dai, S., Wang, X., Zhou, Y., Hower, J.C., Li, D., Chen, W., Zhu, X. (2011): Chemical and mineralogical compositions of silicic, mafic, and alkali tonsteins in the late Permian coals from the Songzao Coalfield, Chongqing, Southwest China. Chemical Geology, 282, 29–44.

Dai, S., Hower, J.C., Finkelman, R.B., Graham, I.T., French, D., Ward, C.R., Eskenazy, G., Wei, Q., Zhao, L. (2020): Organic associations of non-mineral elements in coal: A review. International Journal of Coal Geology, 218, 103347.

Dai, S., Finkelman, R.B., French, D., Hower, J.C., Graham, I.T., Zhao, F. (2021). Modes of occurrence of elements in coal: A critical evaluation. Earth-Science Reviews, 222, 103815.

Espitia-Pérez, L., Arteaga-Pertuz, M., Soto, J.S., Espitia-Pérez, P., Salcedo-Arteaga, S., Pastor–Sierra, K., Galeano–Páez, C., Brango, H., da Silva, J., Henriques, J.A.P. (2018). Geospatial analysis of residential proximity to open-pit coal mining areas in relation to micronuclei frequency, particulate matter concentration, and elemental enrichment factors. Chemosphere, 206, 203-216.

Fiket, Ž., Petrović, M., Medunić, G., Ivošević, T., Fiket, T., Xu, L.Z., Wang, Y., Ding, S. (2021): Evaluation of the Potential Release Tendency of Metals and Metalloids from the Estuarine Sediments: Case Study of Raša Bay. Molecules, 26(21):6656.

Habib, M.A. and Khan, R. (2021): Environmental Impacts of Coal-Mining and Coal-Fired Power-Plant Activities in a Developing Country with Global Context. In: Shit, P.K., Adhikary, P.P., Sengupta, D. (eds), Spatial Modeling and Assessment of Environmental Contaminants. Environmental Challenges and Solutions. Springer, Cham, 421-493.

Hammer, Ø., Harper, D.A.T. and Ryan, P.D. (2001): PAST: Paleontological statistics software package for education and data analysis. Palaeontol. Electron. 4, 1–9. Available online: http://palaeo482 electronica.org/2001_1/past/issue1_01.htm (accessed on May 01, 2022).

Haug, A., Graham, R.D., Christophersen, O.A. and Lyons, G.H. (2007): How to use the world's scarce selenium resources efficiently to increase the selenium concentration in food. Microbial Ecology and Health Disease 19(4), 209-228.

Helsel, D.R., Hirsch, R.M., Ryberg, K.R., Archfield, S.A., and Gilroy, E.J. (2020): Statistical methods in water resources: U.S. Geological Survey Techniques and Methods, book 4, chap. A3, 458 p., https://doi.org/10.3133/tm4a3. [Supersedes USGS Techniques of Water-Resources Investigations, book 4, chap. A3, version 1.1.]

Ketris, M.P. and Yudovich, Y.E. (2009): Estimations of clarkes for carbonaceous biolithes: world averages for trace element contents in black shales and coals. Int. J. Coal Geol., 78, 135–148.

Li, X., Dai, S., Zhang, W., Li, T., Zheng, X., Chen, W. (2014): Determination of As and Se in coal and coal combustion products using closed vessel microwave digestion and collision/reaction cell technology (CCT) of inductively coupled plasma mass spectrometry (ICP-MS). International Journal of Coal Geology, 124, 1–4.

Medunić, G., Rađenović, A., Bajramović, M., Švec, M., Tomac, M. (2016): Once grand, now forgotten: what do we know about the superhigh-organic-sulphur Raša coal? Rudarsko-Geološko-NaftniZbornik, 31(3), 27-45.https://doi.org/10.17794/rgn.2016.3.3

Medunić, G., Kuharić, Ž., Krivohlavek, A., Fiket, Ž., Rađenović, A., Gödel, K., Kampić, Š., Kniewald, G. (2018): Geochemistry of Croatian superhigh-organic-sulphur Raša coal, imported low-S coal and bottom ash: their Se and trace metal fingerprints in seawater, clover, foliage and mushroom specimens. Int. J. Oil Gas Coal Technol., 18, 3–24.

Medunić, G., Grigore, M., Dai, S., Berti, D., Hochella, M.F., Mastalerz, M., Valentim, B., Guedes, A. and Hower, J.C. (2020a.): Characterization of superhigh-organic-sulfurRaša coal, Istria, Croatia, and its environmental implication. International Journal of Coal Geology, 217, 103344. https://doi.org/10.1016/j.coal.2019.103344

Medunić, G., Bucković, D., PrevendarCrnić, A., Bituh, T., GaurinaSrček, V., Radošević, K., Bajramovic, M., &Zgorelec, Z. (2020b):Sulfur, metal(loid)s, radioactivity, and cytotoxicity in abandoned karstic Raša coal-mine discharges (the north Adriatic Sea). Rudarsko-Geološko-NaftniZbornik, 35(3), 1-16. https://doi.org/10.17794/rgn.2020.3.1

Prakash, N.T., Sharma, N., Prakash, R. and Acharya, R. (2010): Removal of Selenium from Se Enriched Natural Soils by a Consortium of Bacillus Isolates. Bull Environ ContamToxicol, 85, 214–218.

Rajak, P.K., Singh, V.K., Singh, A.L., Kumar, N., Kumar, O.P., Singh, V., Kumar, A., Rai, A., Rai, S., Naik, A.S., Singh, P.K. (2020): Study of minerals and selected environmentally sensitive elements in Kapurdilignites of Barmer Basin, Rajasthan, western India: implications to environment. Geosciences Journal, 24, 441–458.

Reimann, C. and de Caritat, P. (1998): Chemical elements in the environment. Factsheets for the geochemist and environmental scientist. Springer-Verlag Berlin Heidelberg, Germany, 398 p.

Reimann, C. andFilzmoser, P. (2000): Normal and lognormal data distribution in geochemistry: death of a myth. Consequences for the statistical treatment of geochemical and environmental data. Environmental Geology, 39, 1001–1014.

Saikia, B.K., Saikia, J., Rabha, S., Silva, L.F.O. and Finkelman, R. (2018): Ambient nanoparticles/nanominerals and hazardous elements from coal combustion activity: Implications on energy challenges and health hazards. Geoscience Frontiers 9, 863-875.

Tang, Y., Chen, C., Li, X., Wei, Q., Guo, X., Finkelman, R.B., Li, W., Huan, X. (2021). The evolution characteristics of organic sulfur structure in various Chinese high organic sulfur coals. Energy Exploration & Exploitation, 39(1), 336–353.

Sažetak

Sumpor i selen iz Raškog ugljena zabilježeni u jezgrama morskog sedimenta (Raški zaljev, Hrvatska): preporučeni koraci statističke analize podataka iz okoliša

Ugljen je možda najsloženija geološka tvar koja je obično obogaćena sumporom (S) i selenom (Se). Izgaranjem ugljena te srodnim industrijskim aktivnostima otpuštaju se dotična dva elementa u okoliš. Obzirom na to da oba elementa mogu imati blagotvorne i štetne učinke na žive sustave, poznavanje njihove sudbine u ekosustavu trebalo bi biti od najveće važnosti. Raški ugljen (Raški zaljev, Hrvatska) ima iznimno visoke koncentracije organskog S i Se, čije razine obično iznose 9-11%, odnosno 50 mg/kg. Nekoliko točkastih izvora ta dva elementa onečišćuje istraživano područje Raše. Cilj ovog istraživanja bio je istražiti dubinske profile koncentracija S i Se u sedam prikupljenih sedimentnih jezgri (do dubina 30-50 cm) iz Raškog zaljeva, te određivanjem njihovih koncentracija pomoću XRF i ICP-MS. Analiza podataka pokazala je da su oba elementa povišena u dvije sedimentne jezgre koje se nalaze najbliže nekadašnjem postrojenju za separaciju i ispiranje ugljena, koje je u razdoblju od 1930-ih do 1960-ih predstavljalo izvor otpadnih voda koje su ispuštane izravno u zaljev. Minimalne do maksimalne razine S i Se u sedimentima bile su 0,22–2,6%, odnosno 0,11–12 mg/kg. U najonečišćenijoj jezgri sedimenta korelacija S-Se iznosila je 0,87 (p = 3,3E-05). Razlike među jezgrama bile su statistički značajne za oba elementa. Ovaj rad prikazuje preporučene korake statističke analize podataka iz okoliša primjenom neparametarskih metoda. Također, ovaj bi rad trebao povećati svijest javnosti o ekološkom statusu Raškog zaljeva.

Ključne riječi: Raški ugljen; sumpor; selen; sedimentne jezgre; neparametarskemetode

Acknowledgment

Author's contribution

Shuai Kang (Ph.D. candidate) conducted element analyses (carbon sulphur analyser and ICP-MS) on collected samples. **Tatjana Ivošević** (Ph.D., assistant professor) performed the field work and assisted with artwork. **Gordana Medunić** (Ph.D., full professor) participated in the field work, conducted data analysis, geochemical interpretations, and presentation of the results. **Shifeng Dai** (Ph.D., full professor) provided financial funds for the research and assisted with expertise on various topics covered by the manuscript.

Analysis of global changes in fossil CO₂ emissions during and after the Covid-19 era

Sonja Koščak Kolin[1]; Lidia Hrnčević[1]; Ivana Šimunović[2]

[1] University of Zagreb Faculty of Mining, Geology and Petroleum Engineering,
Department of Petroleum and Gas Engineering and Energy, Pierottijeva 6, 10000
Zagreb, Croatia, ORCID 0000-0003-0056-4466

[1] University of Zagreb Faculty of Mining, Geology and Petroleum Engineering, Department of Petroleum and Gas Engineering and
Energy, Pierottijeva 6, 10000 Zagreb, Croatia, ORCID 0000-0001-8990-0985

[2] Kompolje 63, Otočac 53220

Abstract

It is well known that the increase in fossil emissions of carbon dioxide (CO_2) is due to the burning of increasing amounts of fossil fuels over the years. The concentration of CO_2 in the atmosphere is increasing because the balance cannot be achieved by natural sinks (removal) of CO_2, which further affects the negative climate change. However, in 2020, there was a significant decrease in global fossil CO_2 emissions due to the restrictive measures taken during the COVID-19 pandemic. Although this decrease in emissions was significant, the trend of fossil CO_2 emissions in 2021, as well as in the future, will mainly depend on the success of the proven energy transition as economies recover from the COVID-19 crisis. This paper presents the mean values, variations and trends in global fossil CO_2 emissions over the period 1959-2020, focusing on the analysis of changes in 2020. It then presents projections and future long-term trends in global fossil CO_2 emissions.

Keywords: fossil CO_2 emissions; emission trends; COVID-19 impact

1. Introduction

Global warming and climate change are the biggest environmental problems of our time. Combustion of ever-increasing amounts of fossil fuels led to a significant increase in fossil emissions of carbon dioxide (CO_2), which negatively affect climate change. The concentration of CO_2 in the atmosphere is has been increasing, because equilibrium cannot be achieved through natural sinks (removal) of CO_2, which has further affected climate change. Although the Earth, in its geological past, had periodically gone through periods of significant climate changes, what is rising serious concern today is the speed at which the changes are taking place. Global temperature during interglacials is thought to be controlled primarily by carbon dioxide concentrations, since existing knowledge of interglacial periods is that they are triggered by Milankovitch cycles that are enhanced by increasing atmospheric carbon dioxide concentrations (**Marsh, 2014**).

In order to assess and to compare the impact of greenhouse gas emissions, it has been internationally agreed that each greenhouse gas is to be assigned the so-called Global Warming Potential (GWP). GWP is the relative value assigned to each greenhouse gas, which describes its impact on climate change, i.e., its ability to absorb the infrared (IR) radiation (heat) over a specific period of time (20, 100 or 500 years) relative to the same amount of CO_2 (**Hrnčević, 2008**). Monitoring and reporting of greenhouse gas emissions is one of the most important elements of the emission reduction program. For better understanding of climate change, it is necessary to constantly record and collect the data on greenhouse gas emissions. The data are collected either from the direct measurements of atmospheric greenhouse gas concentrations or from determining the emissions, as precisely as possible, by using various data sets, such as the data on global energy production and consumption, data on global population, and satellite measurements, etc. Estimation of anthropogenic CO_2 emissions and their redistribution between atmosphere, ocean and the terrestrial biosphere is key to better understanding the global carbon cycle, developing climate policies, and predicting future climate change (**Friedlingstein et al., 2020**).

Five years after the adoption of the Paris Climate Agreement, which follows up the 1997 Kyoto Protocol, the growth in global CO_2 emissions has begun to slow down. Especially during 2020 when the COVID-19 pandemic drastically

Corresponding author: Sonja Koščak Kolin
e-mail address: sonja.koscak-kolin@rgn.unizg.hr

changed the trajectory of fossil CO_2 emissions. Although there has been a significant decline in fossil CO_2 emissions during the pandemic, it is difficult to predict whether this short-term decline will have an impact on the future trend of CO_2 emissions. In most countries, emissions decreased at the peak of Covid-19 restrictive measures, but this peak did not occur in all countries at the same time (**Le Quéré et al., 2021**). The biggest impact on the decline in fossil emissions had the restrictive measures that affected the transport sector.

The European Green Deal is a policy strategy with significant potential to change the European Union's climate policy. While addressing a broader set of environmental and sustainability issues, in the core of the European Green Deal is the climate transition. The ambitious goals of the European Green Deal are to turn the European Union (EU) into a modern and competitive economy and to ensure: net zero greenhouse gas emissions by 2050, economic growth independent on the use of resources, and with regards to all people and regions. All 27 EU Member States have committed to contributing to the transformation of Europe into the first climate-neutral continent by 2050. The Members States have pledged to reduce greenhouse emissions by at least 55% by 2030 compared to 1990 levels (**Šimunović, 2021**). This will create new opportunities for innovation, investments, and job creation, as well as for:

- combating energy poverty,
- reducing dependence on energy originating from non-EU countries,
- improving health and well-being.

The European Commission has proposed to increase the binding target for the share of energy from renewable sources in the EU to 40%. The proposals promote the use of renewable energy sources such as hydrogen in industry and transport and introduce the additional reductional targets. In addition, reduction of energy consumption is necessary to reduce greenhouse gas emissions and energy costs for consumers and industry. To reduce the total primary energy consumption and the final energy consumption by 36-39% by 2030, the Commission has proposed the increase of energy saving targets in EU and to make it binding. Also, a 55% emission reduction from passenger cars is expected by 2030, a 50% emission reduction from trucks and zero emissions from new vehicles by 2035. In addition, road transport will be included in the emissions trading system from 2026, which should set the price of pollution and to encourage the use of cleaner fuels and investment into clean technologies (**https://ec.europa.eu/**).

2. Global CO_2 emissions in the period 1959 - 2019

The concentration of CO_2 in the atmosphere has increased significantly from the beginning of the industrial era to the present day. Before industrial production, CO_2 emissions increased primarily due to deforestation and similar land conversion activities, while today the dominant sources of CO_2 emissions are fossil fuels. The global concentration of CO_2 in the atmosphere increased from $\sim$ 277 ppm in 1750 (**Joos and Spahni, 2008**) to 422.99 ppm in June 2022 (**www.co2.earth**).

Climate change and changes in carbon storage in terrestrial biosphere and ocean are the consequences of the rapid increase in the concentration of CO_2 in the atmosphere. During the assessment of CO_2 emissions the following components are important):

- emissions from the combustion and oxidation of fossil fuels from all energy and industrial processes, including cement production and carbonization (E_{FOS});
- emissions resulting from intentional human activities on land, including those leading to land conversion and forest use (E_{LULUCF});
- their division between the increase of CO_2 concentrations in atmosphere (G_{ATM}), the ocean CO_2 sink (S_{OCEAN}) and terrestrial CO_2 sink (S_{LAND}).

Global emissions and their redistribution between the atmosphere, oceans, and land are in equilibrium, but due to estimation errors and imperfect spatial and temporal data, their sum does not necessarily have to be zero. Due to the sated, a carbon budget imbalance (BIM) is introduced, which shows the mismatch between the estimated emissions and the estimated changes in the atmosphere, terrestrial biosphere and ocean (**Equation 1**) (**Friedlingstein et al., 2020**):

$$E_{FOS} + E_{LULUCF} = G_{ATM} + S_{OCEAN} + S_{LAND} + B_{IM} \tag{1}$$

Where are:
E_{FOS} - fossil CO_2 emissions (GtC/y),
E_{LULUCF} - CO_2 emissions from land use, land use change and forestry (GtC/y),
G_{ATM} - CO_2 concentration in the atmosphere (GtC/y),

S_{OCEAN} - sink (removal) into the ocean (GtC/y),
S_{LAND} - sink (removal) into the terrestrial biosphere (GtC/y),
B_{IM} - budgetary imbalance (GtC/y).

2.1. Methods for estimating global CO₂ emissions

The sources of data analyzed in this chapter have been retrieved from a number of different organizations and research groups listed in **Table 1**.

Components	Literature
National fossil CO_2 emissions by fuel type	Gilfillan et al. (2020) (https://energy.appstate.edu/) UNFCCC (2020) (https://unfccc.int/)
Fossils consumption - based CO_2 emissions by country	Peters et al. (2011)
Net land-use change flux	Average from Houghton and Nassikas (2017), Hansis et al. (2015), Gasser et al. 2020
Growth rate in atmospheric CO_2 concentration	Dlugokency and Tans (2020)
Land sink	Global dynamic vegetation models
Ocean sink	Biogeochemical models and observation-based estimates

Table 1: Summary of main data sources (from **Friedlingstein et al., 2020**)

2.1.1. Fossil CO₂ emissions

Estimation of global and national fossil CO_2 emissions includes the combustion of fossil fuels in various activities: such as heating and cooling, transportation, industry, production of chemicals and fertilizers, and emissions during cement carbonization. Fossil CO_2 emissions include three main fossil fuels: solid (coal), liquid (oil) and gaseous fuels (natural gas). CO_2 emissions from natural gas flare combustion and emissions from cement production can also be added. Combustion of fossil fuels is a major source of anthropogenic CO_2 emissions (**Andres et al., 2012**).

Energy and fossil fuel consumption data are used to estimate fossil CO_2 emissions. In the Global Carbon Budget, the estimate of the uncertainty of global fossil CO_2 emissions is ± 5%, and the data are taken from four main data sets, namely (**Friedlingstein et al., 2020**):
1. Carbon Dioxide Information Analysis Center (CDIAC*)*, for the period 1750 - 2017 - data are derived from energy statistics published by the United Nations (UN). Mass and amount of fuel are converted into fuel energy content using UN-published country-level coefficients and then converted to CO_2 emissions using conversion factors.
2. Official National Greenhouse Gas Inventory 1990-2018 for 42 UNFCCC (United Nations Framework Convention on Climate Change) Annex I countries.
3. Statistical Global Energy Review published by British Petroleum (BP) - this database uses data on energy consumption estimates for the last year, for which UNFCCC and CDIAC estimates are not yet available.
4. Global and national emissions from the cement industry updated by Andrew (2019).

The global total sum, i.e., the estimate, is the sum of fossil CO_2 emissions of individual countries and the data retrieved from fuel consumption, for the international air and maritime transport. National statistics on emissions from CDIAC, UNFCCC and BP represent emissions and greenhouse gases sinks occur within the national territory and submarine area of individual country.

2.1.2. CO₂ emissions from land use and forestry (LULUCF)

In addition to fossil emissions, land use, land use change and forestry contribute to increase of CO_2 emissions. The net CO_2 flow generated by land use, land use change and forestry include CO_2 flows due to deforestation, afforestation, forest degradation, change of cultivation (deforestation for agricultural purposes and then abandonment) and reforestation after logging or abandonment of agricultural activities. Some of these activities lead to increase of CO_2 emissions into the atmosphere, while others act like CO_2 sinks. The annual estimate of CO_2 emissions for the 1959–2019 period was obtained as an average of: an estimate using the land use emissions model (**Hansis et al., 2015**), an estimate published by **Houghton and Nassikas (2017)**, and the assessment according to **Gasser et al. (2020)**. All three models are based on **Houghton's (2003)** original approach that tracks carbon in vegetation and soil before and after land use change. In

addition, the results of seventeen dynamic global vegetation models are used, and they include deforestation and regrowth, but do not represent all the anthropogenic processes on land.

2.1.3. Distribution of CO_2 emissions

The CO_2 released during combustion of fossil fuels has been balanced over several centuries by different carbon sinks in the atmosphere, ocean and terrestrial biosphere. Approximately half of the CO_2 emitted into the atmosphere during fossil fuel combustion remains in the atmosphere, and the other half is absorbed by the ocean and terrestrial biosphere. Oceans are the largest "carbon reservoirs" on Earth, nature's primary mechanisms for absorbing CO_2 from the atmosphere. Oceans can absorb most of the emitted CO_2, but still about 20–40% of the CO_2 remains in the atmosphere, awaiting slower chemical reactions with calcium carbonate and igneous rocks (**Archer et al., 2009**). Carbon isotopes, preserved in deep ocean sediments, reveal a periodical release of carbon into the atmosphere-ocean system, leading to ocean and atmosphere warming and consequently to climate change. A large amount of the absorbed CO_2 acidifies the ocean, but, after a certain period, ocean's pH is restored, but not to its initial value (but to slightly lower one), by excessive dissolution of calcium carbonate from the seabed and shore and by the influence of silicates from land. Ocean's pH recovery restores the ocean's buffer capacity to absorb CO_2, with a tendency of decreasing the absorbed CO_2 concentrations over the next period (**Archer et al., 2009**; **Hrnčević, 2008**).

The sink of carbon in the ocean is estimated by using nine global oceanic biogeochemical models. They represent physical, chemical and biological processes that affect the concentration of CO_2 on the ocean surface, and thus the exchange of CO_2 at the atmosphere-ocean boundary. To verify the results of the biogeochemical model, observational data are used.

Restoring and increasing carbon sinks in the terrestrial biosphere, i.e., the ability of the environment (plants) to absorb CO_2, are the key to achieving the set climate goals. The carbon sink in the terrestrial biosphere is estimated by seventeen dynamic global vegetation models, including all climatic variability and CO_2 effects on land.

2.2. Analysis of global CO_2 emissions changes

2.2.1. Global CO_2 emissions in the period 1959 - 2019

In the period from 1959 to 2019, for which the direct measurements of CO_2 concentrations in the atmosphere are available, 81% of total CO_2 emissions (E_{FOS} + E_{LULUCF}) come from fossil fuels combustion, and 19% from LULUCF. In the stated period, 45% of the total emissions stayed in the atmosphere 24% in oceans and 32% in land, with a budget imbalance of 0% (**Friedlingstein et al., 2020**). In **Table 2** global CO_2 emissions for the period 1960–2019 are shown, and uncertainties are expressed as ± 1 σ. Global fossil CO_2 emissions increased from an average of 3.0 ± 0.2 GtC per year in the period 1960–1969, to 9.4 ± 0.5 GtC per year in the period 2010–2019. CO_2 emissions from LULUCF have remained relatively constant, at about 1.4 ± 0.7 GtC per year for the last half century, but with a large range estimated. The budget imbalance has an uncertainty of more than ± 1 GtC per year, and a positive imbalance means that emissions have been overestimated and / or that the sinks have been underestimated. The growth rate of fossil emissions decreased between the 1960s and 1990s, from 4.3% per year in the 1960s (1960-1969), 3.1% in the 1970s (1970-1979), 1.6% in the 1980s (1980–1989) to 0.9% in the 1990s (1990–1999). After the period 1990–1999, the growth rate began to increase in the 2000s with an average of 3.0% per year, declining to 1.2% in the last decade (2010-2019) (**Šimunović, 2021**).

Mean (GtC/yr)							
	1960-1969	**1970-1979**	**1980-1989**	**1990-1999**	**2000-2009**	**2010-2019**	**2019**
TOTAL EMISSIONS **(EFOS+ELUC)**							
Fossil CO_2 emissions (EFOS)	3±0.2	4.7±0.2	5.4±0.3	6.3±0.3	7.7±0.4	9.4±0.5	9.7±0.5
Land-use change emissions (ELUC)	1.5 ± 0.7	1.3±0.7	1.3±0.7	1.4±0.7	1.4±0.7	1.6±0.7	1.8±0.7
Total emissions	4.5 ± 0.7	5.9±0.7	6.7±0.8	7.6±0.8	9.1±0.8	10.9±0.9	11.5±0.9
PARTITIONING							
Growth rate in atmospheric CO_2 concentration (GATM)	1.8±0.07	2.8±0.07	3.4±0.02	3.2±0.02	4.1±0.02	5.1±0.02	5.4±0.2
Ocean sink (SOCEAN)	1±0.3	1.3±0.4	1.7±0.4	2±0.5	2.1±0.5	2.5±0.6	2.6±0.6
Terrestrial sink (SLAND)	1.3±0.4	2.1±0.4	2.0±0.7	2.6±0.7	2.9±0.8	3.4±0.9	3.1±1.2
BUDGET IMBALANCE							
BIM= EFOS + ELUC - (GATM + SOCEAN + SLAND)	0.5	-0.2	-0.4	-0.1	0	-0.1	0.3

Table 2: Mean values for CO_2 emissions and distribution of emissions by decades (from **Friedlingstein et al., 2020**)

In **Figure 1** global fossil CO_2 emissions, including an uncertainty of ± 5% (grey shading), and emissions extrapolated from BP statistics (black dots) for the period 1960-2020 are shown. The Figure 1 also shows the global CO_2 emissions by fuel type, including coal, oil, natural gas, cement production and cement production reduced by carbon sink (intermittent purple), excluding natural gas flaring. For the same period, the CO_2 emissions (coal, oil, natural gas, natural gas flaring and cement production- solid lines, and consumption emissions- dashed lines) for the three leading countries in terms of CO_2 emissions (USA, China, India) and the European Union (27 Member States; turquoise), as well as the emissions per capita are shown.
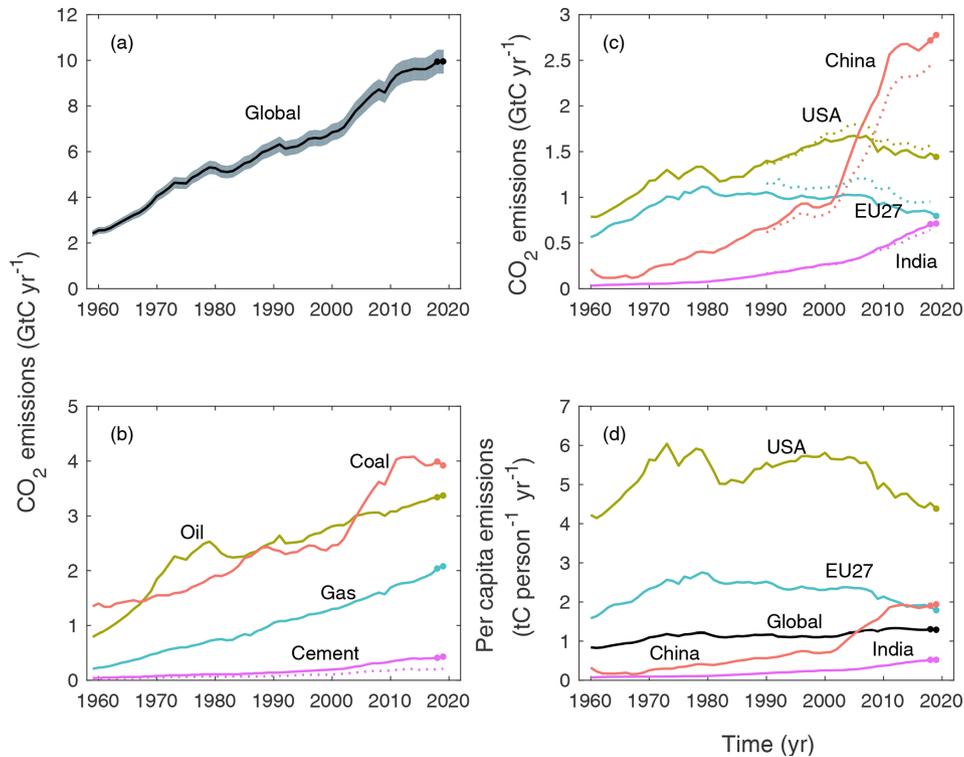
Figure 1: Fossil CO_2 emissions in the period 1960 - 2019 (from **Friedlingstein et al., 2020**)

As it could be seen from **Figure 1**, fossil CO_2 emissions in China (2.7 GtC per year) and India (0.65 GtC per year) record constant growth, especially after 2000, while in the EU27 and the US there is a decline in fossil emissions in the last decade. Emissions in China increased from 0.8 to about 2.7 GtC per year between 2000 and 2019, while in the US they decreased from 1.6 GtC to 1.35 GtC per year. Although fossil CO_2 emissions are on the rise in China, the United States still emits more fossil emissions per capita than China. China is currently on the same volume of emissions as the entire EU, and the US has a declining trend. China emitted 0.65 tC per capita in 2000, and 1.8 tC in 2019, which is an increase of about 1.15 tC per capita. Among fossil fuels, coal combustion has the highest share in emissions, followed by oil and natural gas. Emissions from all types of fossil fuels record increase in period 1960-2020. From 2000 to 2019, coal emissions increased significantly (2.5 GtC to 4.0 GtC per year) due to the increasing coal demand in China (**Šimunović, 2021**).

2.2.2. Global CO_2 emissions in the period 2010 - 2019

During 2010-2019 period, 86% of the total CO_2 emissions ($E_{FOS} + E_{LULUCF}$) were fossil CO_2 emissions, and 14% came from LULUCF, of which 46% remained in the atmosphere, 23% were absorbed by oceans and 31% by the terrestrial biosphere, with a budget imbalance of -1%. Global fossil CO_2 emissions increased at a rate of 1.2% per year with an average of 9.6 ± 0.5 GtC per year excluding the sink of cement carbonization (9.4 ± 0.5 GtC per year with the cement carbonation sink included). Namely, the emissions increased during 2010-2019 by about 94 GtC, which is 21.37% of the total 440 GtC in the period 1850–2019. The average growth rate of atmospheric CO_2 concentration was 5.1 ± 0.02 GtC per year, and sinks in the ocean and terrestrial biosphere were 2.5 ± 0.6 GtC and 3.4 ± 0.9 GtC per year (**Friedlingstein et al., 2020**).

In this decade, China has dominated in increasing fossil CO_2 emissions by an average of 1.2% per year (0.046 GtC per year), followed by India by 5.1% (0.025 GtC per year). In contrast, emissions decreased in the EU27 by 1.4% per year (-0.014 GtC per year), and in the US by 0.7% (-0.01 GtC per year).

2.2.3. Global CO_2 emissions in 2019

In 2019, China had the largest share in the global increase in fossil CO_2 emissions (28%), followed by the USA (14%), the EU27 (8%) and India (7%). These four countries accounted for 57% of global CO_2 fossil emissions, while the

rest of the world contributed 43%, including aviation and marine fuel tanks (3.5% of the total). Emission growth rates for these countries in 2019, compared to the 2018 values, were + 2.2% (China), -2.6% (US), -4.5% (EU27), +1.0% (India) and + 1.8% for the rest of the world. Fossil CO_2 emissions per capita in 2019 were 1.3 tC worldwide and 4.4 tC in the US, 1.9 tC in China, 1.8 tC in the EU27 and 0.5 tC in India (**Friedlingstein et al., 2020**).

Estimates of global fossil CO_2 emissions show slight growth in 2019 (0.1%) compared to 2018, while fossil emissions remain at 9.7 ± 0.5 GtC in 2019. Fossil CO_2 emissions from coal combustion in 2019 accounted for 39% (-1.8%, compared to 2018), followed by fossil emissions from oil 34% (+ 0.8%, compared to 2018) and natural gas 21% (+ 2.0%, compared to 2018).

3. Impact of the Covid-19 pandemic on global CO_2 emissions during 2020

Major changes in CO_2 emissions in 2020 occurred due to the Covid- 19 constraints that led to unprecedented changes in global economy and society. The pandemic and the resulting economic crisis have affected almost all aspects of energy production, supply and consumption worldwide. It has defined energy consumption and emission trends in 2020, has and resulted with the reduction of fossil fuel consumption for most of the year in the most countries worldwide.
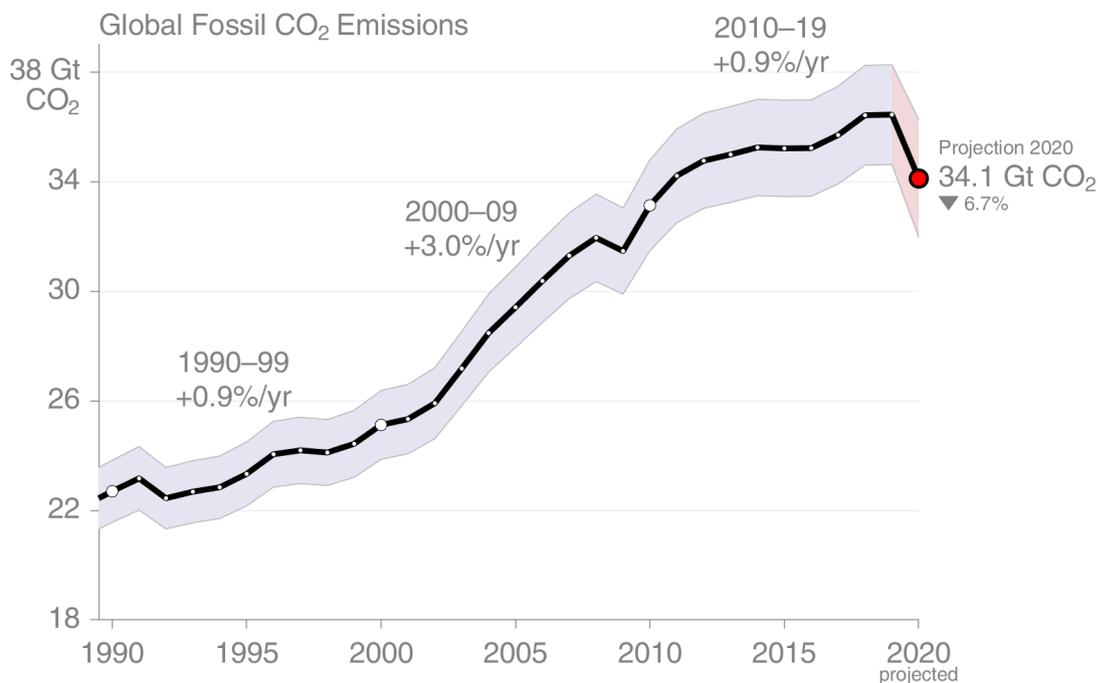
Figure 2: Global fossil CO_2 emissions (from **https://www.globalcarbonproject.org**)

According to the analysis of the Global Carbon Budget 2020, based on several studies and the monthly energy data, global fossil CO_2 emissions for 2020 are estimated at approximately 34 $GtCO_2$, which is 2.4 $GtCO_2$ less than emitted in 2019. Namely, this represents a decrease of about 7% due to the slowdown in economic activities related to the COVID-19 pandemic (**Figure 2**).

3.1. Estimations of global CO_2 emissions

Considering the fact that it is very difficult to accurately determine CO_2 emissions, especially during 2020, the Global Carbon Budget 2020 publication took into account three separate studies as an upgrade to the current method. Emissions were first estimated for part of the year, and then projected for the rest of the year. The studies used for the estimation of CO_2 emissions included **Le Quéré et al. (2020)**, **Forster et al. (2020)**, and **Liu et al. (2020)**.

Le Quéré et al. (2020) estimated CO_2 emissions for six economic sectors based on the data about electricity and coal consumption, steel production, and road and air transport. To estimate absolute daily changes in emissions and to address 67 countries representing 97% of global emissions, the analysis was based on the data about CO_2 emissions by country

for the last available year (2018 or 2019) from the Global Carbon Budget 2019 publication. Until 13th November, all the data had been updated, while the data for the rest of the 2020 were projected, assuming that the Covid-19 measures will remain at the same or lower level until the end of 2020.

Forster et al. (2020) estimated CO_2 emissions primarily on Google's mobility data. The mobility data were used to estimate daily fractional changes in emissions from the energy sector, road transport, industry, housing, and public and commercial sectors. For several countries, primarily China and Iran, Google data were not available, so the data were obtained from the assessment of **Le Quéré et al. (2020)**. The **Forster et al. (2020)** study used a simple extrapolation, assuming that the decline in emissions from base values will remain at 66% of the level in the last 30 days.

Liu et al. (2020) estimated CO_2 emissions based on the data on electricity production, and CO_2 emissions for different sources of electricity from national electricity systems (31 countries), real-time mobility data (416 cities) or indexes (primarily index of industrial production) from national statistics (62 countries and regions), as well as daily emissions from energy sector, industry, transport, and housing. In the study CO_2 emissions were estimated for 2020 and the study did not include any future projections of CO_2 emissions. To enable the comparison other CO_2 emissions estimation methods, a simple extrapolation approach was used, assuming that the values of CO_2 emissions in the remaining months of the year change with the same relative value compared to 2019 in the last month of observation.

Global Carbon Budget (GCB) shows estimations of CO_2 emissions for China, the US, the EU, India, as these are the countries with the highest share in global CO_2 emissions, and for the rest of the world. For China, estimates were done on the basis of the data from the National Bureau of Statistics and Customs, and the emission projections were done on the basis of the previous ratio of monthly and yearly data on CO_2 emissions. For the US, CO_2 emission estimates and projections of the U.S. Energy Information Agency were used. For the EU27, estimates of CO_2 emission from the beginning of the year were done by using the data on monthly consumption of coal, oil and gas converted to CO_2 emissions and scaled to match previous year's emissions. For India CO_2 emission estimates had been updated by **Andrew (2019)**, who calculated the monthly CO_2 emissions directly from the detailed data on energy and cement production. For the CO_2 emissions projections for the remaining months of 2020 (the months from the end of the study till the end of the year) for both, the EU27 and India, the same method as for Carbon Monitor was used. For the rest of the world, no CO_2 emission estimates for the first part of the year were made, while the CO_2 emission projection for 2020 was based on an estimate of GDP combined with the previous editions of the Global Carbon Budget.

3.2. Analysis of changes in global CO_2 emissions

The previously mentioned CO_2 emission estimation/projection studies (methods) used a combination of different data, and gave the CO_2 emission estimations, based on the directly monitored data valid until September 2020, for all regions, except for the EU27, which is based on the data monitored until July 2020. By September 2020, all four studies (methods) show that there has been a decline in fossil CO_2 emissions in 2020 in all countries and regions. The EU and the US showed the declining emission trends even before Covid-19 pandemic, while the pandemic furtherly affected the decline. Similarly, CO_2 emissions in India were declining in 2019, but due to economic problems. However, even in Covid-19 pandemic the long-term trend of increasing emissions in India continues. In 2020 China is recording a smaller drop in CO_2 emissions, which indicates that the impact of the restrictions due to Covid-19 virus occurred earlier than in the rest of the countries and that the Chinese economy has had a longer recovery time. Based on the three studies, that provide sufficient data on the emissions from January to September 2020, global CO_2 emissions decreased by about 8% (median method, based on estimates -7.6%, UEA; -7.6%, Carbon Monitor; -14 .1%, Priestley Centre).

As mentioned earlier, the Global Carbon Budget 2020 estimates that the total global CO_2 emissions have decreased by about 7% in 2020, which is derived from the CO_2 emissions averages of the four previously mentioned studies/methods, with additional uncertainty for each method (-5.8%, GCB; -6.5%, Carbon Monitor; -6.9% (range -2.7 to -10.8%), UEA; -13.0%, Priestley Center) (**Figure 3**).
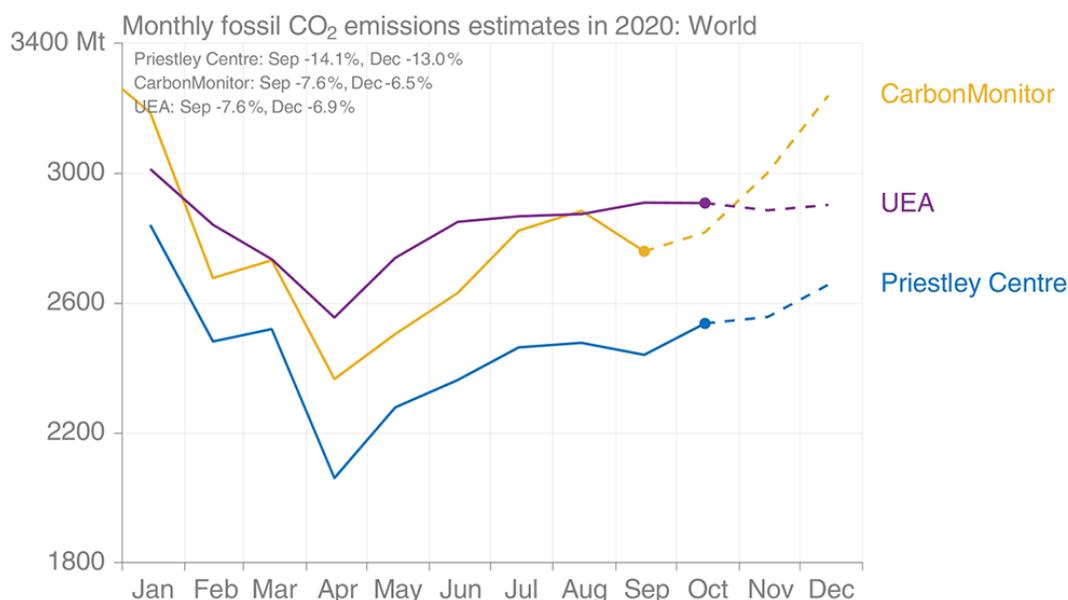
Figure 3: Monthly global estimates of fossil CO_2 emissions in 2020 (from **Friedlingstein et al., 2020**)

Table 3 shows the data on the decline of fossil CO_2 emissions in certain regions and countries in 2020 compared to 2019. The data were obtained as the median of the four aforementioned studies/methods with the note that emissions from the use of fuels for international air and maritime transport are usually not included in the national totals. It can be seen that the largest decline in emissions was in the US (12.2%), followed by the EU (11.3%) and India (9.1%). China recorded the smallest decrease in emissions of only 1.7%, and it quickly began to recover its economic activity. It is one of the first countries to ease the Covid-19 restriction measures, and its CO_2 emissions reached above 2019 levels since April 2020 (**Lehmann et al., 2021**).

Region / Country	2019 emissions (billion tonnes/yr)	2019 growth (%)	2020 projected growth (%)	2020 projected emissions (billion tonnes/yr)
China	10.2	2.2 %	-1.7 %	10.0
USA	5.3	-2.6 %	-12.2 %	4.7
EU27	2.9	-4.5 %	-11.3 %	2.6
India	2.6	1.0 %	-9.1 %	2.4
World	36.4	0.1 %	-6.7 %	34.1

Table 3: CO_2 emissions in 2020 compared to 2019 (from **Friedlingstein et al., 2020; https://www.globalcarbonproject.org**)

Apart from the pandemic at the beginning of 2020, global CO_2 emissions were also affected by the weather conditions. The effect of the pandemic on the global CO_2 emissions became visible in late February, with the decline in global CO_2 emissions peaking by April. However, immediately after the first wave of the pandemic and the regrowth of economic activity, the emissions began to recover by the end of the year. According to the International Energy Agency (IEA, 2021a) report, in December 2020 global CO_2 emissions were 2% higher than in December 2019, so it can be concluded that the changes caused by the Covid-19 measures will not have long-term effect (**Šimunović, 2021**).

3.3. Fossil CO_2 emissions by sector

According to **Le Quéré et al. (2020)** containment and closure Covid- 19 measures led to a reduction in daily global fossil CO_2 emissions by 17 (-11 to -25%) MtCO_2, or 17% (-11 to -25%), by early April 2020 compared to the average daily fossil CO_2 emissions in 2019. Daily fossil CO_2 emissions in early April could be compared to 2006 emission levels,

with the largest daily change in emissions in 2020 occurring on 7th April. For individual countries, the maximum daily decrease was 26% (± 7%) but did not occur on the same day in all countries.

In a study by **Liu et al. (2020)** daily sectoral CO_2 emissions are estimated at the country level from 1 January 2019 to 30 June 2020, based on the results of the international research initiative Carbon Monitor. In this study, only emissions from direct fuel consumption and emissions from chemical processes by the industry sector were taken into account, and emissions related to industry electricity consumption were added to the energy sector CO_2 emissions. CO_2 emission estimates in the energy sector rely on almost real-time hourly or daily electricity data. In the first half of 2020, global fossil CO_2 emissions from the energy sector decreased by 5.0% (-341.4 $MtCO_2$), followed by the decrease of emissions from the industrial sector by 5.5%. For 416 world cities in 57 countries, it is estimated that in the first half of 2020, land transport fossil CO_2 emissions decreased by 18.6% (-613.3 $MtCO_2$), i.e., 17.8% (-685.5 $MtCO_2$) in the first seven months of 2020. Global air transport emissions decreased by 43.9% (-200.8 $MtCO_2$) in the first six months, i.e., 46.7% (-254.5 $MtCO_2$) in the first seven months of 2020, out of which approximately 70% in international air transport.

According to the IEA report (**https://www.iea.org/**), primary energy demand decreased by almost 4% in 2020, which resulted with the decrease of global fossil CO_2 emissions associated with primary energy of 5.6%. **Figure 4** shows the increase in fossil CO_2 emissions in period 1960-2020. Global fossil CO_2 emissions from oil use decreased by about 1.1 $GtCO_2$ (-7.6%), compared to 2019. This is followed by a decline in fossil CO_2 emissions from coal by about 5.1% and natural gas by 3.6% (**https://www.globalcarbonproject.org**).

The decline in road transport activity in 2020 caused a 50% drop in global oil demand, and a decline in air transport by about 35%. The transport sector in 2020 accounted for more than 50% of the total global decline in fossil CO_2 emissions. With various warnings and measures on travel and border closures due to Covid-19 pandemic during 2020, the international air transport was the sector that was the most affected by the pamdemic, and in April experienced the biggest decline of fossil CO_2 emissions of about 70% below the emission level in April 2019. CO_2 emissions from the international air transport decreased by almost 45% or 265 $MtCO_2$ during the year and fell to the levels last seen in 1999 (**https://www.iea.org/**).
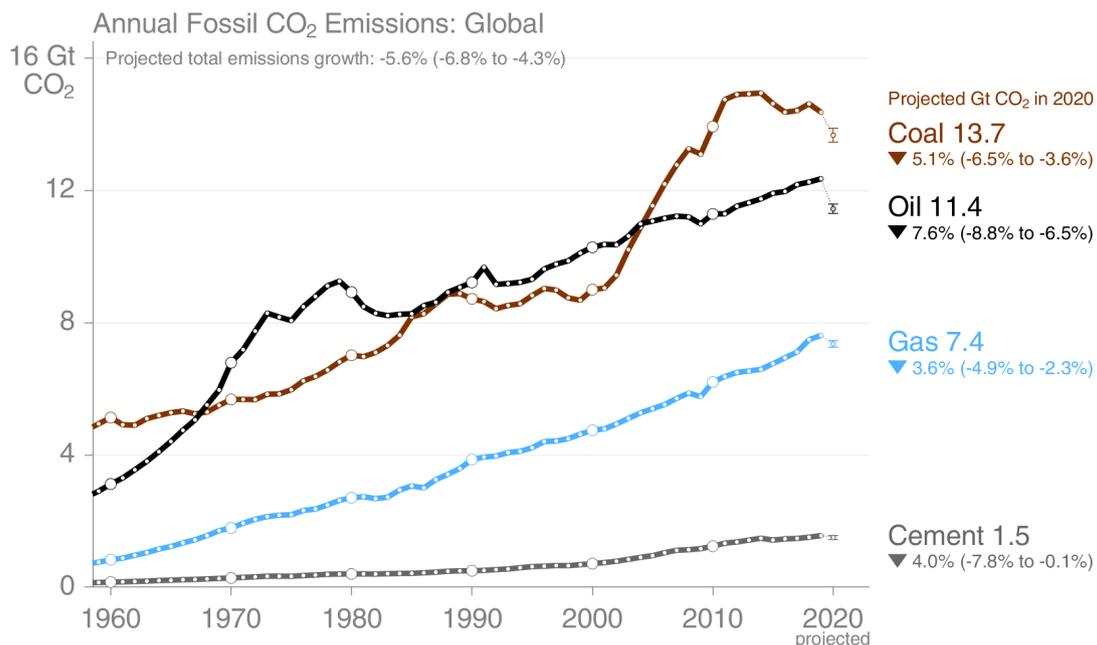
Figure 4: Annual fossil CO_2 emissions with emphasis on 2020 (from **https://www.globalcarbonproject.org**)

4. The impact of the Covid-19 pandemic on future trends of global fossil CO_2 emissions

Although measures to combat the COVID-19 pandemic under the Global Carbon Budget 2020 caused a decline in fossil CO_2 emissions in 2020, they did not in themselves cause a lasting reduction in emissions. The temporary measures have little impact on the infrastructure of the world economy based on the use of fossil fuels. What will happen to energy demand and emissions in 2021, but also later, will depend on how much governments put emphasis on energy transition

during the economy's recovery from the COVID-19 crisis in the future (**Steffen et al., 2020**). Economic incentives at the national level could change the flow of global emissions if investment in green infrastructure increases and investment in fossil energy decreases. However, the real opportunity for political change depends on the capacities of the countries. Significantly, emerging economies such as India, Russia, or Indonesia have issued smaller incentive programs than advanced economies such as the United States or the EU.

4.1. Recovery of global fossil CO_2 emissions in 2021.

The International Monetary Fund (IMF) and the Energy Information Administration (EIA) predict that emissions for the world and US economies will recover by 5.8% and 3.5%, respectively, in 2021. According to an IEA report (2021a), emissions are expected to grow by around 1500 $MtCO_2$ in 2021, but this still leaves global CO_2 emissions by around 400 $MtCO_2$, or 1.2%, below the 2019 peak. Also, energy demand is expected to recover by 4.6%, which will increase global energy consumption by 0.5% above the level before COVID-19 in 2021 (IEA, 2021a). The current economic outlook assumes that global GDP will be higher than in 2019, increasing demand for goods, services and energy, but this depends on COVID-19 measures, the effectiveness of the recovery package and the introduction of vaccines. **Figure 5** shows the growth in demand for goods and services, which also affects the demand for primary energy. Namely, as economies recover from the effects of the pandemic, energy demand will increase, resulting in an increase in fossil CO_2 emissions.
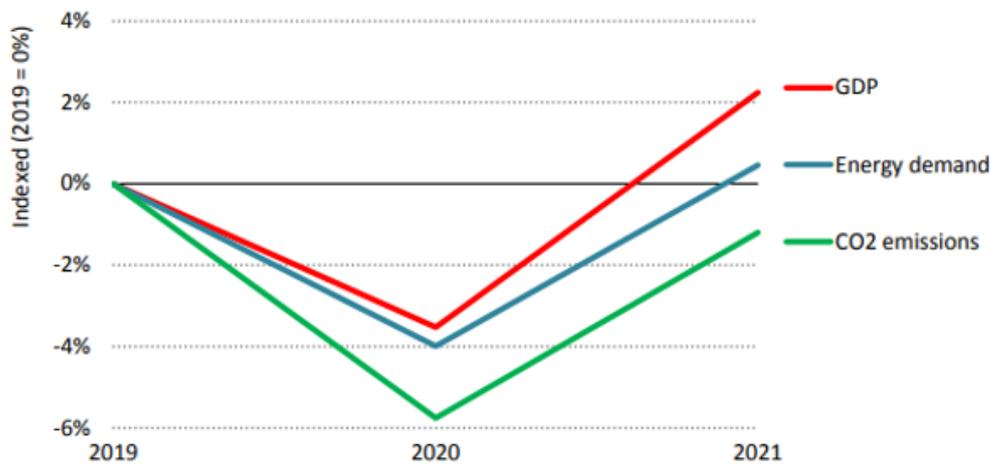
Figure 5: Recovery of global GDP, total primary energy demand and energy-related CO_2 emissions, compared to 2019. (from **https://iea.blob.core.windows.net/**)

Despite the fact that global economic activity has recovered in 2021, and thus energy demand, a full return of CO_2 emissions to pre-crisis levels is not expected. **Figure 6** shows fossil CO_2 emissions for individual regions and countries, and it can be seen that there was an increase in fossil CO_2 emissions in the period January - September 2021 compared to the same period in the previous year. Thus, during 2021, the economy recovered and, consequently, fossil emissions increased in almost all sectors. The sector that still lags behind the rest is air transport due to the restrictive "Covid" measures that were in force. According to the Carbon Monitor, global fossil CO_2 emissions increased by about 6.4% (+1562.8 $MtCO_2$) in 2021. compared to the same period in 2020. In the energy sector, emissions increased by 7.2% (+691.2 $MtCO_2$). The transport sector also experienced a major recovery, with an increase in emissions in road transport of 8.5% (+359.6 $MtCO_2$), followed by 26.8% in domestic air transport (+48.7 $MtCO_2$) and international air transport 4, 6% (+9.9 $MtCO_2$). There is also an increase in emissions in the housing sector by 3.5% (+83.9 $MtCO_2$) and in the industrial sector by 4.8% (+369.5 $MtCO_2$). Brazil can be seen to have the largest increase in CO_2 emissions of 24.2% (66.9 $MtCO_2$), but this figure does not contribute much to the global increase in emissions compared to China (+714.97 $MtCO_2$ in 2021.). In 2021, the countries contributing to the largest increase in fossil CO_2 emissions are China, the US, India and the European Union (**https://carbonmonitor.org/**).
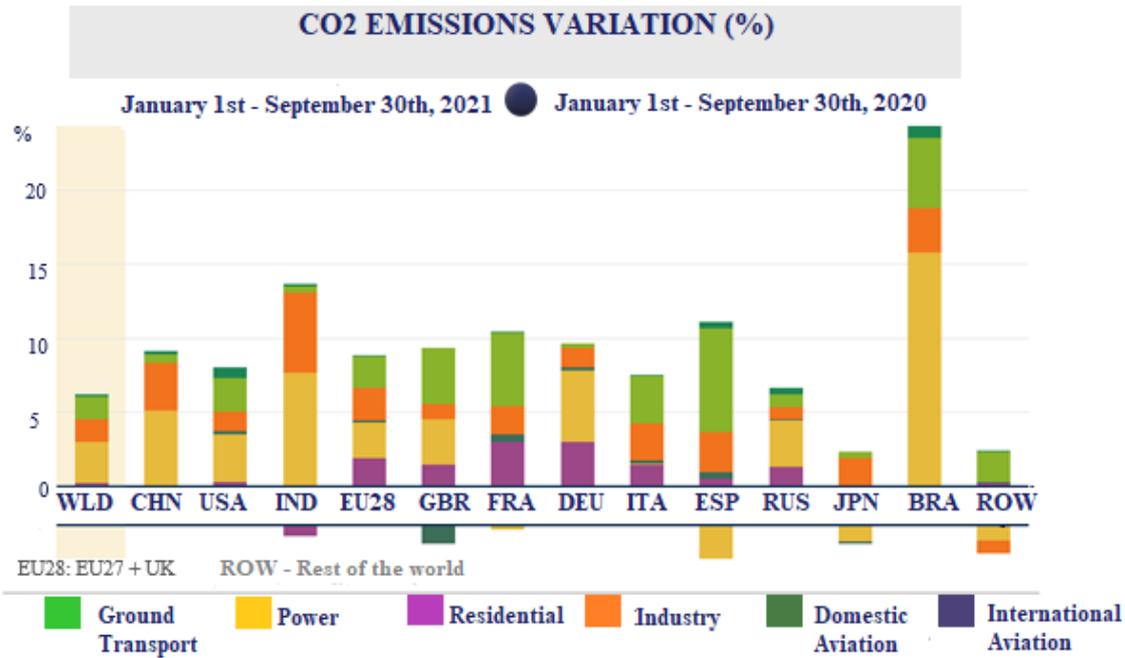
Figure 6: Growth of fossil CO_2 emissions in 2021. compared to 2020. for individual regions and countries (from **https://carbonmonitor.org/**)

4.2. Long-term trend of fossil CO_2 emissions

It is believed that the crisis caused by the Covid-19 pandemic could lead to the social changes needed to mitigate adverse climate change. Namely, the ecological sustainability cannot be allowed at the cost of the social sustainability, because that would trigger various issues. Moreover, this can shape the public opinion to associate energy transition with an excessive restriction of individual rights or with a general economic downturn.

The results of **Hanna et al., 2020** show that the impact of the pandemic on global warming will be insignificant and that without the long-term decarbonization of economy system and major changes in the behaviour of each individual, it cannot significantly affect global climate change. Even if the Covid-19 crisis creates an opportunity for individual change, it will promote environmental sustainability under certain conditions. During the pandemic digitization has progressed, many people worked remotely, but the pandemic also fostered people, who travelled to work by using the public transport, to use private cars to avoid the risk of the infection. Some research even predict that the Covid-19 pandemic could have permanent effects on the public transport and could lead to the increase of dependence on cars, which will consequently result with the increase of fossil CO_2 emissions.

Throughout the history, there have been economic crises that have led to a reduction in CO_2 emissions, but after each crisis there has been an increase again. Some analyses show that during the recovery from the second oil crisis, which began in 1979, fossil CO_2 emissions growth declined by one third. During the period from 1976–1979 the reduction in fossil CO_2 emissions growth was 3.6% per year. and during 1983-1990 2.4% per year. The next major recession was triggered by the collapse of the Soviet Union in 1991. The trajectory of growth of fossil CO_2 emissions decreased by another third, to 1.6% per year during 1994–1997 period (**Hanna et al., 2020**). During the Asian financial crisis of 1998 after a brief recession, fossil CO_2 emissions growth doubled due to the rapid industrial expansion. It was a period of the rise of China, which promoted production and exports, all fuelled by coal. This was followed by the global financial crisis of 2008, after which fossil CO_2 emissions growth declined by 1.6% per year over the next decade. However, the current decline in fossil CO_2 emissions is the largest decline since the World War II (1939–1945) when fossil CO_2 emissions declined by 4% (**Usman et al., 2021**).

But, even if fossil CO_2 emissions follow the same trend as before the pandemic, by 2050 the Covid-19 crisis effects will prevent a cumulative 128 GtCO₂ in the atmosphere - equivalent to roughly three years of emissions at 2018 levels (**Hanna et al., 2020**). However, the further trend of fossil CO_2 emissions will be affected by fiscal incentives for economic recovery. Economies rarely return to pre-crisis conditions. Namely they usually go to either a "green" or "dirty" recovery. In **Figure 7** the three possible recovery scenarios are shown. The black line represents a scenario without the pandemic,

so called business-as-usual (BAU) scenario, the red line represents the economic recovery through fossil fuel investments, and the blue line represents the economic recovery based on the investments in low-carbon technologies. The economic recovery based on fossil fuels use would quickly increase CO_2 emissions again so they will quickly exceed the pre-pandemic emission's trajectory. The economic recovery based on the investments in low-carbon technologies would keep CO_2 emissions under the pre-pandemic levels. The difference between those two scenarios is 230 $GtCO_2$ by 2050, which is equivalent to a change in atmospheric concentration of about 19 ppm. However, it is up to future climate policies to determine in which direction the global economy and thus the trend of fossil CO_2 emissions will move.
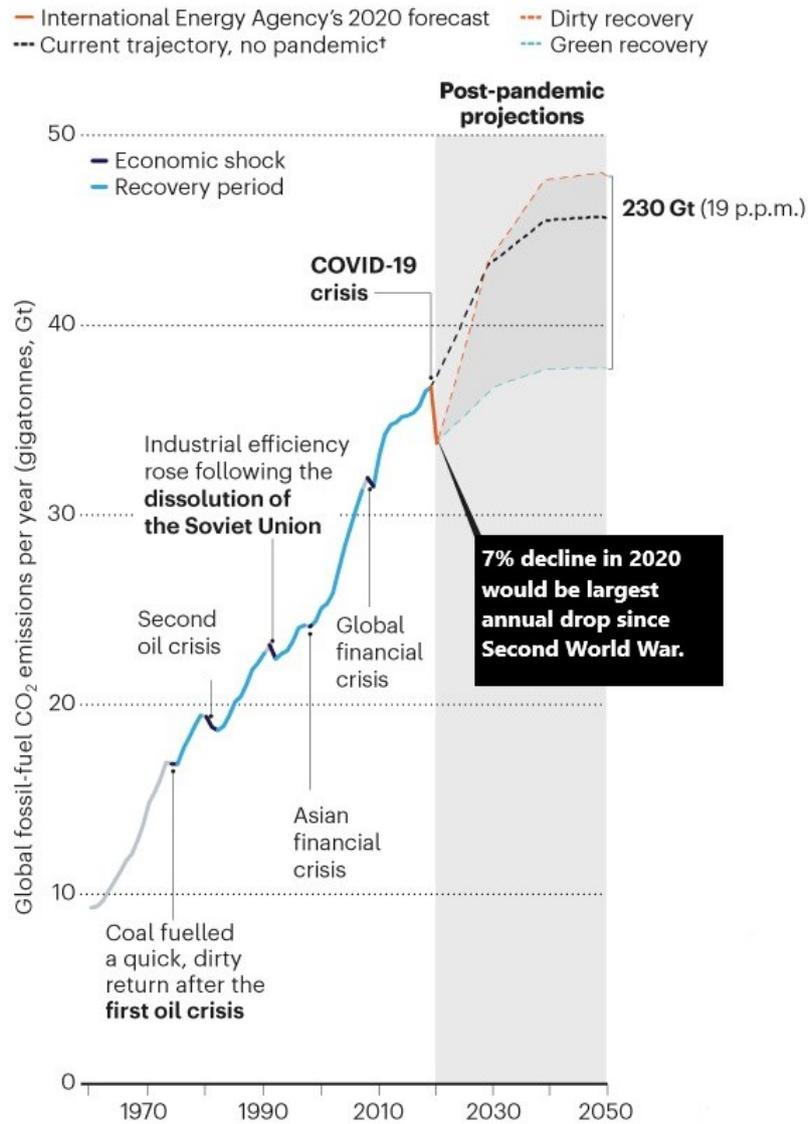
Figure 7: Long-term trend of fossil CO_2 emissions (from **Hanna et al., 2020**)

4.3. Influence of Covid-19 on climate policies

Energy and climate policies will have to adapt to new circumstances that will gradually develop with the progress of the pandemic. Current economic policy interventions were designed under significant time pressure, leaving short time to consider their impact on climate. The pandemic even put under the question the well-established and planned energy policies, especially those affecting the industries that have been severely affected by the current Covid-19 crisis. Some actions caused by the pandemic could have serious unintended consequences for the energy transition. The preliminary results of the studies of the Covid-19 on the realization of the Sustainable Development Goals (SDGs) suggest that the

Covid-19 pandemic has slowed progress in the activities related to 12 of the 17 SDGs, such as no poverty, zero hunger, or reduced inequalities (**Leal et al., 2020**). For the most vulnerable groups, which are at the same time most severely affected by the pandemic, the Covid-19 crisis is not an opportunity for social change, but a threat to everyday survival (**Cho, 2020**).

The impacts of the pandemic may be particularly adverse in the developing countries, where the crisis has resulted in currency inflation and higher loan costs. This particularly undermines investments in renewable energy technologies due to their high capital investment (**Quitzow et al., 2021**). As a result, green investments have been delayed in many countries, with more than half a million renewable energy jobs being lost in the U.S. in the first months of the pandemic (**Blackmon, 2020**).

However, the question is how subsequent fiscal packages for economic recovery during and after the Covid-19 crises will affect climate policies. Most certainly is that the Covid-19 crisis represents a dramatic shock to the global economy that will affect the progress in climate change mitigation activities in many ways. The policy of closing down the countries during the great waves of the pandemic has done a lot in terms of the current reductions in CO_2 emissions, which contribute to achieving the climate goals. Namely, the short-term emission reductions will not have long-term effects if the steps that were started even before the pandemic are not continued. During Covid-19, global CO_2 emissions in 2020. were brought to the 2006. and 2007 levels, and now is the right opportunity for the CO_2 emission's declining trend to continue. Fiscal stimuluses could be either a threat to global climate change or a start to achieving a net energy economy with zero emissions. In the event that remittance and economic recovery investments go to traditional carbon-intensive sectors, this would mean not only a short-term increase in emissions, but also a further embracing of the fossil fuel-based economy. The latest reports show that the G20 countries, plan to invest about 52% of the recovery packages into the fossil fuel-related energy sectors, without any environmental commitments (**Shan et al., 2021**).

Experience from the previous economic crises, especially the economic and financial crisis of 2008/2009, indicates that climate and environmental policies in such situations can be set aside or be of the reduced importance. The fiscal plans of the United Nations Program after the 2008 financial crisis in most G20 countries remained unfulfilled. Only 15% of the $ 3 trillion in fiscal stimulus was spent on "green" stimulus during the recession, accounting for only 0.7% of the G20 GDP. In addition, the results showed that the main contribution to the recovery of CO_2 emissions after the 2008 financial crisis was the decline in energy efficiency. However, it does not necessarily mean that history will repeat itself, but one should be careful and take such cases into account.

Figure 8 shows the different scenarios for fossil CO_2 emissions according to the given fiscal stimulus until the 2024. Depending on the scenario, the results show that the global CO_2 emissions in the period 2020-2024 will range from a decrease of 4.7% to an increase of 16.4%. However, only CO_2 emissions from the economy sector are considered here, so the overall reduction in CO_2 emissions could be less than estimated due to the possible increases in emissions from the housing sector. The green and red areas show the allowed emissions, i.e., the amount of emissions that can be emitted to keep the temperature increase below 2°C and 1.5°C, respectively. The black line represents the basic scenario (BAU) based on the assumption that the Covid-9 pandemic did not occur. The dark green line represents the worst-case scenario, in which it is assumed that if emissions increased at an average rate of 4.3% per year, they would exceed the maximum allowed emissions. However, total CO_2 emissions in 79 countries are projected to decrease by 3.9 to 5.6% between 2020 and 2024, compared to the basic scenario. The worst-case scenario would increase global fossil CO_2 emissions by 16.4% (23.2 Gt) if fiscal packages were directed towards establishing carbon-intensive infrastructure and technologies. In contrast, the "greenest" scenario could reduce fossil CO_2 emissions by 4.7% (6.6 Gt) if fiscal stimulus was allocated to low-carbon technologies (**Shan et al., 2021**).
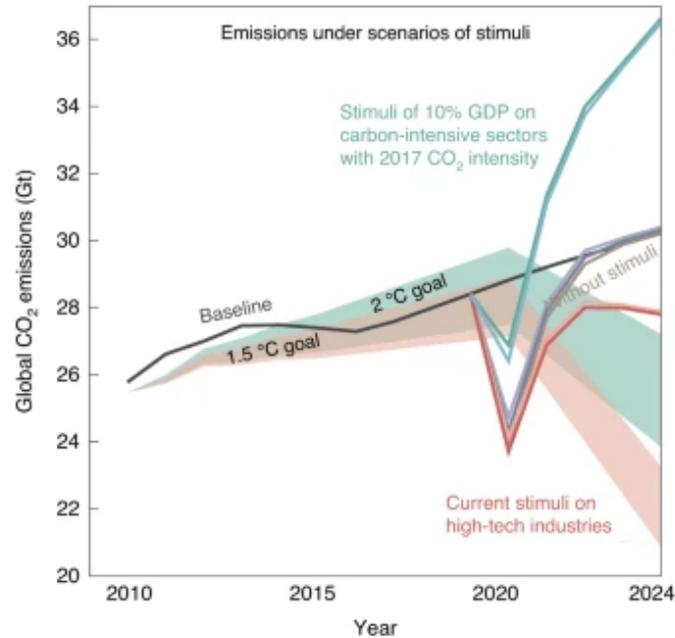
Figure 8: Emissions according to fiscal stimulus scenarios and
comparison with allowed emissions (from **Shan et al., 2021**)

Unlike previous crises, the Covid-19 crisis so far didn't abolish the EU climate policy. In fact, at this point, the crisis has led to strengthening and consolidating of the European Green Deal and the necessary investments, although its implementation might be affected. The Covid-19 crisis could affect the development of the EU climate policies in two respects: (1) further implementation of the European Green Deal and (2) an economy recovery approach from the crisis (**Dupont et al., 2020**).

For now, there is no evidence that the Covid-19 crisis will lead to policies setbacks, other than some initial delays. At this point the crisis caused the strengthening of the policies development and implementation, but in terms of general objectives and directions. On the other hand, most of the energy policy plans are still awaiting implementation, but the current Covid-19 crisis cannot be pointed out as the cause of the nonimplementation. Since it is difficult to predict how the pandemic will develop and what will result with in the future, a certain period of time is needed for a more precise assessment.

5. Deviations from the projections of CO_2 emissions

According to recent data from the Global Carbon Budget 2021, which was published in after the completion of this paper, fossil CO_2 emissions decreased by 5.4% in 2020 compared to 2019, amounting $9.5 \pm 0, 5$ GtC (9.3 ± 0.5 GtC when the cement carbonation sink is involved). Namely, this is ultimately a smaller decrease than the projected value of fossil CO_2 emissions according to the Global Carbon Budget 2020 data. Differences in the budget and deviations for such difficulty quantifiable data are common, which can be seen in **Table 3** for the previous years. As mentioned earlier in the Global Carbon Budget 2020, these are measured data for one part of the year, while for the rest of the year the data are projected. In general, the mean and the trend of the components of the global carbon budget have been consistently estimated in period1959-2020, but there are deviations of 1 GtC between annual to semi-decadal variability in CO_2 emissions trends.

A comparison of CO_2 emissions estimates from several approaches and/or methods shows constant uncertainty in the assessment of fossil CO_2 emissions, but also in the assessment of the emissions from land use, land use change and forestry, and natural sinks. A newer version of the publication is likely to provide more accurate data on global CO_2 emissions, given that the other data and measurements were available after the end of 2020. Global average CO_2 concentration in the atmosphere during 2020 was 412.45 ± 0.1 ppm. Also, preliminary data for 2021 predicted an increase in global fossil CO_2 emissions of 4.9% (4.1% to 5.7%) compared to 2020 (**Friedlingstein et al., 2021**).

6. Conclusions

In 2020, there was a reduction in fossil CO_2 emissions due to the restrictive measures during the Covid-19 pandemic. In some publications the decline in global fossil CO_2 emissions in 2020was 7%, while in more recent publications the decline is estimated to 5.4%. Regardless of the pandemic, global fossil CO_2 emissions have increased by 61% since 1990, although the rate of increase has varied over the years. The primary driver of this increase was the continued growth in fossil fuels energy use such as coal, oil and natural gas. Variations in the pace of the fossil CO_2 emissions growth are often associated with the rise or downturn of large economies, such as China and the Soviet Union. It is encouraging that the rate of the increase in CO_2 emissions has slowed over the last decade, with an average growth rate less than 1% per year, which is significantly less than an average increase of 3% per year during the early 2000s. Nevertheless, to meet the ambitious goals of the Paris Agreement a reduction of 1-2 $GtCO_2$ per year during the 2020s and beyond is needed.

It is difficult to predict the future trajectory of fossil CO_2 emissions, all the Covid-19 consequences and its effects on the future trend of fossil CO_2 emissions. In any case, the fight against Covid-19 virus has encouraged humanity and provided the experience for the development of future strategies in crisis situations such as climate change mitigation. In addition, the Covid-19 crisis has shown that governments can take swift and drastic action when needed, and that they should move in that direction in the development of climate policies. Moreover, the pandemic can turn into a real opportunity to mitigate climate change if individual change is combined with the policy change based on smart and targeted recovery policies. Policies must encourage the investments into economic recovery that will equally address the environmental, economic and social issues. In other words, policy makers, companies, scientists and society as a whole must actively create opportunities and progress towards a "greener" future.

7. References

1. Andres, R.J., Boden1, T.A., Bréon, F.M., Ciais, P., Davis, S., Erickson, D., Gregg, J.S., Jacobson, J., Marland, G., Miller, J., Oda, T., Olivier, J.G.J., Raupach, M.R., Rayner, P. and Treanton, K. (2012): A synthesis of carbon dioxide emissions from fossil-fuel combustion. Biogeosciences, 9, 1845–1871. https://doi.org/10.5194/bg-9-1845-2012

2. Andrew, R.M. (2019): Global CO_2 emissions from cement production, 1928-2018., 11, 1675-1710. https://doi.org/10.5194/essd-11-1675-2019

3. Archer, D., Eby, M., Brovkin, V., Ridgwell, A., Cao, L., Mikolajewicz, U., Caldeira, K., Matsumoto, K., Munhoven, G., Montenegro, A. and Tokos, K. (2009): Atmospheric Lifetime of Fossil Fuel Carbon Dioxide. Earth and Planet. Sci, 37, 117-134. https://doi.org/10.1146/annurev.earth.031208.100206

4. Blackmon, D. (2020): How COVID-19 is hindering the energy transition. Forbes.

5. Cho, R. (2020): COVID-19's long-term effects on climate change-for better or worse. Environmental Science and Pollution Research, 28, 49302-49313.

6. Dupont, C., Oberthür, S. and Von Homeyer, I. (2020): The Covid-19 crisis: a critical juncture for EU climate policy development? J Eur Integr., 42(8), 1095-1110. https://doi.org/10.1080/07036337.2020.1853117

7. Forster, P.M., Forster, H.I., Evans, M.J., Keller, C.A., Lamboll, R.D., Gidden, M.J., Jones, C.D., Quéré, C.L., Rogelj, J., Rosen, D., Schleussner, C.F. and Turnock, S.T. (2020): Current and future global climate impacts resulting from COVID-19. Nature Climate Change, 10, 913–919. https://doi.org/10.1038/s41558-020-0883-0

8. Friedlingstein, P. et al. (2020): Global carbon budget 2020. Earth System Science Data, 12, 3269-3340. https://doi.org/10.5194/essd-12-3269-2020

9. Friedlingstein, P. et al. (2021): Global Carbon Budget 2021. Earth System Science Data, 14, 1917-2005. https://doi.org/10.5194/essd-14-1917-2022

10. Gasser, T., Crepin, L., Quilcaille, Y., Houghton, R.A., Ciais, P. and Obersteiner, M. (2020): Historical CO_2 emissions from land use and land cover change and their uncertainty. Biogeosciences, 17, 4075-4101. https://doi.org/10.5194/bg-17-4075-2020

11. Hanna, R., Xu, Y. and Victor, D. G. (2020): After COVID-19, green investment must deliver jobs to get political traction. Nature, 582(7811), 178-180. https://doi.org/10.1038/d41586-020-01682-1.

12. Hansis, E., Davis, S. J. and Pongratz, J. (2015): Relevance of methodological choices for accounting of land use change carbon fluxes. Global Biogeochemical Cycles, 29(8), 1230-1246. https://doi.org/10.1002/2014GB004997

13. Houghton, R.A. (2003): Revised estimates of the annual net flux of carbon to the atmosphere from changes in land use and land management 1850-2000. Tellus B, 55(2), 378-390. https://doi.org/10.1034/j.1600-0889.2003.01450.x

14. Houghton, R.A. and Nassikas, A A. (2017): Global and regional fluxes of carbon from land use and land cover change 1850–2015. Global Biogeochemical Cycles, 31(3), 456-472. https://doi.org/10.1002/2016GB005546

15. Hrnčević, L. (2008): *Analiza utjecaja provedbe Kyoto Protokola na naftnu industriju i poslovanje naftne tvrtke. (Analysis of the Kyoto Protocol impact on the petroleum industry and petroleum company corporate business), doctoral thesis,* Faculty of Mining, Geology & Petroleum Engineering, University of Zagreb, pp. 361, Zagreb

16. Joos, F. and Spahni, R. (2008): Rates of change in natural and anthropogenic radiative forcing over the past 20,000 years. The Proceedings of the National Academy of Sciences Journal, 105(5), 1425-1430. https://doi.org/10.1073/pnas.0707386105

17. Le Quéré C., Jackson, R.B., Jones, M.W, Smith, A.J.P., Abernethy, S., Andrew, R.M., De-Gol, A.J., Willis, D.R., Shan, Y., Canadell, J.G., Friedlingstein, P., Creutzig, F. and Peters, G.P. (2020): Temporary reduction in daily global CO_2 emissions during the COVID-19 forced confinement. Nature Climate Change, 10, 647-653. https://doi.org/10.1038/s41558-020-0797-x

18. Le Quéré, C., Peters, G.P., Friedlingstein, P., Andrew, R.M., Canadell, J.G., Davis, S.J., Jackson, R.B. and Jones, M.W. (2021): Fossil CO_2 emissions in the post-COVID-19 era. Nature Climate Change, 11, 197-199. https://doi.org/10.1038/s41558-021-01001-02021

19. Leal, F.W., Brandli, L.L, Salvia, A.L., Bacchus, L.R. and Platje, J. (2020): COVID-19 and the UN sustainable development goals: threat to solidarity or an opportunity? Sustainability, 12(13), 5343. https://doi.org/10.3390/su12135343

20. Lehmann, P., de Brito, M.M, Gawel, E., Groß, M., Haase, A., Lepenies, R., Otto, D., Schiller, J., Strunz, S. and Thrän, D. (2021): Making the COVID-19 crisis a real opportunity for environmental sustainability. Sustainability Science, 16, 2137-2145. https://doi.org/10.1007/s11625-021-01003-z

21. Liu, Z. et al. (2020): Near-real-time monitoring of global CO_2 emissions reveals the effects of the COVID-19 pandemic. Nature Communications, 11, 5172. https://doi.org/10.1038/s41467-020-18922-7

22. Marsh, G.E. (2014): Interglacials, Milankovitch Cycles, Solar Activity, and Carbon Dioxide. Journal of Climatology, 2014, 345482. http://dx.doi.org/10.1155/2014/345482

23. Peters, G.P., Minx, J.C., Weber, C.L. and Edenhofer, O. (2011): Growth in emission transfers via international trade from 1990 to 2008. The Proceedings of the National Academy of Sciences Journal, 108(21), 8903-8908. https://doi.org/10.1073/pnas.1006388108

24. Quitzow, R. et al. (2021): The COVID-19 crisis deepens the gulf between leaders and laggards in the global energy transition. Energy Research & Social Science, 74, 101981. 10.1016/j.erss.2021.101981

25. Shan, Y., Ou, J., Wang, D., Zeng, Z., Zhang, S., Guan, D. and Hubacek, K. (2021): Impacts of COVID-19 and fiscal stimuli on global emissions and the Paris Agreement. Nature Climate Change, 11, 200-206. https://doi.org/10.1038/s41558-020-00977-5

26. Steffen, B., Egli, F., Pahle, M. and Schmidt, T.S. (2020): Navigating the Clean Energy Transition in the COVID-19 Crisis. Joule, 4(6), 1137-1141. https://doi.org/10.1016/j.joule.2020.04.011

27. Šimunović, I. (2021): Analiza globalnih promjena fosilnih CO_2 emisija tijekom Covid ere. Rudarsko-geološko-naftni fakultet, Sveučilište u Zagrebu, Zagreb, 50 p.

28. Usman, M., Husnain, M., Riaz, A. and Ali, Y. (2021): Climate change during the COVID-19 outbreak: scoping future perspectives. Environ Sci Pollut Res Int, 1-12. https://doi.org/10.1007/s11356-021-14088-x

Internet sources:

29. URL: https://carbonmonitor.org/ (accessed 28th October 2021)
30. URL: http://www.co2.earth/ (accessed 14th June 2022)
31. URL: https://gml.noaa.gov/ccgg/trends/global.html (accessed 14th August 2021)
32. URL: https://iea.blob.core.windows.net/assets/d0031107-401d-4a2f-a48b-9eed19457335/GlobalEnergyReview2021.pdf. (accessed 1st August 2021)
33. URL: https://unfccc.int/process-and-meetings/transparency-and-reporting/reporting-and-review-under-theconvention/greenhouse-gas-inventories-annex-i-parties/national-inventory-submissions-2020 (accessed 5th October 2021)
34. URL: https://www.iea.org/articles/global-energy-review-co2-emissions-in-2020. (accessed 1st August 2021)
35. URL: https://ec.europa.eu/info/strategy/priorities-2019-2024/european-green-deal/delivering-european-green-deal_hr (accessed 26th September 2021)
36. URL: https://energy.appstate.edu/CDIAC (16th September 2021
37. URL: https://www.globalcarbonproject.org/carbonbudget/archive/2020/GCP_CarbonBudget_2020.pdf (accessed 28th September 2021)

Sažetak

Analiza globalnih promjena fosilnih CO_2 emisija tijekom i nakon Covid-19 ere

Poznato je da do povećanja fosilnih emisija ugljikovog dioksida (CO_2) došlo uslijed izgaranja sve većih količina fosilnih goriva tijekom godina. Koncentracija CO_2 u atmosferi je u porastu, jer se ne može postići ravnoteža putem prirodnih ponora (uklanjanja) CO_2, što je dodatno utjecalo i na nepovoljne klimatske promjene. Međutim, tijekom 2020. godine došlo je do značajnijeg pada globalnih fosilnih emisija CO_2 zbog ograničavajućih mjera tijekom pandemije COVID-19. Iako je ovaj pad emisija bio znatan, trend fosilnih emisija CO_2 u 2021., ali i kasnije, ovisit će uglavnom o uspješnosti provedbe energetske tranzicije, tijekom oporavka gospodarstava od COVID-19 krize. U ovom radu predstavljene su srednje vrijednosti, varijacije i trendovi globalnih fosilnih emisija CO_2 tijekom razdoblja 1959.–2020., s naglaskom na analizu promjena u 2020. godini. Zatim su prikazane procjene i budući dugoročni trendovi globalnih, fosilnih emisija CO_2.

Ključne riječi: fosilne emisije CO_2; trendovi emisija; utjecaj COVIDa-19

Author's contribution

Sonja Koščak Kolin (Assistant professor, PhD, energy engineering, renewable energy resources, well testing, oil and gas production engineering, unconventional oil and gas reservoirs) provided the conceptualization, analysis validation, supervision and writing original draft preparation. **Lidia Hrnčević** (Associate professor, PhD, environmental protection in petroleum industry, oil spill remediation, climate change issues, greenhouse emissions from petroleum industry, petroleum industry process control) provided the resources, performed formal analysis and visualization. **Ivana Šimunović** (mag. ing. petrol., energy engineering, renewable energy resources, sustainable energy) provided the methodology, investigation, interpretations and presentation of the results.

Turbidite lithofacies cut-offs definition, case study Ivanić field, Sava Depression, Croatia

Kristina Novak Zelenika[1]; Ana Majstorović Bušić [2]
[1,2] INA-Oil Industry Plc., Av. V. Holjevca 10, Zagreb,
[1]ORCID: 0000-0002-0090-6879

Abstract

The Ivanić oil field is situated in the central Croatia, in the north-western part of the Sava Depression. Field was discovered in 1963. The secondary phase of reservoir development began 9 years later, in 1972. A total of 87 wells have been drilled so far. A tertiary, EOR phase, started in 2014 and continues up to date. The structure is an asymmetrical brachianticline, with somewhat longer axis of northwest-southeast strike. There are several normal and reverse faults in the field. 11 sandstone intervals have been defined within the Pannonian „Gamma series". They consist of medium to fine-grained quartz-mica sandstones in continuous alternation with marls. During the EOR monitoring parts of the reservoir with remaining hydrocarbon saturation had to be defined. Remaining oil should be found in the parts of the reservoir with lower reservoir properties (porosities and permeabilities). Continuous core pointed out to existence of all transitional lithofacies between pure sandstones and pure marls. To define exact values of cut-offs for different lithofacies, capillary pressure curves and several correlations (porosity-permeability, porosity-irreducible water saturation and porosity-volume of shale) were used. Based on defined cut-offs four lithofacies were determined for all wells in the field (sandstones 20-27% Por, 0-25 % Sw, 0-45% Vsh; marly sandstones 11-20% Por, 25-60% Sw, 45-65, % Vsh; sandy marls 8-11 % Por, 60-85 % Sw, 65-70 % Vsh; marls 0-8% Por, 85-100% Sw, 70-100% Vsh). One injection and one production wells were analyzed. Defined lithofacies were compared with the CO_2 injection and oil production. The part of reservoirs with highest injection of the CO_2 shows a good match with pure channel sandstone, while the highest oil production matches lithofacies with increased content of marl component. Those cases could confirm the assumption that lithofacies with lower reservoir properties may still contain remaining oil.

Keywords: lithofacies definition; EOR; Pannonian reservoirs; Sava Depression; Croatia

1. Introduction

The Ivanić oil field is situated in the north-western part of the Sava Depression, central Croatia. It mostly covers the inhabited part of the Ivanić Grad area, and only the outermost southern edge of the field lies in agricultural area. The terrain is a plain, and agricultural crops and meadows cover the uninhabited part. The Lonja river intersects the central part of the field, in the north-south direction (**Figure 1**).

The first exploration activities began in the period 1940 – 1942 by gravimetric survey of north Croatia. Ivanić Field was discovered in 1963 establishing commercial quantities of hydrocarbons in the „Gamma series" sandstones. A total of 87 wells have been drilled in the field so far.

The secondary phase of reservoir development by injection of water began in 1972. The applied waterflooding system was linear and continuous contour system, with two peripheral injection rows (in the N-W and S-E part of the field) and one "intersecting row" in the middle of the field, with seven production rows.

A tertiary, EOR phase, started in 2014 and continues up to date. During the EOR monitoring, a need for better reservoir understanding occur. Parts of the reservoirs with remaining hydrocarbon saturation had to be defined. The value of the remaining oil saturation depends on different rock properties such as porosity, permeability, capillary pressure, relative permeability etc., but it also depends on the number of pore volumes flooded through the pores. Good pore connectivity can be expected in parts of the reservoir with better reservoir properties, which means that those zones are washed-out. Main assumption was that remaining oil should be found in the channel lobes with lower reservoir properties rather than in the washed-out channel center with high porosities and permeabilities. Depositional channels and lobes of turbidity sandstones are visible on the porosity-thickness maps. Theoretically, such maps describe four lithofacies,

Corresponding author: Ana Majstorović Bušić
Ana.majstorovicbusic@ina.hr

indicating an increase of the marl component, starting from the pure channel sandstones, marly sandstones and sandy marls to pure basinal marls.

Four lithofacies were determined based on cut-off on the shale volume, porosity and water saturation logs and set for all wells in the field. Obtained lithofacies were compared with the oil production. The part of reservoirs with highest injection of the CO_2 shows a good match with pure channel sandstone lithofacies defined in wells, while the highest oil production, in some cases, matches lithofacies with increased content of marl component, like marly sandstones. Those cases could confirm the assumption that lithofacies with lower reservoir properties may still contain remaining oil.
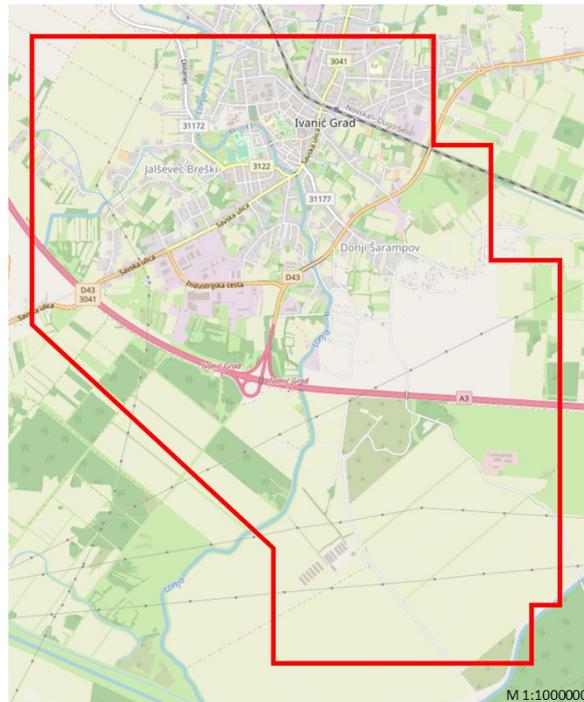
Figure 1: Ivanić exploitation field, situation map

2. Geological overview

Sava Depression represents the south-western margin of the Croatian part of the Pannonian Basin System (CPBS) (e.g. **Pavelić, 2002; Malvić, 2012**). Most of the hydrocarbon prone sandstones were deposited during Late Pannonian. During that time sedimentation was represented with considerable environmental changes where turbiditic currents had been dominant clastic transport mechanisms. The main sources of medium to fine-grained sandstones, deposited from northwest-southeast direction were Eastern Alps. Clastics had been several times redeposited and moved before materials finally entered in the Sava Depression (e.g. **Rögl and Steininger, 1984; Rögl, 1996, 1998**). This mechanism was active periodically, interrupted typical hemipelagic sedimentation in lacustrine environment. Among turbidite events, depression had been filled with mud and clay material, later compacted to marls. That resulted in monotonous alteration of sandstone and marlstone lithofacies (e.g. **Royden, 1988; Velić et al., 2002; Malvić et al., 2005; Ćorić et al., 2009; Vrbanac et al., 2010; Malvić and Velić, 2011; Novak Zelenika et al., 2013**). Upper Pannonian schematic depositional model is shown in **Figure 2**.
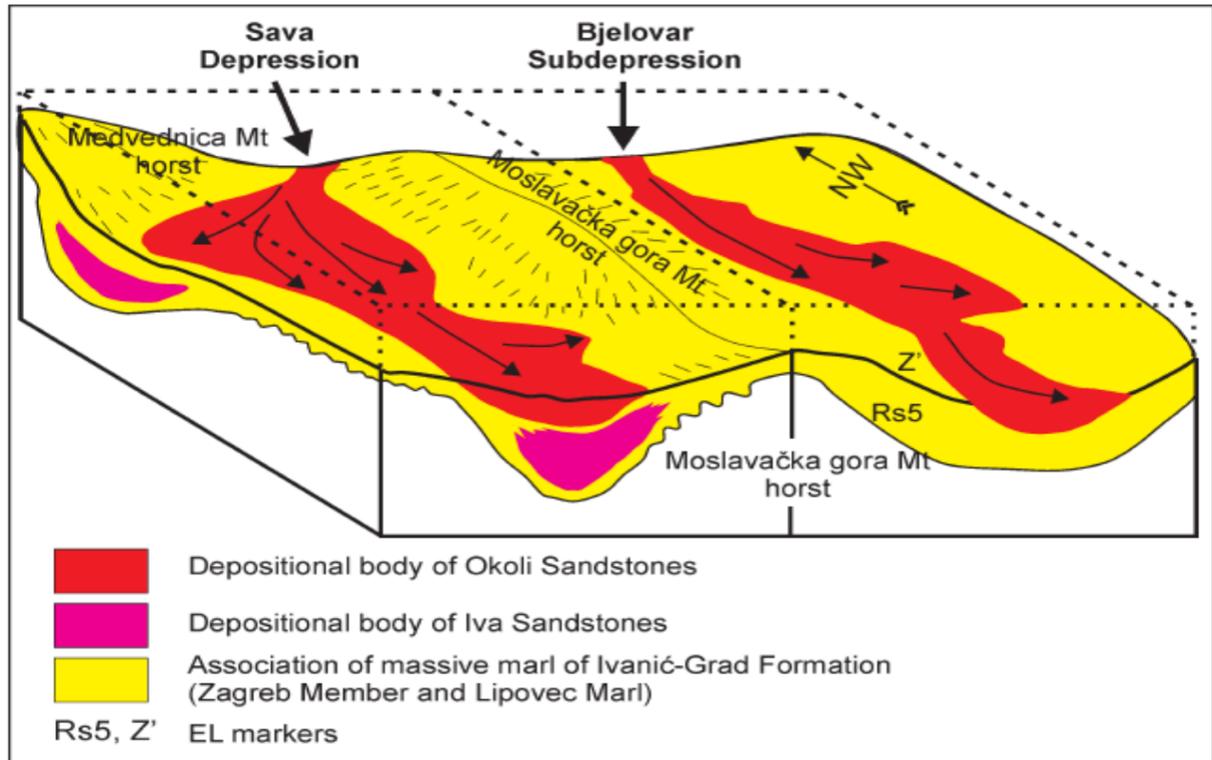
Figure 2: Schematic depositional model during Upper Pannonian (**Vrbanac et al., 2010**)

2.1. Field overview

The Ivanić Structure fits into the structural series that begins in the northwest with the Kloštar Structure, through Ivanić, Žutica to Okoli Field. Starting from Kloštar, the structures subside into the deeper part of the Sava Depression (**Figure 3**).

The Ivanić Field is an asymmetrical brachianticline, with somewhat longer axis of northwest-southeast strike, with slightly pronounced peak in the southern part of the structure. Layers on the limbs of the anticline slightly subside, with the exception of the southern limb, where they relatively steeply subside into the deeper part of the Sava basin. Seismic interpretation established the presence of normal and reverse faults. A normal fault dominates in the eastern limb of the anticline, with a throw of 30 m, of NNW-SSE strike. In the north-eastern part a reverse fault represents the field boundary. A series of faults of NW-SE strike extend along the western part of the field (**Figure 4**).
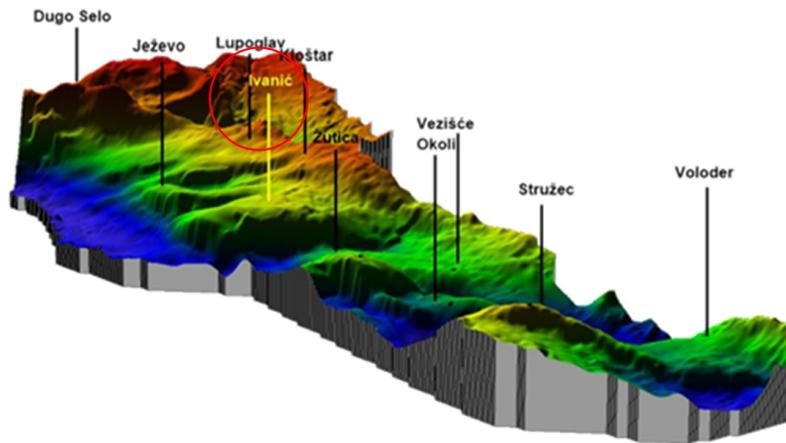
Figure 3: 3D view of the Ivanić Structure
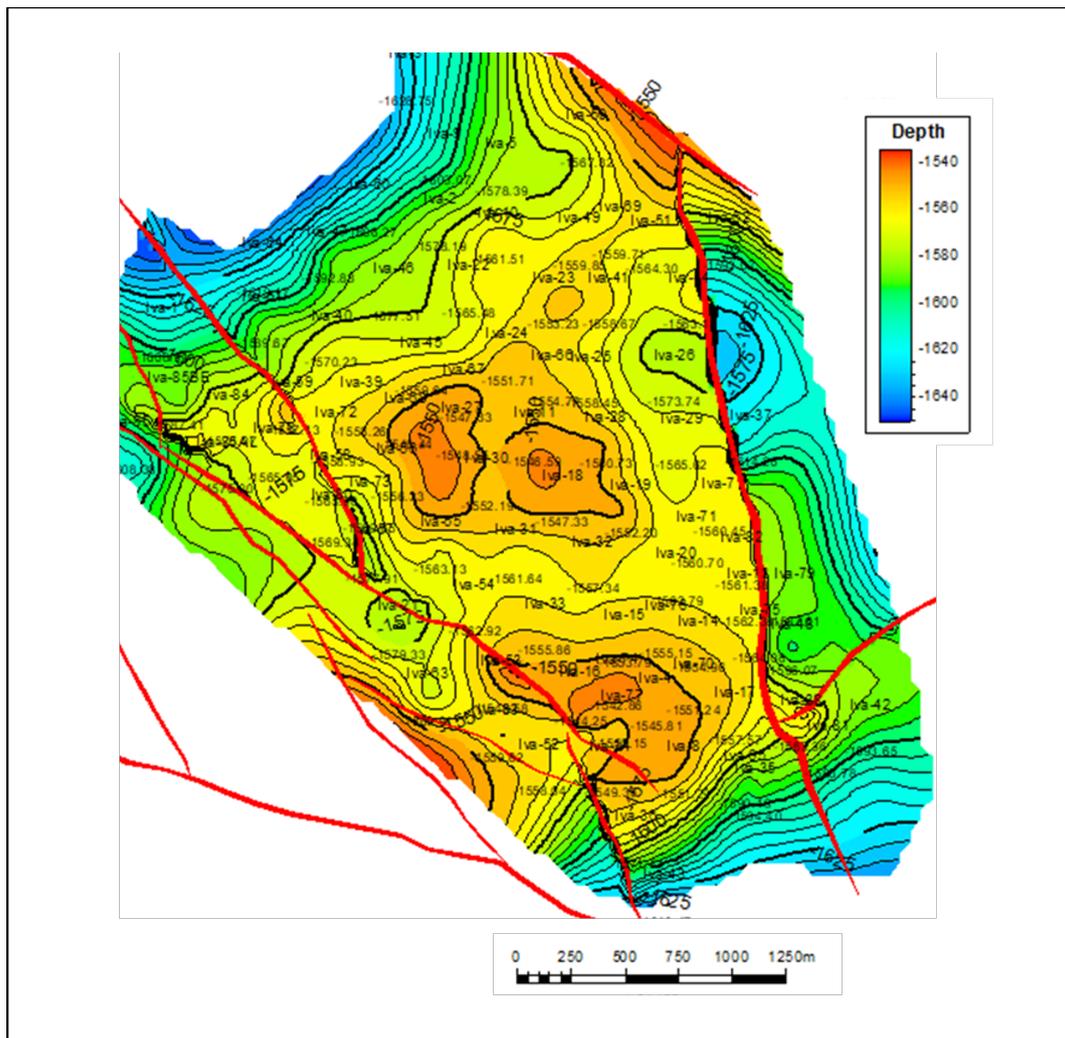
Figure 4: Top map of the Gamma3 reservoir

The Ivanić Field is composed of Neogene and Quaternary deposits. The complex of Neogene sediments transgressively discordantly overlies the consolidated basement in the whole depositional area of the Sava depression. A normal sequence of chronostratigraphic units of the Sava depression was determined from the deepest wells in the field. Based on the well data correlation, 11 intervals have been defined within the „Gamma series", deposited through turbidite currents during the Pannonian in the Sava Depression (**Figure 5**). They consist of medium to fine-grained quartz-mica sandstones in continuous alternation with marls. Marls are compact, dense brown-gray rocks of different horizontal and vertical distributions.
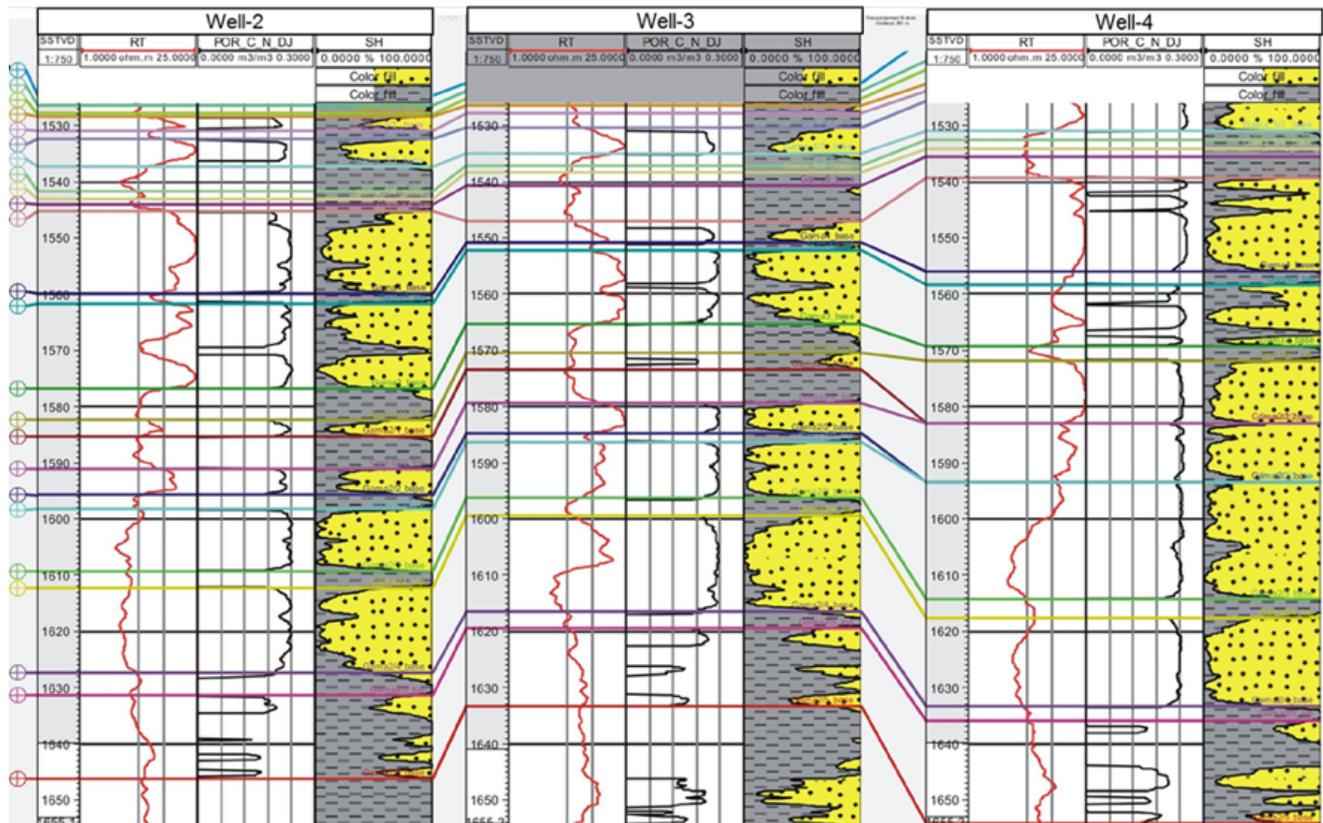
Figure 5: Gamma reservoir: Well-to-well correlation (**Novak Zelenika et al., 2017**)

3. Cut-offs definition in „Gamma series" turbidite sandstones

During the EOR monitoring parts of the reservoir with remaining hydrocarbon saturation had to be defined. Value of the remaining oil saturations depends on different rock properties and good pore connectivity is one of them. Since good pore connectivity can be expected in parts of the reservoir with better reservoir properties, those zones are considered to be washed-out. Main assumption was that remaining oil should be found in the turbidite lobes, rather than in the washed-out turbidite channel centre with high porosities and permeabilities. There are several ways of turbidite facies definitions. According to **Vrbanac et al.** (**2010**) there are four facies associations in Pannonian sediments, defined based on the curve shape. Three are turbidite facies associations and one is massive marl facies association (**Figure 6**).
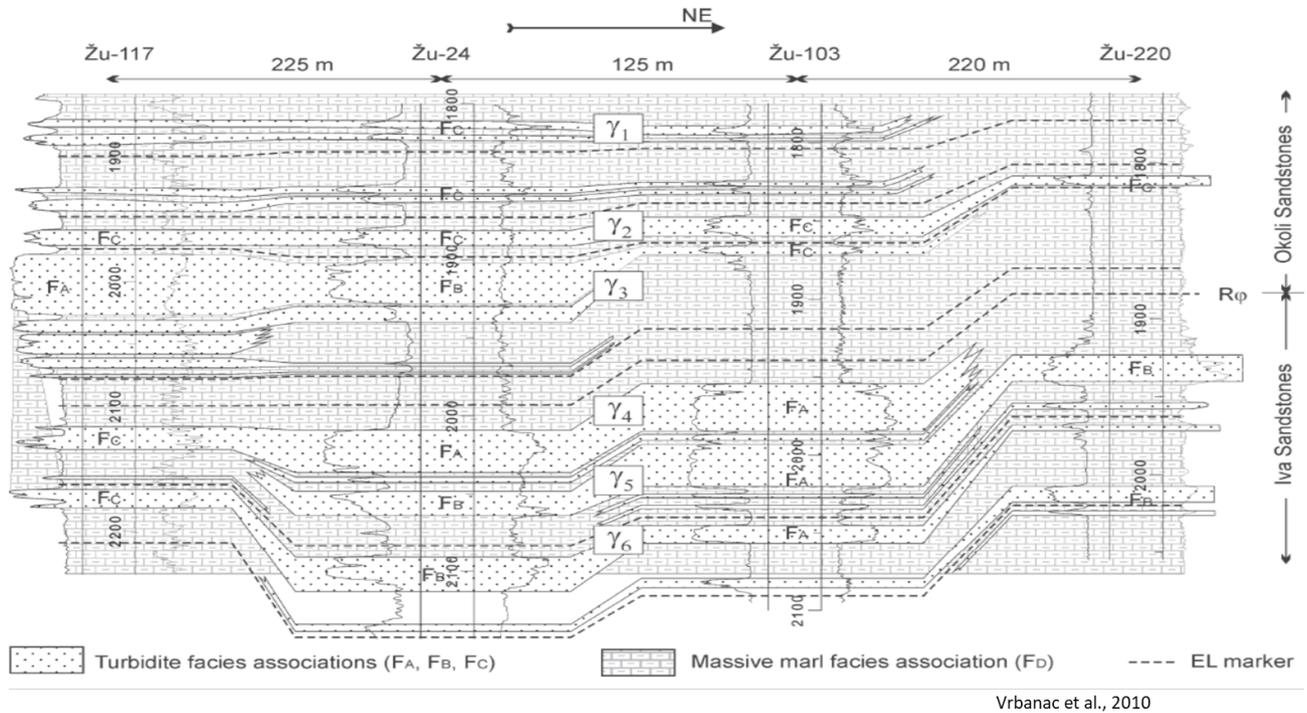
Figure 6: Facies associations in Pannonian sediments (**Vrbanac et al., 2010**)

Another way of turbidite facies definition is based on the Porh maps, which are basically multiplied average porosity and thickness maps created for each reservoir (**Figure 7**). Such maps are described in **Novak Zelenika et al. (2018)** and they enable visibility of turbidite bodies.
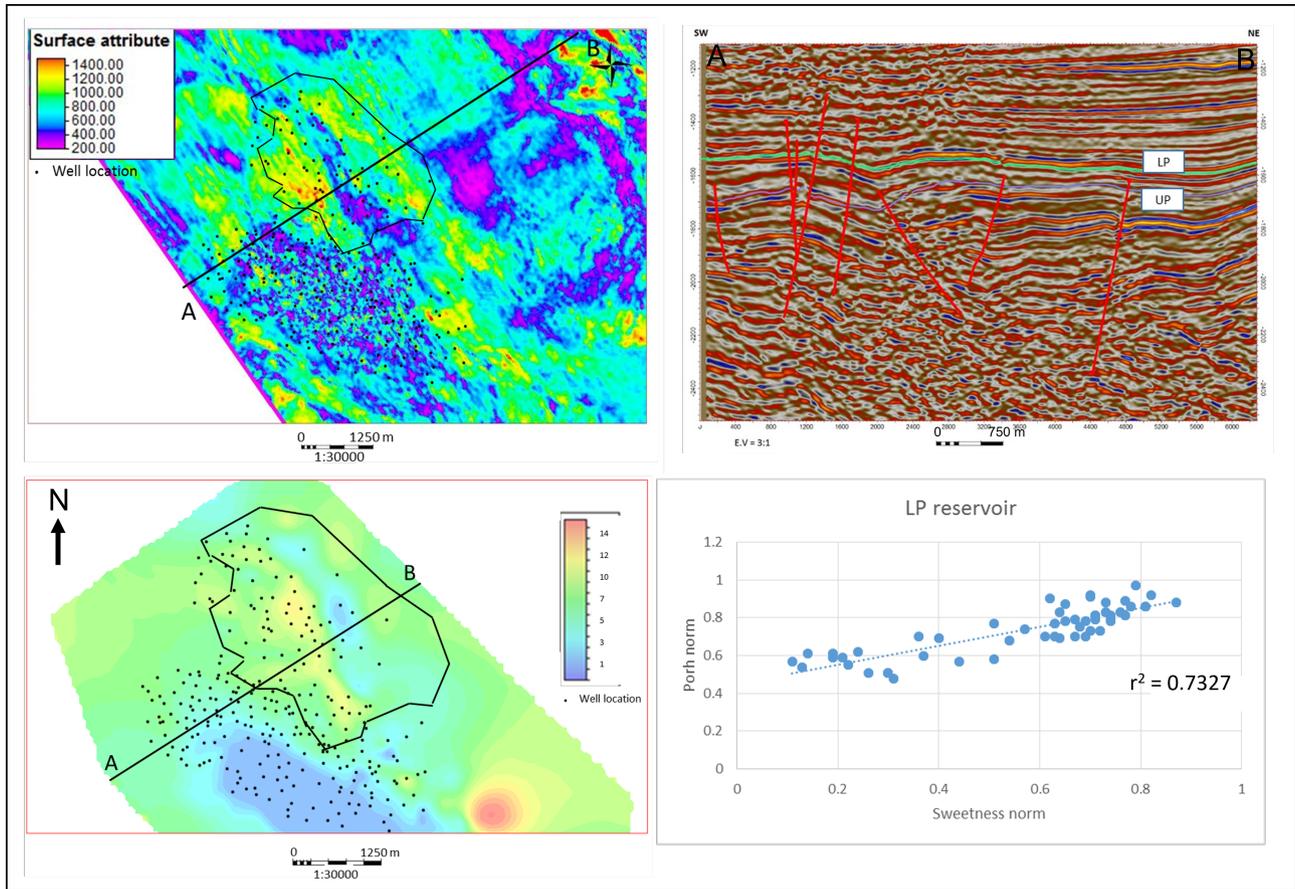
Figure 7: Comparison of the multiplied porosity and thickness maps and sweetness seismic attribute (**Novak Zelenika et al., 2018**)

But none of these ways gives the answer to the question which is the exact value to define turbidite lithofacies? To answer that question well with continuous core, capillary curves and several correlations (porosity - permeability, porosity - water saturation and porosity – volume of shale) were used.

Continuous coring enabled representations of all lithofacies in measured data. First correlation that was used was porosity – permeability correlation (**Figure 8a**). It was used to define cut-off between reservoir and non-reservoir. Lowest value used for fluids to flow is $1*10^{-3}$ μm^2 of permeability, which matches to 11% of porosity. That means that 11% of porosity can be used as border between reservoir and non-reservoir. Next step was to define which Sw_i and Vsh match 11% of porosity. For that purpose, Por-Sw_i and Por-Vsh correlation was established (**Figure 8b and c**). It is clearly visible that 11% of porosity match 60% of Sw_i and 65% of Vsh. Based on the Sw_i value red rectangle in **Figure 8d** shows capillary curves of the permeable part of the reservoir.
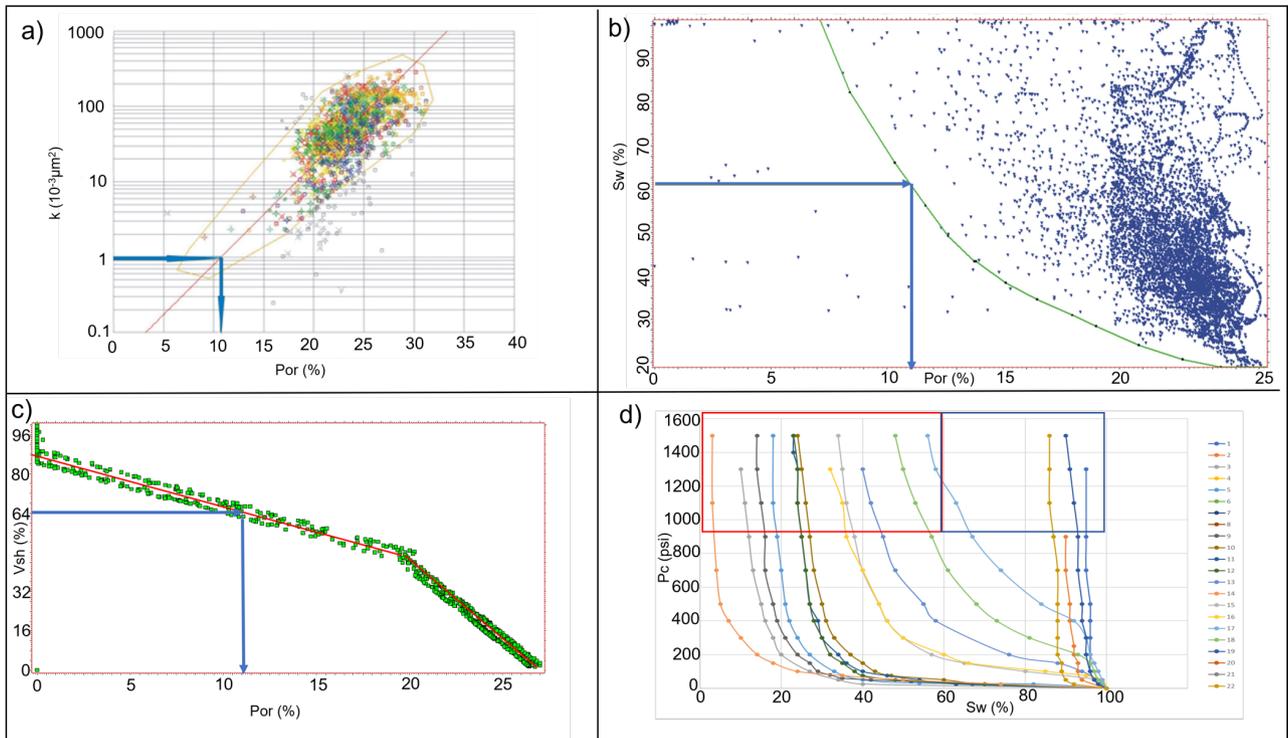
Figure 8: Cross plot diagrams a) porosity vs. permeability, b) porosity vs. water saturation, c) porosity vs. volume of shale, d) capillary curves

Height of the transitional zone in the permeable part of the reservoir (red rectangle in **Figure 8d**) points to two lithofacies groups; one with the low transitional zone and another with high. Border between them is 25% of Sw_i (**Figure 9a**). Those two lithofacies were defined as pure sandstones and marly sandstones. 25% of Sw_i match 20% of porosity, which match 45% of Vsh. (**Figure 9b and c**). Third group in **Figure 9a** represents marls with the highest Sw_i (>85%), which match 8% of porosity and 70% of Vsh (**Figure 9b and c**). In this way cut-offs for four lithofacies were defined (**Table 1**).
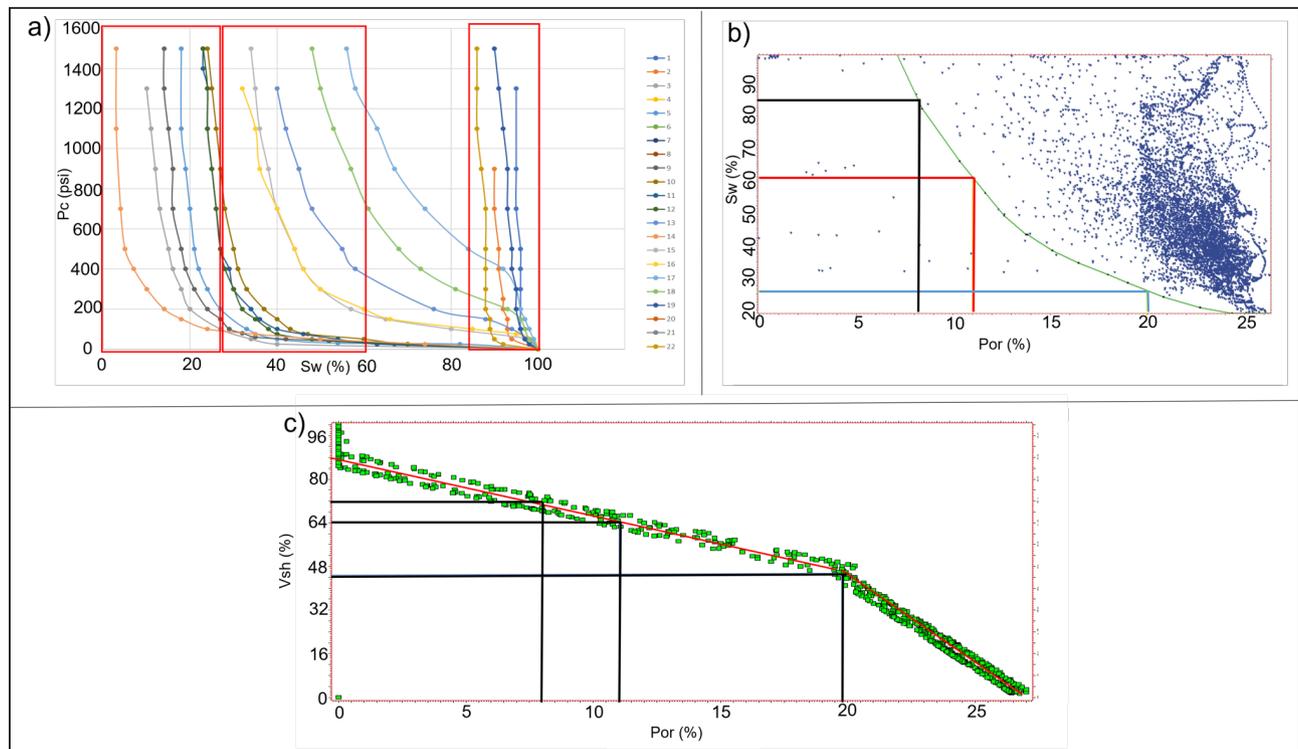
Figure 9: a) Capillary curves of 1. sandstones, 2. marly sandstones, 3. marls; b) cross plot diagram porosity vs. water saturation, c) cross plot diagram porosity vs. volume of shale

Lithofacies	Por (%)	Sw$_i$ (%)	Vsh (%)
Sandstones	20-27	0-25	0-45
Marly sandstones	11-20	25-60	45-65
Sandy marls	8-11	60-85	65-70
Marls	0-8	85-100	70-100

Table 1: Defined cut-offs for four lithofacies

4. Case study and discussion

Based on defined cut-offs four lithofacies were determined for all wells in the field. **Figure 10** represent two wells. Well J is injector and well K is producer. Lithofacies in the wells were defined as LF1 (marl), LF2 (sandy marl), LF3 (marly sandstone) and LF4 (sandstone). In the J well mostly dominates LF4. That assumes that the well is in the channel center with best reservoirs properties. On the contrary, in the K well all four lithofacies are present, which means that the well is a bit further from the center of the channel. Due to increased value of the marl component, well K has lower porosities and permeabilities. According to assumption that remaining oil is in the parts of the reservoir with lower reservoir properties, well K should be good candidate for additional oil production. If you take a look at the well K production history (**Figure 11**), it is clearly visible that after the EOR implementation in 2014 oil production increases. This case could confirm the assumption that remaining oil is still present in lithofacies with increased marl component, i.e., marly sandstones.
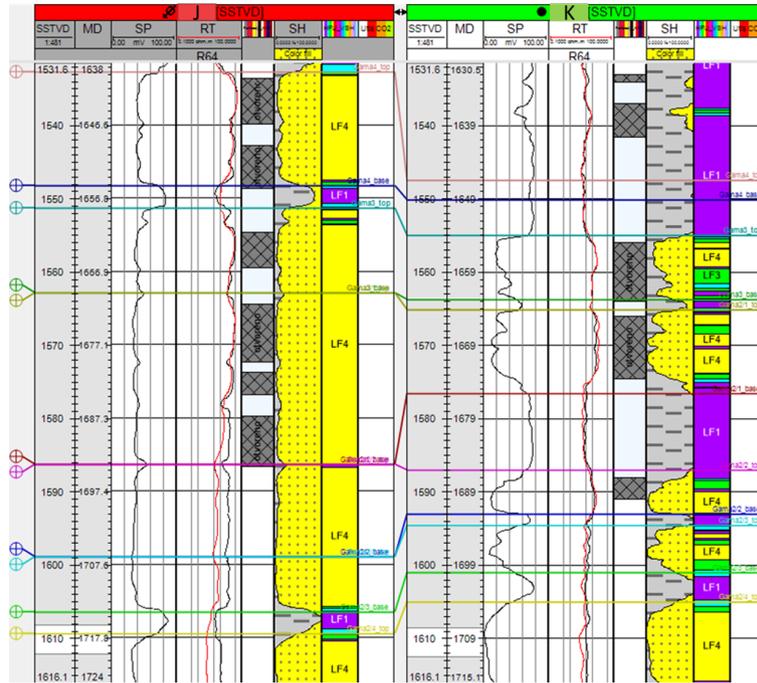
Figure 10: Injector J and producer K wells correlation with defined lithofacies LF1 (marl), LF2 (sandy marl), LF3 (marly sandstone) and LF4 (sandstone)
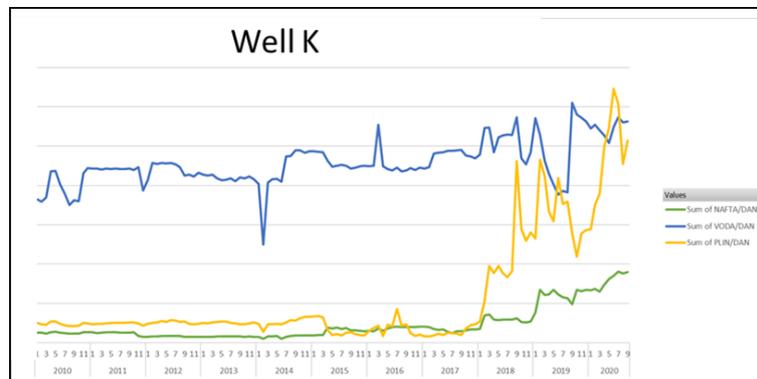
Figure 11: Well K production history

5. Conclusions

Ivanić Field is a brachianticline, with longer axis of northwest-southeast strike. Seismic interpretation established the presence of normal and reverse faults. Some faults represent the field boundary. The field is composed of Neogene and Quaternary sediments. 11 intervals have been defined within the „Gamma series", based on the well data correlation. Sandstones were deposited through turbidite currents during Pannonian. They consist of medium to fine-grained quartz-mica sandstones in continuous alternation with marls.

During the EOR monitoring parts of the reservoir with remaining hydrocarbon saturation had to be defined. Main assumption of this paper was that remaining oil should be found in the parts of the reservoir with lower reservoir properties like turbidite lobes. To define exact values of cut-offs for different lithofacies, several correlations (Por-k, Por-Sw$_i$ and Por-Vsh) as well as capillary pressure curves were used.

Based on defined cut-offs four lithofacies were determined for all wells in the field (sandstones 20-27% Por, 0-25 % Sw, 0-45% Vsh; marly sandstones 11-20% Por, 25-60% Sw, 45-65, % Vsh; sandy marls 8-11 % Por, 60-85 % Sw, 65-70 % Vsh; marls 0-8% Por, 85-100% Sw, 70-100% Vsh). Two wells, one injector and one producer were analyzed. Obtained lithofacies were compared with the oil production. The part of reservoirs with highest injection of the CO_2 in injection well shows a good match with pure channel sandstone (LF4), while the highest oil production in production well

matches lithofacies with increased content of marl component. Those cases could confirm the assumption that lithofacies with lower reservoir properties may still contain remaining oil.

6. References

Ćorić, S., Pavelić, D., Rögl, F., Mandić, O., Vrabac, S., Avanić, R., Jerković, L. and Vranjković, A. (2009): Revised Middle Miocene datum for initial marine flooding of North Croatian Basins (Pannonian Basin System, Central Paratethys). Geologia Croatica, 62, 31-43.

Malvić, T. and Velić, J. (2011): Neogene tectonics in Croatian Part of the Pannonian Basin and reflectance in hydrocarbon accumulations. In: Schattner, U. (ed.): New frontiers in tectonic research: At the midst of plate convergence. – InTech, 215-238 p.

Malvić, T., Velić, J. and Peh, Z. (2005): Qualitative-quantitative analyses of the influence of depth and lithological composition on Lower Pontian sandstone porosity in the central part of Bjelovar Sag (Croatia). Geologia Croatica, 58, 73-85.

Novak Zelenika, K., Novak Mavar, K., Brnada, S. (2018): Comparison of the Sweetness Seismic Attribute and Porosity–Thickness Maps, Sava Depression, Croatia. Geosciences, 8, 426. https://doi.org/10.3390/geosciences8110426

Novak Zelenika, K. (2017). Theory of deterministical and stochastical indicator mapping methods and their applications in reservoir characterization, case study of the Upper Miocene reservoir in the Sava Depression. Rudarsko-geološko-Naftni Zbornik, 32,3, 45–53. https://doi.org/10.17794/rgn.2017.3.5

Novak Zelenika, K., Velić, J. and Malvić, T. (2013): Local sediment sources and palaeoflow directions in Upper Miocene turbidites of the Pannonian Basin System (Croatian part), based on mapping of reservoir properties. Geological quarterly, 57, 17-30.

Rögl, F. (1996): Stratigraphic correlation of the Paratethys Oligocene and Miocene. Mitt. Ges. Geol. Bergbaust. Österr., 41, 65-73.

Rögl, F. (1998): Palaeographic consideration for Mediterranean and Paratethys seaways (Oligocene to Miocene). Ann. Naturhist. Mus. Wien, 99A, 279-310.

Rögl, F. and Steininger, F. (1984): Neogene Paratethys, Mediterranean and Indo-Pacific seaways. Geol. Jour., Spec. issue, 11, 171-200.

Royden, L.H. (1988): Late Cenozoic tectonics of the Pannonian Basin System. AAPG Mem., 45, 27-48.

Velić, J., Weisser, M., Saftić, B., Vrbanac, B. and Ivković, Ž. (2002): Petroleum-geological characteristics and exploration level of the three Neogene depositional megacyclus in the Croatian part of the Pannonian basin. Nafta, 53, 239-249.

Vrbanac, B., Velić, J. and Malvić, T. (2010): Sedimentation of deep-water turbidites in main and marginal basins in the SW part of the Pannonian Basin. Geologia Carpathica, 61, 55-69.

Sažetak

Definiranje graničnih vrijednosti turbiditnih litofacijesa na primjeru polja Ivanić. Savska depresija, Hrvatska

Polje Ivanić se nalazi u središnjoj Hrvatskoj, u SZ dijelu Savske depresije. Polje je otkriveno 1963. godine. Sekundarna faza razrade ležišta započela je 9 godina kasnije, 1972. Ukupno je u polju izrađeno 87 bušotina. Tercijarna EOR faza, koja je još uvijek u tijeku, započela je 2014. godine. Struktura polja je asimetrična brahiantiklinala s dužom osi pružanja sjeverozapad-jugoistok. U polju je utvrđeno postojanje nekoliko normalnih i reverznih rasjeda. Unutar panonske Gamma "serije" izdvojeno je 11 pješčenjačkih intervala. Pješčenjaci su kvarc-tinjčasti srednjozrnati, proslojeni bazenskim laporima. Tijekom EOR monitoringa javila se potreba za definiranjem dijelova ležišta koji sadrže preostalo zasićenje ugljikovodicima. Takvo zasićenje je prisutno u dijelovima koji imaju lošija petrofizikalna svojstva (šupljikavosti Ii propusnosti). Kontinuirano jezgrovanje ukazalo je na postojanje svih prijelaznih litofacijesa od čistih pješčenjaka do čistih lapora. Kako bi se definirale točne granične vrijednosti pojedinih litofacijesa korištene su krivulje kapilarnih tlakova te korelacije šupljikavosti-propusnosti, šupljikavosti-ireducibilnog zasićenja vodom i šupljikavosti-volumena šejla. Na temelju tako definiranih graničnih vrijednosti izdvojena su četiri litofacijesa (pješčenjaci, laporoviti pješčenjaci, pjeskoviti lapori i lapori). Analizirane su dvije bušotine, jedna utisna i jedna proizvodna. Litofacijesi u bušotinama su uspoređeni s količinom utisa CO_2 i proizvodnjom nafte. Dijelovi ležišta s najvećom količinom utisa CO_2 odgovaraju čistim kanalskim pješčenjacima, dok je najveća proizvodnja nafte iz litofacijesa s povećanim udjelom laporovite komponente. Takvi slučajevi bi mogli potvrditi pretpostavku da litofacijesi s lošijim petrofizikalnim karakteristikama još uvijek sadrže preostalo zasićenje naftom.

Ključne riječi: definiranje litofacijesa; EOR; panonska ležišta; Savska depresija; Hrvatska

Author's contribution

Kristina Novak Zelenika (PhD, scientific associate, reservoir modelling expert) provided idea, method selection cut-offs calculation, writing and review, **Ana Majstorović Bušić** (PhD, geological expert) provided the geological overview, writing and review

Isotopic signature of the Sikirevci well field and its connection with the Sava River

Vedrana Filipović [1]; Zoran Kovač [2*]; Jasna Kopić [3]; Zoran Nakić [4]; Jelena Parlov [5]; Ferid Skopljak [6]

[1] Faculty of Mining, Geology and Petroleum Engineering, University of Zagreb, Pierottijeva 6, 10000 Zagreb

[2] Faculty of Mining, Geology and Petroleum Engineering, University of Zagreb, Pierottijeva 6, 10000 Zagreb, https://orcid.org/0000-0001-8091-7975

[3] Vinkovci Waterworks and Sewage Company, Dragutina Žanića-Karle 47a, Vinkovci

[4] Faculty of Mining, Geology and Petroleum Engineering, University of Zagreb, Pierottijeva 6, 10000 Zagreb, https://orcid.org/0000-0001-6353-8500

[5] Faculty of Mining, Geology and Petroleum Engineering, University of Zagreb, Pierottijeva 6, 10000 Zagreb, https://orcid.org/0000-0002-2862-7222

[6] Federal Institute for Geology; Ustanička 11, 71210 Sarajevo, Bosnia & Herzegovina, https://orcid.org/0000-0003-4114-0539

Abstract

The Sikirevci well field is one of the most important well fields in the eastern Slavonia used for the public water supply. In this study, stable isotopes of water were used to determine the origin of water from pumped aquifer, but also to test its connection with the Sava River. From August 2020 till July 2021, groundwater samples were collected from four pumping wells, while historical chemical analyses were used to determine the hydrogeochemical facies. The isotopic signature of the Sava River was found to be different from that of the sampled aquifer. The stable isotopes of hydrogen and oxygen (δ^2H and $\delta^{18}O$) of the groundwater are more negative than those of the Sava River, indicating that the Sikirevci well field pumps water from the deeper part of the aquifer where Sava River does not have such a strong influence, although the d-excess values do not show such a large difference. Moreover, the isotopic composition of the groundwater is very stable and does not change over time. This is consistent with the presence of iron, manganese and arsenic concentrations in groundwater, which indicate reductive conditions. However, the variations in the concentrations of the observed potentially toxic metals indicate that different geochemical conditions prevailed during the study period. Most of the water samples had hydrogeochemical facies $CaMg-HCO_3$, while two samples had slightly higher levels of sodium and magnesium. Results of this research indicate different conclusions when observing main isotopic composition with respect to d-excess values. Although d-excess is observed as a second order parameter, it can greatly help in data interpretation.

Keywords: stable water isotopes; Sikirevci well field; Sava River; hydrogeochemical facies

1. Introduction

The Sikirevci well field is located in the Brodsko-Posavska County, in the eastern part of Croatia, between the settlement of Sikirevci and the Sava River. It has four active pumping wells (Z2-Z5, Figure 1). It is located in the zone of typical lowland relief. The climate is temperate continental, characterized by a variety of weather conditions with frequent and intense changes throughout the year. The inflow area of the Sikirevci well field extends over the territory of the Republic of Croatia and the Federation of Bosnia and Herzegovina (Kopić, 2016; Kopić et al., 2016).

The wellfield Sikirevci captures Quaternary deposits with transmittivities ranging from 3000 to 6000 m²/day. It is a gravelly-sandy aquifer, semi-confined to unconfined type, with a thickness of over 90 m. Pumping wells capture three aquifer layers (29 - 36 m, 51 - 57 m and 69 - 75 m), while the total thickness of aquifers and less permeable interlayers between them is 50 to 60 m. The aquifer belongs to the alluvial sediment of the Bosna River. The Sikirevci wellfield has a very high pumping capacity (about 1000 l/s) and exceptional water quality (**Kopić, 2016; Kopić et al., 2016**). The average hydraulic conductivity is about 150 m/day (**Briški et al., 2013**), which is in accordance with the lithological composition of the aquifer. The shallow, semi-permeable layers of the Sava plain consist of alternations of clay, silt and

Corresponding author: Zoran Kovač
zoran.kovac@rgn.unizg.hr

sand deposits whose lithologic diversity and individual permeability cause varying infiltration into the aquifer layers. Due to small thickness of semi-permeable layers, the riverbed is cut into the shallowest aquifer, resulting in direct contact between surface water and groundwater, so that the Sava maintains a high piezometric level at high water levels (**Brkić et al., 2009**). At high water levels, the aquifer is fed by the Sava River, and at low and medium water levels the Sava River drains the groundwater, especially in the downstream parts (**Briški et al., 2013**).

In recent years, isotope hydrology research in Croatia was mainly focused to the unconfined aquifers in the northwestern part of Croatia, especially in Zagreb (**Kovač et al., 2018; Parlov et al., 2019; Barešić et al., 2020**) and in the Varaždin aquifer (**Marković et al., 2020**), as well as on soil hydrology related to hillside vineyards (**Kovač et al., 2022**). On the other side, in the eastern part of Croatia, conduction of isotope hydrology research is not that common.

The main objectives of this research were to evaluate the isotopic signature of the groundwater and the Sava River in the area of the Sikirevci well field and to study their relationship using the water stable isotopes ($\delta^{18}O$ and δ^2H). In addition, we used the concentrations of major ions to define the hydrogeochemical facies and evaluate whether it changes over time.
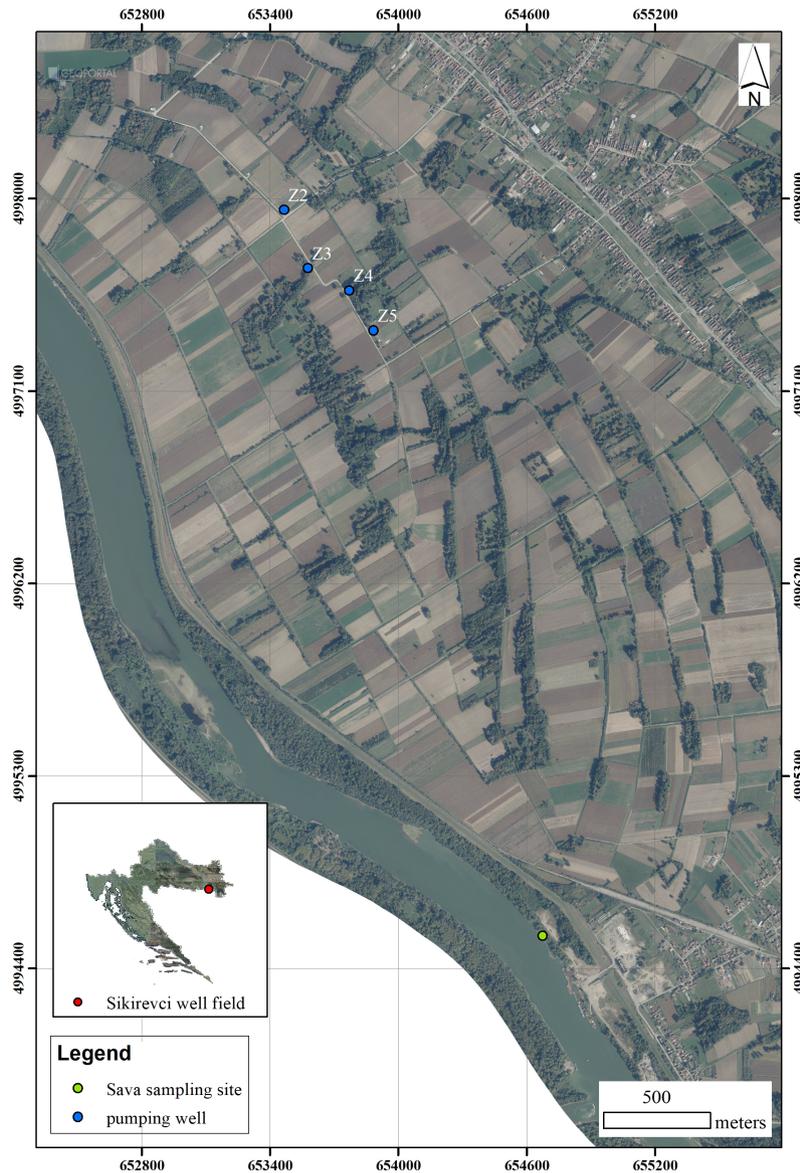
Figure 1: Location of sampled pumping wells and Sava River sampling site in the research area

2. Methods and data

Monthly sampling of groundwater and Sava River water was conducted between August 2020 and July 2021. All four pumping wells were sampled, as well as the Sava River (**Figure 1**). Due to the COVID-19 epidemiological situation and related technical problems, samples were not taken in all months, which primarily refers to the Sava River. Stable isotopes of groundwater and Sava River (δ^2H and $\delta^{18}O$) were determined at the Laboratory for Spectroscopy of the Faculty of Mining, Geology, and Petroleum Engineering, University of Zagreb, using a Liquid Water Isotope Analyzer (LWIA-45-EP, Los Gatos Research). Data preparation and interpretation were performed using the Laboratory Information Management System (LIMS for lasers 2015; **Coplen and Wassenaar, 2015**). The measurement precision of duplicate samples was ±0.19‰ for $\delta^{18}O$ and ±0.9‰ for δ^2H, while all results are presented with respect to VSMOW (Vienna Standard Mean Ocean Water). Hydrogeochemical facies were determined based on available historical data from 2012 to 2020. The chemical analyses were performed at the Teaching Institute for Public Health of Osijek-Baranja County, while the data are available on the website of the Vinkovci Waterworks and Sewage Company.

Data interpretation was done in four steps. First, the isotopic signature of the Sava River and groundwater is compared with the LMWLs (Local Meteoric Water Lines) of Zagreb and Ljubljana based on the available data from GNIP (Global Network of Isotopes in Precipitation; **IAEA/WMO, 2021 – URL 1**). In the second step, the change of $\delta^{18}O$ of the Sava River and groundwater over time is evaluated, while in the third step the d-excess value is investigated. In the fourth step, the hydrogeochemical facies was determined together with the concentrations of iron, manganese, and arsenic. Analyses of major ion concentrations were available only for mixed water from all pumping wells.

3. Results and discussion

In **Figure 2** isotopic composition of the Sikirevci well field and the Sava River, together with the LMWLs of Zagreb and Ljubljana are presented. It can be clearly seen that the isotopic signature of the Sava River is different from that of the groundwater pumped from the Sikirevci well field. This corresponds to the evaluation of the $\delta^{18}O$ in time (**Figure 3**). Furthermore, the results suggest that the isotopic signature of the Sava River is primarily related to the precipitation which falls in Slovenia (**Filipović, 2021**), which corresponds to the results of previous studies in the Zagreb area (**Parlov et al., 2019**). Groundwater from the well field Sikirevci is more negative than the Sava River, indicating that well field Sikirevci pumps water from deeper aquifer layers that are not in the direct contact with the Sava River. This is consistent with previous research (**Kopić et al., 2016**). Furthermore, it is evident from all results that the isotopic composition of the Sava River varies more than that of the groundwater, which is generally very stable.
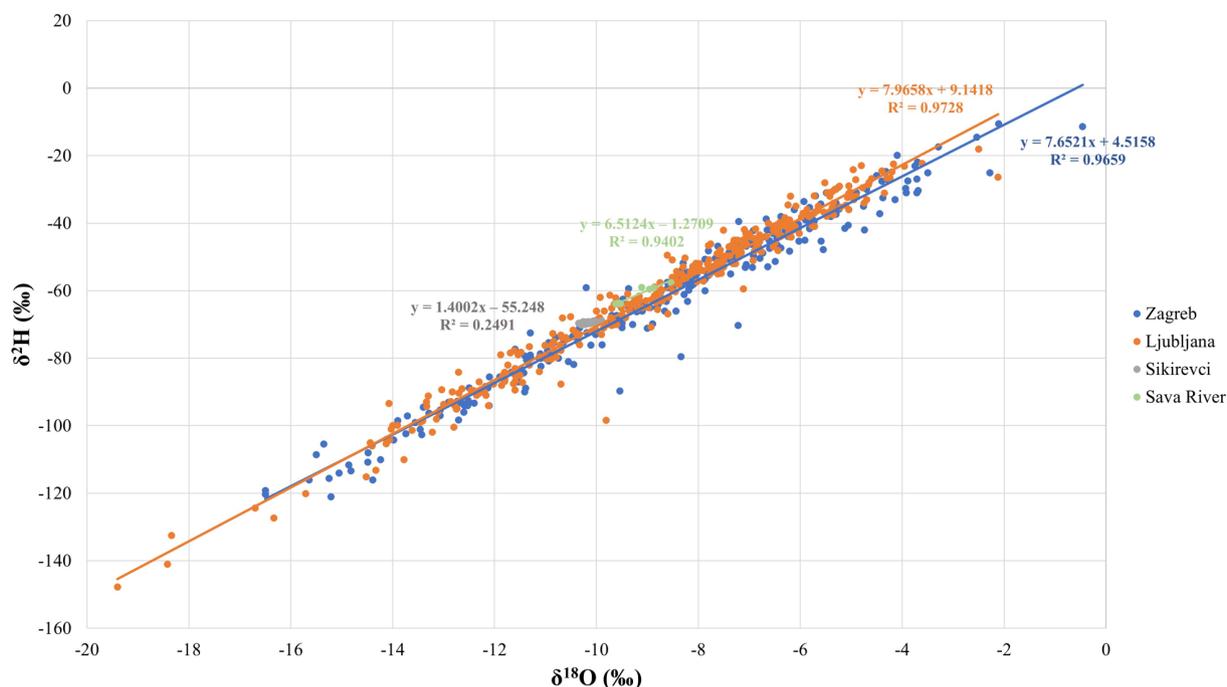
Figure 2: Isotopic composition of the well field Sikirevci and Sava River with respect to LMWLs of Zagreb and Ljubljana (modified from **Filipović, 2021**)
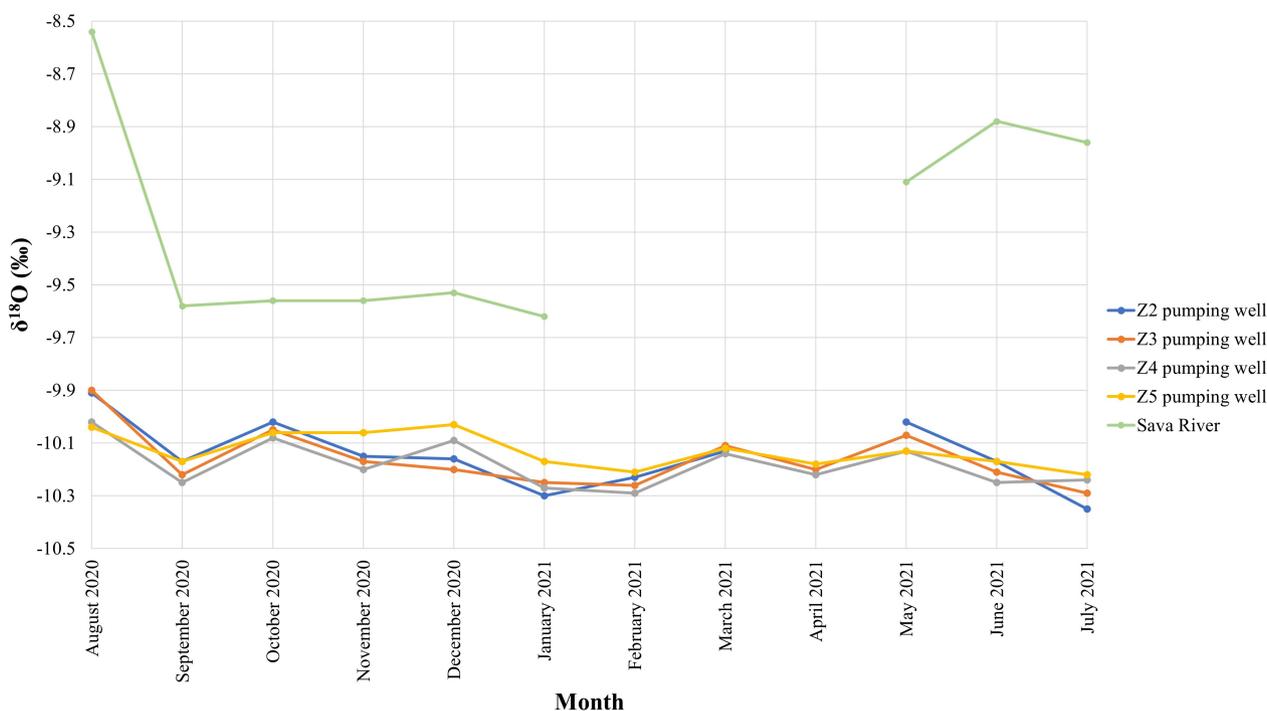
Figure 3: Variability of the δ¹⁸O values of the well field Sikirevci and Sava River in time

Although the primary evaluation of the isotopic signature shows a difference between the Sava River and the groundwater, the d-excess values, as a second order parameter, have similar average values, while the minimum and maximum values are not so different (**Table 1; Figure 4**). The d-excess values indicate that connection between Sava River and groundwater from deeper layers exist. **Figure 4** shows that the d-excess values of the groundwater follow a similar pattern to those of the Sava River. In this case, without evaluating the d-excess, the isotopic composition would likely lead to incorrect conclusions. This is consistent with other soil hydrology research where d-excess was defined as a better tracer (**Lee et al., 2007**). The initial isotopic results suggest that the relationship between the Sava River and groundwater is complicated and needs to be studied in much more detail, including the influence of the Bosna River.

Parameter	Groundwater			Sava River		
	δ^2H (‰)	$\delta^{18}O$ (‰)	d-excess (‰)	δ^2H (‰)	$\delta^{18}O$ (‰)	d-excess (‰)
Average	-69.44	-10.15	11.80	-61.58	-9.26	12.50
Minimum	-70.11	-10.35	10.10	-63.90	-9.62	10.75
Maximum	-68.94	-9.90	13.19	-57.57	-8.54	13.90
Standard deviation	0.25	0.10	0.71	2.67	0.40	0.88

Table 1: Statistical parameters of water isotope composition of groundwater from the well field Sikirevci and Sava River
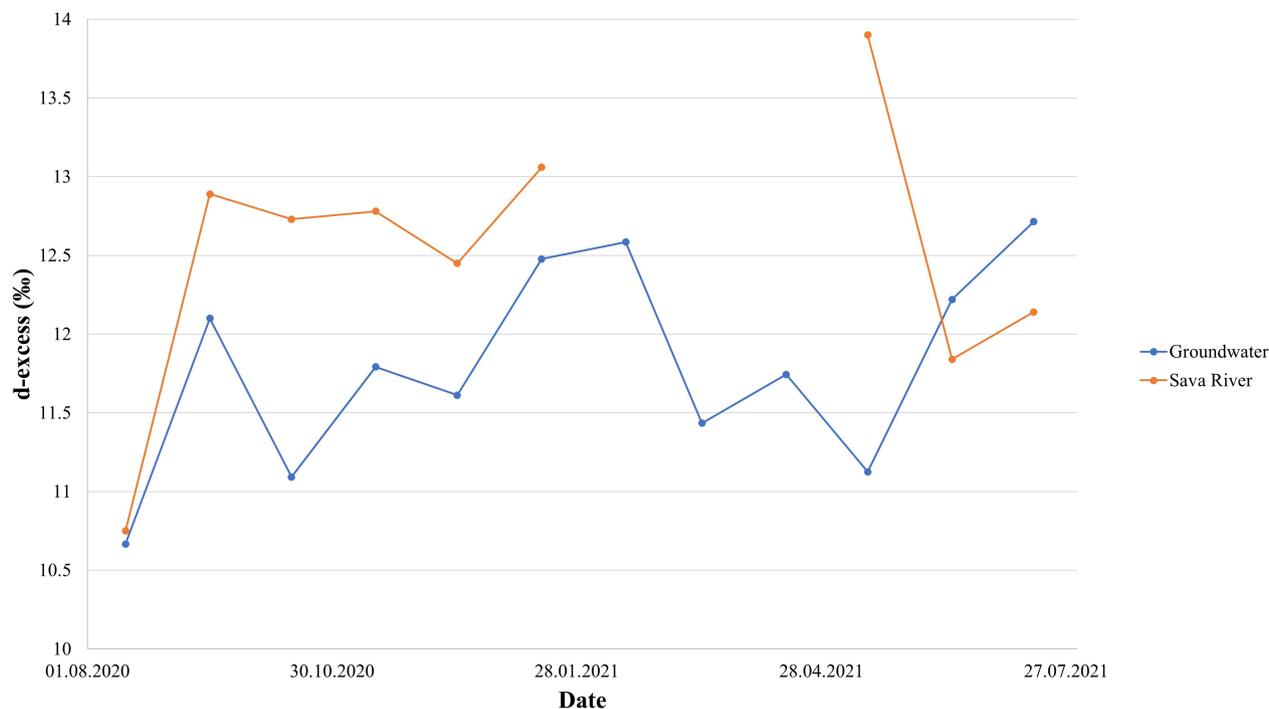
Figure 4: Variability of average d-excess values between groundwater and Sava River

The hydrogeochemical facies of the groundwater from the Sikirevci well field is shown in **Figure 5**. In general, CaMg-HCO$_3$ facies was detected in almost all samples. In 2016, slightly higher sodium values were observed, which resulted in the CaMgNa-HCO$_3$ hydrogeochemical facies. In 2020, magnesium concentrations were the highest in all analyses which resulted in MgCa-HCO$_3$ hydrogeochemical facies (**Filipović, 2021**). In the previous research (**Kopić et al., 2016**) cluster analysis showed that the groundwater quality parameters are a consequence of the dissolution of alumosilicates, mostly clay minerals, organic matter, but also an anthropogenic input (probably related to the agriculture influence). One of the subgroups was defined as a group of complex parameter affinities of different origin, more or less related to geochemical processes, which include the presence of organic matter and its decomposition. Within that group, sodium concentrations were defined, while the origin of the concentrations was defined as anthropogenic or/and natural. Third subgroup, where one of the parameters was magnesium, was defined as non-reactive group which origin was probably natural. From this point of view, it is still unclear why higher sodium and magnesium concentrations were observed and whether they were of natural or anthropogenic origin. If higher sodium concentrations are the consequence of human influence, they probably represent further evidence that infiltration from the surface into deeper aquifer layers is possible. The concentrations of potentially toxic metals are very interesting: iron, manganese, and arsenic (group **Figure 6**). While arsenic concentrations (**Figure 6a**) do not vary much over time, i.e., are generally very stable, concentrations of iron (**Figure 6b**) and manganese (**Figure 6c**) show much greater variation. Iron concentrations vary from about 11 µg/l to about 91 µg/l. Manganese concentrations vary from about 1 µg/l up to 20 µg/l. The observed concentrations of potentially toxic metals are consistent with those observed in previous studies (**Kopić et al., 2016**). In general, they are lower than the maximum contaminant levels (MCLs) defined by Croatian law. However, this variation suggests the presence of a different geochemical environment that changes over time (probably dominantly reductive), possibly leading to mixing of water between different aquifer layers and possible infiltration of surface water. It must be emphasised that in this case the limited amount of data does not allow strict and reliable conclusions. From that perspective detail hydrogeological and hydrogeochemical investigations, which include determination of stable isotopes on all types of water (surface water, precipitation and groundwater), should be done. This applies not only to the Croatian part, but also to the part located in the Federation of Bosnia and Herzegovina, which is primarily related to the Bosna River and its influence on the Sikirevci well field.
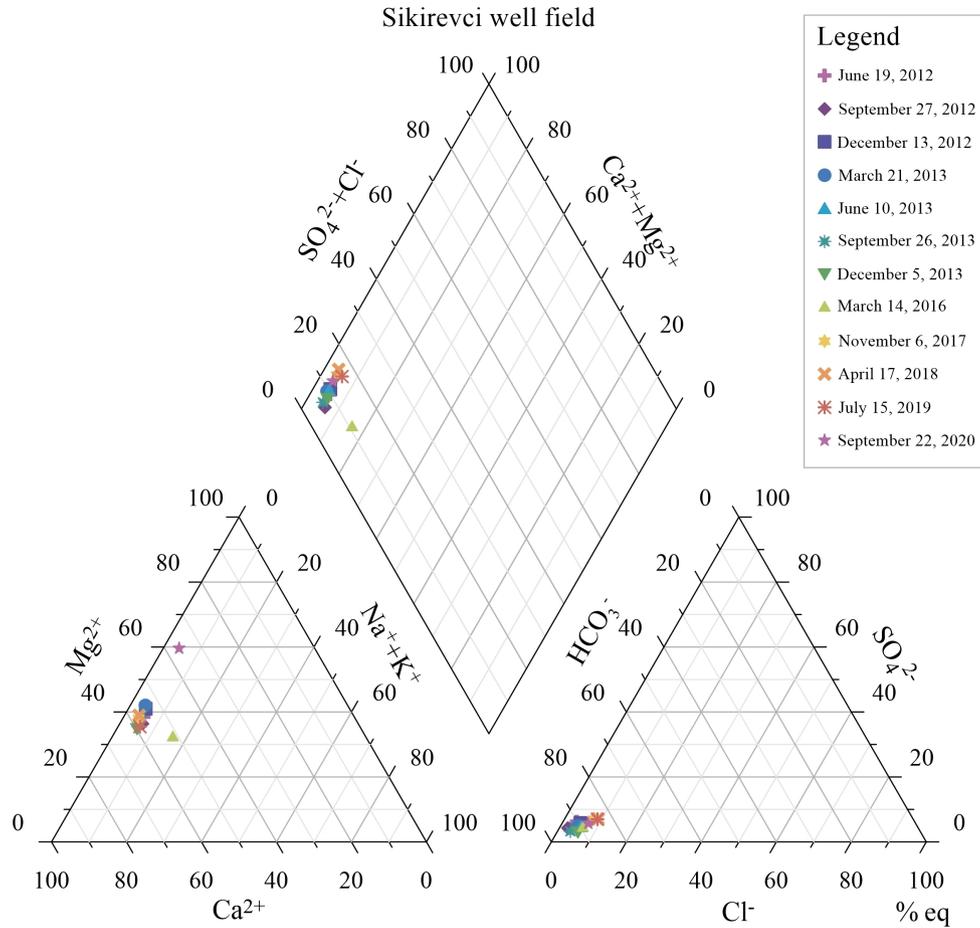
Figure 5: Hydrogeochemical facies at the well field Sikirevci (modified from **Filipović, 2021**)
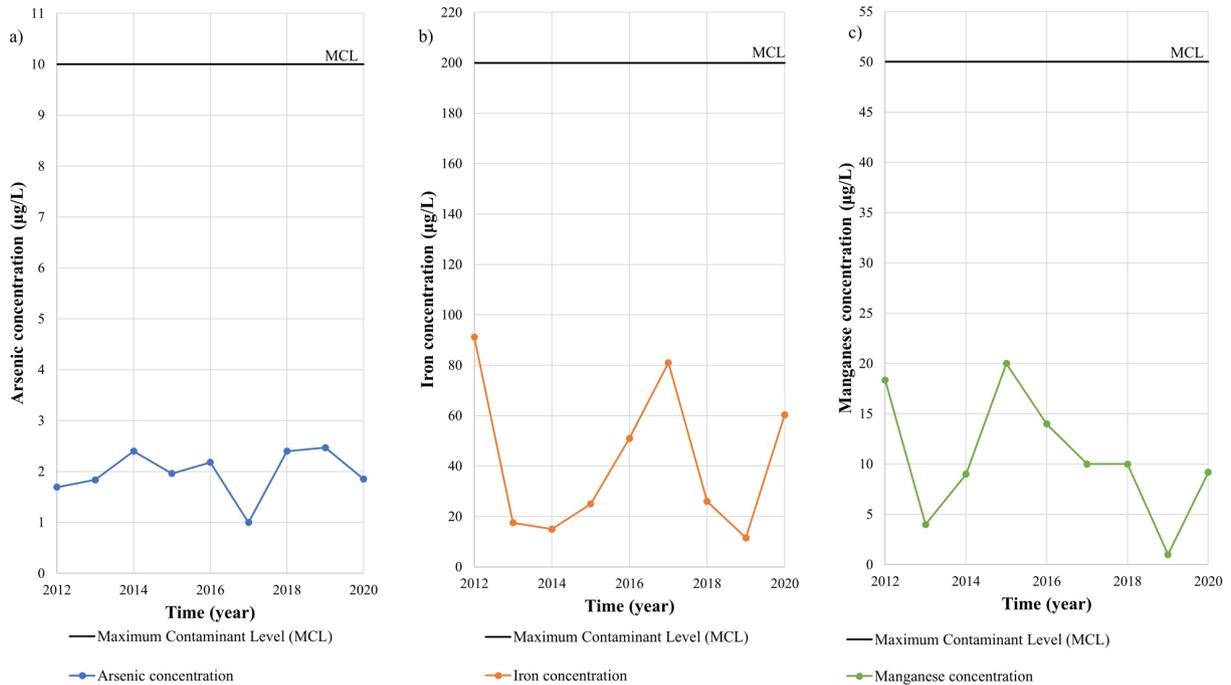
Figure 6: Concentrations of potentially toxic metals at the well field Sikirevci: a) arsenic concentration, b) iron concentration, c) manganese concentration (modified from **Filipović, 2021**)

4. Conclusions

The wellfield Sikirevci presents one of the main and most important well fields in the eastern part of the Slavonia. In this paper, the isotopic composition of the Sava River and groundwater from the Sikirevci well field is studied. Although the primary isotopic signature has shown a different isotopic composition between the two compartments, the d-excess values suggest that there is a connection between the Sava River and the deeper groundwater. However, this connection is not very strong, probably because the pumping wells of the Sikirevci well field pump water from deeper aquifer layers, while the Sava River is in direct contact only with the shallow aquifer layer. In addition, the hydrogeochemical composition showed a dominant $CaMgHCO_3$ facies, while the variations in iron and manganese concentrations indicate a possible change in the geochemical environment, which is mostly reductive. All results suggest the need for more detailed hydrogeological and hydrogeochemical research which should include both the Republic of Croatia and Federation of Bosnia and Herzegovina, as they are transboundary aquifers very important for public supply in both countries, in order to achieve sustainable groundwater management and provision of potable water for future generations.

5. References

Barešić, J., Parlov, J., Kovač, Z., Sironić, A. (2020): Use of nuclear power plant released tritium as groundwater tracer. Rudarsko-geološko-naftni zbornik 35, 25 – 34, doi: 10.17794/rgn.2020.1.3.

Briški, M., Brkić, Ž., Urumović, K. (2013): Konceptualni model vodonosnog sustava na širem području Sikirevaca. (The conceptual model of groundwater system in a wider area Sikirevci). Proceedings V. Geological Consulting in Bosnia and Herzegovina), 77-78, Pale (in Croatian).

Brkić, Ž., Kolarić, J., Larva, O., Lukač Reberski, J., Marković, T., Urumović, K. (2009): Ocjena stanja i rizika cjelina podzemnih voda u panonskom dijelu Republike Hrvatske. Project, Croatian Geological Society, Zagreb ((in Croatian).

Coplen, T.B., Wassenaar, L.I. (2015): LIMS for Lasers for achieving long-term accuracy and precision of δ^2H, $\delta^{17}O$, and $\delta^{18}O$ of waters using laser absorption spectrometry. Rapid Communications in Mass Spectrometry, 29, 2122–2130, doi: 10.1002/rcm.7372.

Filipović, V. (2021): Origin and water quality at well field Sikirevci. Undergraduate thesis, Faculty of Mining, Geology and Petroleum Engineering, University of Zagreb, Croatia, 21 p. (in Croatian).

Kopić, J. (2016): Određivanje specifične ranjivosti vodonosnika u priljevnom području regionalnog crpilišta "Istočna Slavonija". PhD thesis, Faculty of Mining, Geology and Petroleum Engineering, University of Zagreb (in Croatian).

Kopić, J., Loborec, J., Nakić, Z. (2016): Hydrogeological and hydrogeochemical characteristics of a wider area of the regional well field Eastern Slavonia – Sikirevci. Rudarsko-geološko-naftni zbornik 31 (3), 47-66, doi: 10.17794/rgn.2016.3.4.

Kovač, Z., Nakić, Z., Barešić, J., Parlov, J. (2018): Nitrate Origin in the Zagreb Aquifer System. Geofluids, 2789691, 15, doi: 10.1155/2018/2789691.

Kovač, Z., Krevh, V., Filipović, L., Defterdarović, J., Buškulić, P., Han, L., Filipović, V. (2022): Utilizing stable water isotopes (δ^2H and $\delta^{18}O$) to study soil-water origin in sloped vineyard: first results. Rudarsko-geološko-naftni zbornik 37 (3), doi: 10.17794/rgn. 2022.3.1.

Lee, K-S., Kim, J.M, Lee, D.R., Kim, Y., Lee, D. (2007): Analysis of water movement through an unsaturated soil zone in Jeju Island, Korea using stable oxygen and hydrogen isotopes. Journal of Hydrology 345: 199–211. Doi: 10.1016/j.jhydrol.2007.08.006.

Marković, T., Karlović, I., Perčec Tadić, M., & Larva, O. (2020): Application of Stable Water Isotopes to Improve Conceptual Model of Alluvial Aquifer in the Varaždin Area. Water, 12, 379, doi: 10.3390/w12020379.

Parlov, J., Kovač, Z., Nakić, Z., Barešić, J. (2019): Using water stable isotopes for identifying groundwater recharge sources of the unconfined alluvial Zagreb aquifer (Croatia). Water 11(10), 2177, doi: 10.3390/w11102177.

URL 1: IAEA/WMO, 2021. Global Network of Isotopes in Precipitation. The GNIP Database. https://nucleus.iaea.org/wiser (23.8.2021.)

Sažetak

Izotopni sastav crpilišta Sikirevci i njegova povezanost sa rijekom Savom

Crpilište Sikirevci jedno je od najvažnijih crpilišta u istočnoj Slavoniji koje se koristi za javnu vodoopskrbu. U ovom istraživanju korišteni su stabilni izotopi vode za određivanje porijekla vode iz crpljenog vodonosnika, ali i za ispitivanje njegove povezanosti s rijekom Savom. Od kolovoza 2020. do srpnja 2021. godine uzorci podzemne vode prikupljeni su iz četiri zdenca, dok su povijesne kemijske analize korištene za određivanje hidrogeokemijskog facijesa. Utvrđeno je da se izotopni sastav rijeke Save razlikuje od uzorkovanog vodonosnika. Stabilni izotopi vodika i kisika (δ^2H i δ^{18}O) podzemne vode imaju negativnije vrijednosti od onih u rijeci Savi, što ukazuje na to da zdenci crpilišta Sikirevci crpe vodu iz dubljeg dijela vodonosnog sloja na koji rijeka Sava nema tako jak utjecaj, iako vrijednosti viška deuterija ne pokazuju tako veliku razliku. Štoviše, izotopni sastav podzemne vode je vrlo stabilan i ne mijenja se tijekom vremena. To je u skladu s prisutnošću koncentracija željeza, mangana i arsena u podzemnoj vodi, što ukazuje na postojanje dominantno reduktivnih uvjeta. Međutim, varijacije u koncentracijama promatranih potencijalno toksičnih metala ukazuju na to da su tijekom razdoblja istraživanja prevladavali različiti geokemijski uvjeti. Većina uzoraka vode imala je CaMg-HCO$_3$ hidrogeokemijski facijes, dok su dva uzorka imala nešto više koncentracija natrija i magnezija.

Ključne riječi: stabilni izotopi vode; crpilište Sikirevci; rijeka Sava; hidrogeokemijski facijes

Acknowledgment

Author's contribution

Vedrana Filipović (student in the graduate studies of Geological Engineering) participated in writing of original draft, data interpretation and presentation of the results. **Zoran Kovač** (PhD, Assistant Professor, hydrogeology, hydrogeochemistry and isotope hydrology) made the isotope analysis, and participated in conceptualization, writing of the original draft and data interpretation. **Jasna Kopić** (PhD, hydrogeology), performed the field work (sampling of groundwater and Sava River) and participated in data interpretation. **Zoran Nakić** (PhD, Full Professor, hydrogeology, hydrogeochemistry) participated in conceptualization, review, and editing. **Jelena Parlov** (PhD, Associate Professor, hydrogeology, isotope hydrology) participated in the interpretation and presentation of the results, as well as review and editing. **Ferid Skopljak** (PhD, hydrogeology, geology) participated in data interpretation and review and editing.

Modeling of watershed basins using weighted graphs and presenting an algorithm to select suitable sample locations for reducing sampling and analysis costs

Elham Sharifi Yazdi[1]; Farhad M. Torab[2]

[1] Department of Computer Engineering, Imam Javad University College, Yazd, Iran, 0000-0003-0152-3551

[2] Department of Minning and Metallurgical Engineering, Yazd University, Yazd, Iran, 0000-0002-2291-4319

Abstract

Watershed sampling is one of the most important prospecting methods applied for mineral exploration. The objective of this study is mathematical modeling of watersheds for proper sampling and optimization of sample numbers for reduction of sampling and analysis costs. For this purpose, the mathematical modeling of the catchment basins of the studied area was carried out using DEM in GIS by constructing a directed graph with weighting of the upper catchment basins. Then the matrix model of the graph was prepared and assigned weight based on the relevant indexes using codes in the MATLAB and outlet basins and their related weights were determined. In the next step, critical paths were determined in the simulated graph and in each critical path, the key basins were determined for sampling. The proposed algorithm was implemented on a watershed network as a case study and the results showed that this algorithm is able to reduce the costs of sampling and analysis by one quarter.

Keywords: watershed; weighted graph; directed graph; sampling; analysis

1. Introduction

The study of watersheds and stream sediments in order to explore mineral resources, could be carried out by modeling and sampling of the catchments. In all these cases, the goal can be achieved using sampling from the watersheds and analysis of the samples to conclude the results. However, due to the vast network of watersheds, it is not possible to sample and analyze the samples from all of the catchments. The traditional methods are time consuming and require high cost which is not cost effective. Over the years, many studies have been conducted in this field that the main purpose of all these studies is to find the optimal points for sampling in order to reduce the number of samples and consequently reduce the cost and time to reach the desired points. Therefore, the issue of designing and modeling the network of watershed and catchments to find the optimal sampling points has been raised for many years.

In this regard, for the first time, Sharp was able to find the optimal points for sampling by specifying the topological center of the watershed network **(Sharp, 1971)**. The theory of this method was first proposed by some researchers and its implementation began in practice in the seventies **(Scheidegger, 1965**; **Shreve, 1967**; **Steinhaus, 1969)**.

Using Sharp method, there was no need to sample all points of catchments and analyze them, but one of the disadvantages of this method is that the factors of catchments do not play a role in determining the optimal points. In Sharp method, all primary basins have the same value and the values given to the intermediate basins have nothing to do with the parameters of the respective catchment and the characteristics of the upstream catchments. Sharp implemented the algorithm on a district of South Carolina with an area of approximately 1.9 square kilometers and 145 catchments, and finally 8 catchments were identified for final sampling.

Harmancioglu et al. presented an algorithm that took into account the properties of catchments for optimal sampling **(Harmancioglu et al., 2004)**. The basis of this algorithm was based on the method used by Lettenmaier et al. to detect contamination of the American water network, and they were able to reduce the number of samples from 81 to 47 by using this method **(Lettenmaier et al., 1984)**. By implementing this algorithm on Gadiz watershed in Turkey, Harmancioglu et al. were able to increase the number of watershed stations from 33 to 14. In this method, dynamic programming was used to find the optimal basins **(Harmancioglu et al., 2004)**. Dixon et al. proposed a method for

Corresponding author: Elham Sharifi Yazdi
e-mail address: sharifiyazdielham@yahoo.com

determining the optimal sampling points using the simulated annealing algorithm. They implemented the algorithm on the Logan and Albert River areas in Queensland, Australia, and eventually introduced eight stations for optimal sampling (**Dixon et al., 1999**).

In this paper for modeling the watershed network, using DEM images in the GIS, a graph model is presented and a matrix model related to the graph is implemented. In the next step, the information of catchments is considered as a matrix and by presenting a new algorithm which has been developed from Sharp theory and coding in MATLAB, the key catchments are identified. According to this presented algorithm, using assigned weights and matrix operations, the critical paths are introduced and the optimal points are selected for sampling. The purpose of this algorithm is to reduce the number of sampling points and adjust the cost of sample analysis.

2. Methods

In this section we describe the mathematical methodology and algorithm that have been used for watershed modeling and sample location design.

2.1. Mathematical graph modeling of watershed network

In this section, special graphs made based on the network of watersheds and matrix patterns are used to analyze them. Due to the extent of watersheds, which sometimes extend for kilometers, it is necessary that this area is modeled to be able to analyze them using mathematical models and the main goal is to select the optimal sampling points from thousands. First, the geographical information of the catchments needs to be modeled. In this regard, the experts developed a technical method which prepare digital elevation model (DEM) using satellite images, topography and geomorphology of the region and river network. Using satellite images, these areas are divided into partition of 20-30 meters and each area is considered as a point. Then, using the information received from the satellite, an average altitude is assigned to each area (**Carranza, 2009**). The grid is formed based on the height of the areas from the highest to the lowest area (**Figure 1**).
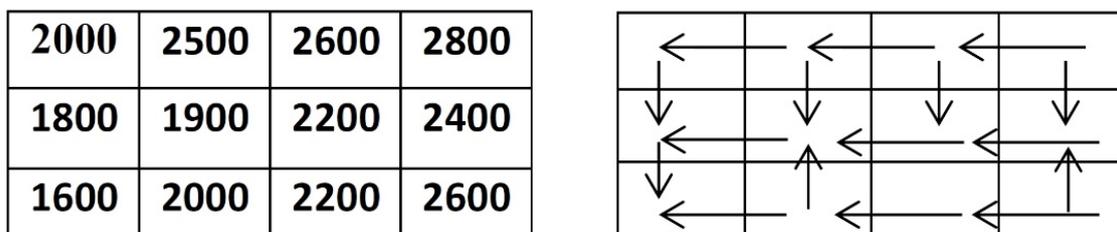
Figure 1: River network model based on the height of the areas obtained from DEM images

Sorting the catchment is carried out using the importance of its branches. In this method, the branches of the catchments are numbered in such a way that to each branch of the network, a number equal to the total number of upstream branches is assigned. In this way, the number 1 is assigned to the primary or input branches and the number 2 is assigned to the branch that consists of two first order branches. Suppose two small rivers with order m_1 and m_2 are connected at one point. It is obvious that the larger river originating from these two rivers has the order of $m_1 + m_2$ (**Sharp, 1971**). In **Figure 2**, the watershed network is sorted using the above method and as can be seen, the outlet branch is ranked as 16, which indicates the total number of sub-branches.
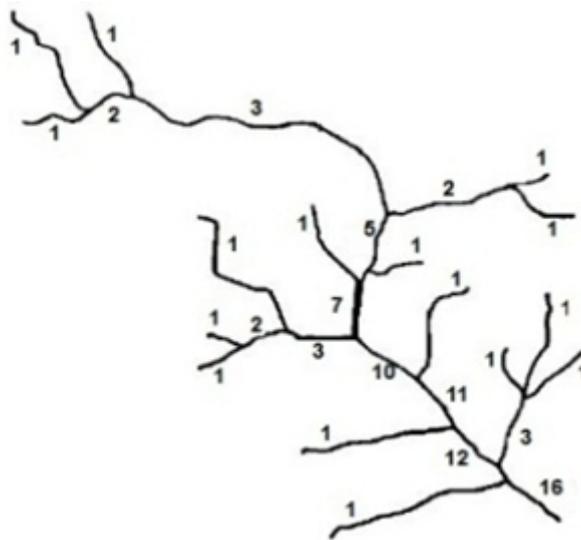
Figure 2: An example of watershed ranking (**Sharp, 1971**)

A river system can be supposed as a directed graph by considering a corresponding vertex for each branch of the watershed and determining the connection between the watershed network by directed edges in the graph. It is also possible to consider a vertex corresponding to each catchment, and based on which catchment water flows into another catchment, the connection between these two vertices is determined with a directed edge. As a result, the catchment network is modeled with a directed graph (**Figure 3**).
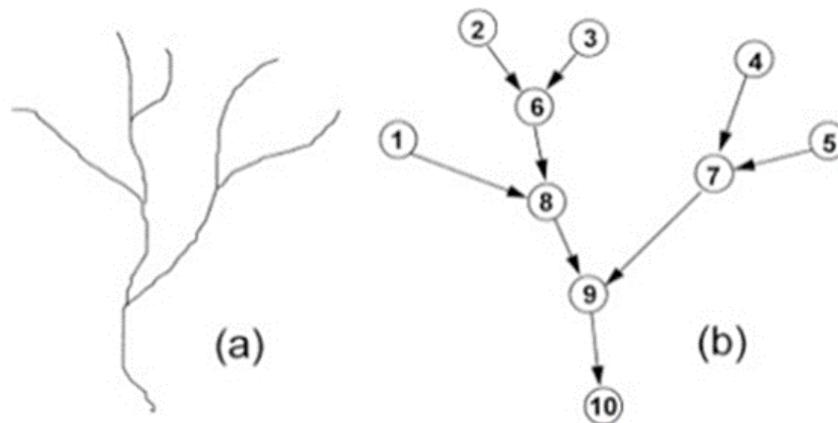
Figure 3: (a) A watershed network (b) Modeling by directed graph (**Dixon et al., 1999**)

Generally, every directed graph G can be modeled by a matrix. This matrix is called adjacency matrix. If we denote this matrix as A, in this matrix the entry a_{ij} is equal to 1 if there is a directed edge starting from the vertex v_i to the vertex v_j, otherwise it has a value of zero (**Harari, 1972**). As an example, a directed graph (**Figure 4**) is modeled as follows using its adjacency matrix (**Figure 5**).
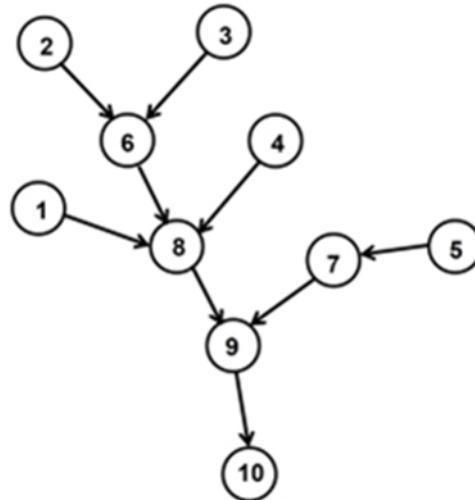
Figure 4: An example of directed graph modeled from the catchment network

$$A = \begin{bmatrix} 0 & 0 & 0 & 0 & 0 & 0 & 0 & 1 & 0 & 0 \\ 0 & 0 & 0 & 0 & 0 & 1 & 0 & 0 & 0 & 0 \\ 0 & 0 & 0 & 0 & 0 & 1 & 0 & 0 & 0 & 0 \\ 0 & 0 & 0 & 0 & 0 & 0 & 0 & 1 & 0 & 0 \\ 0 & 0 & 0 & 0 & 0 & 0 & 1 & 0 & 0 & 0 \\ 0 & 0 & 0 & 0 & 0 & 0 & 0 & 1 & 0 & 0 \\ 0 & 0 & 0 & 0 & 0 & 0 & 0 & 0 & 1 & 0 \\ 0 & 0 & 0 & 0 & 0 & 0 & 0 & 0 & 1 & 0 \\ 0 & 0 & 0 & 0 & 0 & 0 & 0 & 0 & 0 & 1 \\ 0 & 0 & 0 & 0 & 0 & 0 & 0 & 0 & 0 & 0 \end{bmatrix}$$

Figure 5: Adjacency matrix of directed graph corresponding to **Figure 4**

The powers of adjacency matrix A are widely used in watershed network analysis. Suppose A is the adjacency matrix of the directed graph G with n vertices. In this case, the entry of the row i and the column j of the matrix A^m is equal to the number of paths of length m from the vertex v_i to the vertex v_j ($1 \leq m \leq n$) (**Harari, 1972**). Therefore, in the matrix A^2 corresponding to the graph in **Figure 4**, the entry a^2_{ij} is equal to 1 whenever water flows from the catchment i through an intermediate catchment to the catchment j, otherwise its value is zero. Also, in matrix A^3 related to this graph, the value a^3_{ij} is equal to 1 whenever water flows from catchment i through two intermediate catchments to catchment j otherwise its value is equal to zero.

According to the physical properties of watersheds, the graphs modeled on the catchment network are the union of several directed trees. Also in the matrix M, which is considered as the following **Equation 1**:

$$M = A + A^2 + A^3 + \ldots + A^n \tag{1}$$

the elements of this matrix have the value of zero or one. It should be noted that the ones in row i represent the downstream catchments of catchment i and the ones in column j represent the upstream catchments of catchment j. Because each catchment flows into itself, the I + M matrix can be constructed to take this into account, which I is the identity matrix. Using the sum of the values in each column of this matrix, we can realize the importance of the catchment corresponding to that column. In addition, the column that has the most ones represents the outlet catchment. Also, columns with exactly one non-zero entry is known as inlet catchments. Due to the large number of the catchments, for calculation of I + M matrix, it can be simply used the following **Equation 2**:

$$I + M = (I - A)^{-1} \tag{2}$$

where $(I - A)^{-1}$ is inverse matrix $(I - A)$. The correctness of the **Equation 2** can be easily proved by calculating $(I - A)(I + M)$ and vice versa and reaching to the identity matrix (I).

2.2. Algorithm and methodology

Due to the fact that the sampling of all watershed catchments is time consuming and costly task, there are a number of stations in each catchment that are the most important which need to be sampled. As a result, in order to access the optimal samples, unused stations should be eliminated in each catchment area and stations where the possibility of having an optimal sample is high should be considered. Suppose N_r is the total number of stations in the region and N_s is the number of stations that must be remained in the entire network. In this case, the number of selections for the stations that should be totally remained is calculated using **Equation 3** binomial coefficients as follows **(Harmancioglu et al., 2004)**:

$$C(N_r, N_s) = \binom{N_r}{N_s} = \frac{N_r!}{N_s! \, (N_r - N_s)!} \tag{3}$$

Where are:
N_r- *the total number of stations in the region,*
N_s- *the number of stations that must be remained in the entire network.*

Obviously, this number depends on the values of N_r and N_s and can be a large number of choices. Consider that the area is divided into k primary catchments. Suppose the number of stations in each catchment of i (i =1, 2, …, k) is equal to r_i and the number of stations remaining in that catchment is equal to s_i, therefore we have **Equation 4**:

$$N_r = \sum_{i=1}^{k} r_i \, , \ \ N_s = \sum_{i=1}^{k} s_i \tag{4}$$

Where are:
r_i- *the number of stations in each catchment i,*
s_i- *the number of stations remaining in catchment i.*

Because the number of stations that must be remained in the initial catchment i is not yet known, therefore s_i can select any of the values $0, 1, . . ., r_i$. If the number of selections for the total number of stations remaining in the area is denoted with the variable F and the number of selections for the total number of stations remaining in the catchment i is denoted with F$_i$, we have **Equations 5** and **6**:

$$F_i = \sum_{s_i=0}^{r_i} C(r_i, s_i) = 2^{r_i} - 1 \tag{5}$$

$$F = \prod_{i=1}^{k} F_i \tag{6}$$

As a result, F will have a very large value. Therefore, it is necessary to reduce the number of stations for sampling. In a sampling network, significant criteria must first be considered for selection of the optimum stations. These criteria should be used as a prioritized list at stations. In this way, the number of stations can be reduced by considering the priorities. For this purpose, for each initial catchment i, weight is allocated according to the existing criteria as follows (**Equation 7**):

$$W_i = \sum_{j=1}^{r_i} \sum_{l=1}^{m} w_{ijl} \tag{7}$$

Where are:
w_{ijl}- *uniform data in the range (1,0) for property l in catchment i and for station j,*
m- *the number of properties that are considered as existing criteria.*

In the Sharp method, each primary catchment is given the same weight. In this method, by determining the topological centre of the network, an optimal method for sampling of stream sediments can be achieved (**Sharp, 1971**). By definition, the topological centre of a watershed network is the branch that divide the network into two topological areas so that the number of outermost branches of two sides of the basin is equal. However, in our algorithm, the real

value of the catchments is not the same and each branch does not have the same weight due to the topographical situation, length and slope of the branches, and the variety of geological units in the basin. Therefore, according to the weights assigned to the catchments, the first topological centre of the entire network can be calculated as follows (**Equation 8**):

$$w_{k1} = \frac{w_{ko}+1}{2}$$ (8)

Where are:
w_{k1}- *the first topological centre of the entire network for every basin k.*
w_{ko}- *the weight assigned to the outflow catchment in the basin k.*

Now suppose w_{s1} is the closest weight of the catchment to w_{k1} that exists in the basin network. Therefore, the relevant catchment is considered as a key catchment in the sampling priority after the outlet sample. The same steps are continued to find the catchments for the next optimal sampling and in step i in the remaining part, the topological centre is calculated as the following **Equation 9**:

$$w_{ki} = \frac{w_{ko}-\sum_{j=1}^{i-1} w_{sj}+1}{2}$$ (9)

Where are:
w_{ki}- *the ith topological centre of the entire network for every basin k.*
w_{sj}- *the closest catchment weight to w_{kj}.*

This algorithm uses a combination of geographic information system (GIS), graph theory and the development of the Sharp method. Thus, a matrix model of watershed network has been prepared using GIS and graph theory. This matrix contains accumulated information and the location of samples in the catchment area, such as the catchment area and its physical and geomorphological properties, etc. This algorithm can use this matrix to provide the best combination of samples. In the proposed algorithm in this paper, at first the corresponding graph of the catchments is modeled using MATLAB software. Then, considering that each region has its own characteristics, the weight of catchments is determined based on the physical and geological characteristics of the catchments. Information about catchments is also stored in a matrix. By considering the output catchments and evaluating the upstream catchment areas and developing the Sharp method using the mentioned matrix and programming in MATLAB software, the optimal sampling points are determined. The implementation steps of this algorithm are presented in a flowchart as shown in **Figure 6**:

3. Case study

The study area is Khoy basin in West Azerbaijan in Iran. Khoy city is located in the south-eastern part of the region. This area on the basis of climatic situation has usually cold and semi-arid winters and mild summers and the average annual rainfall is 334 mm. The Aqchai and Aland rivers are the most important waterway systems in the region, which originate from the north-western highlands and the central mountainous regions, respectively, and flow into the Aras River. The valleys that appear in these areas are usually deep and their topographic slope in some areas exceeds 70 degrees. In this study, using geographical information system (GIS) and topography and slope of waterways, the region is divided into 457 catchments. According to the slope of the waterways and the geological condition of the region, the relationship between sub-basin catchments is determined. **Figure 7** shows the division map of the basins and the status of waterways in each catchment and the connections between these waterways in the study area.
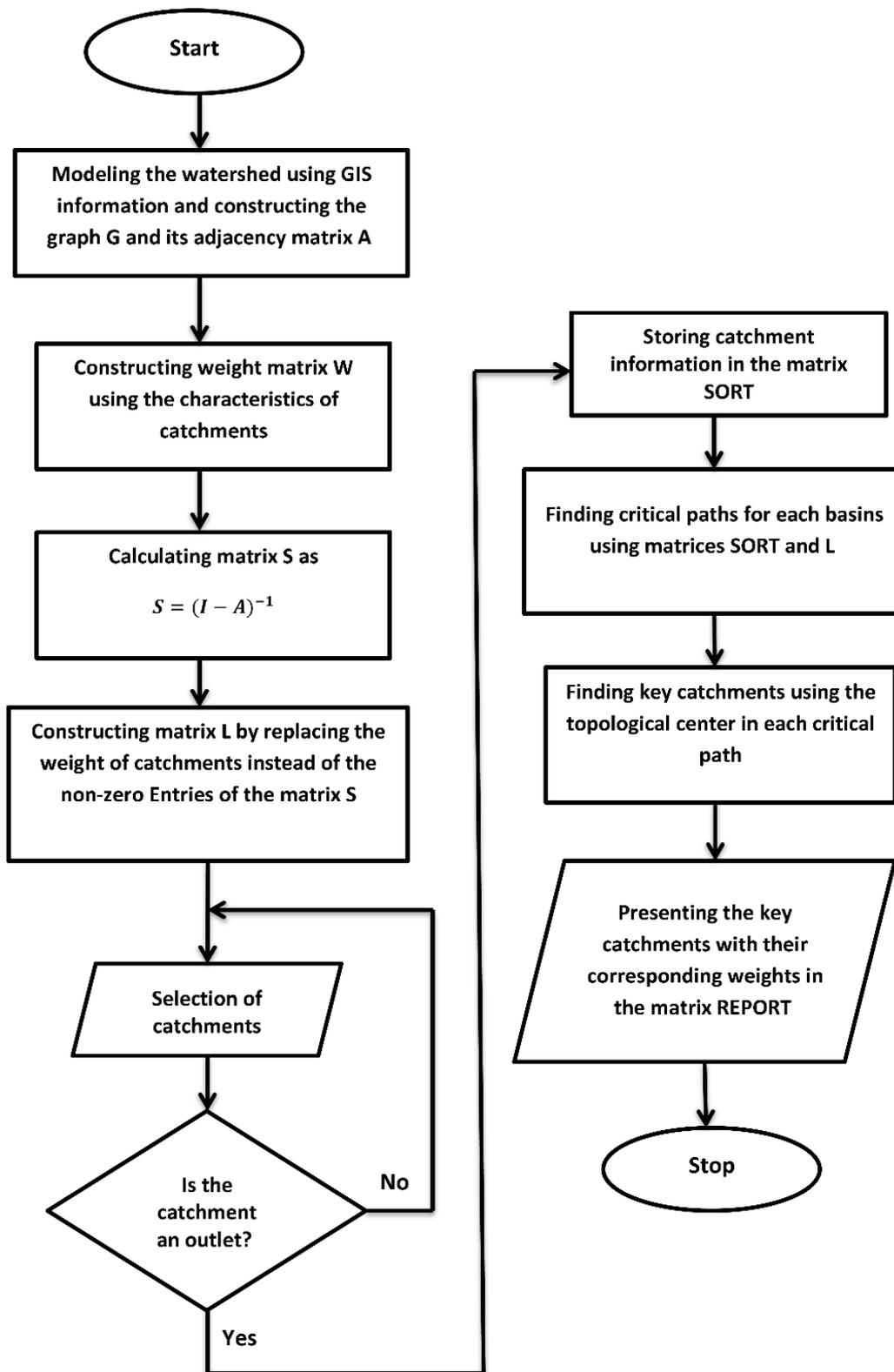
Figure 6: Flowchart presenting algorithm for finding key catchments
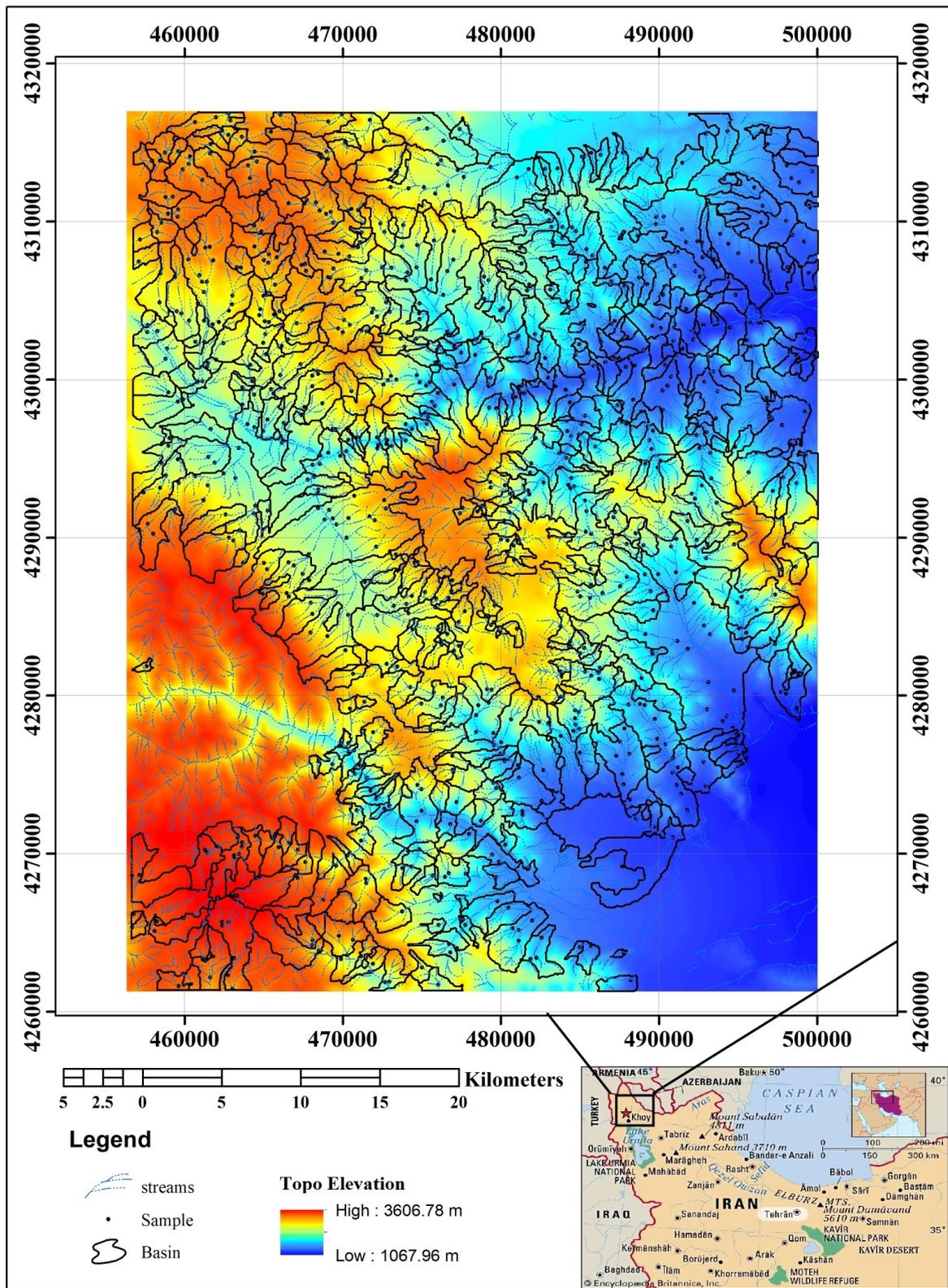
Figure 7: Condition of waterways, altitude changes and catchments of the region

In this section, at first one vertex corresponding to each catchment is considered and according to the connection status of upstream and downstream catchments, the directed graph and its adjacency matrix is formed. This matrix has 457 rows and 457 columns, which are shown in **Figure 8** as part of the adjacency matrix corresponding to the directed graph of the catchments, related to rows 111 to 133 and columns 116 to 140.

	116	117	118	119	120	121	122	123	124	125	126	127	128	129	130	131	132	133	134	135	136	137	138	139	140
111	1	0	0	0	0	0	0	0	0	0	0	0	0	0	0	0	0	0	0	0	0	0	0	0	0
112	0	0	0	1	0	0	0	0	0	0	0	0	0	0	0	0	0	0	0	0	0	0	0	0	0
113	0	0	0	0	0	0	0	0	0	0	0	0	0	0	0	0	0	0	0	0	0	0	0	0	0
114	0	0	0	0	0	0	0	0	0	0	0	0	0	0	0	0	0	0	0	1	0	0	0	0	0
115	0	0	0	0	0	0	1	0	0	0	0	0	0	0	0	0	0	0	0	0	0	0	0	0	0
116	0	0	0	0	0	0	0	0	0	0	0	0	0	0	0	0	0	0	0	0	0	0	0	0	0
117	0	0	0	0	0	0	0	0	0	0	0	0	0	0	0	0	0	0	0	0	0	0	0	0	0
118	0	0	0	0	0	0	0	0	0	0	0	0	0	0	0	0	0	0	0	0	0	0	0	0	0
119	0	0	0	0	0	0	0	0	0	0	0	0	0	0	0	0	0	0	0	0	0	0	0	0	0
120	0	0	0	0	0	0	0	0	0	0	0	0	0	0	0	1	0	0	0	0	0	0	0	0	0
121	0	0	0	0	0	0	0	0	0	0	0	0	0	0	0	0	0	0	0	0	0	0	0	0	0
122	0	0	0	0	0	0	0	0	0	0	0	0	0	0	0	0	0	0	0	0	0	0	0	0	0
123	0	0	0	0	0	0	0	0	0	0	0	0	0	0	0	0	0	0	0	0	0	0	0	0	0
124	0	0	0	0	0	1	0	0	0	0	0	0	0	0	0	0	0	0	0	0	0	0	0	0	0
125	0	0	0	0	0	0	0	0	0	0	0	0	1	0	0	0	0	0	0	0	0	0	0	0	0
126	0	0	1	0	0	0	0	0	0	0	0	0	0	0	0	0	0	0	0	0	0	0	0	0	0
127	0	0	0	0	0	0	0	0	0	0	0	0	0	0	0	0	0	0	0	0	0	1	0	0	0
128	0	0	0	0	0	0	0	0	0	0	0	0	0	0	0	0	0	0	0	0	0	0	0	0	0
129	0	0	0	0	0	0	0	0	0	0	0	0	0	0	0	0	0	0	0	0	0	0	0	0	0
130	0	0	0	0	0	0	0	0	0	0	0	1	0	0	0	0	0	0	0	0	0	0	0	0	0
131	0	0	0	0	0	0	0	0	0	0	0	0	0	0	0	0	0	0	0	0	0	0	0	0	0
132	0	0	0	0	0	0	0	0	0	0	0	0	0	0	0	0	0	0	0	0	0	0	0	0	0
133	0	0	0	0	0	0	0	0	0	0	0	0	0	0	0	0	0	0	0	0	0	0	0	0	0

Figure 8: A part of adjacency matrix

Using the adjacency matrix and MATLAB program, the directed graph of the catchments in the region was prepared. Part of this graph is presented in **Figure 9**. Using this graph, it is possible to easily identify the connections between the catchments and the upstream and downstream of a particular catchment.
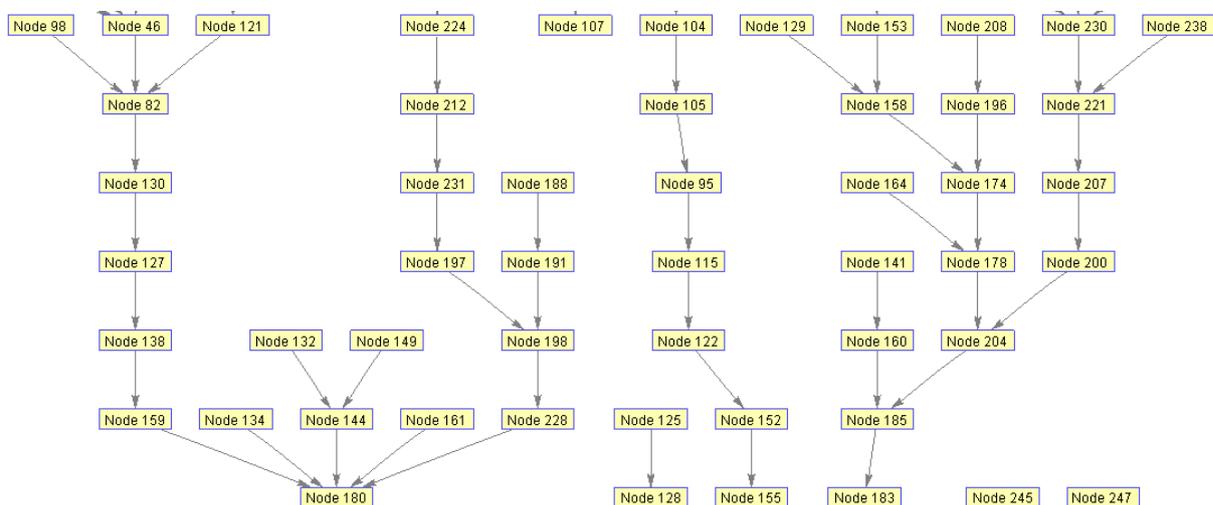
Figure 9: A part of directed graph corresponding to catchment situation

Using geographic information system (GIS), the desired parameters of each catchment including the area of the catchment, the total length and the number of waterways of each catchment, the number of rock units and the average slope of the catchment were extracted. The geological classes were considered in our study and one of the factors influencing to the weights is number of rock units in the catchments. These rock units of the district are very various, consist of sedimentary, partially metamorphic and in some parts ultrabasic to acidic volcanic and intrusive rocks. Due to the importance of the above parameters, a special weight was assigned to each of these indicators and as a result of combination of this information, a specific statistical weight was assigned to each of the catchments. This weight shows the importance of each catchment to be sampled. Table 1 shows a part of the weight matrix W.

Catchment No.	Weight	Catchment No.	Weight
1	2.72	26	2.71
2	2.03	27	1.44
3	2.55	28	2.32
4	3.32	29	3.40
5	3.42	30	1.82
6	3.50	31	3.17
7	2.51	32	2.51
8	2.22	33	1.42
9	1.28	34	4.31
10	2.43	35	2.32
11	1.63	36	3.20
12	2.62	37	1.86
13	2.08	38	3.28
14	3.51	39	2.00
15	2.86	40	3.87
16	2.70	41	1.80
17	1.77	42	1.99
18	1.64	43	2.96
19	3.09	44	1.92
20	1.73	45	2.94
21	2.54	46	3.78
22	2.42	47	3.65
23	2.16	48	2.51
24	2.83	49	2.89
25	3.01	50	3.95

Table 1: A part of weight matrix W assigned to the catchments

As explained in the flowchart (**Figure 6**), the matrix L was constructed using the weight matrix W and the mentioned steps of the algorithm. Using this matrix and MATLAB program, the outflow catchments and their corresponding numbers and their degree of importance are determined and the results were stored in the matrix SORT. Finally, using this matrix (SORT) and finding the critical path corresponding to each outflow catchment and applying **Equation 9**, the key catchments were identified (**Table 2** and **Figure 10**).

Catchment No.	Value	Catchment No.	Value	Catchment No.	Value
135	224.47	70	14.28	436	3.87
421	118.91	79	13.32	426	3.85
183	112.64	226	12.91	444	3.65
180	110	312	12.86	428	3.39
413	87.9	301	12.76	123	3.37
235	65.95	60	12.51	417	3.35
367	65.09	331	12.49	44	3.34
241	63.72	412	12.46	86	3.24
349	60.06	440	11.38	61	3.2
221	58.15	229	10.71	36	3.2
399	55.22	22	10.54	181	3.17
82	54.72	304	10.53	353	3.1
386	43.33	91	10.34	391	3.1
264	33.06	136	10.05	169	3
246	32.62	225	10.04	72	2.98
177	32.46	415	10.04	328	2.96
342	30.22	163	10.02	85	2.93
388	29.61	55	9.98	49	2.89
198	27.56	326	9.57	296	2.82
323	27.09	437	9.43	335	2.82
400	26.68	15	8.89	120	2.82
174	25.65	302	8.3	255	2.76
318	24.88	109	7.74	26	2.71
107	24.12	196	7.29	325	2.66
455	23.55	242	6.96	222	2.66
365	23.27	252	6.89	445	2.66
168	21.95	145	6.73	432	2.39
146	21.61	77	6.3	276	2.37
89	20.96	347	6.04	193	2.27
21	20.31	311	5.61	355	2.23
179	18.85	97	5.48	362	2.2
102	18.61	54	5.4	65	2.19
457	17.32	84	5.29	71	1.95
434	17.09	256	5.26	322	1.94
223	16.86	232	5.24	280	1.93
289	16.5	58	5.16	134	1.92
2	16.26	28	5.03	132	1.9
383	16.17	454	4.59	272	1.85
411	15.56	293	4.57	321	1.84
122	14.91	420	4.55	41	1.8
43	14.71	422	4.06	33	1.42
451	14.34	59	3.91		

Table 2: Selected Catchments for optimal priority sampling and their importance values

Figure 10: The location map of the optimal sample points (for better demonstration only some of the number of optimal catchments related to **Table 2** was shown in this figure)

4. Results
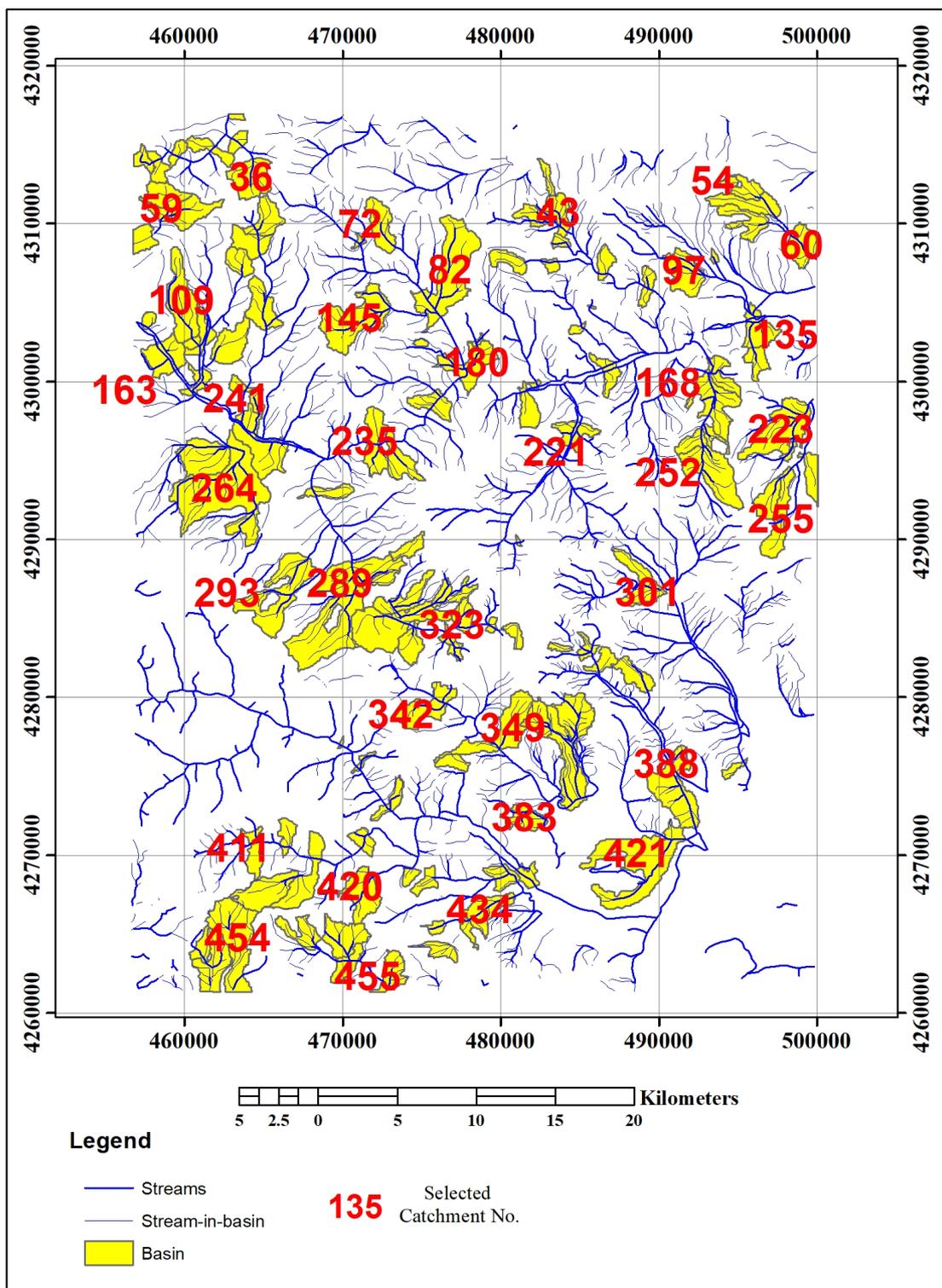
Using the proposed algorithm implemented on the Khoy region as a case study, the optimal catchments with their degree of importance for optimal sampling are specified and shown in **Table 2** and **Figure 10**. As can be seen in the table, the value of each catchment allows the sampler to be aware of its importance for the priority of the catchment sampling design. In this sampling system, sampling starts from the most important outlet with highest value and goes up towards the critical path of the relevant tree. In the second sampling priority, the outlet of the next high value tree is then sampled and thus the sampling work continues to reach to the source. Undoubtedly, the number and type of the rock units, catchment area, waterway length, catchments slope and so on are effective in tracking and determining the source of mineralization and must be considered in the designing of the sampling in order to achieve the goal with the minimum number of the samples. All of these important factors are considered in this algorithm.

Recent study shows that the use of this algorithm is able to reduce the number of required optimal samples to about one quarter. If the total number of catchments in the region is assumed to be 457, using a mathematical model and the algorithm presented in this research and finding critical paths, only 125 samples are required and this method is able to reduce the costs of sampling and analysis by one quarter.

5. Discussion and conclusion

Watershed sampling using traditional methods by taking the samples throughout area from all catchments and their subbranches is very expensive and time consuming. This research proposed a scientific methodology to optimize this sampling method. In this paper, the presented algorithm used a graph base watershed modelling that on the basis of GIS data implements weights on the main factors. These factors consist of area of the catchment, the total length and the number of waterways of each catchment, the number of rock units and the average slope of the catchment. We expect that this new algorithm can be used for precise modelling the watershed system and presenting the optimum points of sampling.

The proposed algorithm was implemented on a watershed network as a case study and the results showed that this algorithm is able to reduce the costs of sampling and analysis by one quarter.

6. References

Carranza, EJM. (2009): Handbook of Exploration and Environmental Geochemistry, Geochemical Anomaly and Mineral Prospectivity Mapping in GIS: Elsevier. 11 p.

Dixon, W., Smyth, G. and Chiswell, B. (1999): Optimized selection of river sampling sites. Water Research, 33, 4, 971-978.

Harary, F. (1972). Graph Theory. Addison-Wesley Publishing Company. Inc.

Harmancioglu, NB., Icaga, Y. and Gul, N. (2004): The use of an optimization method in assessment of water quality sampling sites. European Water, 5, 6, 25-34.

Lettenmaier, DP., Anderson, DE. and Brenner, RN. (1984): Consolidation of a stream quality monitoring network, Water Resources Bulletin. AWRA. 20, 4, 473-481.

Scheidegger, AE. (1965): The algebra of stream-order numbers. U.S. Geological Survey Professional Paper, 525B, 178-186.

Sharp, WE. (1971): A topologically optimum water sampling plan for rivers and streams. Water Resources Research, 7, 6, 1641-1646.

Shreve, RL. (1967): Infinite topologically random channel networks. Journal of Geology.,75, 178-186.

Steinhaus, H. (1969): Mathematical Snapshots. Oxford University Press, New York.

Sažetak

Modeliranje bazenske vododjelnice uporabom težinskih dijagrama te predstavljanje algoritma za odabir primjerenoga smjestišta uzorkovanja s ciljem smanjivanja troškova uzorkovanja i analiza

Uzorkovanje u području vododjelnice je najvažnija istraživačka metoda kod pridobivanja mineralnih sirovina. Ovdje je prikazano matematičko modeliranje vododjelnice s ciljem odgovarajućega uzorkovanja i optimiziranja broja uzoraka te smanjivanja cijene njihova uzimanja i analiziranja. Načinjeno je matematičko modeliranj odabranoga slivnoga područja uporabom DEM-a u GIS-u konstruiranjem izravnih grafova s otežavanjem u gornjem slivu. Zatim je načinjen matrični model kojemu su pridruženi težinski koeficijenti pomoću indeksa, uporabom koda u MATLAB-u. Time su opisani otjecajni dijelovi bazena te su određeni težinski koeficijenti za ta područja. Na kraju su izračunati kritični putovi toka pomoću simuliranih grafova te su za svaki takav tok određeni ključni bazeni glede uzorkovanja. Prikazani algoritam je provjeren na mreži vododjelnica u odabranom prostoru i rezultati su potvrdili kako je troškove uzorkovanja i analiza moguće smanjiti za četvrtinu.

Ključne riječi: vododjelnica; otežani grafovi; izravni grafovi; uzorkovanje; analiza

Author's contributions

Both authors equally participate in all aspects of presented work.

Estimation of the maximum amount of water available for infiltration from precipitation, Velika Gorica well field

Ana Rečić [1*]; **Zoran Kovač** [2]; **Laura Bačani** [3]; **Kristijan Posavec** [4]; **Jelena Parlov** [5]

[1] Faculty of Mining, Geology and Petroleum Engineering, University of Zagreb, Pierottijeva 6, 10000 Zagreb

[2] Faculty of Mining, Geology and Petroleum Engineering, University of Zagreb, Pierottijeva 6, 10000 Zagreb, https://orcid.org/0000-0001-8091-7975

[3] Faculty of Mining, Geology and Petroleum Engineering, University of Zagreb, Pierottijeva 6, 10000 Zagreb, https://orcid.org/0000-0003-2064-4439

[4] Faculty of Mining, Geology and Petroleum Engineering, University of Zagreb, Pierottijeva 6, 10000 Zagreb, https://orcid.org/0000-0002-5392-9329

[5] Faculty of Mining, Geology and Petroleum Engineering, University of Zagreb, Pierottijeva 6, 10000 Zagreb, https://orcid.org/0000-0002-2862-7222

Abstract

Zagreb aquifer presents one of the main sources of potable water for the inhabitants of the City of Zagreb and Zagreb County. It presents strategic water reserves protected by the Croatian State. In the first sanitary protection zone of the Velika Gorica well field, which is one of the major well fields, pedological pit was excavated and scientific research polygon was established. Long-term goals of the research are related to the modelling of groundwater flow and transport through unsaturated zone and quantification of effective infiltration. In this study, various equations for estimating evaporation and evapotranspiration were evaluated in detail to determine the maximum amount of water available for infiltration in 2019. The modified Penman-Monteith (CIMIS), Meyer, Turc, Hargreaves and Jensen-Haise equations were used. Due to different input parameters, linear regression was used to test the relationship between the most important parameters. In general, reference evapotranspiration estimated with different equations showed differences up to ±30%. Correlation and regression analysis between the evapotranspiration, evaporation, temperature, and solar radiation showed statistically significant positive correlations, with the highest correlation coefficient and coefficient of determination observed for solar radiation and reference evapotranspiration. However, only the equations of Meyer and Turc gave smaller values of evaporation and evapotranspiration than precipitation. The equations used for reference evapotranspiration gave higher values that ultimately resulted in unrealistic values for water available for infiltration. The annual Turc equation was chosen as the most appropriate equation for the investigated area, estimating the maximum available water for infiltration in 2019 to be about 269 mm.

Keywords: evaporation; evapotranspiration; infiltration; Velika Gorica well field

1. Introduction

The Zagreb aquifer presents the main source of potable water for the citizens of the City of Zagreb and Zagreb County. It is proclaimed as strategic water reserves protected by the Republic of Croatia. In recent years, hydrogeological research in the study area has focused mainly on determining the origin of nitrates (**Kovač et al., 2018**), evaluation of groundwater and surface water interaction (**Posavec et al., 2017; Kapuralić et al., 2018; Parlov et al., 2019**), estimation of groundwater velocities (**Barešić et al., 2020**) and groundwater level trends (**Vujević & Posavec, 2018**). Soil and unsaturated zone research was mainly associated to the estimation of the unsaturated hydraulic conductivity variation in Fluvisols (**Ružičić et al., 2017**), influence of agriculture activities (**Ružičić et al., 2018**), definition of relationship between physicochemical properties and soil permeability (**Ružičić et al., 2019**), sorption of cadmium, zinc and copper in dominant soils (**Kovač et al., 2022a**), as well as to soil hydrology research in the hillslope

Corresponding author: Ana Rečić
ana.recic@rgn.unizg.hr

vineyard (**Kovač et al., 2022b**). However, there has not been a lot of research related to the estimation of infiltration through unsaturated zone into the aquifer.

Within this research we present results related to the estimation of evaporation and evapotranspiration through different equations in order to determine the maximum amount of water available for infiltration in year 2019, at well field Velika Gorica, located in the southeastern part of the Zagreb aquifer (**Figure 1**).
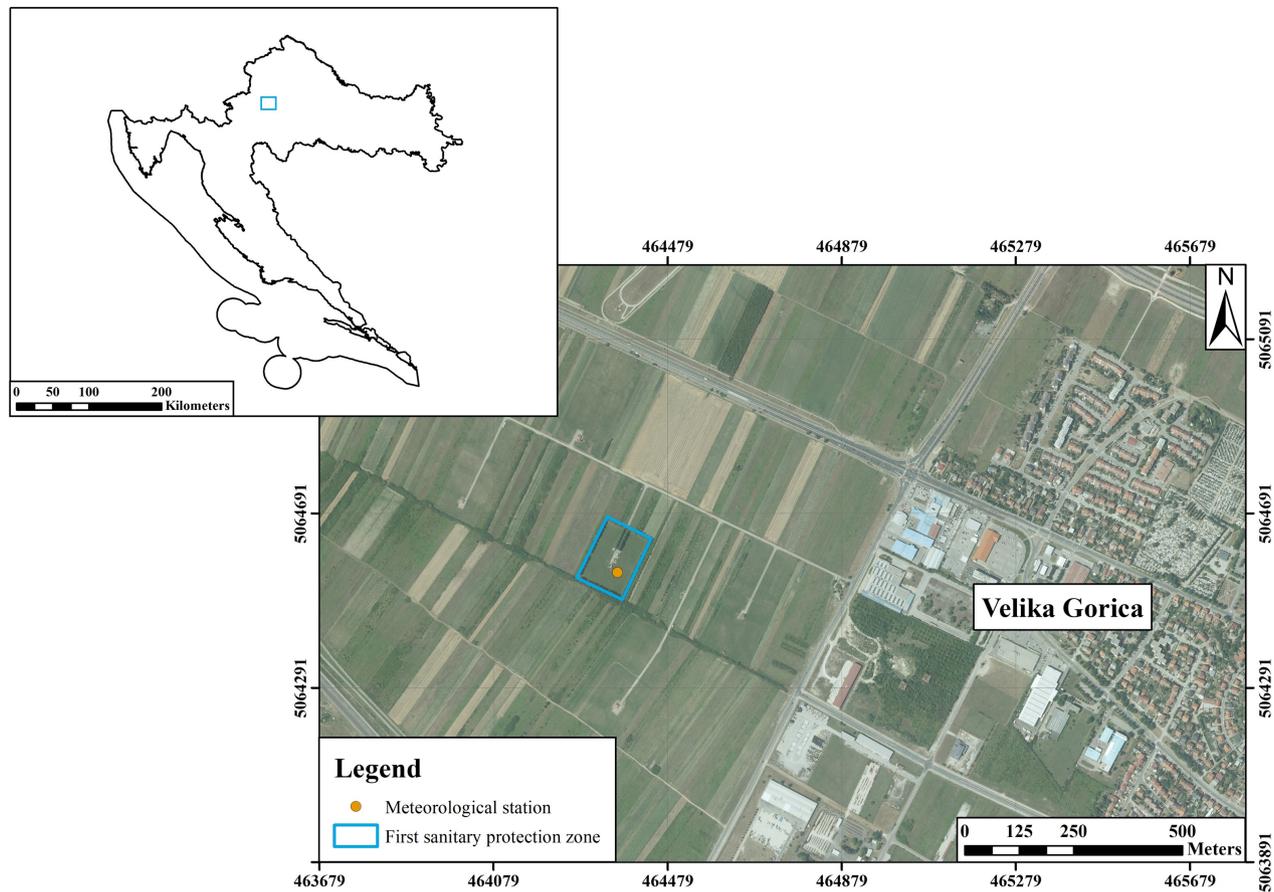
Figure 1: Research area (modified according to **Rečić, 2020**)

2. Methods and data

The research was conducted in the first sanitary protection zone of the Velika Gorica well field, where a new scientific research polygon of the Faculty of Mining, Geology and Petroleum Engineering was established. Within this polygon pedological pit was excavated and a meteorological station Davis Vantage Pro 2 was set. The hourly data of the Davis Vantage Pro 2 station from 2019 were used, while the global radiation values for the research area were ceded by the Croatian Meteorological and Hydrological Service. Meteorological station Davis Vantage Pro 2 has incorporated Penman-Monteith equation (**Penman, 1948; Allen et al., 1998**) for the calculation of reference evapotranspiration which was modified by California Irrigation Management Information System (CIMIS). This reference evapotranspiration was available only from April to December because additional sensors related to radiation have been additionally installed to the meteorological station. Furthermore, Meyer equation (**Meyer, 1915**) was used for the calculation of monthly evaporation, Turc equation (**Turc, 1953**) for the calculation of average annual evapotranspiration, Hargreaves equation for reference monthly evapotranspiration (**Hargreaves and Samani, 1985; Jensen et al., 1990; Fernandes et al., 2012**) and Jensen-Haise equation for daily reference evapotranspiration (**Jensen and Haise, 1963; Sediyama et al., 1997; Fernandes et al., 2012**). The choice of equations was made based on the availability of the meteorological variables. Correlation and regression analysis were performed in Microsoft Excel by testing the relationship between evaporation, reference evapotranspiration, air temperature and solar radiation. Estimation of the maximum amount of water available for infiltration was done by subtracting evapotranspiration/evaporation from precipitation.

The Penman-Monteith equation modified by CIMIS (URL 1) works with hourly data and is expressed as (**equation 1**):

$$ETo = W \cdot Rn + (1 - W) \cdot VPD \cdot FU2 \qquad (1)$$

where:
ET_o – is reference hourly evapotranspiration (mm/h);
W - is a dimensionless partitioning factor;
Rn – is net radiation (W/m²);
VPD – is vapor pressure deficit (kPa);
FU2 – is empirical wind function (mm/h/kPa).

The Meyer equation (**Meyer, 1915**) is expressed as (**equation 2**):

$$E = 11.25\, E_t\, (1 - R_v)\, (1 + 0.225\, v) \qquad (2)$$

where:
E – evaporation (mm/month);
E_t – saturated air vapor pressure at temperature t (mbar);
R_v – relative humidity (%);
v – air sped (m/s).

Due to the lack of measurements regarding saturated air vapor pressure, it was calculated using **Buck (1981)** equation with temperature in Celsius degrees (**equation 3**):

$$P_s(T) = 6.1121 e^{\left(18.678 - \frac{T}{234.5}\right)\left(\frac{T}{257.14+T}\right)} \qquad (3)$$

where:
P_s (T) – water vapor pressure (hPa=mbar);
e – Euler`s number;
T – air temperature (°C).

The Turc equation (**Turc, 1953**) was expressed as (**equation 4**):

$$E_T = \frac{P}{\sqrt{0,9 + \frac{P^2}{L^2}}} \qquad (4)$$

where:
P – average annual precipitation (mm);
L = 300 + 25T + 0.05T³;
T – average annual air temperature (°C).

The Hargreaves equation is expressed as (**Jensen et al., 1990; Fernandes et al., 2012; equation 5**):

$$ET_O = 0.0135\, Rs\, (Tmean + 17.8) \qquad (5)$$

where:
ET_O – reference evapotranspiration (mm/month);
Rs = is the global radiation at surface (MJ/m²day = 0.408 mm/day);
Tmean – average monthly air temperature (°C).

The Jensen-Haise equation is expressed as (**Sediyama et al., 1997; Fernandes et al., 2012; equation 6**):

$$ET_O = (0.0252\ Tmean + 0.078)\ Rs \qquad (6)$$

where:

ET_O – reference evapotranspiration (mm/day);
Rs – is the global radiation at surface (MJ/m²day = 0.408 mm/day);
$Tmean$ – average monthly air temperature (°C).

3. Results and discussion

Figure 2 shows the monthly precipitation and average air temperature for 2019. Precipitation values ranged from 28.2 mm in January to 162.4 mm in May. Very high precipitation values were also observed in September and November. The annual precipitation sum was 819.6 mm (**Rečić, 2020**). The average monthly air temperature varied from 0.71 °C in January up to approximately 23 °C in June, July and August. According to the **Meyer (1915)** equation monthly evaporation was highest in June, and then in July and August, which corresponds to the observed temperatures. Smallest evaporation was recorded in period from November to January (**Figure 3**). Total annual evaporation was estimated to be 573.93 mm, which is very similar to the values of annual evapotranspiration calculated by **Turc (1953)** equation, i.e., 550.88 mm.
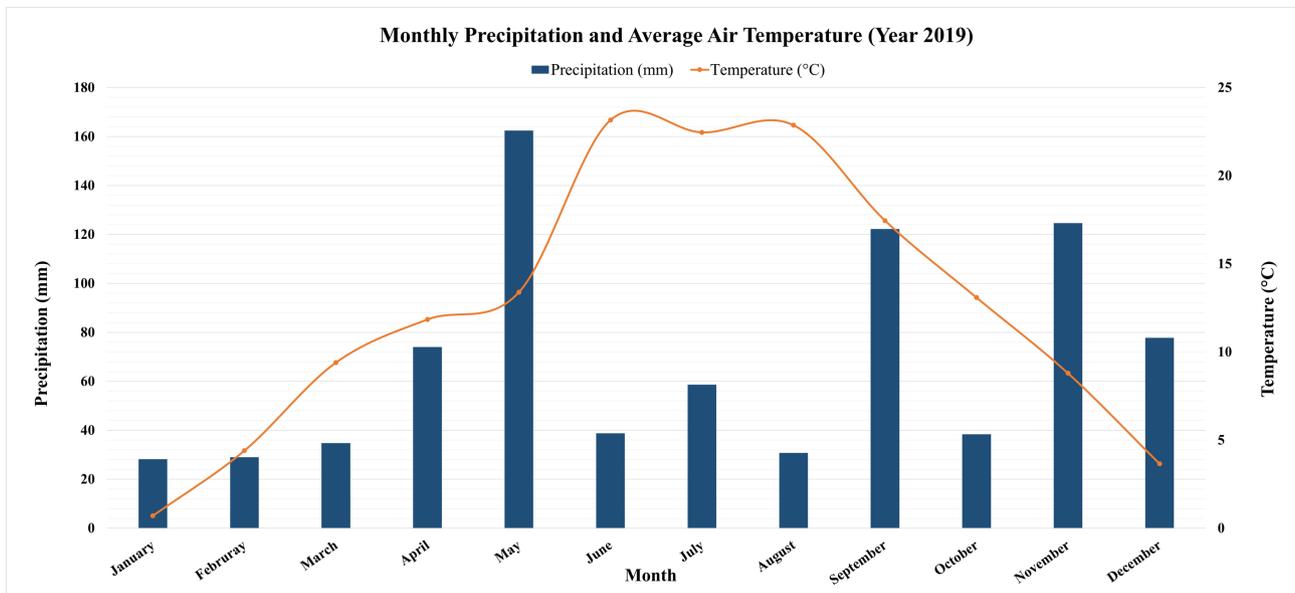
Figure 2: Monthly precipitation and average air temperature (modified according to **Rečić, 2020**)
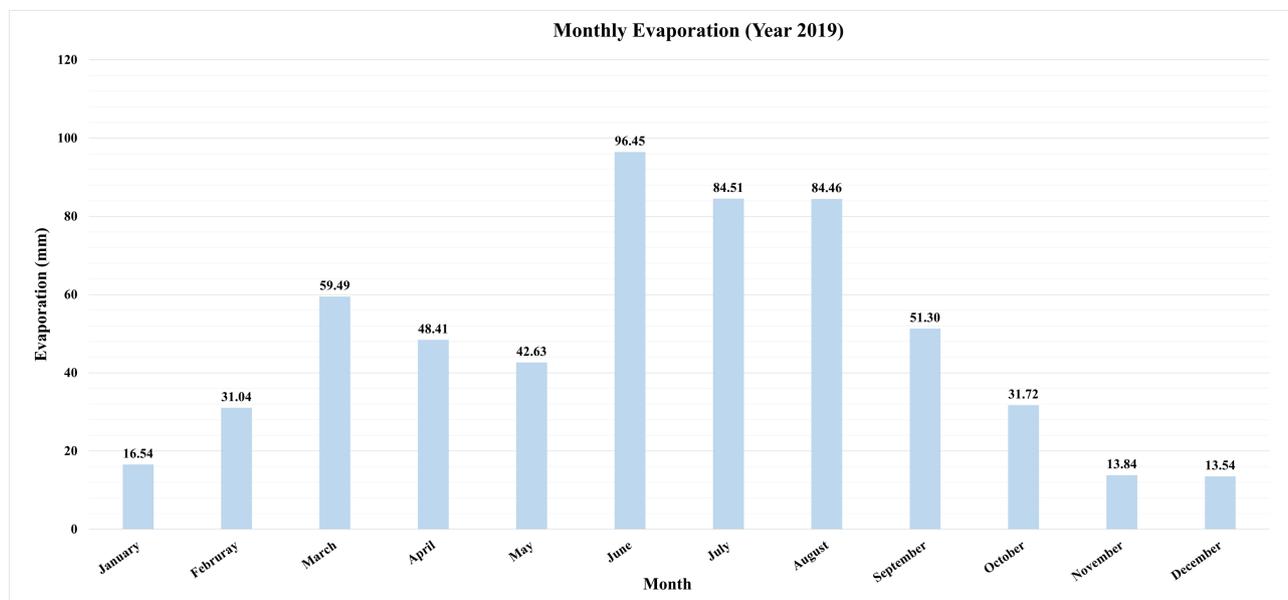
Figure 3: Monthly evaporation (modified according to **Rečić, 2020**)

Reference evapotranspiration calculated by Hargreaves equation (**Jensen et al., 1990; Fernandes et al., 2012**) and Jensen-Haise equation (**Sediyama et al., 1997; Fernandes et al., 2012**) gave much higher values. It must be emphasized here that the daily values calculated with the Jensen-Haise equation were summed to obtain monthly values. **Figure 4** shows the monthly values of evapotranspiration. Values observed directly by Davis Vantage Pro 2 were only available from April. In **Figure 4** it can be clearly seen that all three equations gave the highest values of evapotranspiration in June, then July and August. Furthermore, Jensen-Haise values were the highest (898.72 mm), followed by lower Hargreaves (840.07 mm) and Vantage Pro 2 values (668.83 mm from April to December). However, large differences can only be seen in summer months when the values are highest. In all other months, except December, the estimation of reference evapotranspiration is very similar. In general, reference evapotranspiration estimated with different equations showed differences up to ±30%. The only higher difference was observed in December when Jensen-Haise equation resulted with reference evapotranspiration almost half the value with respect to the other two equations. In addition, results showed that values estimated by meteorological station Vantage Pro 2 are much closer to Hargreaves equation in comparison to the Jensen-Haise equation.
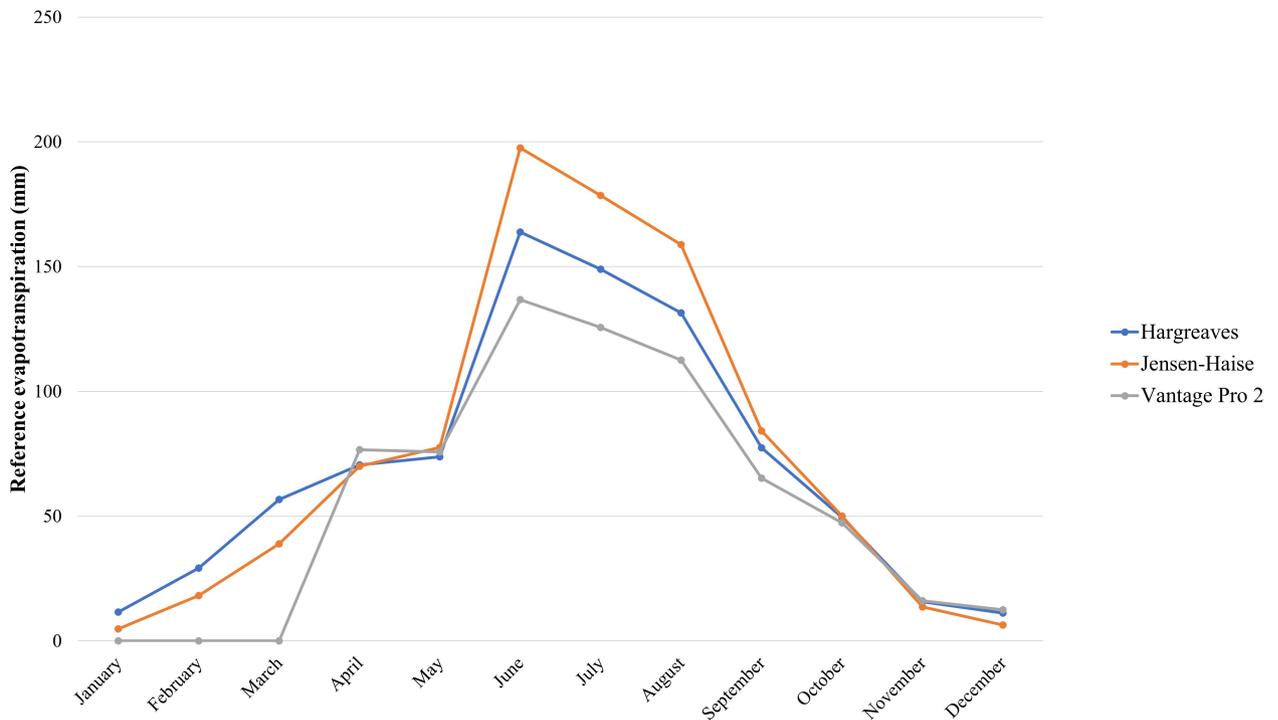
Figure 4: Monthly reference evapotranspiration according to Hargreaves and Jensen-Haise equations

Looking more closely at all the equations used it is clear that most of them use solar radiation and temperature values. To test their relationship, a linear regression analysis was performed. It was performed based on monthly data, while for the reference evapotranspiration results estimated by the Hargreaves equation were used as relevant. The regression analysis was done between the values of evaporation/reference evapotranspiration, temperature, and solar radiation. Firstly, inspection of visual fit for determination of the goodness of fit is presented (**Figure 5**). This is an effective way to examine the goodness of fit because the coefficient of determination (R^2) can be large even when the linear/nonlinear approximation is poor (**Montgomery and Runger, 2003**). In **Table 1** statistical results of linear regression analysis are presented. Results show statistically significant positive correlation in all cases, with higher coefficients of correlation and determination obtained when reference evapotranspiration was observed, which can be also seen through visual inspection on **Figure 5**. The lowest correlation coefficient, although also high, was found between evaporation and temperature.

In general, the results show that only the values of Meyer`s evaporation and Turc`s annual evapotranspiration have values lower than the annual precipitation. Reference evapotranspiration generated higher values than precipitation which makes it unsuitable for estimating the maximum amount of water available for infiltration in this case, i.e., reference evapotranspiration is higher than precipitation. Looking at the values on the annual level, the maximum amount of water available for infiltration would be 245.67 mm (when using Meyer`s evaporation value) and 268.72 mm (when using Turc`s evapotranspiration value; **Rečić, 2020**). Although the differences are not that great, Turc`s evapotranspiration seems to be the most appropriate equation to use for this area and this type of analysis.
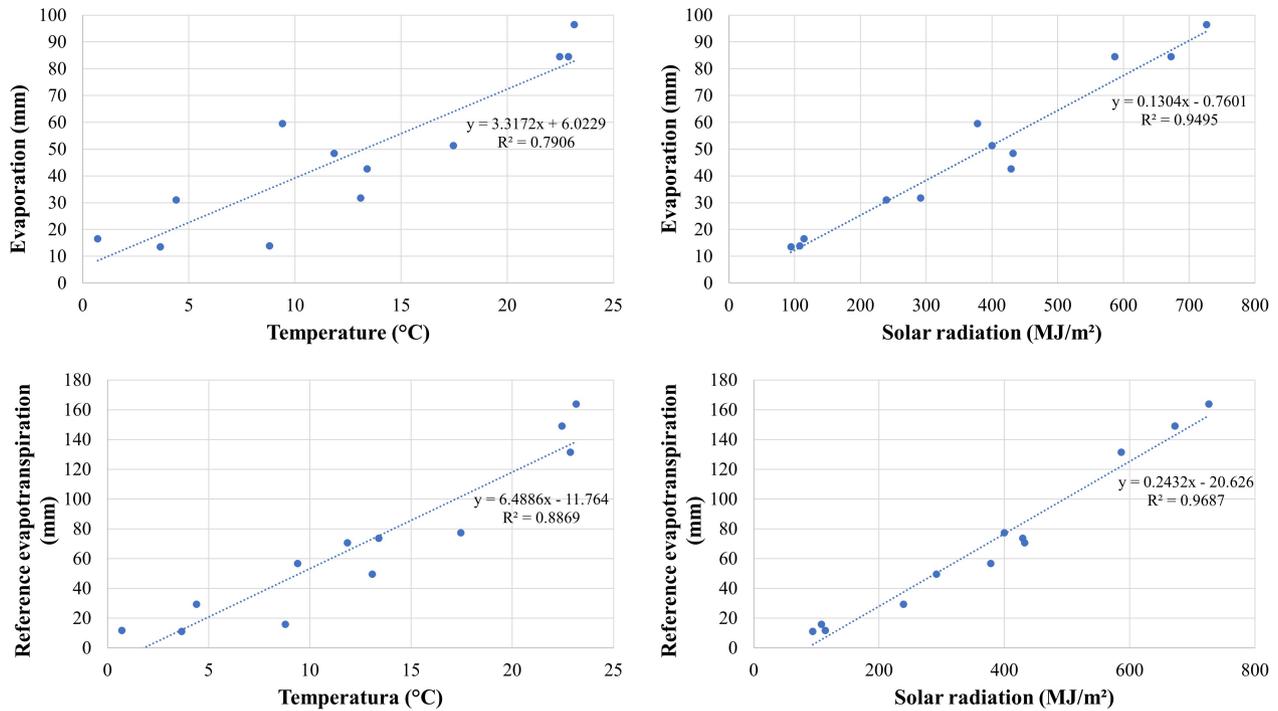
Figure 5: Visual fit of regression analysis between observed meteorological parameters

Parameters	p-value	Statistical significance (α=0.05)	Correlation coefficient	Coefficient of determination
Evaporation vs. temperature	1.09E-04	Yes	0.88917	0.7906
Evaporation vs. solar radiation	8.25E-08	Yes	0.97443	0.9495
Reference evapotranspiration vs temperature	4.78E-06	Yes	0.94177	0.8869
Reference evapotranspiration vs solar radiation	7.49E-09	Yes	0.98423	0.9687

Table 1: Results of regression analysis (modified according to **Rečić, 2020**)

4. Conclusions

This paper presents the first estimation of evaporation and evapotranspiration values at the new scientific research polygon of the Faculty of Mining, Geology and Petroleum Engineering established in the first sanitary protection zone of the Velika Gorica well field. Different equations have been used for the estimation of evaporation, actual evapotranspiration, and reference evapotranspiration in order to quantify the maximum available water for infiltration in the research area in year 2019. Results showed that only Meyer`s evaporation and Turc`s evapotranspiration had values which were smaller than the value of the precipitation. Reference evapotranspiration showed higher values than precipitation, which is not characteristic for the study area. Results suggest, if annual values of evapotranspiration want

to be estimated, Turc`s equation seems to be the most appropriate. Maximum available water for infiltration was estimated to be about 269 mm. Furthermore, in most cases, it has been shown that the reference evapotranspiration estimated with different equations can have differences of up to ±30%, but also that the values of reference evapotranspiration are more related to solar radiation than to air temperature. However, it must be emphasized that long-term monitoring and more detailed studies must be conducted to obtain more reliable results, especially if long-term goals want to be achieved, i.e., modelling groundwater flow and transport through unsaturated zone and quantifying effective infiltration.

5. References

Allen, R.G., Pereira, L.S., Smith, M. (1998): Crop evapotranspiration, FAO Irrigation and Drainage, paper 56. Roma. FAO Rome.

Barešić, J., Parlov, J., Kovač, Z., Sironić, A. (2020): Use of nuclear power plant released tritium as groundwater tracer. Rudarsko-geološko-naftni zbornik 35, 25 – 34, doi: 10.17794/rgn.2020.1.3.

Buck, A.L. (1981): New equations for computing vapor pressure and enhancement factor. Journal of Applied Meteorology 20, 12, 1527-1532.

Fernandes, L.C., Paiva, C.M., Rotunno Filho, O.C. (2012): Evaulation of Six Empirical Evapotranspiration Equations – Case Study: Campos Dos Goytacazes/RJ. Revista Brasileira de Meteorologia 27, 3, 272 – 280, doi: 10.1590/S0102-77862012000300002.

Hargreaves, G.H., Samani, Z.A. (1985): Reference crop evapotranspiration from temperature. Transactions of the ASAE 1, 2, 96-99.

Jensen, M.E., Haise, H.R. (1963): Estimating Evapotranspiration from Solar Radiation. Journal of the Irrigation and Drainage Division 89, 15-41.

Jensen, M.E., Burman, R., Allen, R.G. (1990): Evapotranspiration and irrigation water requirements. American Society of Civil Engineers, New York, NY.

Kapuralić, J., Posavec, K., Kurevija, T., Macenić, M. (2018): Identification of river Sava temperature influence on groundwater tem-perature of the Zagreb and Samobor-Zaprešić aquifer as a part of shallow geothermal potential. Rudarsko-geološko-naftni zbornik 33, 59 – 69, doi: 10.17794/rgn.2018.5.6.

Kovač, Z., Nakić, Z., Barešić, J., Parlov, J. (2018): Nitrate Origin in the Zagreb Aquifer System. Geofluids, 2789691, 15, doi: 10.1155/2018/2789691.

Kovač, Z., Ružičić, S., Rubinić, V., Nakić, Z., Sertić, M. (2022a): Sorption of cadmium, zinc and copper in dominant soils of the Zagreb aquifer system, Croatia. Geologia Croatia 75 (1), 177-188, doi: 10.4154/gc.2022.05.

Kovač, Z., Krevh, V., Filipović, L., Defterdarović, J., Buškulić, P., Han, L., Filipović, V. (2022b): Utilizing stable water isotopes (δ^2H and δ^{18}O) to study soil-water origin in sloped vineyard: first results. Rudarsko-geološko-naftni zbornik 37, 3, 1-14, doi: 10.17794/rgn. 2022.3.1.

Montgomery, C.M., Runger, G.C. (2003): Applied Statistics and Probability for Engineers. 3rd ed. New York: John Wiley & Sons Inc.

Meyer, A.F. (1915): Computing Run-Off from Rainfall and Other Physical Data. Trans. ASCE, vol.79, 1056-1224.

Parlov, J., Kovač, Z., Nakić, Z., Barešić, J. (2019): Using water stable isotopes for identifying groundwater recharge sources of the unconfined alluvial Zagreb aquifer (Croatia). Water 11,10, 2177, doi: 10.3390/w11102177.

Penman, H.L. (1948): Natural Evaporation from Open Water, Bare Soil and Grass. Proceedings of the Royal Society A 193, 129-145, doi: 10.1098/rspa.1948.0037.

Posavec, K., Vukojević, P., Ratkaj, M., Bedeniković, T. (2017): Cross-correlation modelling of surface water-groundwater interaction using the Excel spreadsheet application. Rudarsko-geološko-naftni zbornik 32,1, 25–32, doi: 10.17794/rgn.2017.1.4.

Rečić, A. (2020): Calculation of reference and actual evapotranspiration at well field Velika Gorica. Undergraduate thesis, Faculty of Mining, Geology and Petroleum Engineering, University of Zagreb, Croatia.

Ružičić, S., Kovač, Z., Nakić, Z., Kireta., D. (2017): Fluvisol permeability estimation using soil water content variability. Geofizika 34, 141–155, doi: 10.15233/gfz.2017.34.9.

Ružičić, S., Kovač, Z., Perković, D., Bačani, L., Majhen, Lj. (2019): The Relationship between the Physicochemical Properties and Permeability of the Fluvisols and Eutric Cambisols in the Zagreb Aquifer, Croatia. Geosciences 9 (10), 416, doi: 10.3390/geosciences9100416.

Ružičić, S., Kovač, Z., Tumara, D. (2018): Physical and chemical properties in relation to soil permeability in the area of the Velika Gorica well field. Rudarsko-geološko-naftni zbornik 33,2, 73–81, doi: 10.17794/rgn.2018.2.7.

Sediyama, G.C., Villanova, N.A., Pereira, A.R. (1997): Evapo(transpi)ração. Piracicaba, Editora Universitária ESALQ, 183 p.

Turc, L. (1953): Le bilan d'eau des sols: Relations entre les precipitations, l'evaporation et l'ecoulement. Institut national de la recharge agronomique, 1-252, Paris.

Vujević, M., Posavec, K. (2018): Identification of Groundwater Level Decline in the Zagreb and Samobor-Zapresic Aquifers since the Sixties of the Twentieth Century. Rudarsko-geološko-naftni zbornik 33, 4, 55–64, doi: 10.17794/rgn.2018.4.5.

URL 1: https://cals.arizona.edu (Azmet Computation of Reference Crop Evvapotranspiration, accessed 23. 6. 2022)

Sažetak

Procjena maksimalne količine vode raspoložive za infiltraciju iz oborina, crpilište Velika Gorica

Zagrebački vodonosnik predstavlja jedan od glavnih izvora pitke vode za stanovnike Grada Zagreba i Zagrebačke županije. Pripada u strateške zalihe podzemnih voda zaštićenih od strane Republike Hrvatske. U prvoj zoni sanitarne zaštite na području crpilišta Velika Gorica, koje je jedno od glavnih crpilišta, iskopana je pedološka jama i uspostavljen je istraživački poligon. Dugoročni ciljevi istraživanja odnose se na modeliranje toka podzemne vode i transport kroz nesaturiranu zonu te kvantifikaciju efektivne infiltracije. U ovoj studiji, detaljno su evaluirane različite jednadžbe za procjenu evaporacije i evapotranspiracije kako bi se odredila maksimalna količina vode dostupna za infiltraciju u 2019 godini. Korištene su sljedeće jednadžbe: modificirana Penman-Monteith (CIMIS), Meyer, Turc, Hargreaves i Jensen-Haise. Zbog različitih ulaznih parametara, korištena je linearna regresija kako bi se testirala veza između najvažnijih parametara. Generalno, referentna evapotranspiracija procijenjena različitim jednadžbama pokazivala je razlike do ±30 %. Korelacijske i regresijske analize između evapotranspiracije, evaporacije, temperature i solarnog zračenja pokazale su statistički značajne pozitivne korelacije, a najveći korelacijski koeficijent i koeficijent determinacije dobiven je za solarno zračenje i referentnu evapotranspiraciju. Međutim, samo Meyerova i Turcova jednadžba su dale manje vrijednosti evaporacije i evapotranspiracije nego oborine. Jednadžbe korištene za izračun referentne evapotranspiracije dale su veće vrijednosti što je naposljetku rezultiralo nerealnim iznosima u količinama vode dostupne za infiltraciju. Turcova jednadžba na godišnjoj razini odabrana je kao najreprezentativnija jednadžba za istraživano područje, procijenjena maksimalna količina vode dostupna za infiltraciju u 2019 godini bila je oko 269 mm.

Ključne riječi: evaporacija; evapotranspiracija; infiltracija; crpilište Velika Gorica

Author's contribution

Ana Rečić (student in the graduate studies of Geological Engineering) participated in writing of original draft, data interpretation and presentation of the results. **Zoran Kovač** (PhD, Assistant Professor, hydrogeology, hydrogeochemistry) participated in conceptualization, writing of the original draft and data interpretation. **Bačani Laura** (PhD candidate – research assistant, hydrogeology) performed the field work (data collection and data interpretation) and visualization of the results. **Kristijan Posavec** (PhD, Full Professor, hydrogeology) participated in conceptualization, review, and editing. **Jelena Parlov** (PhD, Associate Professor, hydrogeology) participated in the interpretation and presentation of the results, as well as review and editing.

Improving the national monitoring of groundwater chemical status by applying the R$_u$ index

Borna-Ivan Balaž[1]; Krešimir Pavlić[2]; Zoran Nakić[3]; Jasna Kopić[4]

[1] University of Zagreb, Faculty of Mining, Geology and Petroleum Engineering, Pierottijeva 6, Zagreb, Croatia, ORCID: 0000-0002-2642-3576

[2] University of Zagreb, Faculty of Mining, Geology and Petroleum Engineering, Pierottijeva 6, Zagreb, Croatia, ORCID: 0000-0003-3315-2900

[3] University of Zagreb, Faculty of Mining, Geology and Petroleum Engineering, Pierottijeva 6, Zagreb, Croatia, ORCID: 0000-0001-6353-8500

[4] Vinkovci water supply and sewerage, Dragutina Žanića-Karle 47a, 32100 Vinkovci, Croatia

Abstract

Two complementary proposals were given to improve the national monitoring of groundwater chemical status in the grouped groundwater body "Eastern Slavonia - Sava River Basin". The aim of this research was to ensure an even distribution of monitoring stations in the study area and systematic monitoring of groundwater quality in deeper parts of the aquifer system. This is important as the national monitoring stations are used to assess the status of a grouped groundwater body according to the methodology in accordance with the provisions of the Water Framework Directive as well as the Groundwater Directive. Based on hydrogeological and geological characteristics of the investigated area, an objective assessment of the representativeness of the monitoring stations, using the R$_U$ index, was done. Representativity Index (R$_U$ index) is used to measure monitoring network homogeneity expressed in percentages. The first proposal of improvement of the national monitoring of groundwater chemical status includes 11 monitoring stations, with a R$_U$ index of 80.10%, two of which, as new observation wells, should be drilled at shallow depth of the aquifer system. Seven observation wells and two pumping wells around Gunja and Đakovo are part of the existing national monitoring system. The second proposal complements the first one and includes 17 monitoring stations, with a Ru index of 82.48%, six of which, as new observation wells, should be drilled at a greater depth of the aquifer system. These proposals would enable better confidence of groundwater chemical status and trend assessment, as well as more reliable determination of ambient background values of groundwater quality parameters. Implementing these proposals in practice and getting insight into new hydrogeochemical data from the deeper part of the aquifer system would give the possibility of delineating the grouped groundwater body "Eastern Slavonia – Sava River Basin" by depth into two new groundwater bodies, the shallower and deeper.

Keywords: groundwater monitoring, groundwater body, eastern Slavonia, alluvial aquifer system, R$_U$ index, chemical status

1. Introduction

Monitoring of groundwater chemical status ensures a comprehensive overview of the chemical status of groundwater in the river basin district and allows determining the presence of a significant and persistently growing pollution trend. National groundwater monitoring includes surveillance monitoring, used to assess the long-term chemical status of groundwater in groundwater bodies, and operational monitoring, used to determine the chemical status of groundwater and/or to assess the risk at of failure to achieve good chemical status of groundwater bodies. Since national monitoring stations are used for assessing the chemical status of groundwater bodies, it is important that each monitoring station representatively presents area where it is located. An objective assessment of homogeneity of a monitoring network on a grouped groundwater body is ensured by applying the Representativity Index (R$_U$ index) that should be 80% or higher (**Grath et al., 2001**).

In the investigated area of the grouped groundwater body "Eastern Slavonia - Sava River Basin" (**Figure 1**) the existing network of groundwater monitoring stations does not consider properly the representativeness of stations according to the conceptual hydrogeological model, R$_U$ index, hydrogeological characteristics, or vertical delineation (**Nakić et al., 2016**; **Nakić et al., 2018**).

Corresponding author: Borna-Ivan Balaž
borna-ivan.balaz@rgn.unzg.hr

In this paper, two proposals were given to improve the national monitoring of groundwater chemical status in the grouped groundwater body "Eastern Slavonia - Sava River Basin". The aim of this research was to ensure an even distribution of monitoring stations in the study area and systematic monitoring of groundwater quality in deeper parts of the aquifer system, based on geological and hydrogeological data, aquifer vulnerability and technical data from available observation and pumping wells.
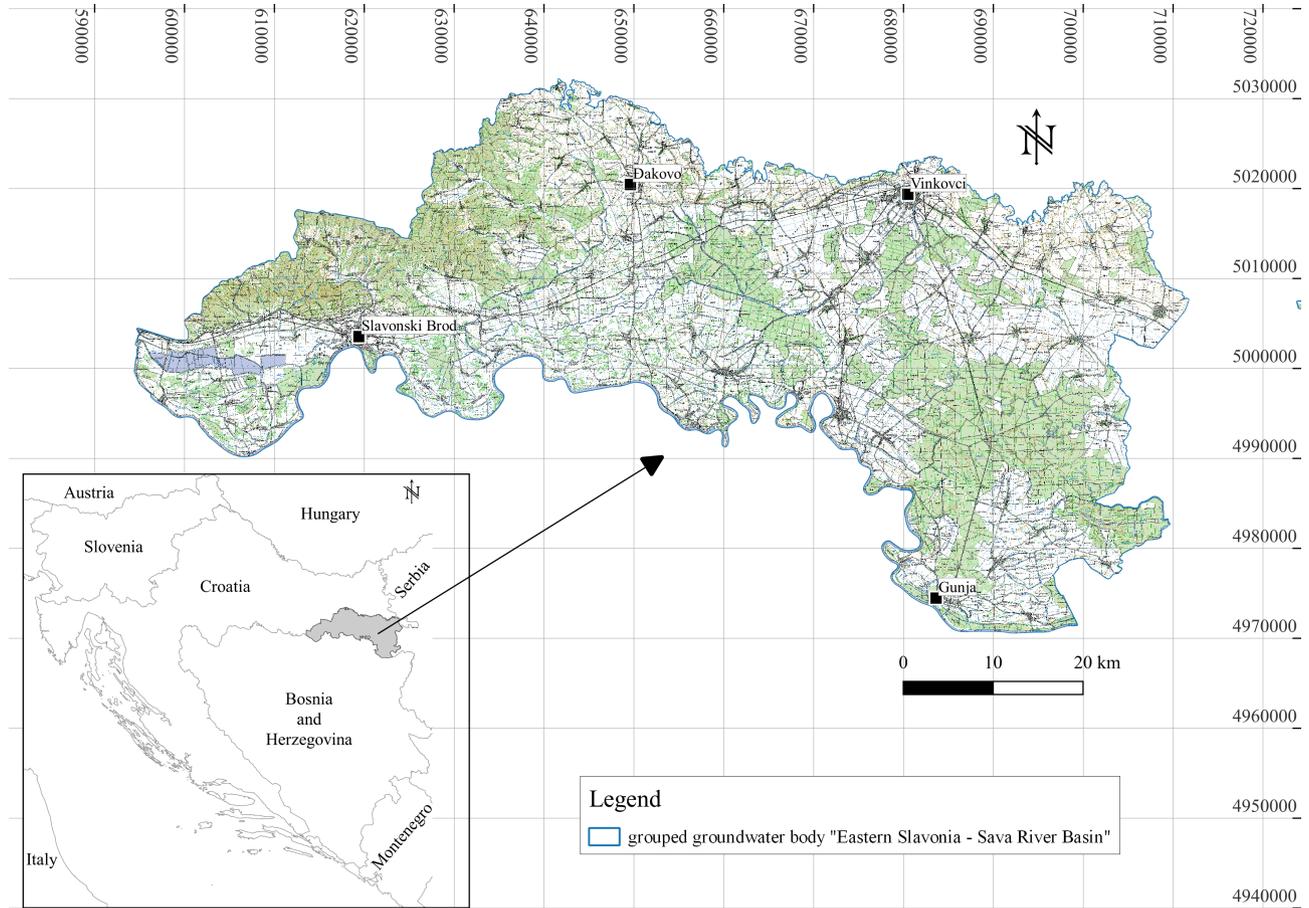
Figure 1: Grouped groundwater body "Eastern Slavonia - Sava River Basin"

2. Methods

As stated earlier, an appropriate and representative number of monitoring stations is the first prerequisite for objective assessment of groundwater chemical status. The first step for improving groundwater monitoring network is to collect the existing data in the investigated area. That includes all technical data from pumping and observation wells as well as all relevant geological and hydrogeological data (**Figure 2**). In addition, data on aquifer vulnerability was also used to locate new observation wells. Finally, the Representativity Index was used to make an objective assessment of existing and new monitoring networks representativity.

2.1. Collecting data

In 2021, the national monitoring of groundwater chemical status included 18 stations with a R_U index of 62.07%. For these stations, technical data were collected from "Đakovo water supply", "Vinkovci water supply and sewerage" and "Croatian Waters". A review of collected data found that for eight observation wells there is data on the depth and positions of the filter, for two wells there is data on depth and for one well there is data only on filter positions and well depth respectively. For other five wells, no data on the position and depth of the filter were available. In addition, data on filter positions were collected for another 19 pumping and observation wells in the investigated area.

Hydrogeological and geological data were collected from the literature review and include the following: lithological units in the investigated area (**Velić & Vlahović, 2009**); thickness of the Quaternary aquifer complex (**Hernitz, 1983**); total aquifer thickness (**Bačani, 1997; Miletić et al., 1975a; Miletić et al., 1975b; Nakić & Mayer, 2003**); aquifer productivity (**Brkić et al., 2009**) and aquifer vulnerability (**Brkić et al., 2009; Nakić et al., 2016**).
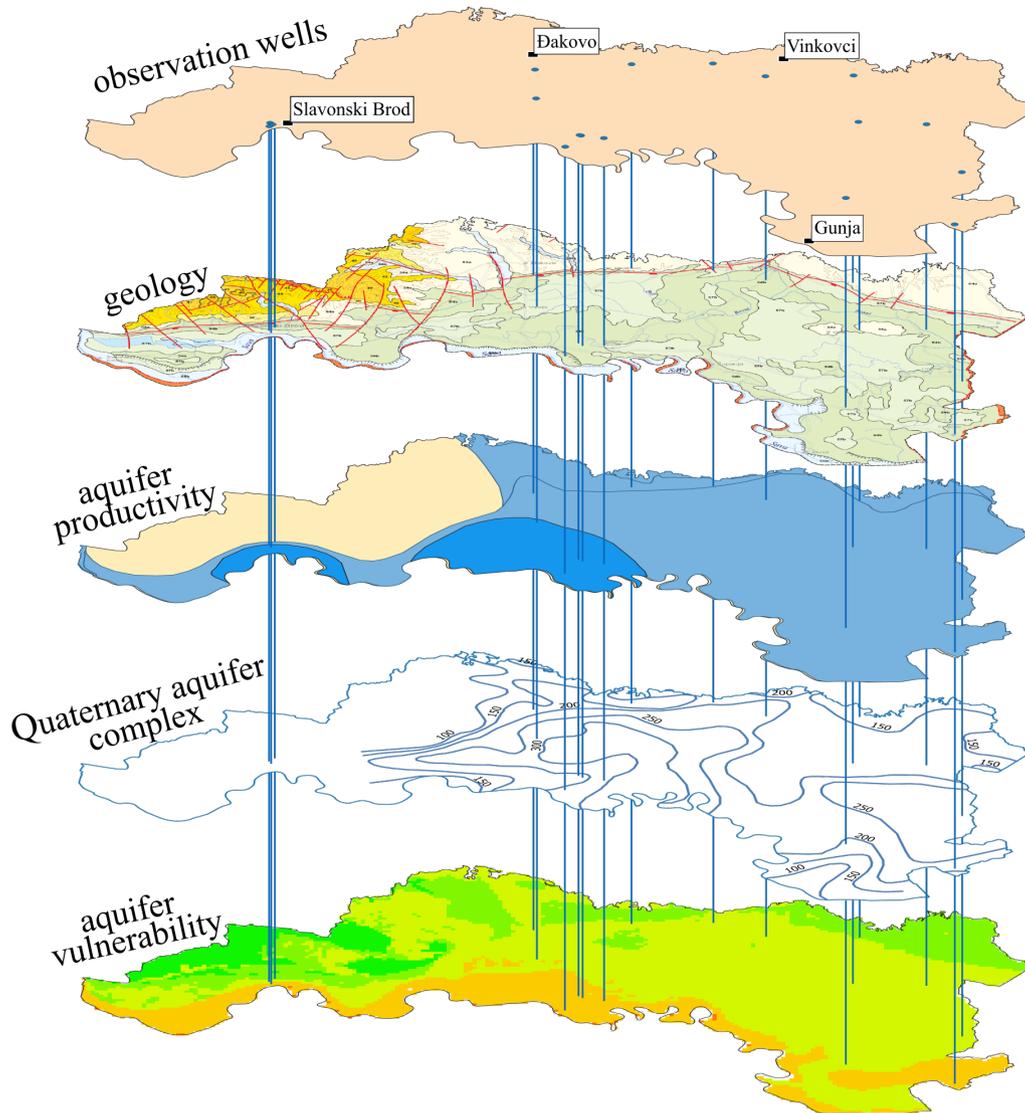
Figure 2: Data used to improve groundwater chemical status monitoring network in investigated area

2.2. R_U index

To assess the homogeneity of monitoring stations in the grouped groundwater body "Eastern Slavonia - Sava River Basin", the R_U index was used. It is defined as the average minimum distance between any location in the area to the closest sampling site and expressed as percentage of the average minimum distance for an optimal network (**Grath et al., 2001**). It is calculated according to the **Equation 1** (**Grath et al., 2001**).

$$R_U = \frac{37,7}{dist_{ave}\sqrt{\dfrac{k}{Area}}} \ [\%]$$

[1]

Where are:
k – number of sites,
dist$_{ave}$ – average minimum distance between any location in the area to the closest sampling site,
Area – size of the area.

The term "optimal network" is represented as a theoretical network with an optimal triangular pattern of sites for which R$_U$ index will be 100**% (Grath et al., 2001)**. In real conditions, as previously mentioned, the Representativity Index needs to be 80% or higher for the network of monitoring stations to be considered homogeneous (**Grath et al., 2001**).

3. Results and discussion

The first proposal to improve network of groundwater monitoring stations includes 11 stations, and the R$_U$ index is 80.10%. Out of a total of 11 stations, seven of them are part of the existing national monitoring system, which would certainly contribute to cost rationalization if this proposal was implemented. These are the stations marked in green in **Figure 3**. Two stations include the existing water wells for public water supply in Gunja and Đakovo (marked in purple in **Figure 3**), which should be included in the monitoring program to increase better spatial coverage and R$_U$ index. Within this proposal, two new stations should be established, i.e., new observation wells would have to be drilled. One station would be in the zone of the productive aquifer (third map from the top on **Figure 2**) in the far west, and the other in the centre of the eastern part of the investigated area (marked in blue in **Figure 3**). Productive and non-productive aquifers can be distinguished in the observed area, whereby productive aquifers are divided into primary and secondary aquifers. Primary aquifers have high hydraulic properties, while secondary aquifers have lower hydraulic properties with spring yields less than 20 l/s. In the area of unproductive aquifers, the yields of the springs are less than 5 l/s. Existing stations (observation wells and pumping wells) would cover most of the grouped groundwater body and productive aquifer distribution areas, while new wells were proposed due to the lack of monitoring stations in parts of investigated area. Both new proposed stations contribute to the even distribution of points and increase the R$_U$ index and should contribute to get a new hydrogeological data of the aquifer system. No detailed hydrogeological data were available in the western part of the investigated area. In the eastern part of the observed area, the thickness of the Quaternary aquifer complex is between 150 and 200 m and more detailed hydrogeological data were used for more precise site selection (**Bačani, 1997**).

The first proposal and consequently the second proposal include observation and pumping wells in their monitoring networks. Both types of monitoring stations are included to rationalize the costs of eventual implementation of the proposal since the collected data can be compared. This refers to the results of chemical analysis of groundwater for the purposes of national monitoring, which are used in the overall assessment of the chemical status of a grouped groundwater body. Since the primary purpose is to comply with the guidelines for assessing the status of grouped groundwater bodies in accordance with EU legislation, the only requirement for valid chemical analysis is that the sampled groundwater is not pre-conditioned. For this reason, it is possible to use pumping wells in the monitoring system.
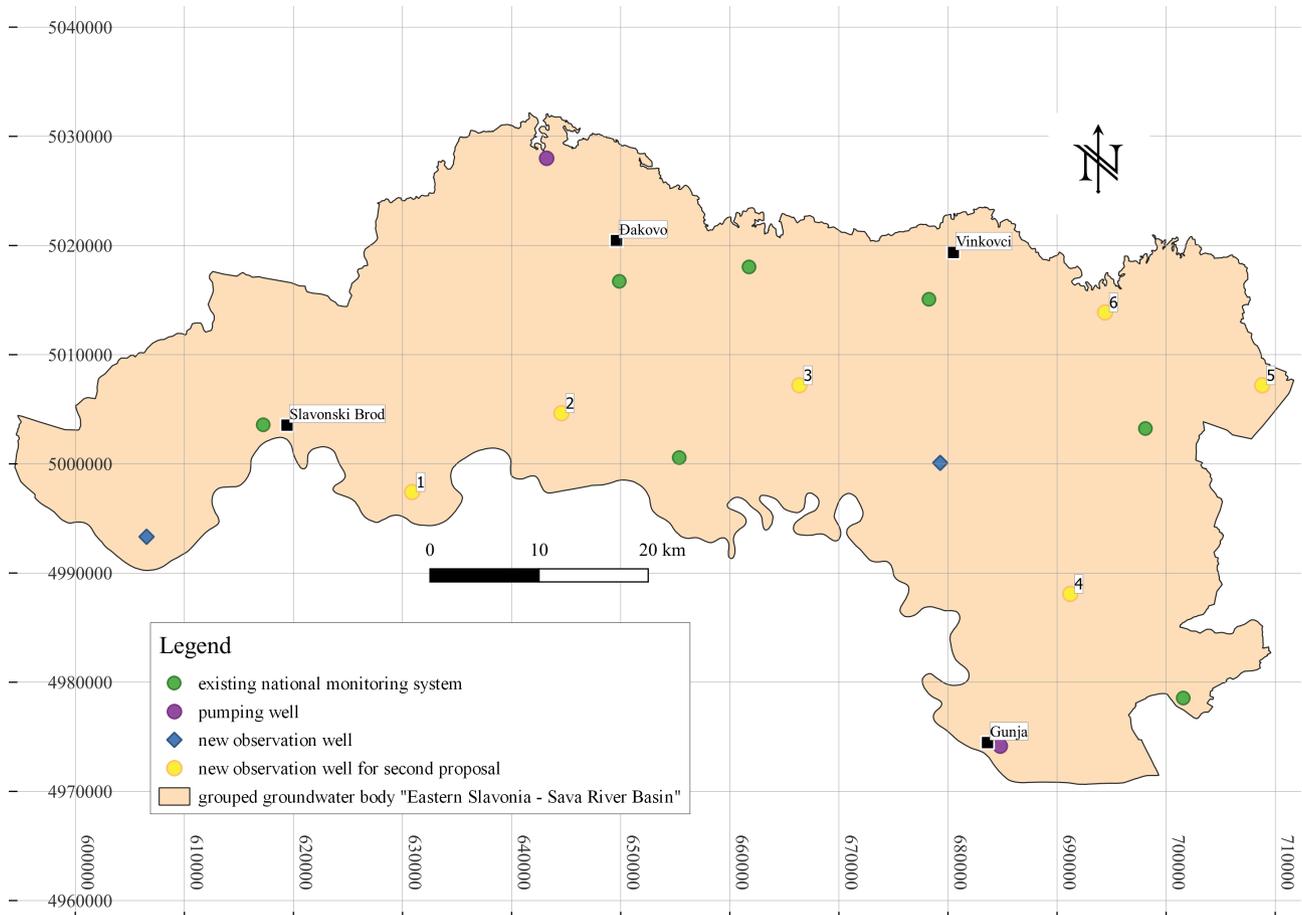
Figure 3: The proposal of improvement of the national groundwater monitoring network

The second proposal complements the first proposal and includes in total 17 stations, with an R_U index of 82.48%. In this proposal, six new observation wells are proposed (marked in yellow in **Figure 3** with marks 1 to 6), which would need to be drilled to a depth greater than 100 m. The new wells should reach deeper sandy aquifers, which probably differ from the shallower gravelly and coarse-grained sandy layers in terms of lithological composition and groundwater chemical composition. The layout of the wells follows zones of moderate and increased vulnerability of aquifers. At the location of wells 1, 5 and 6, the bottom of the Quaternary aquifer complex lies at a depth of 150 m; at the location of well 2 it lies at a depth of 250 m; at the location of well 3 it lies at a depth over 300 m, and at the location of well 4 it lies at depths between 200 and 250 m. The total thickness of aquifers at locations of well 2 and 3 is between 70 and 100 m; at location of well 4 its thickness is from 50 to 75 m, while at locations of wells 5 and 6 aquifers its thickness is less than 50 m (**Bačani, 1997; Hernitz, 1983**). Therefore, in addition to the R_U index, lithology, thickness of the Quaternary aquifer complex, total aquifer thickness, aquifer productivity and aquifer vulnerability were used for the preparation of the monitoring proposal. The results of chemical analysis of groundwater are also available for stations from the existing national monitoring system. However, these data were not used since the wells were located in a shallower part of the aquifer system that has already been well explored and described in the literature. Any data from chemical analysis from the proposed wells that cover a deeper part of the aquifer system could be used in the future to further improve the monitoring system in this area.

Such a spatial arrangement of groundwater monitoring stations would enable comprehensive chemical monitoring of groundwater laterally as well as vertically in the grouped body of groundwater "Eastern Slavonia - Sava River Basin". After drilling new observation wells and the establishment of improved groundwater monitoring network, a new chemical and hydrogeological data would be gathered, based on which conclusions could be made about the hydrogeochemical characteristics of deeper aquifers. In addition, it would be possible to assess the suitability of delineating the grouped groundwater body "Eastern Slavonia – Sava River Basin" by depth into two new groundwater bodies, the shallower and deeper.

4. Conclusions

This paper analyses the representativity of the national groundwater monitoring network in the grouped groundwater body "Eastern Slavonia - Sava River Basin". The new proposal is done using hydrogeological and geological data of the investigated area: the thickness of the Quaternary aquifer complex, total thickness of aquifers, aquifer productivity, aquifer vulnerability, technical data on drilled wells and R_U index.

Two monitoring proposals have been made for this purpose; the first one, which ensures the coverage of the area of the grouped body more evenly, and the second proposal that complements the first proposal, enabling more comprehensive monitoring of deeper aquifers.

These two proposals would enable an adequate assessment of groundwater quality in this grouped body with high reliability according to the methodology for assessing the condition of grouped groundwater bodies **(Croatian Waters, 2016)**, a relevant chemical trend assessment as well as a more precise determination of ambient background values of groundwater parameters in the investigated area. The implementation of the first proposal would increase the representativeness of the monitoring network, and at the same time rationalizing investment costs. The implementation of the second proposal would enable the assessment of the possibility of delineation of the grouped groundwater body "Eastern Slavonia - Sava River Basin" in depth into two new groundwater bodies, shallower and deeper.

5. References

Bačani, A. (1997): Characteristics of hydraulic boundaries of aquifers at the watershed of the Sava and Drava basins in eastern Slavonia (Značajke hidrauličkih granica vodonosnih slojeva na vododjelnici Savskog i Dravskog porječja u istočnoj Slavoniji). Doctoral dissertation, Faculty of Mining, Geology and Petroleum Engineering, University of Zagreb. (*in Croatian without abstract in English*)

Brkić Ž., Larva O. and Marković T. (2009): Assessment of the status and risk of groundwater bodies in the Pannonian part of the Republic of Croatia (Ocjena stanja i rizika cjelina podzemnih voda u panonskom dijelu Republike Hrvatske). Study, Croatian Geological Survey, Zagreb. (*in Croatian without abstract in English*)

Croatian Waters (2016): River Basin Management Plan (RBMP) 2016 – 2021 (Plan upravljanja vodnim područjima 2016 – 2021).

Grath, J., Scheidleder, A., Uhlig, S., Weber, K., Kralik, M., Keimel, T. and Gruber, D. (2001): The EU Water Framework Directive: Statistical aspects of the identification of groundwater pollution trends, and aggregation of monitoring results. Final Report.

Hernitz, Z. (1983): Deep structural tectonic relations in the area of Eastern Slavonia (Dubinski strukturno-tekstonski odnosi u području istočne Slavonije). Doctoral dissertation. Jugoslavenski komitet svjetskog kongresa za naftu, „Nafta", 1–221, Zagreb. (*in Croatian without abstract in English*)

Miletić, P., Nowinski, A. and Urumović, K. (1975a): About the second hydrogeological zone of northern Croatia (O drugoj hidrogeološkoj zoni sjeverne Hrvatske). Proceedings: "Zbornik radova RGN fakulteta III. 97-100, Zagreb". (*in Croatian without abstract in English*)

Miletić, P., Urumović, K., Blašković, V. (1975b): Regional hydrogeological research and hydrogeological zoning of northern Croatia (Regionalna hidrogeološka istraživanja i hidrogeološka rajonizacija sjeverne Hrvatske). Proceedings: "Zbornik radova RGN fakulteta III. 93-95, Zagreb". (*in Croatian without abstract in English*)

Nakić, Z. and Mayer, D. (2003): Study of the first phase of research with the proposal of protection zones of the Vrpolje well field area (Elaborat prve faze istraživanja s prijedlogom zaštitnih zona crpilišta Vrpolje). Technical report, Faculty of Mining, Geology and Petroleum Engineering, University of Zagreb. (*in Croatian without abstract in English*)

Nakić, Z., Bačani, A., Parlov, J., Duić, Ž., Perković, D., Kovač, Z., Tumara, D., Mijatović, I., Špoljarić, D., Ugrina, I., Stanek, D. and Slavinić, P. (2016): Defining trends and groundwater status assessment in the Pannonian part of Croatia (Definiranje trendova i ocjena stanja podzemnih voda na području panonskog dijela Hrvatske). Study, Faculty of Mining, Geology and Petroleum Engineering, University of Zagreb. (*in Croatian without abstract in English*)

Nakić, Z., Parlov, J., Perković, D., Kovač, Z., Buškulić, P., Špoljarić, D., Ugrina, I., and Stanek, D. (2018): Defining criteria for determining background concentrations and limit values of pollutants in groundwater bodies in the Pannonian part of Croatia (Definiranje kriterija za određivanje pozadinskih koncentracija i graničnih vrijednosti onečišćujućih tvari u tijelima podzemne vode u panonskom dijelu Hrvatske). Study, Faculty of Mining, Geology and Petroleum Engineering, University of Zagreb. (*in Croatian without abstract in English*)

Velić, I. and Vlahović, I. (2009): Interpreter of the geological map of the Republic of Croatia at the scale 1:300.000. – Croatian Geological Survey, Zagreb, 147 p. (*in Croatian without abstract in English*)

Sažetak

Unapređenje nacionalnog monitoringa kemijskog stanja podzemnih voda primjenom R$_U$ indeksa

U ovome radu prikazani su prijedlozi za poboljšanje nacionalnog monitoringa kemijskog stanja podzemnih voda na grupiranom tijelu podzemne vode "Istočna Slavonija - sliv Save". Cilj ovog istraživanja bio je osigurati ravnomjernu distribuciju monitoring postaja na istraživanom području i omogućiti sustavno praćenje kakvoće podzemnih voda u dubljim dijelovima vodonosnika. Na temelju hidrogeoloških i geoloških karakteristika istraživanog područja izvršena je objektivna procjena reprezentativnosti monitoring postaja, korištenjem RU indeksa. Prvi prijedlog poboljšanja uključuje 11 monitoring postaja, s Ru indeksom od 80,10%, od kojih bi dvije nove bušotine trebale biti izvedene u plićem dijelu vodonosnog sustava. Sedam pijezometara i dva izvorišta u Gunji i Đakovu dio su postojeće infrastrukture za praćenje kemijskog stanja podzemne vode. Drugi prijedlog nadopunjuje prvi i uključuje 17 monitoring postaja, s Ru indeksom od 82,48%, od kojih bi šest novih bušotina trebalo izvesti u dubljem dijelu vodonosnog sustava. Ovi prijedlozi omogućili bi veću pouzdanost prilikom ocjene kemijskog stanja podzemnih voda i relevantniju procjenu trenda, kao i pouzdanije određivanje pozadinskih vrijednosti parametara kakvoće podzemnih voda. Provedba ovih prijedloga u praksi i stjecanje uvida u nove hidrogeokemijske podatke iz dubljeg dijela vodonosnog sustava potencijalno bi omogućili delineaciju grupiranog tijela podzemne vode „Istočna Slavonija – sliv Save" po dubini na dva nova tijela podzemne vode, pliće i dublje.

Ključne riječi: monitoring podzemnih voda, tijelo podzemne vode, istočna Slavonija, aluvijalni vodonosni sustav, R$_U$ indeks, kemijsko stanje

Author's contribution

Borna-Ivan Balaž (mag. ing. geol., univ. spec. oecoing., environmental geology) provided the interpretation and presentation of the results. **Krešimir Pavlić** (PhD, Assistant Professor, geophysics, hydrology) provided the interpretation and analysis of the results. **Zoran Nakić** (PhD, Full Professor, hydrogeology) provided the presentation of the results and overview of the research area. **Jasna Kopić** (PhD, hydrogeology) provided the interpretation of results and technical data of wells on the observed area.

Numerical analysis of the Middle Miocene *Panopea* bivalves (geoducks) from the southwestern margin of the Central Paratethys, Croatia

Marija Bošnjak[1]; Jasenka Sremac[2]; Dijana Bigunac[3]; Davor Vrsaljko[1]

[1] Croatian Natural History Museum, Demetrova 1, 10000 Zagreb, Croatia, http://orcid.org/0000-0002-1851-1031; http://orcid.org/0000-0002-6829-7774

[2] Faculty of Science, Department of Geology, University of Zagreb, Horvatovac 102a, 10000 Zagreb, Croatia; http://orcid.org/0000-0002-4736-7497

[3] INA - Industrija nafte d.d., Avenija Većeslava Holjevca 10, 10020 Zagreb, Croatia; Dijana.Bigunac@ina.hr

Abstract

Here presented numerical analysis shows a variety of shell morphologies of the genus *Panopea*, based on the geoduck samples from the Middle Miocene (Badenian) deposits of Northern Croatia (southwestern margin of the Central Paratethys), previously considered as different species/subspecies. Specimens were measured, analyzed using PAST software, and data were compared with the available measurements from earlier studies. Results showed morphological variability of the geoducks shell shape from all localities, with Lower Badenian geoducks showing the lower median shell values than the Upper Badenian geoducks. Consistency with the comparative material is also concluded. Despite the shape varieties, which are also present in the modern geoducks, they are all considered as ecotypes of the morphologically variable species *Panopea* (*Panopea*) *menardi* (Deshayes, 1828). Middle Miocene climate shifts were probably the main cause of the shell size variability.

Keywords: numerical analysis; *Panopea*; Middle Miocene; Central Paratethys; Croatia

1. Introduction

Fossil bivalves from the genus *Panopea* Ménard de la Groye, 1807 have been recorded in Northern Croatia in the Middle Miocene – Badenian (Langhian) deposits. Species *Panopea* (*Panopea*) *menardi* (Deshayes, 1828) was described from Medvednica Mt. (Gornje Vrapče and Gornji Stenjevec localities) in **Kochansky (1944)**, **Budak (1974)**, **Butković (1979)**, **Vrsaljko et al. (2006)**, **Šoić (2011)** and **Fio et al. (2014)**, Pokupsko area in **Bigunac (1990)** and **Dželalija (2007)**, and Zrinska Gora Mt. in **Pikija (1987a,b)**. Several findings from Medvednica Mt. have been described as *Panopea* sp. considering slightly different shell morphology of the panopean casts and molds (**Šoić, 2011**; **Fio et al., 2014**).

Genus *Panopea* has medium-sized to large, elongated and thick shells, rounded anterior region and truncate posterior region that is widely gaping; subcentral beaks; a weak hinge plate, equal in both valves; a deeply impressed pallial line and a triangular pallial sinus (**Moore, 1969**; **Bosio et al., 2021**). The shape and depth of the pallial sinus vary among species (**Leyva-Valencia et al., 2015** after Yonge, 1971). Genus *Panopea* is recorded since the Cretaceous (maybe even Triassic) to recent (**Moore, 1969**).

Today clams of the genus *Panopea*, known as geoducks, represent one of the largest burrowing bivalves in the world, which can be found in the Pacific Ocean, the Mediterranean Sea, Australia and New Zealand, and in the Atlantic Ocean where one species is endemic to its southwestern part (**Leyva-Valencia et al., 2012 and references therein**; **Aragón-Noriega et al., 2015 and references therein**). Modern representatives of *Panopea* species live in sandy and muddy substrate, and are found from the intertidal zone to depths greater than 110 m, with most live individuals recorded from above 60 m. They live buried in the sediment up to a depth of 1 m, with large incurrent and excurrent siphons extending upward with the tip above the sea bed (**Bureau et al., 2002**; **Thomsen et al., 2009**; **Wood et al., 2018**; **Bosio et al., 2021**). Species of the genus *Panopea* can reach shell length over 200 mm (e.g., **Aragón-Noriega et al., 2019 and references therein**). Within five years they reach their mean size, and rapid growth is present during the

Corresponding author: Marija Bošnjak
marija.bosnjak@hpm.hr

first ten years and slower in the later years (e.g., **Thomsen et al., 2009**; **Zaidman & Morsan, 2015**). Recent geoducks are long-living bivalves, with life span up to 168 years (**Bureau et al., 2002**).

This paper presents numerical analysis of the panopean casts and molds shape morphology. Analyzed panopeans were found in the Upper Badenian deposits of the Medvednica Mt. (Gornje Vrapče and Gornji Stenjevec localities; e.g., **Kochansky, 1944**; **Šikić et al., 1977, 1979**; **Vrsaljko et al., 2006**; **Pezelj et al., 2016** and references therein) and determined as *Panopea* (*Panopea*) *menardi* (Deshayes, 1828) species, and in the Lower Badenian deposits of Pokupsko area which were determined as *Panope menardi rudolphii* Eichwald, 1934 subspecies after **Bigunac (1990)** (**Figures 1 and 2**). Results of the numerical analysis were compared with the measurements of **Šoić (2011)**, who described *in situ* panopean findings from the Upper Badenian deposits from Gornje Vrapče locality, Medvednica Mt. (**Figure 1**). Goal of this research was to check whether two panopean species can be distinguished based on the numerical analysis of the shell shape morphology, or the differences in the shell shape are the consequence of the morphological variability within a single geoduck species.
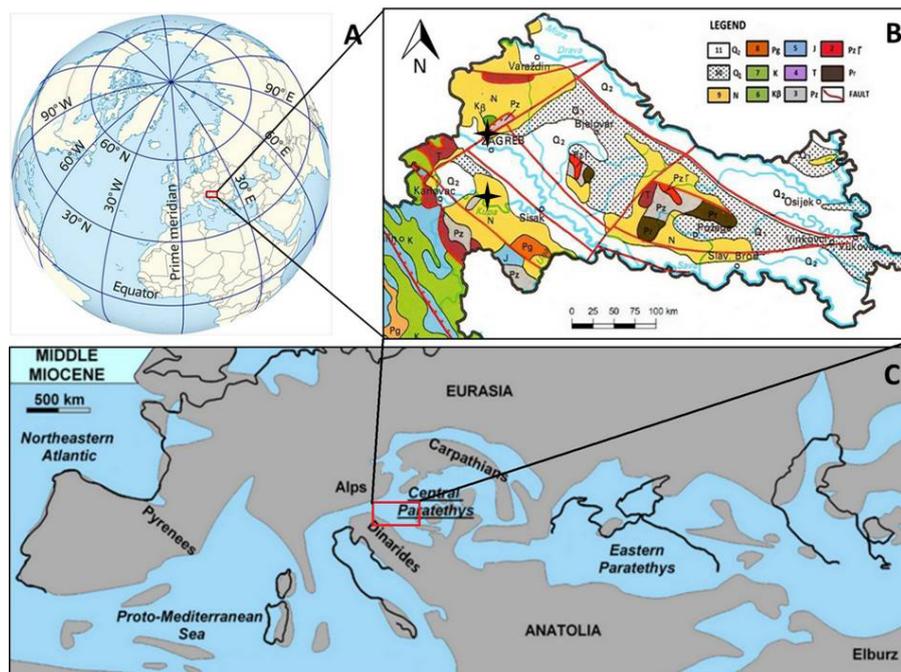
Figure 1: Geographical and paleogeographical location of the Badenian localities in Northern Croatia: (**A**) Geographic position of Croatia marked by red rectangle (modified after https://www.sailingissues.com/navcourse1.html). (**B**) Geographical location of the Badenian localities (**from Sremac et al., 2022, map after Velić & Velić, 1995**) where the panopean findings analyzed in this paper have been recorded (Medvednica Mt. near Zagreb, with Gornje Vrapče and Gornji Stenjevec localities, and Pokupsko area near the River Kupa). Four-Point stars in Figure B mark Medvednica Mt. near Zagreb (Gornje Vrapče and Gornji Stenjevec localities) and Pokupsko area localities; (**C**)Paleogeographical location of the Badenian localities in Northern Croatia (modified after **Harzhauser & Landau, 2019 and Sremac et al., 2022 and references therein**). Red rectangle in Figure C marks the area of North Croatian Basin in the Central Paratethys during Badenian. Legend (after **Sremac et al., 2022 and references therein**): 1. Precambrian metamorphic rocks; 2. Paleozoic granites; 3. Paleozoic sedimentary rocks; 4. Triassic carbonates, sporadically clastites; 5. Jurassic carbonates with scarce volcanoclastites; 6. Cretaceous dominantly carbonate rocks; 7. Cretaceous basalts; 8. Paleogene limestones; 9. Neogene clastic and carbonate rocks; 10. Pleistocene, dominantly unconsolidated clastites; 11. Holocene unconsolidated clastites.

Figure 2: Part of the analyzed *Panopea* (*Panopea*) *menardi* specimens. Scale bar: 10 mm.

2. Material and methods

In total 24 fossil panopeans were included in this numerical analysis. Specimens are preserved as casts and molds, and collected at three Badenian sites in Croatia; two Upper Badenian sites are located in the southwestern part of the Medvednica Mt. (Gornji Stenjevec and Gornje Vrapče localities, e.g., **Kochansky, 1944**; **Šikić et al., 1977, 1979**; **Vrsaljko et al., 2006**; **Pezelj et al., 2016** and references therein), and the third site of the Lower Badenian age (after **Bigunac, 1990**) is in the Pokupsko area (**Figure 1**). From the Medvednica Mt. (**Figure 1**) 12 specimens were measured; 6 of them are part of the Academician Vanda Kochansky-Devidé collection, housed at the Croatian Natural History Museum (CNHM) in Zagreb, and other 6 specimens were collected by Professor Jasenka Sremac and donated to the CNHM. Specimens from the V. Kochansky-Devidé collection (specimens VKD 1 – VKD 6) were determined as *Glycymeris menardii* Deshayes in **Kochansky (1944)**, today classified as *Panopea* (*Panopea*) *menardi* (Deshayes, 1828) (e.g., **Studencka, 1986 and references therein**; **fossilworks.org**). Specimens collected by Professor J. Sremac (specimens JS 1 – JS 6) are determined as *Panopea* (*Panopea*) *menardi* (Deshayes, 1828). From the Pokupsko area (**Figure 1**) 12 specimens collected by Dijana Bigunac (specimens DB 1 – DB 12) were measured. These geoducks were determined as *Panopea menardi rudolphii* Eichwald, 1934 and described in D. Bigunac Master Thesis (**Bigunac, 1990**). On these 24 specimens length, height and width of the *Panopea* casts and molds was measured as shown in **Figure 3**. Data on the analyzed *Panopea* specimens are presented in **Table 1**. Part of the specimens show more elongated shape comparing to the other specimens in the sample (e.g., see **Figure 2**, specimen DB 4, and **Šoić, 2011**), and the elongate specimens were initially classified as well as *Panopea* sp.? (see **Table 1, Figure 2**). Three specimens (VKD 2, VKD 6 and DB 12) were discarded from the analysis because they represent fragmented *Panopea* molds.

In order to fulfill the numerical analysis, the directly obtained measurements from this study (**Table 1**) were compared with those from the Gornje Vrapče locality (SW Medvednica Mt.) which are described and measured in **Šoić (2011)** as a part of his Master Thesis, and later in **Fio et al. (2014)**. Comparative material is shown in **Table 2**. As described in **Šoić (2011)**, the author also noticed differences in *Panopea* shape and marked those specimens as *Panopea* sp.

Numerical analysis of the here presented *Panopea* shells is done in the PAST software (**Hammer et al., 2001**) using the XY graphs, boxplots and cluster analysis, showing the values and the relations between the measured shell elements, as well as the morphological variability of the *Panopea* (*Panopea*) *menardi* species.
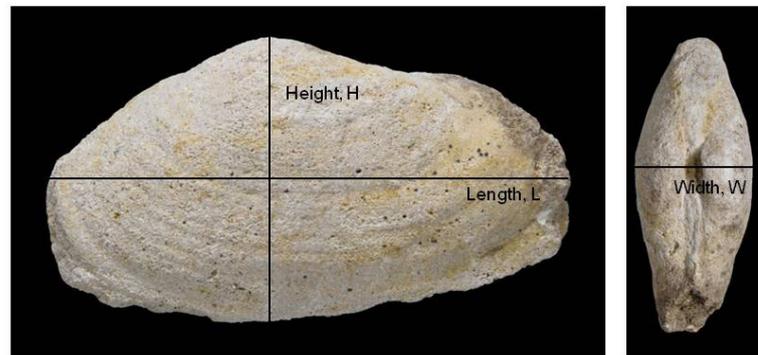
Figure 3: Measured elements of the *Panopea* shell: length (L), height (H) and width (W)

SPECIMEN	Name	Length, L (mm)	Height, H (mm)	Width, W (mm)	Locality
VKD 1	*Panope*a (*Panoepa*) *menardi* (Deshayes, 1828)	74.1	39.47	28.57	Gornji Stenjevec, Medvednica Mt.
VKD 2*	*Panope*a (*Panoepa*) *menardi* (Deshayes, 1828)	45	44.82	15.71	Gornji Stenjevec, Medvednica Mt.
VKD 3**	*Panope*a (*Panoepa*) *menardi* (Deshayes, 1828)	138.46	67.25	32.25	Gornji Stenjevec, Medvednica Mt.
VKD 4	*Panope*a (*Panoepa*) *menardi* (Deshayes, 1828)	130.57	76.58	45.59	Gornji Stenjevec, Medvednica Mt.
VKD 5	*Panope*a (*Panoepa*) *menardi* (Deshayes, 1828)	95.33	65.97	49.82	Gornji Stenjevec, Medvednica Mt.
VKD 6*	*Panope*a (*Panoepa*) *menardi* (Deshayes, 1828)	60.84	60.46	45.85	Gornje Vrapče, Medvednica Mt.
JS 1	*Panope*a (*Panoepa*) *menardi* (Deshayes, 1828)	122.36	72.82	52.25	Gornje Vrapče, Medvednica Mt.
JS 2**	*Panope*a (*Panoepa*) *menardi* (Deshayes, 1828)	130	73.77	52.94	Gornje Vrapče, Medvednica Mt.
JS 3	*Panope*a (*Panoepa*) *menardi* (Deshayes, 1828)	122.08	71.21	49.64	Gornje Vrapče, Medvednica Mt.
JS 4	*Panope*a (*Panoepa*) *menardi* (Deshayes, 1828)	124.83	65.13	44.69	Gornje Vrapče, Medvednica Mt.
JS 5	*Panope*a (*Panoepa*) *menardi* (Deshayes, 1828)	114.95	72.83	51.26	Gornje Vrapče, Medvednica Mt.
JS 6**	*Panope*a (*Panoepa*) *menardi* (Deshayes, 1828)	108.59	64.61	47.44	Gornje Vrapče, Medvednica Mt.
DB 1	*Panope menardi rudolphii* Eichwald, 1934	125.23	79.06	57.08	Pokupsko area
DB 2	*Panope menardi rudolphii* Eichwald, 1934	105.31	67.51	51.08	Pokupsko area
DB 3**	*Panope menardi rudolphii* Eichwald, 1934	141.1	64.16	44.33	Pokupsko area
DB 4**	*Panope menardi rudolphii* Eichwald, 1934	147.76	75.45	59.95	Pokupsko area
DB 5	*Panope menardi rudolphii* Eichwald, 1934	149.29	76.64	48.97	Pokupsko area
DB 6	*Panope menardi rudolphii* Eichwald, 1934	103.76	57.94	38.35	Pokupsko area
DB 7	*Panope menardi rudolphii* Eichwald, 1934	85.62	58.09	40.37	Pokupsko area
DB 8	*Panope menardi rudolphii* Eichwald, 1934	90.72	60.48	38.43	Pokupsko area
DB 9	*Panope menardi rudolphii* Eichwald, 1934	83.67	56.41	30.71	Pokupsko area
DB 10	*Panope menardi rudolphii* Eichwald, 1934	86.77	55.86	35.79	Pokupsko area
DB 11	*Panope menardi rudolphii* Eichwald, 1934	93.59	52.81	33.02	Pokupsko area
DB 12*	*Panope menardi rudolphii* Eichwald, 1934	58.32	40.43	22.76	Pokupsko area

Table 1: Determinations and measurements of the analyzed *Panopea* (*Panopea*) *menardi* specimens. Localities shown in **Figure 1**. Legend: VKD 1 – VKD 6: specimens from the Academician Vanda Kochansky-Devidé collection (**Kochansky, 1944**); JS 1 – JS 6: specimens collected by Professor Jasenka Sremac; DB 1 – DB 12 specimens from D. Bigunac Master Thesis (**Bigunac, 1990**). All specimens are today housed at the CNHM. * marks fragmented specimens which are excluded from the numerical anaylsis. ** marks *Panopea* (*P.*) *menardi* specimens which are also observed as *Panopea* sp. ?

SPECIMEN	Name	Length, L (mm)	Height, H (mm)	Locality
V-1	*Panopea menardi* Deshayes, 1828	112	72	Gornje Vrapče, Medvednica Mt.
V-2	*Panopea menardi* Deshayes, 1828	122	75	Gornje Vrapče, Medvednica Mt.
V-3	*Panopea menardi* Deshayes, 1828	104	74	Gornje Vrapče, Medvednica Mt.
V-4	*Panopea menardi* Deshayes, 1828	112	60	Gornje Vrapče, Medvednica Mt.
V-5	*Panopea menardi* Deshayes, 1828	123	70	Gornje Vrapče, Medvednica Mt.
V-7	*Panopea menardi* Deshayes, 1828	110	74	Gornje Vrapče, Medvednica Mt.
V-6	*Panopea* sp. A	80	65	Gornje Vrapče, Medvednica Mt.
V-8	*Panopea* sp. B	110	57	Gornje Vrapče, Medvednica Mt.
V-9	*Panopea* sp. B	129	71	Gornje Vrapče, Medvednica Mt.

Table 2. Comparative *Panopea* specimens after **Šoić (2011)** and **Fio et al. (2014)**. Locality is shown in **Figure 1.**

Abbreviations used in text (in alphabetical order):
CNHM: Croatian Natural History Museum
DB 1 – DB 12: specimens from D. Bigunac Master Thesis (Bigunac, 1990)
H: shell height
JS 1 – JS 6: specimens collected by J. Sremac
L: shell length
V-1 – V-9: comparative specimens from N. Šoić (2011)
VKD 1 - VKD 6: specimens collected by Academician V. Kochansky-Devidé
W: shell width

3. Results

In order to analyze morphological variability of the panopean shells (**Figure 3**), the measured elements (length and height, after **Figure 3** and **Table 1**) were plotted in XY graph and compared with the measurements of *Panopea* shells from Medvednica Mt. (Gornje Vrapče locality) by **Šoić (2011) (Table 2)**, as shown in **Figure 4**.

Plotted shell measurements show dispersity of data (**Figure 4**), although two possible trends could be recognized (**Figure 4A**). Specimens from the Upper Badenian Gornje Vrapče locality on Medvednica Mt. are showing the best correlation, and geoducks from the Lower Badenian deposits of Pokupsko area are the most dispersed (**Figures 1 and 4**). As seen in **Figure 4**, Lower Badenian geoducks show smaller values of shell dimensions, than the Upper Badenian specimens from Medvednica Mt. (**Figure 4B, C** and **D**). The assumed *Panopea* sp. specimens are grouping well with the *Panopea* (*P.*) *menardi* specimens. As seen in **Figure 4**, this species shows the lowest and the highest values of shell length and height (from both, Medvednica Mt. and Pokupsko area), while the assumed *Panopea* sp. specimens fit between those minimum and maximum values.
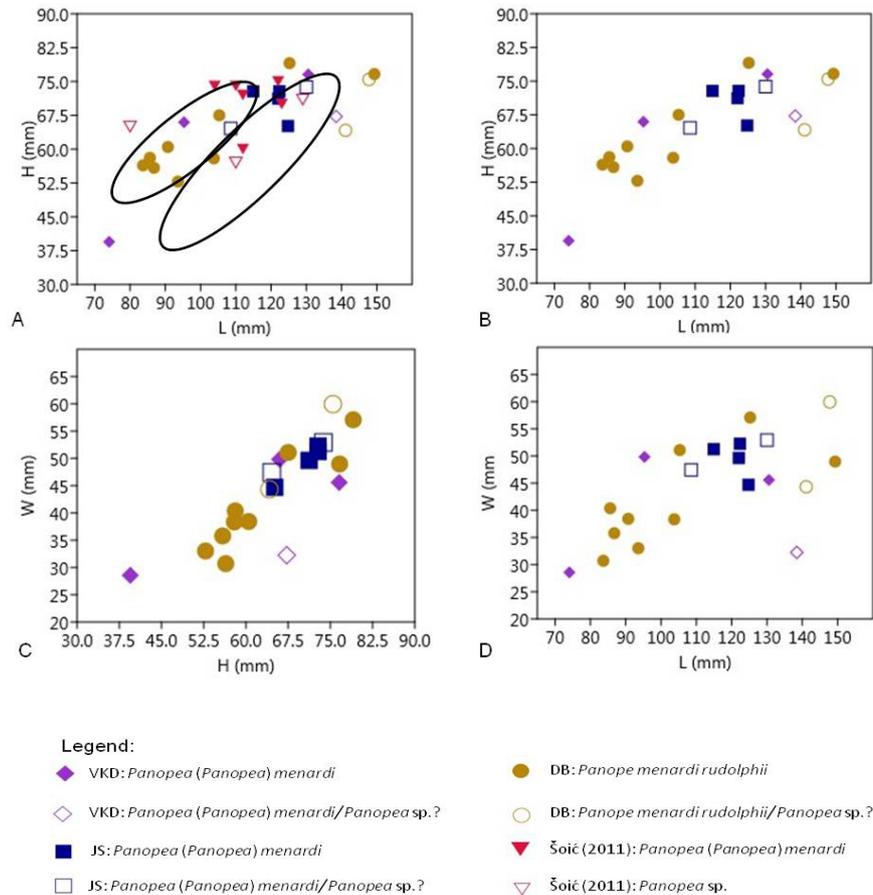
Figure 4: Correlation of the measured shell elements of the analyzed *Panopea* specimens. (**A**)Length and height of the analyzed geoducks compared to the measurements of **Šoić (2011)**; black ellipses: possible trends of the specimens. (**B**) Length and height of the analyzed specimens housed at the CNHM (**C**) Height and width of the analyzed specimens housed at the CNHM (**D**) Length and width of the analyzed specimens housed at the CNHM. For measurements and determinations of specimens see **Tables 1 and 2**. Legend: L – length (mm); H – height (mm); W – width (mm). Samples DB are collected in the Lower Badenian deposits of the Pokupsko area and determined as *Panope menardi rudolphii* Eichwald, 1834. Samples VKD, JS and V are collected from the Upper Badenian deposits on Medvednica Mt. and determined as *Panopea (P.) menardi* and *Panopea* sp. (see **Figure 1, Tables 1 and 2**).

Further comparison of the analyzed specimens is shown in **Figure 5**. All specimens were compared, and, afterwards specimens from Medvednica Mt. were separated from the ones from the Pokupsko area. As it can be seen in **Figure 5** and **Table 3**, median length value of the specimens is 114.95, and looking at the separated localities, specimens from Medvednica Mt. have higher median length value which is 122.22, and Pokupsko area specimens have lower median value of 103.76. Median height value of all specimens is 65.97; however, geoducks from the Pokupsko area have lower median height value (60.48) than the ones from Medvednica Mt (69.23), as shown in **Figure 5** and **Table 3**. Median width value of all specimens is 45.59 (**Figure 5**, **Table 3**), except again for Medvednica Mt, where it is higher (48.54), and Pokupsko area specimens where it is lower (40.37).

The comparative measurements of *Panopea* specimens from Gornje Vrapče locality, Medvednica Mt. after **Šoić (2011)** are shown in **Figure 6** and **Table 3**. As it can be seen, the median length value of all those specimens is 112, and the median height value is 71. The separated *Panopea* (*P.*) *menardi* samples after **Šoić (2011)** are shown in **Figure 6B**, and they show the same median length value, and slightly higher median height value of 73.
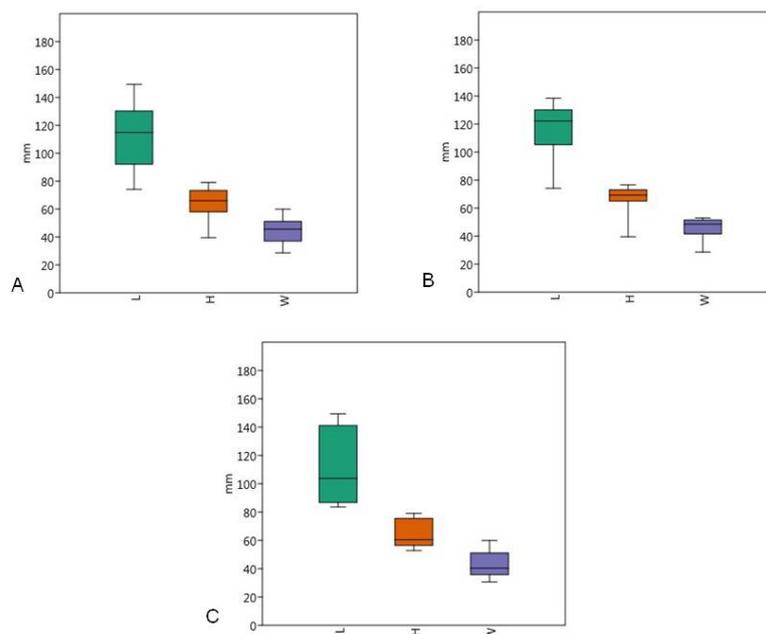
Figure 5: Boxplot of the analyzed *Panopea* specimens. **(A)** Localities Medvednica Mt. and Pokupsko area (all measured specimens). **(B)** Medvednica Mt. locality (all measured specimens). **(C)** Pokupsko area (all measured specimens). For each sample, the 25-75 percent quartiles are drawn using a box. The median is shown with a horizontal line inside the box. The minimal and maximal values are shown with short horizontal lines ("whiskers") (**Hammer et al., 2001**). Legend: L – length, H – height, W – width.
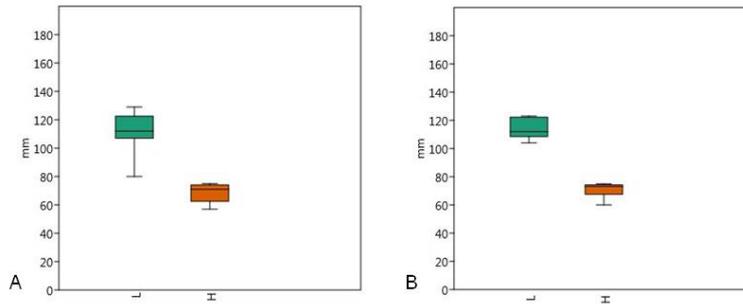
Figure 6: Boxplot of the compared measurements of *Panopea* specimens from **Šoić (2011)**. **(A)** All specimens from Gornje Vrapče locality, Medvednica Mt. **(B)** Specimens determined as *Panopea* (*P.*) *menardi* from Gornje Vrapče locality, Medvednica Mt. For each sample, the 25-75 percent quartiles are drawn using a box. The median is shown with a horizontal line inside the box. The minimal and maximal values are shown with short horizontal lines ("whiskers") (**Hammer et al., 2001**). Legend: L – length, H – height, W – width.

In order to compare the measured samples determined as *Panopea* (*P.*) *menardi* with those from **Šoić (2011)**, they are plotted separately (**Figure 7**). Specimens marked as VKD and JS (Table 1) from the Gornje Vrapče locality show median length values of 122.08, median height value 71.21, and median width value of 49.64 (**Figure 7A** and **Table 3**). Specimens from the Pokupsko area are showing lower values, with the median length value of 93.59, median height value of 58.09, and the median width value of 38.43 (**Figure 7B** and **Table 3**).
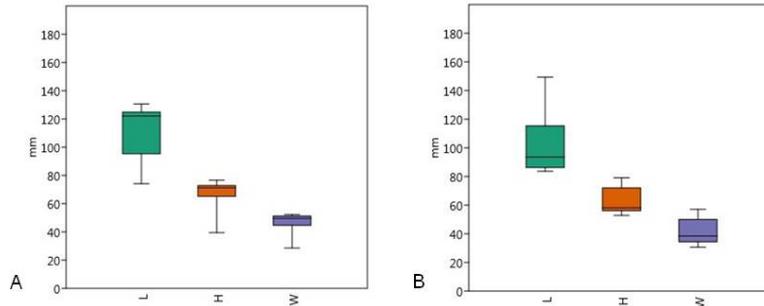
Figure 7: Boxplot of the measured *Panopea* (*P.*) *menardi* specimens. **(A)** Gornje Vrapče and Gornji Stenjevec localities, Medvednica Mt. **(B)** Pokupsko area. For each sample, the 25-75 percent quartiles are drawn using a box. The median is shown with a horizontal line inside the box. The minimal and maximal values are shown with short horizontal lines ("whiskers") (**Hammer et al., 2001**). Legend: L – length, H – height, W – width.

The measured specimens from Medvednica Mt. and Pokupsko area were also analyzed by cluster analysis, which confirmed the dispersion of the measured data.

SPECIMENS	MEDIAN LENGTH	MEDIAN HEIGHT	MEDIAN WIDTH
VKD, JS, DB	114.95	65.97	45.59
VKD, JS	122.22	69.23	48.54
VKD, JS (except **)	122.08	71.21.	49.64
DB	103.76	60.48	40.37
DB (except **)	93.59	58.09	38.43
V	112	71	/
V (except **)	112	73	/

Table 3. Median values of the measured shell parameters. For specimens determinations see **Tables 1 and 2.**

4. Discussion

The analyzed and measured Middle Miocene *Panopea* specimens from the southwestern margin of the Central Paratethys (**Figure 1**) show slight differences between the two analyzed localities: Medvednica Mt. and Pokupsko area. Specimens from Pokupsko area show lower median length, height and width values than the specimens from Medvednica Mt. (**Figure 5**, **Table 3**). Here presented specimens from Medvednica Mt. and Pokupsko area (**Tables 1 and 3**) have slightly higher median length value and lower median height value compared to the *Panopea* specimens from Medvednica Mt. by **Šoić (2011)** (**Tables 2 and 3**, **Figures 5A and 6A**).

Specimens determined as *Panopea* (*Panopea*) *menardi* (**Table 1**) from Medvednica Mt. show higher median length value than the comparative samples of the same species and locality by **Šoić (2011)** (**Tables 2 and 3**), while the median height value is lower (**Figures 6 and 7**). Specimens of *Panopea* (*Panopea*) *menardi* from Pokupsko area have lower median length and height values than the samples from Medvednica Mt., both here presented samples and the comparative ones (**Figures 6 and 7**, **Table 3**).

Considering the above mentioned and as shown in **Figure 4**, the highest dispersity of data is visible in the specimens from Pokupsko area, and better grouping of the data in the specimens from Medvednica Mt., which also have higher length and height values. That grouping of higher shell elements values could also indicate a second trend in height/length ratio (**Figure 4**).

Specimens which were questioned to belong to *Panopea* (*Panopea*) *menardi* species and marked as *Panopea* sp.? (**Table 1**) show good fitting between the minimum and maximum length and height values of *Panopea* (*Panopea*) *menardi* specimens (**Figure 4**), so this could point to the differences in the shell morphology of the single, *Panopea* (*P.*) *menardi* species.

In the studies on the recent species of the genus *Panopea*, intraspecific variability of the shell size and shape has been recorded among the different regions (e.g., **Bureau et al., 2002**; **Aragón-Noriega et al., 2015, 2019 and references therein**; **Zaidman & Morsan, 2015**; **Wood et al., 2018 and references therein**). **Bureau et al. (2002)** mention earlier results by **Goodwin & Pease (1991)** who found a link between the sediment type and panopean length, with larger specimens found in the sand and sand/mud than in the mud or pea gravel. **Wood et al. (2018)** show significant differences in *Panopea generosa* valve length, with specimens reaching larger sizes in areas with colder water and higher primary productivity, what is also mentioned in earlier papers (e.g., **Goodwin & Pease, 1987 in Bureau et al., 2002 and references therein**). Authors also show spatial variability in shell morphology of the species *P. generosa*; specimens from subtidal and intertidal differed based on the shell compression in the dorsoventral region. Similar results to **Wood et al. (2018)**, considering the different growth parameters of modern *Panopea generosa* between the different regions and among sites have been recorded also in other studies, e.g., **Leyva-Valencia et al. (2012 and references therein)**, **Aragón-Noriega et al. (2015, and differences therein)**. **Leyva-Valencia et al. (2012)** discuss problems regarding identification of modern *Panopea* species considering the morphometric plasticity that occurs in the genus, differences in shell morphology influenced by environmental factors (temperature, tidal excursion, wave exposure, water currents, sediment type) and genetic difference, and the unknown relationship between the local environmental conditions and shell morphology (**Leyva-Valencia et al., 2012 and references therein**). **Zaidman & Morson (2015 and references therein)** mention results of studies that show connection of size and growth of modern geoducks to environmental factors, and conclude that their work on the recent *Panopea abbreviata* species growth variability suggests that growth is mainly governed by local environmental conditions.

The two *Panopea* sites mentioned in this study are of different stratigraphic age; Gornji Stenjevec and Gornje Vrapče localities on Medvednica Mt. belong to the Upper Badenian (e.g., **Kochansky, 1944**; **Šikić et al., 1977, 1979**; **Vrsaljko et al., 2006**; **Pezelj et al., 2016 and references therein**), while the Pokupsko area belongs to the Lower Badenian age (after **Bigunac, 1990**), as shown in **Figure 8**. According to **Bigunac (1990)**, the Pokupsko area deposits can be asserted to the Lower Badenian Upper Lagenidae Zone, with the most common foraminifer *Borelis melo* (Fichtel & Moll, 1798). This means that these sediments were deposited during the Miocene Climatic Optimum (**Figure 8**). Geoduck specimens from Medvednica Mt. were collected in younger, Upper Badenian deposits (**Figure 8**). These specimens have generally higher median shell height, length and width values than those from the Pokupsko area specimens, as presented in the chapter Results and described above. Modern geoduck shell growth studies showed that the panopeans reach larger sizes in the cooler waters (e.g., **Wood et al., 2018 and references therein**). This could also be a factor in the panopean shell growth during the Badenian; the older Badenian panopeans corresponding to the time of the Miocene Climatic Optimum have smaller values of the measured shell parameters (**Figure 3**), than the panopeans of the younger Badenian age, living in cooler climate, after the Miocene Climatic Optimum. The authors consider this

as a hypothesis, where more results are needed to make more conclusions on the variability of the geoduck shell variability.
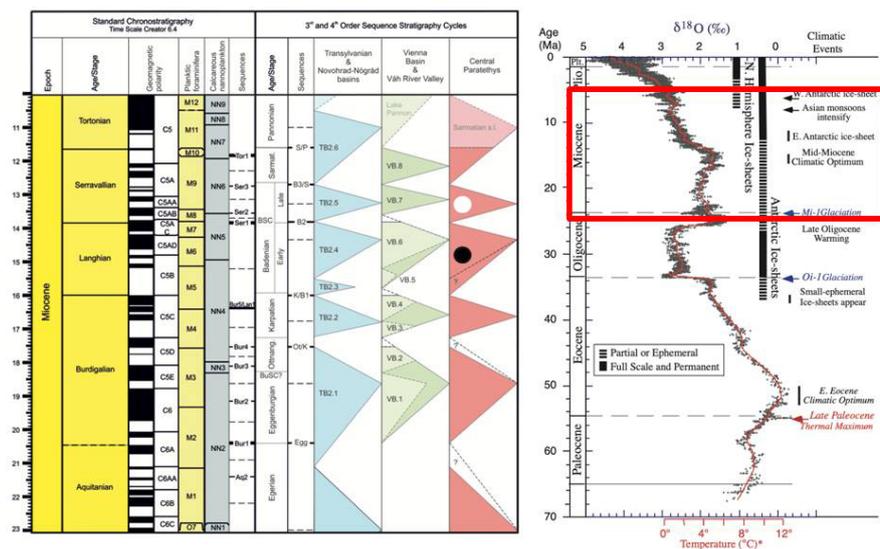

Figure 8: Stratigraphic age of the localities where analyzed panopean specimens were collected (after **Kováč et al., 2018**), and Neogene temperature curve with mentioned major climatic events (after **Zachos et al., 2001**). Black circle marks Pokupsko area locality (after **Bigunac, 1990**), and white circle marks the Medvednica Mt. localities (**Kochansky, 1944**; **Šikić et al., 1977, 1979**; **Vrsaljko et al., 2006**; **Pezelj et al., 2016 and references therein**).

The length and height deviations of the specimens assumed as another *Panopea* species or subspecies as seen in **Figure 4**, are most probably the consequence of the intraspecific morphological variability of the species *Panopea* (*P.*) *menardi*. These morphological varieties previously resulted with the recognition of different *Panopea* species (e.g., **Studencka, 1986 and references therein**). **Studencka (1986)** describes *Panopea* (*P.*) *menardi* specimens from the Badenian sediments of southern Poland, and discusses their morphology and their assignment to one or more panopean species. Taking into account all the above mentioned, the authors agree with the opinion of **Studencka (1986 and references therein)** that variable Middle Miocene (Badenian) panopeans, despite their variability of the shell shape, represent the ecotypes of a single *P.* (*P.*) *menardi* species.

5. Conclusions

Performed numerical analysis on the Middle Miocene (Lower and Upper Badenian) geoducks from the two areas (three localities) situated at the southwestern margin of the Central Paratethys in Croatia showed the following results:

(1) Measured parameters of the panopean casts and molds (height, length and width) show morphological variability of the shell shape seen through the dispersity of data on the presented graphics;

(2) Geoducks initially determined on the genus level (*Panopea* sp.?) group well into the plotted graphs with the measured elements of *Panopea* (*Panopea*) *menardi*, supporting the hypothesis that they are also the ecotypes of *Panopea* (*P.*) *menardi*;

(3) The numerical results can be grouped according to the geoduck stratigraphic age: Lower Badenian geoducks show lower median length, height and width values than the Upper Badenian geoducks;

(4) Hypothesis is made that the smaller size of the Lower Badenian geoducks is the consequence of higher water temperature during the Miocene Climatic Optimum. On the contrary, Upper Badenian geoducks, living in cooler seas, are larger, a pattern also recognized in studies of the modern geoducks;

(5) Further analysis of Badenian geoducks is needed to record more ecotypes of the *Panopea* (*Panopea*) *menardi* species and to test the validity of suggested hypothesis based on the climatic effects on the geoducks shell shape and its connection in the fossil record.

6. References

Aragón-Noriega, E.A. and Rodríguez-Domínguez, G. (2015): Comparison of growth curves of four *Panopea* species. Journal of Shellfish Research, 34, 1, 147–151. DOI: 10.2983/035.034.0118

Aragón-Noriega, E.A., Alcántara-Razo, E., Cruz-Vásquez, R., Castillo-Vargasmachuca, S.G., Rodríguez-Domínguez, G., Ponce-Palafox, J.T. and López-Sánchez, J.A. (2019): Growth variations in the geoduck *Panopea globosa* in different climatological regions of northwestern Mexico. Journal of Shellfish Research, 38, 2, 279–286. DOI: 10.2983/035.038.0208

Bigunac, D. (1990): Fauna badenskih naslaga okolice Pokupskog [Fauna from the Badenian deposits of Pokupsko area]. Unpublished Graduation Thesis, Unviersity of Zagreb, Faculty of Mining, Geology and Petroleum Engineering, 41 pp. (*in Croatian*).

Bosio, G., Bracchi, V. A., Malinverno, E., Collareta, A., Coletti, G., Gioncada, A., Kočí, T., Di Celma, C., Bianucci, G. and Basso, D. (2021): Taphonomy of a *Panopea* Ménard de la Groye, 1807 shell bed from the Pisco Formation (Miocene, Peru). Comptes Rendus Palevol, 20, 8, 119-140. https://doi.org/10.5852/cr-palevol2021v20a8

Budak, M. (1974): Razvoj tortona i njegove faune u području Dubravice kod Gornjeg Stenjevca – jugozapadni dio Zagrebačke gore [Development of Tortonian deposits and fauna in the Dubravica area near Gornji Stenjevec locality, southwestern part of Zagreb Mt.]. Unpublished Graduation Thesis, University of Zagreb, Faculty of Science, 24 pp. (*in Croatian).*

Bureau, D., Hajas, W., Surry, N.W., Hand, C.M., Dovey, G. and Campbell, A. (2002): Age, Size Structure and Growth Parameters of Geoducks (*Panopea abrupta*, Conrad 1849) from 34 Locations in British Columbia Sampled Between 1993 and 2000. Canadian Technical Report Fisheries and Aquatic Sciences. Nanaimo, British Columbia, Canada. no. 2413. 84 pp.

Butković, B. (1979): Makrofosili tortona Gornjeg Vrapča [Tortonian macrofossils from Gornje Vrapče locality]. Unpublished Graduation Thesis, University of Zagreb, Faculty of Science, 47 pp. (*in Croatian*).

Dželalija, S. (2007): Stratigraphy and facies of Miocene deposits in the southwestern part of Petrinja. Unpublished Bachelor of Sc. Thesis, University of Zagreb, Faculty of Science, Department of Geology, 35 pp. (*in Croatian*, *with English abstract*).

Fio, K., Sremac, J. and Šoić, N. (2014): Large deep burrowing bivalves in Middle Miocene (Badenian) of Central Paratethys; examples from Northern Croatia. In: Cvetković, V. (ed.): XVI Serbian Geological Congress: Proceedings (National Congress with International Participation), Donji Milanovac, 22-25.05.2014, Serbian Geological Society, 181-191.

Hammer, Ø., Harper, D.A.T. and Ryan, P.D. (2001): PAST: Paleontological statistics software package for education and data analysis. Palaeontologia Electronica, 4, 1, 9pp.

Harzhauser, M.and Landau, B. (2019): Turritellidae (Gastropoda) of the Miocene Paratethys Sea with considerations about turritellid genera. Zootaxa, 4681, 1–136.

Kochansky, V. (1944): Fauna marinskog miocena južnog pobočja Medvednice (Zagrebačke gore) [Miozäne marine Fauna des südlichen Abhanges der Medvednica (Zagreber Geibrge)]. Vjestnik Hrv.drž. geol. zav. i Hrv. drž. geol. muz., II/III, 171-280 (*in Croatian, with German Abstract*).

Kováč, M., Halásová, E., Hudáčková, N., Holcová, K., Hyžný, M., Jamrich, M. and Ruman, A. (2018): Towards better correlation of the Central Paratethys regional time scale with the standard geological time scale of the Miocene Epoch. Geologica Carpathica, 69, 3, 283-300. doi: 10.1515/geoca-2018-0017

Leyva-Valencia, I., Álvarez-Castañeda, S.T., Lluch-Cota, D.B., González-Peláez, S., Pérez-Valencia, S., Vadopalas, B., Ramírez-Pérez, S. and Cruz-Hernández, P. (2012): Shell shape differences between two *Panopea* species and phenotypic variation among *P. globosa* at different sites using two geometric morphometrics approaches. Malacologia, 55, 1–13. DOI: http://dx.doi.org/10.4002/040.055.0101

Leyva-Valencia, I., Cruz-Hernández, P., Álvarez-Castañeda, S.T., Rojas-Posadas, D.I., Correa-Ramírez, M.M., Vadopalas, B. and Lluch-Cota, D.B. (2015): Phylogeny and phylogeography of the geoduck *Panopea* (Bivalvia: Hiatellidae). Journal of Shellfish Research, 34, 1, 11–20. DOI: 10.2983/035.034.0104

Moore, R. C. (Ed.) (1969): Treatise on Invertebrate Paleontology. Part N, volume 2, Mollusca 6, Bivalvia. The Geological Society of America and the University of Kansas, pp. N491-N952.

Pezelj, Đ., Sremac, J. and Bermanec, V. (2016): Shallow-water benthic foraminiferal assemblages and their response to the palaeoenvironmental changes — example from the Middle Miocene of Medvednica Mt. (Croatia, Central Paratethys). Geologia Croatica, 67, 4, 329-345. doi: 10.1515/geoca-2016-0021

Pikija, M. (1987a): Osnovna geološka karta SFRJ 1:100.000, list Sisak, L 33-93 (Basic geological map of SFRY 1: 100.000, Sisak sheet, L 33-93). Savezni geološki zavod, Beograd (*in Croatian*).

Pikija, M. (1987b): Osnovna geološka karta SFRJ 1:100.000. Tumač za list Sisak, L 33-93 (Basic Geological Map of SFRY 1:100.000. Geology of Sisak sheet). Institut za geološka istraživanja, Zagreb (1986), Savezni geološki zavod, Beograd, pp. 51 (*in Croatian*).

Sremac, J., Bošnjak, M., Velić, J., Malvić, T. and Bakrač, K. (2022): Nearshore Pelagic Influence at the SW Margin of the Paratethys Sea—Examples from the Miocene of Croatia. Geosciences, 12, 120. https://doi.org/10.3390/geosciences12030120

Studencka, B. (1986): Bivalves from the Badenian (Middle Miocene) marine sandy facies of southern Poland. Palaeontologia Polonica, 47, 3-128.

Šikić, K., Basch, O. and Šimunić, A. (1977): Osnovna geološka karta SFRJ 1:100.000, list Zagreb, L 33–80 (Basic geological map 1:100.000, Zagreb sheet, L 33-80). Institut za geološka istraživanja, Zagreb (1972), Savezni geološki zavod, Beograd.

Šikić, K., Basch, O. and Šimunić, A. (1979): Osnovna geološka karta SFRJ 1:100.000. Tumač za list Zagreb, L 33–80 (Basic geological map 1:100.000, Geology of the Zagreb sheet).– Institut za geološka istraživanja, Zagreb (1972), Savezni geološki zavod, Beograd, 75 pp.

Šoić, N. (2011): The bivalve *Panopea* and its role in Miocene of Paratethys; an example from locality Gornje Vrapče (*in Croatian, with an English abstract*). Unpublished Graduation Thesis, University of Zagreb, Faculty of Science, Department of Geology, 44 pp.

Thomsen, E., Knudsen, J. and Koskeridou, E. (2009): Fosssil panopeans (Bivalvia, Hiatellidae) from Rhodes, Greece. Steenstrupia 30 (2), 163–176.

Velić, I. and Velić, J. (1995): Geological Map of Croatia. In Proceedings of the First Croatian Geological Congress, Opatija, Croatia, 18–21, October 1995.

Vrsaljko, D., Pavelić, D., Miknić, M., Brkić, M., Kovačić, M., Hećimović, I., Hajek-Tadesse, V., Avanić, R. and Kurtanjek, N. (2006): Middle Miocene (Upper Badenian/Sarmatian) palaeoecology and evolution of the environments in the area of Medvednica Mt. (North Croatia). Geol. Croatica, 59, 51-63.

Wood, G., Hamilton, S.L., Vadopalas, B., Stevick, B. and Leyva-Valencia, I. (2018): Geographic variation in the life history and morphology of the pacific geoduck *Panopea generosa*. Journal of Shellfish Research, 37, 5, 919–931. DOI: 10.2983/035.037.0502

Zachos, J., Pagani, M., Sloan, L., Thomas, E. and Billups, K. (2001): Trends, Rhythms, and Aberrations in Global Climate 65 Ma to Present. Science, 292, 686-693.

Zaidman, P.C. and Morson, E. (2015): Growth variability in a metapopulation: The case of the southern geoduck (*Panopea abbreviata*). Fisheries Research, 172, 423-431. http://dx.doi.org/10.1016/j.fishres.2015.08.011

Internet sources:

URL: https://www.sailingissues.com/navcourse1.html
URL: www.fossilworks.org

Sažetak

Numerička analiza srednjomiocenskih školjkaša iz roda *Panopea* („geoducks") iz jugozapadnog dijela Centralnog Paratethysa, Hrvatska

U radu je prikazana numerička analiza koja pokazuje raznolikost morfologije ljušture školjkaša iz roda *Panopea*, poznatih u engleskom jeziku kao „geoducks". Primjerci su prikupljeni u srednjomiocenskim (badenskim) naslagama Sjeverne Hrvatske (jugozapadni rub Centralnog Paratethysa). U starijoj literaturi se za primjerke ove jedne vrste panopeja smatralo da je riječ o više vrsta/podvrsta ovih školjkaša. Analizirani primjerci su izmjereni i obrađeni u software-u PAST. Dobiveni podatci su uspoređeni s dostupnim mjerenjima ovih školjkaša u ranijim istraživanjima. Rezultati su pokazali morfološku varijabilnost oblika ljušture panopeja iz donjobadenskih i gornjobadenskih naslaga, pri čemu donjobadenske panopeje pokazuju niže vrijednosti medijana mjerenih parametara ljušture od gornjobadenskih panopeja. Također je zaključeno slaganje s komparativnim materijalom. Usprkos raznolikosti oblika, koje su prikazane u analiziranim primjercima, svi se obrađeni primjerci smatraju ekotipovima morfološki varijabilne vrste *Panopea* (*Panopea*) *menardi* (Deshayes, 1828). Mogući glavni uzrok varijabilnosti oblika ljušture panopeja bile su srednjomiocenske klimatske promjene.

Ključne riječi: numerička analiza; *Panopea*; srednji miocen; Centralni Paratethys; Hrvatska

Author's contribution

Marija Bošnjak (Dr.sc., senior curator, geology, paleontology, geomathematics) measured the analyzed material, provided the numerical analysis, data analysis, data and paleoenvironmental interpretations, and presentation of the results. **Jasenka Sremac** (Dr.sc., Full Professor, retired, geology, paleontology, paleoenvironment) provided the field work, collected and determined part of the analyzed fossil bivalves, provided the paleontological analysis, paleoenvironmental interpretation and presentation of the results. **Dijana Bigunac** (Dr.sc., senior expert geophysicist, sedimentology, geophysics) provided the field work, collected and determined part of the analyzed fossil bivalves, and contributed in the taxonomic discussion. **Davor Vrsaljko** (Dr.sc., geology, paleontology, biostratigraphy, malacology) provided the paleoenvironmental interpretations, and discussion on the taxonomy and broader regional geological context.

Statistical analysis of oil pipeline spills in Croatia

Karolina Novak Mavar[1]; Katarina Žbulj[1]; Lidia Hrnčević[1]; Katarina Simon[1]
[1] University of Zagreb, Faculty of Mining, Geology and Petroleum Engineering, Pierottijeva 6, Zagreb

Abstract

Petroleum upstream activities pose a certain risk to the environment. Pipelines, as the most efficient hydrocarbon transport means, are irreplaceable in the petroleum industry activities. Corrosive media being transported contributes to a higher risk of pipeline failure and resulting release. Prevention and risk mitigation approaches require proper maintenance and inspection of pipelines. Continuous statistical tracking and identification of pipeline sections with the highest spill frequency is required. For that purpose, descriptive statistics are commonly used. Time series data analyses allows trends to be observed and future results to be predicted. The paper presents the practical application of statistical methods in pipeline spills analysis in the context of oil and gas production in the continental part of Croatia. The analysis covers a ten-year period. To enable comparison with the CONCAWE methodology, only leakages ≥ 1 m^3 were considered and presented. The negative trend of spill occurrence is consistent with the CONCAWE results. Unlike the CONCAWE Report on European cross-country oil pipelines, where 88 % of all accidents are caused by third party activities, while corrosion and mechanical failures account for 5 % and 2 % respectively, in the case of Croatian gathering and transportation pipelines, more than 70 % of spill accidents were caused by corrosion. The high age of pipelines and exposure to aggressive and corrosive media stand out as the main failure causes. However, a slight negative trend has been observed, which is due to reconstruction/replacement of critical pipeline sections.

Keywords: pipeline transport; oil spill; gathering pipeline; transmission pipeline; statistical tools

1. Introduction

Because of the operating conditions, fluids involved, and long-lasting complex infrastructure, petroleum industry activities pose significant threat to the environment. Hydrocarbon spills can occur throughout the life cycle of an oil field, whether from well blow-out, equipment damage or failure, or human factor. To minimise the risk of spill, demanding standards for well integrity and safety of oil and gas production and transportation system must be ensured. Through the selection of adequate equipment materials and safety systems, as well as by regular maintenance and process control and monitoring systems, accident occurrence can be minimised. Adherence to safety regulations, relevant procedures and best practice, helps prevent the occurrence of accident and improves the efficiency of remediation (**Owens, 2002; Ivshina et al., 2015**).

However, despite all measures applied, hydrocarbon releases into the environment continue to occur. An oil spill is any unplanned and uncontrolled release of hazardous substances into the environment. Oil and gas production usually involves the leakage of hydrocarbons, brine and process water, different chemicals, hydraulic fluids, mud, etc. into the soil, and ground and surface water. Spills can also occur during transportation of the produced fluids through pipelines, rail cars, trucks or tankers. Pipeline leakages are mostly caused by corrosion, mechanical failure, operational system failures (design or material related), natural disasters or third-party activities (**Jernelöv, 2010; Anderson et al., 2012; Ivshina et al 2015**).

Management commitment to certified standards based management systems ensures that negative impact of production processes on the environment are constantly monitored, reduced and prevented. Having responsibility for their actions, oil and gas companies, within their annual reports, provide information on spills and undertake remediation measures, being in line with the corporate social responsibility commitment (**Frynas, 2012**).

The aim of this research is to present an overview of the available methods used in pipeline spills risk analysis in oil and gas production processes. The presented analysis covers the leakages ≥ 1 m^3 that occurred in the gathering-transmission system in the continental part of Croatia, during a ten-year period. The results have been compared with the CONCAWE methodology (**CONCAWE, 2015**) and can serve as a reliable database with the local conditions for spill risk analysis as a common basis for decision making.

Corresponding author: Karolina Novak Mavar
karolina.novak-mavar@rgn.unizg.hr

2. Statistical tools in analysis of environmental impacts

In the process of managing specific impacts on the environment, different statistical tools can be used. In a statistical analysis of environmental impacts, there is a distinction between the cross-sectional data analysis and the time series data analysis. While in cross-sectional data analysis the data is obtained at the same time, the time series data approach refers to collecting the data in a defined period. Environmental management uses both, cross-sectional and time series data.

Furthermore, the data can be determined as either qualitative or quantitative. Qualitative data may be nominal (categorical data obtained by labelling) or ordinal (having ordered categories), while quantitative data has some numeric values (measured data) (**Benčić et al., 2008; Malvić and Rusan, 2009; Matanović et al., 2014; Novak, 2015; Gaurina-Međimurec and Novak Mavar, 2017**).

Descriptive statistics, i.e., tabular and graphical representation of data (line, stripe, cake, Box & Whiskers (B & W) diagrams etc.) is commonly used in environmental management. The B & W plot can be particularly suitable for environmental data representation, since environmental processes in general do not follow normal distribution. This means that the probability curve does not have a symmetrical shape, and the data dispersion is very large (**Benčić et al., 2008**).

In order to get relevant risk analysis, different databases are consulted and used. The most relevant databases available are operated by CONCAWE, European Gas Pipeline Incident Data Group (EGIG), and US Department of Transportation (US DoT) (**Hosseinnia Davatgar et al., 2021**).

2.1. CONCAWE Report Analysis

The Concawe Oil Pipelines Management Group (OPMG) has been collecting a database of pipeline safety and environmental performance in Europe since 1971 (**Simon et al., 2013; CONCAWE, 2021**). It includes all pipelines used for transportation of crude oil or petroleum products, in a length ≥ 2 km, which are running cross-country, as well as the pump stations, intermediate aboveground installations and intermediate storage facilities. CONCAWE only considers international pipelines. Available database covers all reported leakages over 1 m^3 occurred in the period from 1971 to 2020. However, if the spilled fluid does not reach the environment, such an extraordinary event is not considered a spill, but is defined as a Loss of Primary Containment (LOPC) event. Oil pipeline leakages assorted by the causes that occurred in Europe in the period from 2011 to 2020 are shown in **Table 1** and **Figure 1**. According to CONCAWE the spill causes can be classified into five general categories: mechanical failure, operational, corrosion, natural hazard and third party (**Table 1**). In case of mechanical failures, the failure is generated by design or material fault, caused, for instance, by some metallurgical defect, or inadequate material selection, or can be generated by some construction fault. This category also includes the failure of sealing devices. Operational failures are caused by operational malfunctions or process control systems (e.g., instrumentation, mechanical pressure relief system, etc.) errors or failures. This category also covers operator (human) errors. Corrosion failures refer to internal, external and stress corrosion cracking. Natural hazard failures are caused by natural phenomena and include lightning strikes, landslides, flooding, etc. Third party failures are damages inflicted by accidental or intentional third-party activities, including "incidental" damage, detected later in time (**CONCAWE, 2021**).

Spillage accidents	2011	2012	2013	2014	2015	2016	2017	2018	2019	2020	Total
Mechanical failure	1	1	3	1	3	1	0	1	2	2	15
Operational	0	1	1	0	0	0	2	0	1	0	5
Corrosion	2	3	1	0	3	3	0	0	3	1	16
Natural hazard	0	0	0	0	0	0	0	0	0	0	0
Third party activity	4	8	21	57	87	62	11	11	0	5	266
Total	7	13	26	58	93	66	13	12	6	8	302

Table 1: Oil pipeline leakages in Europe from 2011 to 2020 (**CONCAWE, 2015; CONCAWE, 2018; CONCAWE, 2021**)
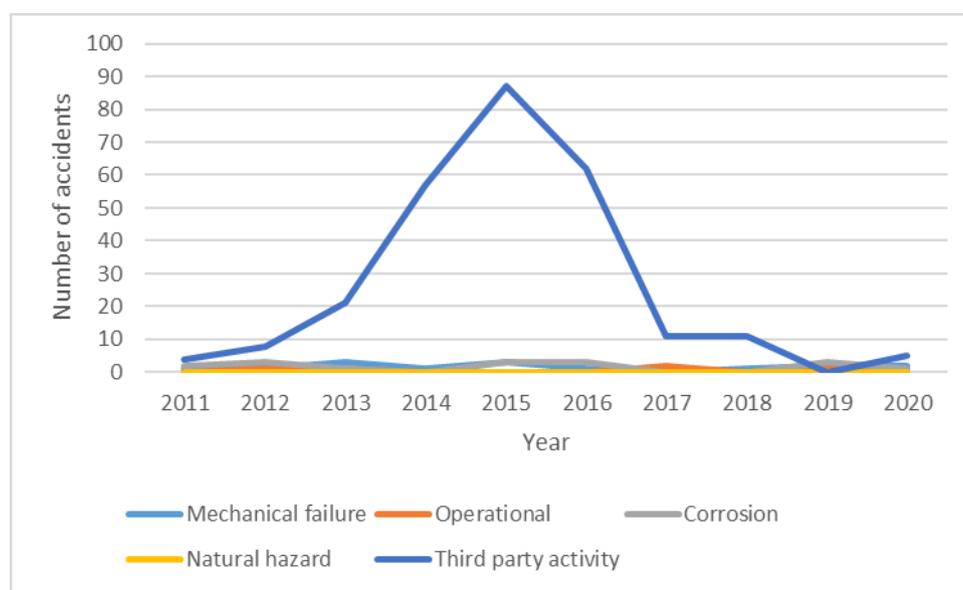
Figure 1: Oil pipeline leakages assorted by the causes that occurred in Europe in the period from 2011 to 2020 (according to **CONCAWE, 2021**)

Although there has been a slight increase in the number of accidents in 2020 compared to 2019, it can be observed that the pipeline accident frequency in the EU has shown a decreasing trend over the last decade. In fact, such a steadily decreasing trend can be observed from the mid-1970s until today. According to the Report, third party activities, accounting for 88 % of all incidents, represent the most common cause of hydrocarbon spill to the environment, while corrosion and mechanical failures contribute individually with 5 % and 2 % respectively. The reported spillage frequency of 0.12×10^{-3} spillages per km per year was consistent with the 5- year average, but well below the long-term average of 0.43×10^{-3} spillages per km of line (**CONCAWE, 2021**).

3. Case study

Hydrocarbon exploitation in the continental part of the Republic of Croatia takes place in the Pannonian Basin at 55 production fields (37 oil fields and 17 gas fields) (**Figure 2**). In 2020, domestic crude oil production amounted to 631.8 $\times 10^3$ tons. In the same year, natural gas production was 849.0 $\times 10^6$ m^3, with onshore production accounting for more than 67 % (**INA Plc., 2020; EIHP, 2021**). The extended history of hydrocarbon extraction in Croatia has resulted in relatively mature fields. The first concession for oil production in Croatia was granted in 1860 for the Peklenica Field

near Mursko Središće (**Malvić & Velić, 2021**). In accordance with INA's Annual report for 2020, the average age of Croatian onshore oil fields is 45 years, while the gas fields are on average 35 years old (**INA Plc, 2020**).

Figure 2: Oil and gas fields in the Croatian part of the Pannonian Basin System (**Velić et al., 2016**)

Pipelines are irreplaceable as an efficient means of transporting oil and gas upstream in the petroleum industry. In Croatia, there are two types of systems for collecting production fluids (**Figure 3**). In the first type, wells are connected through pipelines to the metering station collector, from where the produced fluid (a mixture of oil and brine) is directed to the metering/gathering separators on gathering stations. After treatment of the extracted fluid, the crude oil is transported from the gathering stations to the refineries via pipelines with the help of pumps, while the water is injected into the subsurface. In the second type, the gathering system involves transporting the produced fluid from the wells to the collector line through flowlines, from where the fluid is transported through two gathering lines to a metering/gathering separator at the gathering station. The rest of the fluid flow is identical to the previously described system.
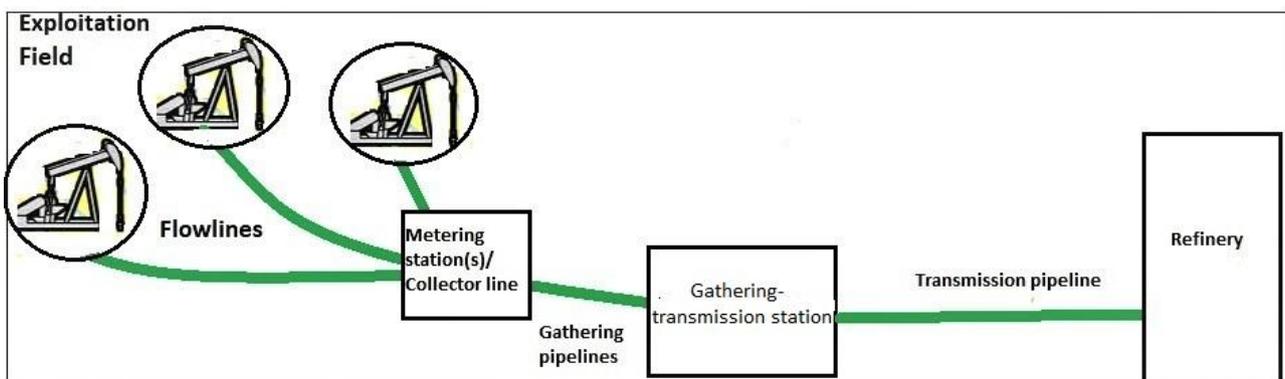
Figure 3: Oilfield gathering systems i Croatia

In order to determine the spill trend in the 2010 to 2019 period in the Republic of Croatia, hydrocarbon leakages from pipelines were analysed. The analysis includes all active pipelines in the process of hydrocarbon exploitation (flowlines, gathering pipelines and transmission pipelines) with a total length of 3×10^3 km, of which about 1420 km are flowlines, 700 km gathering pipelines and 830 km transmission pipelines. The longest part of the transportation and gathering system (the flowlines) is also the most vulnerable part of the system due to the fact that it is exposed to the aggressive fluid, that the inline inspection of this part of the system is not conducted and that it is one of the oldest parts of the system. The Croatian transmission oil and gas pipeline network is shown in **Figure 4**.
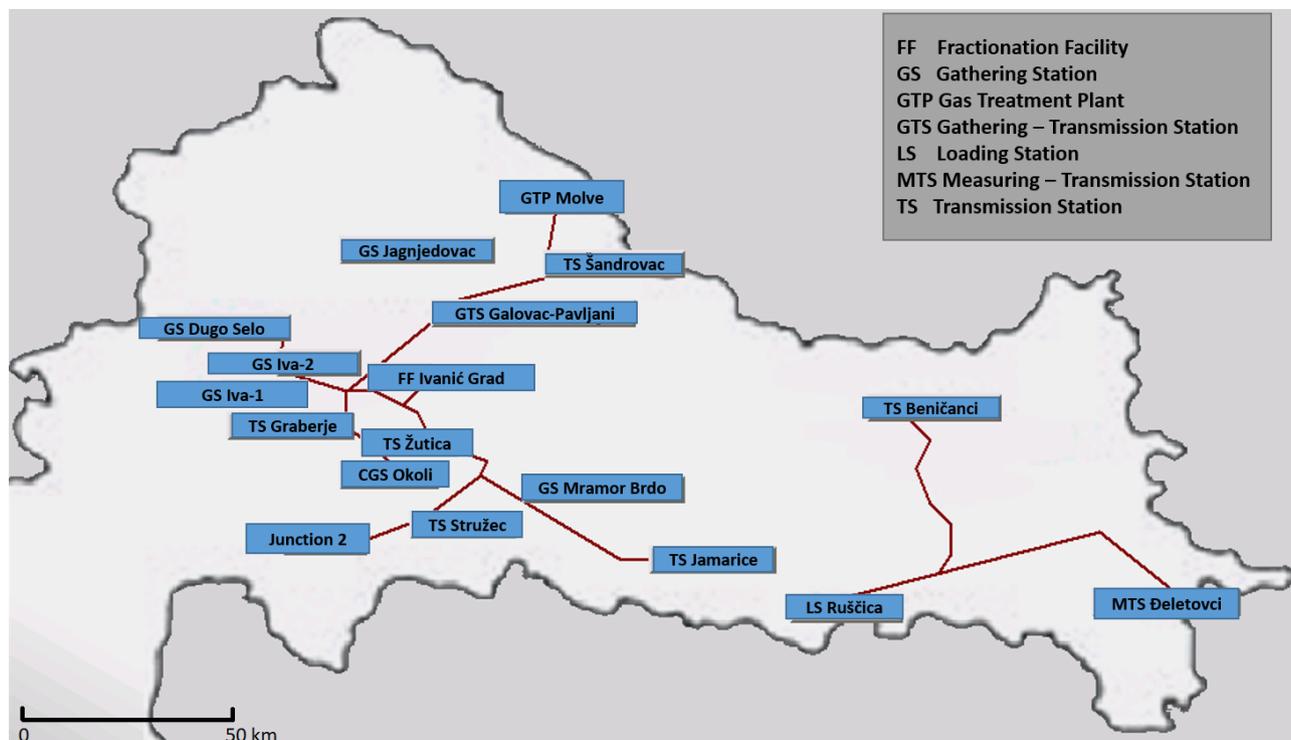
Figure 4: Croatian transmission pipeline map (**Kaličanin, 2012**)

For the analysis of the pipeline spills in the observed period descriptive statistics tools have been used. To enable comparison with CONCAWE data, oil leakages larger or equal to 1 m³, that occurred in gathering and transmission pipelines in Croatia in the period from 2010 to 2019, were analysed (**Table 2**). Gathering and transmission pipelines meet the CONCAWE criteria regarding pipeline diameter and length.

YEAR	NUMBER OF SPILLS	NUMBER OF SPILLS PER PIPELINE TYPE		NUMBER OF SPILLS PER SPILLED QUANTITIES	
		Gathering pipeline	Transmission pipeline	Less than 1 m³	Equal to or greater than 1 m³
2010	7	4	3	3	4
2011	15	10	5	15	0
2012	17	5	12	15	2
2013	19	11	8	17	2
2014	17	5	12	16	1
2015	7	7	0	6	1
2016	5	4	1	3	2
2017	2	1	1	0	2
2018	8	6	2	6	2
2019	13	13	0	12	1
TOTAL	**110**	**66**	**44**	**93**	**17**

Table 2: Data on spills in the period from 2010 to 2019 (**Žbulj, 2021**)

3.1. Pipeline spills analysis

Table 2 shows that there was a total of 110 pipeline related hydrocarbon spills into the ground and surface water during transportation of produced fluid. In terms of quantities spilled, 17 spills (15.5 %) were equal to or greater than 1.0 m^3.

Pipeline related spills in hydrocarbon exploitation in Croatia in the period from 2010 to 2019 are shown in **Figure 5**. Although there is some discrepancy (in 2013 there were 19 spills, while in 2017 there were a total of 2 spills ≥1 m^3 occurred), there were on average 11 spills per year in the observed period. When it comes to the major spills (≥1 m^3) they are mostly related to the gathering pipelines (60 %), while 40 % of spills occurred in transmission pipelines.
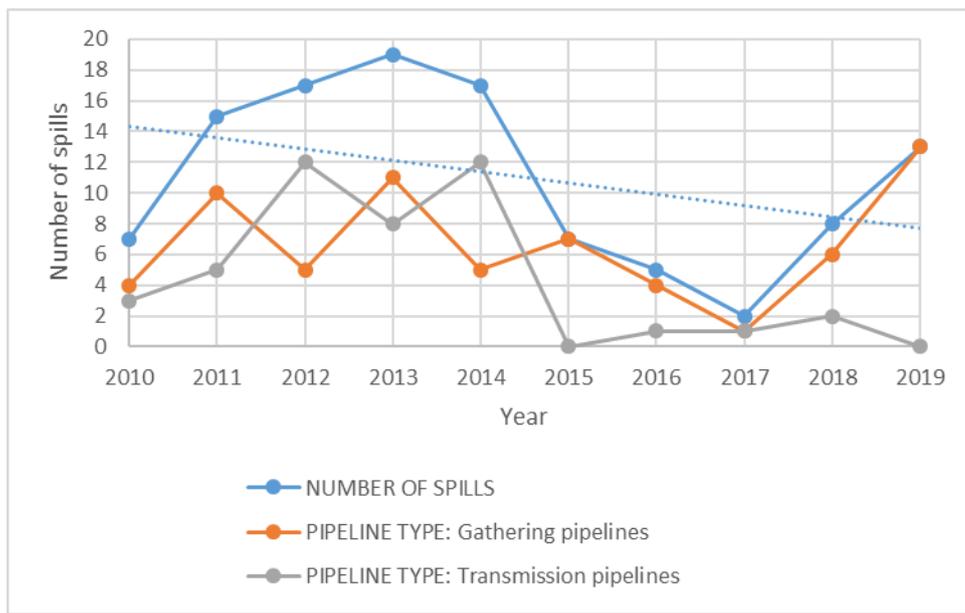
Figure 5: Pipeline related spills in hydrocarbon exploitation in Croatia in the period from 2010 to 2019

Considering the total number of spills and each individual length of each pipeline type: gathering pipelines (G) and transmission pipelines (T), annual failure frequency is calculated. As shown in **Figure 6**, annual failure frequency ranges between 0 per year per km (transmission pipelines in 2015 and 2019) and 18.6×10⁻³ per year per km (gathering pipelines in 2019). The higher average spill frequency for the ten-year period is related to gathering pipelines (9.4×10⁻³ per km) compared to 5.3×10⁻³ per km calculated for transmission pipelines. However, when it comes to the spills ≥1 m^3, as it can be seen in **Figure 7,** both gathering and transmission pipelines show a slightly negative trend in the number of accidents. Nevertheless, calculated ten years average major spill frequency is greater for gathering pipelines (1.71×10⁻³ per km compared to 6.02×10⁻⁴ per km in case of transmission pipelines). The CONCAWE report identified smaller pipelines to be more prone to leakage, due to lower levels of awareness around smaller pipelines (accidental failures caused by third party activities) and corrosion. The obtained ratio of smaller diameter pipelines leakages in total number of leakages is in line with the CONCAWE report (**CONCAWE, 2021**).
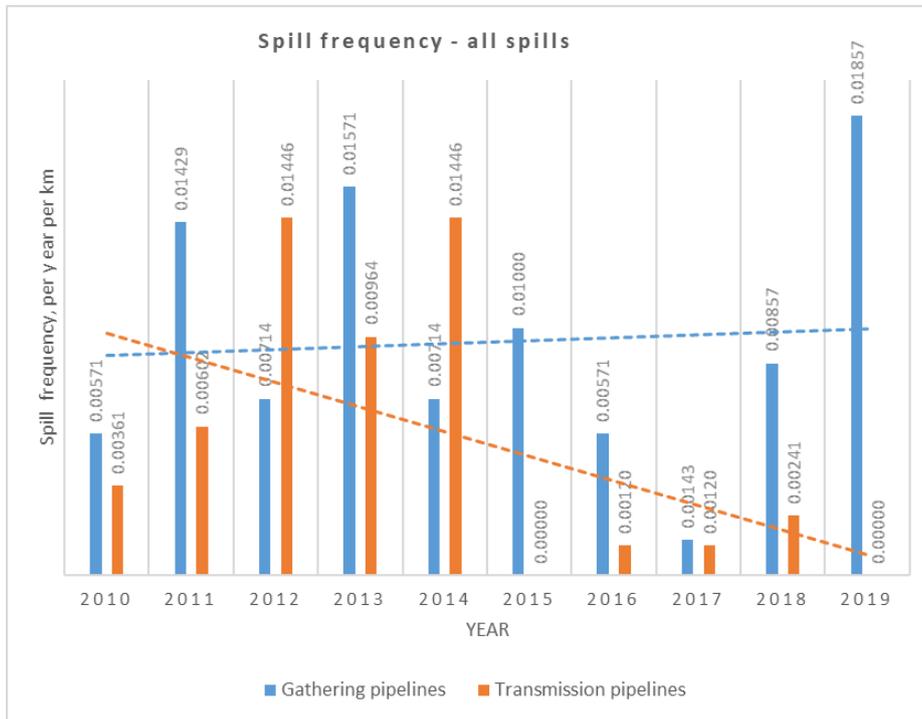
Figure 6: All spills frequency per pipeline types with ten-year trend
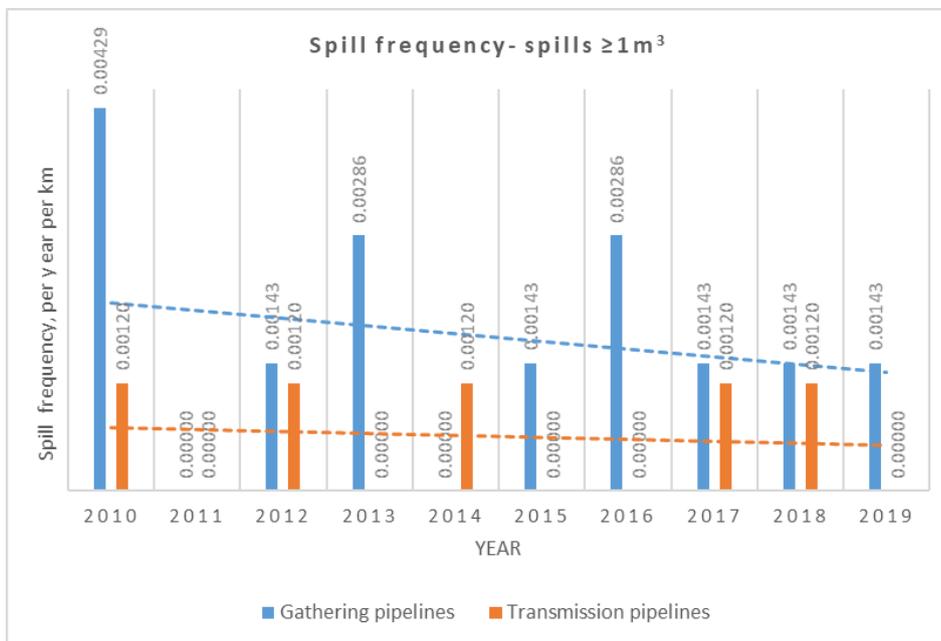
Figure 7: Major spills frequency per pipeline types with ten-year trend

With regards to leakage causes, the analysis shows that major spills (leakages $\geq 1m^3$) that occurred on the gathering and transmission pipelines were caused by corrosion or third-party activities. Corrosion was the cause in more than 70 % of accidents in the observed period, which is not surprising since most of pipelines are old and exposed to aggressive fluids for a long period. Pipeline spills caused by corrosion have a slight negative trend which may be due to reconstruction/replacement of critical pipeline sections. The remaining share belongs to the third-party activities, mostly related to illegal connections to the pipelines. Prevention of illegal connections intended for theft of products is almost an impossible task for the oil and gas industry to complete due to the significant lengths of pipelines. However, the number of illegal connections shows a negative trend, which can be attributed to enhanced monitoring and good cooperation with the local police (**Figure 8**).
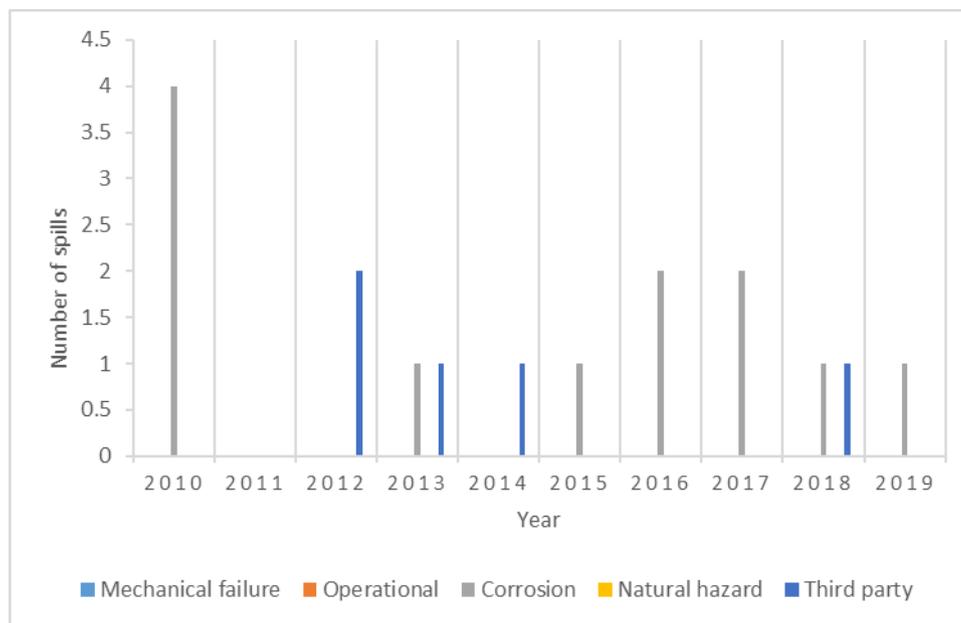
Figure 8: Pipeline failure causes

4. Conclusions

Environmental management considers monitoring and supervision of all identified issues (environmental aspects), in order to improve overall environmental performance. Pipeline spillage represents a significant environmental impact for the oil and gas production industry, which is highly dependent on the pipeline integrity management system in place. One of the most important elements relates to systematic maintenance of the pipeline transport systems in compliance with approved plans and programs.

The first step in preventing hydrocarbon leakage is pipeline maintenance and inspection, along with continuous statistical tracking and identification of pipeline sections with the highest leakages. Descriptive statistics are typically used for this purpose. Time series data analysis allows trends to be observed and future results to be predicted. The following conclusions can be drawn from the study, which covers all spills occurred in upstream pipeline transportation system in the continental part of the Republic of Croatia (gathering and transmission pipelines) with oil leakages ≥ 1 m^3 in the period from 2010 to 2019:

- 17 spills (15.5 %) can be classified as major since spilled quantities are equal to or greater than 1.0 m^3.
- About 60 % of spills ≥ 1 m^3 are related to gathering pipelines. Calculated ten-year average spill frequency is greater in case of gathering pipelines (1.71×10^{-3} per km compared to 6.02×10^{-4} per km in case of transmission pipelines).
- Both gathering and transmission pipelines show a slightly negative trend in the number of accidents.
- About 70 % of pipeline spill accidents (leakage ≥ 1 m^3) were caused by corrosion which is not surprising since the majority of pipelines are old and exposed to aggressive fluids for a long period.
- The pipeline system on oil and gas fields in Croatia is old and the percentage of brine in the transported fluid is high. Consequently, this results in frequent accidents, especially on flowlines and gathering pipelines. In the observed period there is a negative trend in corrosion related accidents occurrence, which appears as the result of reconstruction/replacement of critical pipeline sections.
- In the future it could be expected that the application of planned production optimization projects will also positively affect the transportation and gathering system.
- Illegal connections cases show a negative trend, which is due to increased monitoring and good cooperation with the local police.
- The calculated 10-year averages for the frequency of the gathering and transmission pipeline spills are 1.71×10^{-3} and 6.02×10^{-4} per km respectively, which is significantly higher than the long-term running average of 0.43×10^{-3} spillages per km of line calculated by CONCAWE. This is not surprising given that major part of the system is not subject to smart pigging.

- Regardless of the reasons, a well-defined pipeline maintenance plan should include regular inspections and pipeline maintenance, pipeline condition analysis and proper functioning of the safety system.

5. References

Anderson, C.M.; Mayes, M. and LaBell, R. (2012): Update of Occurrence Rates for Offshore Oil Spills. BOEM & BSEE, Herndon, VA, USA, 76 p.

Benčić, A., Buntak, K. and Babić, T. (2008) Statistički alati za analizu aspekata okoliša i njihovog utjecaja u sustavu upravljanja okolišem (*Statistical Tools for the Analysis of Environmental Aspects and their Impact in the Environmental Management System*). Proceedings of 9th Croatian Quality Conference, Zadar, Croatia, April 21.-23. (*in Croatian*)

CONCAWE (2015): Performance of European Cross-Country Oil Pipelines Detailed Description Of Reported Spillages 2005+. Available online: https://www.concawe.eu/wp-content/uploads/2017/01/spillage-descriptions-2005-2.pdf (accessed on 1 6 2022)

CONCAWE (2018): Performance of European Cross-Country Oil Pipelines. Report 6/18. Available online: URL https://www.concawe.eu/wp-content/uploads/2018/03/Rpt_18-6-2.pdf (accessed on 1 06 2022)

CONCAWE (2021): Performance of European Cross-Country Oil Pipelines. Report 6/22. Available online: URL https://www.concawe.eu/wp-content/uploads/Rpt_22-6.pdf (accessed on 1 06 2022)

EIHP (2021) Energy in Croatia. Available online: URL https://www.eihp.hr/wp-content/uploads/2022/01/Velika_EIHP_Energija_2020.pdf

Frynas, J. G. (2012). Corporate Social Responsibility or Government Regulation? Evidence on Oil Spill Prevention. Ecology and Society, 17, 4, 13 p.

Hosseinnia Davatgar, B.; Paltrinieri, N. and Bubbico, R. (2021) Safety Barrier Management: Risk-Based Approach for the Oil and Gas Sector. Journal of Marine Science and Engineering, 9, 7, 722.

INA-Oil Industry, Plc. (2020): Integrated Annual Report 2020. Available online: URL https://www.ina.hr/godisnje-izvjesce-2020/

Ivshina,I.B.; Kuyuklina,M.S.; Krivoruchko,A.V.; Elkin, A.A.; Makarov, S.O:, Cunningham, C.J.; Peshkur, T.A.; Atlasd , R.M. and Philp, J.C. Oil Spill Problems and Sustainable Response Strategies Through New Technologies. Environmental Sciences: Processes and Impacts, 17, 1201-1219.

Kaličanin, I. (2012): Utvrđivanje rizika od propuštanja naftovoda i razvoj sustava za upravljanje cjevovodima u Republici Hrvatskoj (*Pipeline Leakage Risk Assessment and the Development of Pipeline Management System in Croatia*). Doctoral thesis, Faculty of Mining, Geology and Petroleum Engineering, Zagreb, 2012. (*In Croatian*)

Jernelöv A. (2010): The Threats from Oil Spills: now, then, and in the Future. Ambio, 39, 5, 6; 353-366.

Malvić, T. and Rusan, I. (2009) Investment Risk Assessment in Potential Hydrocarbon Discoveries in a Mature Basin, Case Study from the Bjelovar Sub-Basin Croatia. Oil Gas European Magazine 2, 67-72.

Malvić, T. and Velić, J. (2021): Nafta. Hrvatska tehnička enciklopedija, Leksikografski Zavod Miroslav Krleža. Available online: URL: https://tehnika.lzmk.hr/nafta/ (*in Croatian*)

Matanović, D., Gaurina-Međimurec, N., Simon, K. et al. (2014) (Ed.) Risk Analysis for Prevention of Hazardous situations in Petroleum and Natural Gas Engineering. IGI Global, Hershey, PA, USA, 415 p.

Novak, K. (2015): Modeliranje površinskoga transporta i geološki aspekti skladištenja ugljikova dioksida u neogenska pješčenjačka ležišta sjeverne hrvatske na primjeru polja ivanić (*Surface Transportation Modelling ad Geological Aspects of Carbon-Dioxide Storage into Northern Croatian Neogene Sandstone Reservoirs, Case Study Ivanić Field*). Doctoral thesis, Faculty of Mining, Geology and Petroleum Engineering, Zagreb, 185 p. (*in Croatian*)

Owens, E.H. (2002): Response Strategies for Spills on Land. Spill Science & Technology, 7, 115–117

Patterson, L.A. et al. (2017): Unconventional Oil and Gas Spills: Risks, Mitigation Priorities, and State Reporting Requirements. Environmental Science & Technology, 51, 5, 2563-2573

Simon, K.; Novak K. and Malnar, M. (2013): Leakage Analysis of Gathering Pipelines in Croatia. Proceedings of the 13th SGEM Geo Conference on Science and Technologies In Geology, Exploration and Mining, Albena, Bulgaria, June 16 – 22.

Velić, J., Kišić, K. and Krasić, D. (2016): The Characteristics of the Production and Processing of Oil and Natural Gas in Croatia from 2000 to 2014. The Mining-Geology-Petroleum Engineering Bulletin 2016, 31/2, 69-112.

Žbulj, K. (2021): Odabrani biljni ekstrakti kao inhibitori korozije čelika u proizvodno-transportnim sustavima ugljikovodika (*Extracts of Selected Plants as Steel Corrosion Inhibitors in Hydrocarbon Production and Transportation Systems*). Doctoral thesis, Faculty of Mining, Geology and Petroleum Engineering, Zagreb, 145 p. (*in Croatian*)

Sažetak

Statistička analiza puknuća naftovoda u Hrvatskoj

Aktivnosti istraživanja i proizvodnje nafte i plina predstavljaju određenu prijetnju okolišu. Cjevovodi, kao najučinkovitije transportno sredstvo ugljikovodika, nezamjenjivi su u naftnoj industriji. Korozivni medij koji se transportira pridonosi većem riziku od puknuća i posljedičnog izlijevanja u okoliš. Pristup koji se zasniva na prevenciji i ublažavanju rizika zahtijeva adekvatno održavanje i nadzor cjevovoda. Potrebno je kontinuirano statističko praćenje s ciljem identifikacije dionica s najvećom učestalošću izlijevanja. U tu svrhu obično se koristi deskriptivna statistika. Analize podataka vremenskih serija osiguravaju promatranje trendova i predviđanje budućih ishoda. U radu je prikazana analiza propuštanja cjevovoda u procesima sabiranja i otpreme nafte u kontinentalnom dijelu Hrvatske. Analiza obuhvaća desetogodišnje razdoblje. Kako bi rezultati bili usporedivi s CONCAWE metodologijom, uzeta su u obzir samo puknuća naftovoda koja su rezultirala s izlijevanjem ≥ 1 m^3. Negativan trend izlijevanja u skladu je s nalazima CONCAWE izvješća. Za razliku od CONCAWE-ovog izvješća, gdje je 88 % svih incidenata uzrokovano aktivnostima "treće strane", dok korozija i mehanički kvarovi doprinose pojedinačno s 5 %, odnosno 2 %, u slučaju hrvatskih sabirnih i otpremnih naftovoda, više od 70 % akcidenata uzrokovano je korozijom. Starost cjevovoda i izloženost agresivnim i korozivnim medijima ističe se kao glavni uzrok puknuća. Međutim, uočen je blagi negativni trend kao rezultat rekonstrukcije/zamjene kritičnih dionica cjevovoda

Ključne riječi: transport cjevovodom; izlijevanje nafte; sabirni cjevovod; otpremni cjevovod; statistički alati.

Author's contribution

Karolina Novak Mavar (1) provided conceptualization, methodology and writing original draft preparation. **Katarina Žbulj (2)** provided resources, investigation and formal analysis. **Lidia Hrnčević (3) p**rovided formal analysis and visualisation **Katarina Simon (4)** performed analysis validation and supervision.

Hydrogeochemical facies of groundwater in the influence area of the Velika Gorica well field

Patricia Buškulić[1]; Jelena Parlov[2]

[1] University of Zagreb, Faculty of Mining, Geology and Petroleum Engineering,
Pierottijeva 6, Zagreb, Croatia, ORCID: 0000-0002-6124-9083

[2] University of Zagreb, Faculty of Mining, Geology and Petroleum Engineering,
Pierottijeva 6, Zagreb, Croatia, ORCID: 0000-0002-2862-7222

Abstract

This research defines hydrogeochemical characteristics in the influence area of the Velika Gorica well field, which is located in the southern part of the Zagreb aquifer. Investigated area is characterized by various lithology, pedology, hydraulic properties and land use. The three main factors that determine the chemical characteristics of groundwater are the petrographic composition of soil and aquifer, the permeability and hydrological system topography. According to the amount of the dissolved substance and chemical composition, groundwater can be divided into hydrogeochemical facies. The data used to define the hydrogeochemical facies were provided by Croatian Waters. The EC value of groundwater indicates a low enrichment of salts, as well as the value of pH indicates an alkaline groundwater. The water samples were classified as very hard, as the TH is more than 300 mg/L. Ca^{2+} is the dominant ion among the cations with a mean value of 108.4 mg/L. The predominant ion dissolved in groundwater samples is HCO_3^- with a mean value of 393.9 mg/L. According to the results, the groundwater in the influence area of the Velika Gorica well field can be determined as the $CaMgHCO_3$ water type, which coincides with the results of previous research.

Keywords: groundwater, hydrogeochemical facies, Piper diagram, Zagreb aquifer

1. Introduction

The groundwater of the Zagreb aquifer is the only source of potable water for the citizens of the Zagreb County and part of the country's strategic water reserves. Nowadays, the Zagreb aquifer is threatened due to increasing concentrations of pollutants and decreasing water quantity (**Nakić et al., 2013**). The Velika Gorica well field is one of the major well field and consists of five wells which provide drinking water for the City of Zagreb and the City of Velika Gorica.

The chemical quality of groundwater reflects the combined effects of numerous processes along the groundwater flow path. The quality is affected by the chemical composition of the rocks, sediments, and soils through which it moves under numerous physico-chemical conditions. Subsurface water flow is generally very slow, and water has sufficient time to react with the rocks and sediments (**Fetter, 1988**). In addition, water changes its chemical composition through other processes such as ion exchange, oxidation, reduction, biological processes, etc. (**Schoeller, 1959**).

Water quality analyses vary in completeness, from a basic analysis of major species to a more detailed analysis that include minor and trace elements, dissolved gases, bacteria, contaminants etc. Drinking water quality monitoring requires a more comprehensive list of analytes (**Clark, 2015**).

To understand the chemical composition of groundwater, the concentrations of the major cations and anions should be determined because they contribute most to the ionic strength of a solution. The three most important factors affecting the chemical characteristics of groundwater are the petrographic composition of the soil and aquifer, the permeability, and the topography of the hydrological system (**Halle, 2004**). Depending on the chemical composition and amount of dissolved substances, water can be classified into groups, i.e. hydrogeochemical facies. The Piper diagram is the most commonly used graphical representation of water composition in hydrogeology and is a very powerful tool for visualizing the relative abundance of major ions in groundwater samples (**Halle, 2004**). While, there are other types of diagrams that can be used to show the abundance of ions in water, this type of diagram is particularly useful because it allows multiple samples to be plotted on the same diagram and the differences in their chemistry are immediately apparent.

According to the results of previous research (**Nakić et al., 2005; Vlahović et al., 2009; Parlov et al., 2019**), the groundwater in the shallower aquifer part belongs to the calcium-magnesium-hydrogen carbonate ($CaMgHCO_3$) type.

Corresponding author: Patricia Buškulić
patricia.buskulic@rgn.unizg.hr

The main goal of the research presented in this paper was to determine the hydrogeochemical characteristics in the influence area of the Velika Gorica well field. For this purpose, geochemical data of groundwater, statistics of chemical parameters and Piper diagrams were used.

2. Materials and methods

Hydrogeochemical investigations in the Zagreb aquifer are carried out on 4 monitoring wells (**Figure 1**), located near the Velika Gorica well field.

2.1. Investigated area

The Zagreb aquifer is situated in the northwestern part of the Republic of Croatia along the Sava River, between the Medvednica Mountain in the north and the hills of Vukomeričke Gorice in the south. It covers an area of about 350 km². The studied area is located in the southern part of the Zagreb aquifer (**Figure 1**).

The Zagreb aquifer is an unconfined aquifer and it consists of three major units: unsaturated zone, shallow layer and deep layer. The thickness of the unsaturated zone in the Zagreb region varies from two meters (SE part) to eight meters (NW part). The lower part of this zone contains gravels, while the upper part is composed of silty to sandy material (**Ružičić et al., 2012**). The aquifer layers composed of unconsolidated Quaternary sediments that are mainly consisting of sand, gravel and silt or silty clays. These sediments were deposited during the Middle and Upper Pleistocene and the Holocene (**Velić & Saftić, 1991**). The deep layer contains Pleistocene lacustrine-marshy deposits, while the shallow layer contains Holocene alluvial deposits of the Sava River (**Velić & Durn, 1993; Velić et al., 1999**). The shallow aquifer is in direct hydraulic connection with the Sava River, which is the main source of groundwater recharge (**Posavec et al., 2017**). Fluctuations in the water level of the Sava River primarily influence changes in the groundwater levels. During high water, the Sava River gives water to the aquifer, while during low and medium water it drains the aquifer (**Posavec, 2006**). The general groundwater flow direction is from west to east or south-east, which coincides with the flow direction of the Sava River. The area of the Zagreb aquifer system consists of three major pedological units: Fluvisols, Stagnic Podzoluvisols and Eutric Cambisols on the Holocene deposits (**Bogunović et al., 1998**).
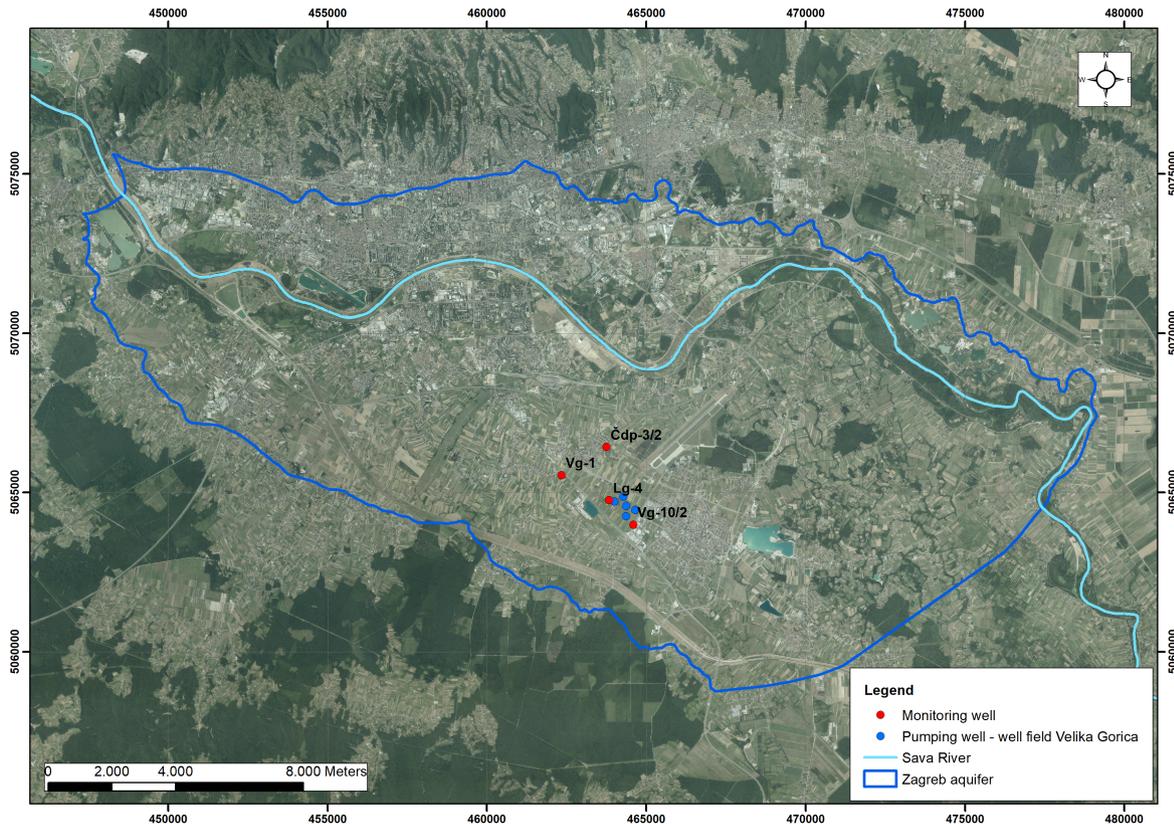

Figure 1: Location of monitoring wells in the influence area of the Velika Gorica well field

2.2. National monitoring of groundwater

Data used to define hydrogeochemical characteristics in the influence area of the Velika Gorica well field were provided by Croatian Waters for each monitoring well in the form of an Excel file. The total number of analyses was 410 for the period from 2001 to 2020. The raw data were sorted, filtered and processed. The research was based on the following hydrochemical parameters: electrical conductivity (EC), pH, total hardness (TH), calcium (Ca^{2+}), magnesium (Mg^{2+}), sodium (Na^+), potassium (K^+), bicarbonate (HCO_3^-), chloride (Cl^-), sulphate (SO_4^{2-}), fluoride (F^-) and nitrate (NO_3^-). During data preparation, 352 analyses with incorrect data, laboratory results below detection or quantitation limits and incomplete anion-cation measurements were removed.

2.3. Charge balance error

The validity and reliability of a geochemical analysis can be tested by comparing the sum of negative charges with the sum of positive charges in solution. Laboratory analyses were converted to equivalents or milliequivalents (meq/L = (mg/L) x valence/atomic mass) for major cations and anions (**Clark, 2015**). The total concentration of cations, Ca^{2+} + Mg^{2+} + Na^+ + K^+ in milliequivalents per liter, should be equal to the total concentration of anions, Cl^- + HCO_3^- + CO_3^{2-} + SO_4^{2-} expressed in the same units. The following **Equation 1** was used to calculate the charge balance error of each water sample (**Freeze & Cherry, 1979**):

$$Charge\ balance\ error = \left(\frac{\sum Cations - \sum Anions}{\sum Cations + \sum Anions}\right) \times 100 \tag{1}$$

The groundwater quality data measurement is considered acceptable if the error of the ion balance is ± 10%, otherwise the measurement does not pass the validation test (**Katz & Collins, 1998**). Among the 58 analyses, 6 analyses had been excluded due to an error of more than ± 10% and therefore research work was continued with 52 analyses.

2.4. Piper diagram

Hydrogeochemical facies were determined from Piper diagrams created by the Visual Basic macro in Microsoft Excel. The concentrations of major anions (Cl^-, HCO_3^-, CO_3^{2-}, SO_4^{2-}) and cations (Ca^{2+}, Mg^{2+}, Na^+, K^+) were used to generate the Piper diagrams. The criteria for determining the hydrogeochemical facies are shown in **Figure 2**.

Figure 2: Hydrogeochemical facies in Piper diagram (**Freeze & Cherry, 1979; modified by Buškulić, 2019**)

2.5. Statistical tests

Statistical methods were used to calculate the arithmetic mean (**Equation 2**), standard deviation (**Equation 3**) and coefficient of variation (**Equation 4**) for 12 chemical parameters (EC, pH, TH, Ca^{2+}, Mg^{2+}, Na^+, K^+, HCO_3^-, Cl^-, SO_4^{2-}, F^- and NO_3^- of 52 groundwater samples, using Microsoft Excel. This reflects a significant impact on hydrogeochemical conditions.

$$Arithmetic\ mean\ (\bar{x}) = \left(\frac{\sum x_i}{n}\right) \tag{2}$$

Where are:
x_i – each value in the data set,
n – total number of values in the data set.

$$Standard\ deviation\ (\sigma) = \sqrt{\sum \frac{(x_i - \bar{x})^2}{n}} \tag{3}$$

Where are:
x_i – each value in the data set,
$\bar{x}$ – mean of all values in the data set,
n – total number of values in the data set.

$$Coefficient\ of\ variation\ (CV) = \left(\frac{\sigma}{\bar{x}}\right) \times 100 \tag{4}$$

Where are:
σ – standard deviation,
$\bar{x}$ – mean of all values in the data set.

3. Results and discussion

Statistics of chemical parameters, Piper diagrams, and hydrogeochemical facies were obtained after data preparation and the cation-anion balance procedure for a total of 52 analyses and for 4 monitoring wells, respectively. The EC is the ability of materials to conduct electric current. The higher EC is, the greater the enrichment of dissolved salts in groundwater. The EC value of groundwater samples ranges from 470 to 802 µS/cm, with a mean value of 705.6 µS/cm (**Table 1**), indicating low enrichment of salts (EC < 1,500 µS/cm).

The pH is a measure of how acidic or basic the water is. The pH varies from 7.1 to 7.4 (**Table 1**), with a mean value of 7.3, indicating that the groundwater is alkaline. The main ions responsible for TH are Ca^{2+} and Mg^{2+}. The value of TH ranges from 308 to 472 mg/L (**Table 1**), therefore the water samples can be classified as very hard because TH is more than 300 mg/L (**Davis & Dewiest, 1966**).

The concentration of Ca^{2+} varies from 83.2 to 127 mg/L, while the concentration of Mg^{2+} ranges from 16.5 to 50.4 mg/L (**Table 1**). Among the cations, Ca^{2+} is the dominant ion with a mean value of 108.4 mg/L. The concentration of Na^+ varies between 4.5 and 13.9 mg/L, with a mean value of 8.3 mg/L (**Table 1**). The value of K^+ ranges from 1.1 to 2.1 mg/L, which is the lowest concentration among the cations (**Table 1**).

The content of HCO_3^- ranges from 292.9 to 439.3 mg/L, with a mean value of 393.9 mg/L (**Table 1**), the dominant ion dissolved in groundwater. The higher concentration of HCO_3^- in water indicates dominance of mineral dissolution (**Stumm & Morgan, 1996**). The value of Cl^- ranges from 11.9 to 24.3 mg/L (**Table 1**), with a mean value of 17.8 mg/L. The concentration of SO_4^{2-} ranges from 27.6 to 38.2 mg/L, making it the second largest ion among the anions after bicarbonate (**Table 1**). The values of F^- in groundwater range from 0.01 to 0.7 mg/L, while the concentration of NO_3^- varies from 10.2 to 23.5 mg/L (**Table 1**). In areas not affected by human activities and pollution, NO_3^- concenration in water does not exceed 10 mg/L (**Panno et al., 2006**), so these higher concentrations indicate anthropogenic pollution.

Parameters	Unit	Min	Max	Mean	SD	CV	MCL
EC	μS/cm	470.0	802.0	705.6	62.6	8.9	2500
pH	pH unit	7.1	7.4	7.3	0.1	1.1	6.5 – 9.5
TH	$CaCO_3$ mg/L	308.0	472.0	395.6	27.8	7.0	-
Ca^{2+}	mg/L	83.2	127.0	108.4	9.4	8.6	-
Mg^{2+}	mg/L	16.5	50.4	27.9	5.4	19.4	-
Na^+	mg/L	4.5	13.9	8.3	1.8	22.0	200
K^+	mg/L	1.1	2.1	1.6	0.3	21.6	12
HCO_3^-	mg/L	292.9	439.3	393.9	28.7	7.3	-
Cl^-	mg/L	11.9	24.3	17.8	3.7	20.6	250
SO_4^{2-}	mg/L	27.6	38.2	32.4	3.1	9.5	250
F^-	mg/L	0.01	0.7	0.1	0.1	165.6	1.5
NO_3^-	mg/L	10.2	23.5	16.7	3.7	22.3	50

Table 1: Statistics of groundwater quality parameters. EC is electrical conductivity at 25 °C, TH is total hardness, SD is standard deviation, CV is coefficient of variation in %, MCL is maximum contaminant level, μS/cm = microSiemens per centimetre, mg/L = milligram per liter

According to the results, groundwater belongs to calcium-magnesium-hydrogen carbonate water type ($CaMgHCO_3$) in 51 analyses and only one sample belongs to calcium-hydrogen carbonate type of water ($CaHCO_3$) (**Figure 3**). In September 2001, 177 mm of rain fell in Zagreb County, twice as much as usual for that time of year. The different hydrogeochemical facies of that one sample could be due to the extreme rainfall. In addition, monitoring well Čdp-3/2 is very shallow and captures mainly freshly infiltrated precipitation water that has not yet had time to react with the surrounding rocks and sediments. Therefore, the groundwater in the influence area of the Velika Gorica well field can be assigned to the $CaMgHCO_3$ type of water which coincides with the results of previous research.
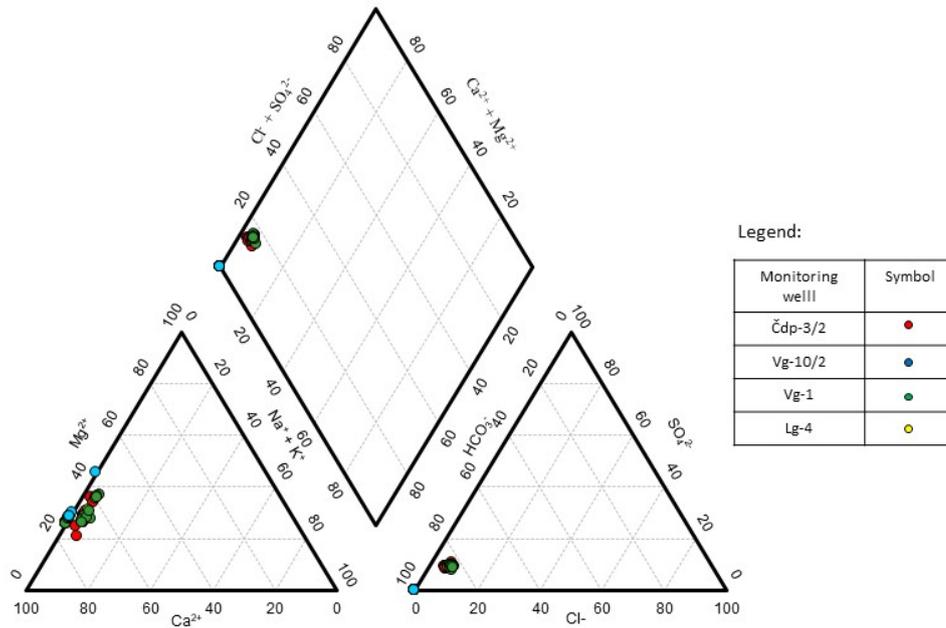
Figure 3: Piper diagram showing the hydrogeochemical facies of groundwater, in the influence area of the Velika Gorica well field, based on the data of 52 water analyses

4. Conclusions

The Velika Gorica well field is located in the southern part of the Zagreb aquifer. Velika Gorica is one of the major well fields and consists of five wells that supply the City of Zagreb and the City of Velika Gorica with drinking water. According to the chemical composition and amount of dissolved substances, water can be classified into hydrogeochemical facies, as well as Piper diagram is mostly used graphical representation of water composition in hydrogeology and very powerful tool. The data used to define the hydrogeochemical characteristics in the influence area of the Velika Gorica well field were provided by Croatian Waters. Research was based on the following hydrochemical parameters: electrical conductivity (EC), pH, total hardness (TH), calcium (Ca^{2+}), magnesium (Mg^{2+}), sodium (Na^+), potassium (K^+), bicarbonate (HCO_3^-), chloride (Cl^-), sulphate (SO_4^{2-}), fluoride (F^-) and nitrate (NO_3^-). The statistics of chemical parameters and hydrogeochemical facies were obtained after the data preparation and charge balance error procedure for a total of 52 analyses (4 monitoring wells). The EC value of groundwater indicates a low enrichment of salts (EC < 1,500 µS/cm), as well as the value of pH indicates an alkaline groundwater. The water samples were classified as very hard, as the TH is more than 300 mg/L. Ca^{2+} is the dominant ion among the cations with a mean value of 108.4 mg/L. The value of K^+ ranges from 1.1 to 2.1 mg/L, which is the lowest concentrations among the cations. The content of HCO_3^- ranges from 292.9 to 439.3 mg/L, with a mean value of 393.9 mg/L. It is the predominant ion dissolved in groundwater. The concentration of SO_4^{2-} ranges from 27.6 to 38.2 mg/L. Thus, SO_4^{2-} is the second largest ion among anions after bicarbonate. In areas not affected by human activities and pollution, NO_3^- concentration in water does not exceed 10 mg/L, so higher nitrate concentration in these groundwater samples indicates anthropogenic pollution. According to the results, groundwater belongs to the calcium-magnesium-hydrogen carbonate type of water ($CaMgHCO_3$) in 51 analyses and one sample belongs to calcium-hydrogen carbonate type of water ($CaHCO_3$). Accordingly, the groundwater in the influence area of the Velika Gorica well field mostly belongs to a $CaMgHCO_3$ type of water.

5. References

Bačani, A. and Posavec, K. (2009): Elaborat zaštitnih zona vodocrpilišta Velika Gorica. Fond stručnih dokumenata Zagrebačke županij (*Study of protection zones of the Velika Gorica well field. Zagreb county documents fund*). 2-39. (*in Croatian without abstract in English*)

Bogunović, M., Vidaček, Ž., Husnjak, S. and Sraka, M. (1998): Inventory of soils in Croatia. Agriculturae conspectus scientificus, 63, 105-112.

Buškulić, P. (2019): Hidrogeokemijske značajke podzemne vode u panonskom dijelu Republike Hrvatske (*Hydrogeochemical characteristics of groundwater in the Panonian part of the Republic of Croatia*). Master's Thesis, University of Zagreb, Faculty of Mining, Geology and Petroleum Engineering. (*in Croatian*)

Clark, I. (2015): Groundwater geochemistry and isotopes. Taylor and Francis Group, Boca Raton, 456 p.

Davis, S.N., and Dewiest, R.J.M. (1966): Hydrogeology. Wiley, New York, 463 p.

Fetter, C.W. (1988): Applied hydrogeology. Charles E. Merrill, Columbus.

Freeze, R.A. and Cherry, J.A. (1979): Groundwater. Prentice-Hall Inc., Englewood Cliffs, New Jersey, 604 p.

Halle, R. (2004): Kemizam i obradba vode (*Chemistry and water treatment*). University of Zagreb, Faculty of Mining, Geology and Petroleum Engineering, Zagreb.

Katz B. G. and Collins J. J. (1998): Evaluation of chemical data from selected sites in the Surface-Water Ambient Monitoring Program (SWAMP) in Florida. Open-File Report, 98-559, USGS, p. 4.

Nakić, Z., Horvat, S. and Bačani, A. (2005): Statistical indicators of groundwater geochemical characteristics in a quaternary aquifer from the Mala Mlaka well field catchment area (Zagreb, Croatia). Geologia Croatica, 58, 87-99.

Nakić, Z., Ružičić, S., Posavec, K., Mileusnić, M., Parlov, J., Bačani, A. and Durn, G. (2013): Conceptual model for groundwater status and risk assessment – case study of the Zagreb aquifer system. Geologia Croatica, 66, 55-76, doi: 10.4154/gc.2013.05.

Panno, S., Kelly, W., Martinsek, A. and Hackley, K.C. (2006): Estimating background and threshold nitrate concentrations using probability graphs. Groundwater, 44, 697-709.

Parlov, J., Kovač, Z., Nakić, Z. and Barešić J. (2019): Using water stable isotopes for identifying froundwater recharge sources of the unconfined alluvial Zagreb aquifer (Croatia). Water, 11, doi:10.3390/w11102177.

Posavec, K. (2006): Identifikacija i prognoza minimalnih razina podzemne vode zagrebačkog aluvijalnog vodonosnika modelima recesijskih krivulja (*Identification and prediction of minimum ground water levels of Zagreb alluvial aquifer using recession curve models*). PhD Thesis, University of Zagreb, Faculty of Mining, Geology and Petroleum Engineering. (*in Croatian*)

Posavec, K., Vukojević, P., Ratkaj, M. and Bedeniković, T. (2017): Cross-correlation modelling of surface water-groundwater interaction using the Excel spreadsheet application. Rudarsko Geolosko Naftni Zbornik., 32, 25-32.

Ružičić, S., Mileusnić, M. and Posavec, K. (2012): Building conceptual and mathematical model for water flow and solute transport in the unsaturated zone at Kosnica site. Rudarsko Geolosko Naftni Zbornik, 25, 21-31.

Schoeller H (1959): Arid zone hydrology, recent developments. UNESCO, Paris

Stumm, W. and Morgan, J. J. (1996): Aquatic chemistry. Wiley, New York, 1022 p.

Velić, J. and Durn, G. (1993): Alternating lacustrine-marsh sedimentation and subaerial exposure phases during Quaternary: Prečko, Zagreb, Croatia. Geologia Croatica, 46, 71-90.

Velić, J. and Saftić, B. (1991): Subsurface spreading and facies characteristics of middle Pleistocene deposits between Zaprešić and Samobor. Geology Bulletin, 44, 69-82.

Velić, J., Saftić, B. and Malvić, T. (1999): Lithologic composition and stratigraphy of Quaternary sediments in the area of the "Jakuševec" waste depository (Zagreb, Northern Croatia). Geologia Croatica, 52, 119-120.

Vlahović, T., Bačani, A. and Posavec, K. (2009): Hydrogeochemical stratification of the unconfined Samobor aquifer (Zagreb, Croatia). Environ. Geol., 57, 1707-1722, doi 10.1007/s00254-008-1452-4.

Sažetak

Hidrogeokemijski facijesi šireg priljevnog područja crpilišta Velika Gorica

Ovim istraživanjem definirane su hidrogeokemijski facijesi u priljevnom području crpilišta Velika Gorica koje se nalazi u južnom dijelu zagrebačkog vodonosnika. Značajke istraživanog područja su različita litologija, pedologija, hidraulička svojstva i korištenje zemljišta. Tri glavna čimbenika koja određuju kemijska obilježja podzemne vode su

petrografski sastav tla i vodonosnika, propusnost i topografija hidrološkog sustava. Prema količini otopljene tvari i kemijskom sastavu, podzemna voda se može podijeliti na hidrogeokemijske facijese. Facijesi su određeni na temelju podataka nacionalnog monitoringa kakvoće podzemne vode ustupljenih od strane Hrvatskih voda. Podzemna voda je prema pH vrijednosti lužnata, dok EC vrijednosti vode ukazuju na niski sadržaj soli. Podzemna voda je klasificirana kao vrlo tvrda zbog totalne tvrdoće koja iznosi više od 300 mg/L. Ca^{2+} je dominantan ion među kationima sa srednjom vrijednosti od 108.4 mg/L. Dominantan ion otopljen u uzorcima podzemne vode je HCO_3^- sa srednjom vrijednosti od 393.9 mg/L. Prema rezultatima, podzemna voda šireg priljevnog područja crpilišta Velika Gorica pripada $CaMgHCO_3$ tipu vode, što se podudara s rezultatima prethodnih istraživanja.

Ključne riječi: podzemna voda, hidrogeokemijski facijes, Piperov dijagram, zagrebački vodonosnik

Acknowledgment

Author's contribution

Patricia Buškulić (mag. ing. geol., environmental geology) provided overview of the research area, the interpretation and presentation of the results. **Jelena Parlov** (PhD, dipl. ing., Associate Professor, hydrogeology) provided the interpretation of the results.

Testing the validity of "dark data" on the Late Miocene freshwater cockles housed in the CNHM

Anja Jarić Matanović[1]; Marija Bošnjak[2]; Jasenka Sremac[3]

[1] Tratinska ulica 57, 10000 Zagreb, Croatia; ajaric90@gmail.com, https://orcid.org/0000-0003-3364-2280

[2] Croatian Natural History Museum, Demetrova 1, 10000 Zagreb, Croatia, marija.bosnjak@hpm.hr; https://orcid.org/0000-0002-1851-1031

[3] University of Zagreb, Faculty of Science, Horvatovac 102a, 10000 Zagreb, Croatia; jsremac@geol.pmf.hr, https://orcid.org/0000-0002-4736-7497

Abstract

Late Miocene freshwater cockles from the Croatian Natural History Museum (CNHM) were studied in order to recognize the size patterns within the population and reveal the possible subjective approach to the collecting process (size or preservation quality preferences). The most abundant taxa, *Tauricardium baraci* (Brusina, 1884), *Lymnocardium diprosopum* (Brusina, 1884), *L. inflatum* (Gorjanović–Kramberger, 1889), *L. majeri* (M. Hörnes, 1862), *L. riegeli* (M. Hörnes, 1862), *L. rogenhoferi* (Brusina, 1884), *Prosodacnomya vutskitsi* (Brusina, 1902) and *Pseudocatillus simplex* (Fuchs, 1870), from the localities: Okrugljak (SW Medvednica), Glogovnica (S Kalnik), Glogovac (Bilogora) and Kindrovo, were chosen for comparative studies. Relations between the length (L) and height (H) (=surface) and length (L)/height (H)/width (W) (=volume) values were calculated for each taxon and compared within a single species and within the cockle populations from the same locality. Calculations yielded the following results: (1) Volume (L/H/W) compared to surface (L/H) studies proved to be the better choice in population analyses; (2) size distribution values group independently of species dimensions, but can be well correlated within the finding-sites; (3) cockles from Bilogora-Kalnik area show normal value distribution, while all taxa from Okrugljak locality present a similar slight asymmetry of size distribution; (4) such distribution probably points to the different taphonomical processes in these two depositional basins. This research has proved that the CNHM Late Miocene cockle collections can be successfully studied from all paleontological aspects, even when field outcrops are no more available, because fossils were collected objectively, taking all available specimens from the site, regardless of their size or preservation quality.

Keywords: Lymnocardiinae; CNHM collection; biometry; Late Miocene; Croatia

1. Introduction

From the seventies to the present, paleoecology has gained more importance and more attention is given to the sampling methods and criterion, which effect diversity, or recording geographic and stratigraphic data. As a result, many older museum collections lack information that is valuable for modern paleobiological research (e.g., **Lawrence, 1971; Allmon, 2005**). The problem of museum collections has recently emerged and there are not many available studies that could resolve it, but can give a new perspective on the museum „dark data" (**Marshall, 2018**). Because every collection is a case for itself, there is a need to carefully choose which data we want and can get from the chosen collections (e.g., **Dominici et al., 2020**).

Upper Miocene – Panonnian deposits are widely distributed in Northern Croatia (**Figure 1**) and comprise rich findings of freshwater Lymnocardiinae, also known as cockles (e.g. **Basch, 1990; Vrsaljko, 1999; Kovačić et al., 2004; Vrsaljko et al., 2005; Sebe et al., 2020; Magyar, 2021**). Majority of these cockle fossils are today housed in the Croatian Natural History Museum (CNHM). Considering the fact that the original outcrops are no longer available, we numerically analyzed the relations between the surface and volume measured values of the cockle shells housed in the CNHM, in order to study the best promising tool for the population analysis based on the museum collections. We tested the possible size sampling bias during the collecting work, wandering if the museum collection has stored only the biggest and best looking samples or does it include versatility. These results may affect further research and our ability to include the museum samples in the paleobiological studies.

Specimens for this research were chosen from three localities in Northern Croatia (**Figure 1**), which yielded so far the richest collections of cockle species housed in the CNHM. Analysis of these cockles is a part of the test model for A. Jarić Matanović PhD dissertation, where part of the Upper Miocene cockles from northern Croatia will be studied.

Corresponding author: Anja Jarić Matanović
ajaric90@gmail.com

Analyzed Lymnocardiinae were collected from the Upper Miocene – Pannonian – *Rhomboidea* beds at the Okrugljak locality, Bilogora and Kalnik area (**Figure 1**). Okrugljak locality is situated near Zagreb, the capital of Croatia, but outcrops are no longer available, due to the expansion of buildings and tram rails. Fossil cockles were mostly collected by **Brusina** (**1874, 1897, 1902**) and **Kiseljak** (**1889**). After exploring the Okrugljak area, I. Kiseljak in agreement and advised by S. Brusina, set out to explore the Glogovnica locality (Kalnik Mt.), which is the second analyzed locality in this paper (**Figure 1; Kochansky-Devidé, 1982**), described in **Poljak and Šuklje** (**1934**), with the age of fossils belonging to the Pannonian (after **Šimunić et al., 1990**). Third locality is Glogovac locality (Bilogora Mt.) (**Figure 1**), where **Šuklje** (**1933**) processed the coal mine macrofauna of fossil mollusks and concluded that their age is the upper Pannonian *Rhomboidea* beds. The latest revision on Lymnocardiinae from the CHNM collections was made by **Basch** (**1990**) and the results are included in this analysis.
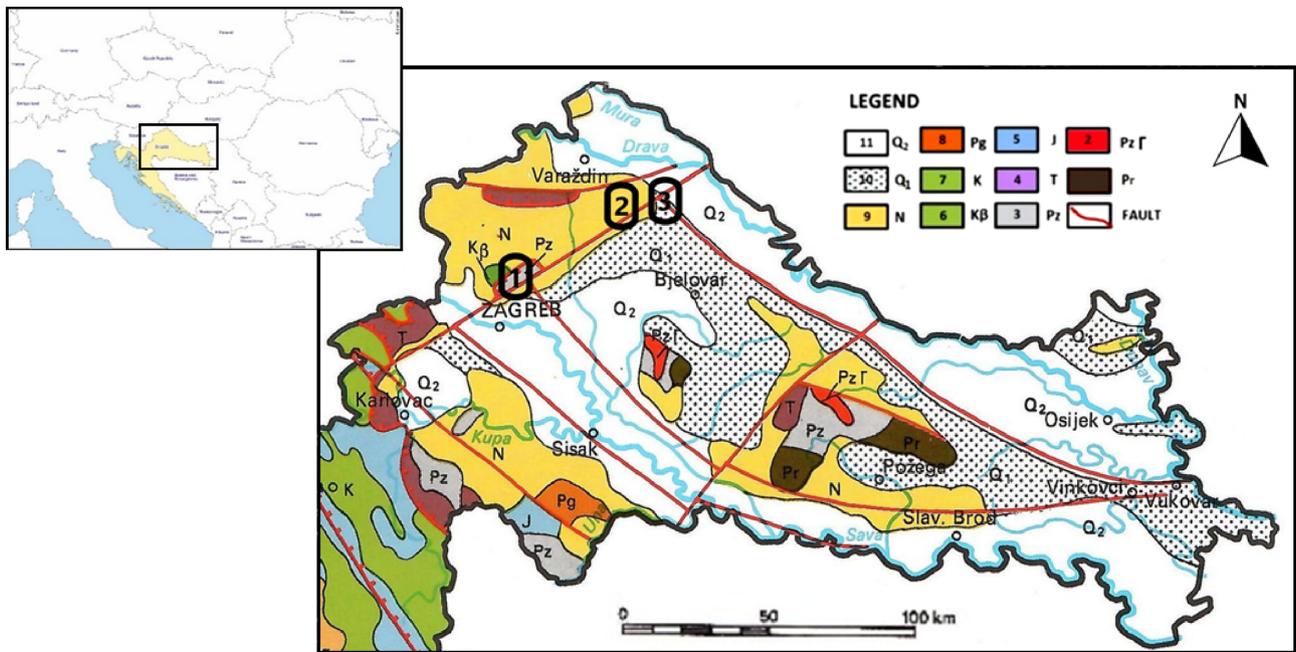

Figure 1: Geographic position of studied localities in Northern Croatia (modified after **Velić and Velić 1995**; https://d-maps.com/carte.php?num_car=2242&lang=en: 1. Okrugljak locality; 2. Glogovnica (Kalnik Mt.); 3. Glogovac Bilogora Mt.). Legend (after **Sremac et al., 2022**): 1. Precambrian metamorphic rocks; 2. Paleozoic granites; 3. Paleozoic sedimentary rocks; 4. Triassic carbonates, sporadically clastites; 5. Jurassic carbonates with scarce volcanoclastites; 6. Cretaceous dominantly carbonate rocks; 7. Cretaceous basalts; 8. Paleogene limestones; 9. Neogene clastic and carbonate rocks; 10. Pleistocene, dominantly unconsolidated clastites; 11. Holocene unconsolidated clastites.

2. Materials and methods

For the here presented numerical analysis, 402 fossil cockles from the CNHM collection were measured. Analyzed specimens include four species from Okrugljak locality, two species from Glogovnica locality, one species from Glogovac locality and one species from Kindrovo locality (**Table 1, Figure 1**). Specimens of *Pseudocatillus simplex* from Kindrovo were too fragile so they were excluded from the further analysis, although the number of specimens was sufficient. Species *Lymnocardium majeri* is also excluded from the numerical analysis, because most of the smaller specimens were stored in sealed tubes. For this occasion, these small specimens were not available for measurement, and the authors did not include this species further because the lack of smaller measurements would affect the analysis results.

CNHM Inventory number	Species	Number of specimens	Locality
83., 84., 85., 86., 87., 811., 813.	*Lymnocardium rogenhoferi* (Brusina, 1884)	34	Okrugljak
73., 74., 75., 76., 77., 78., 79., 80.	*Lymnocardium majeri* (M. Hörnes, 1862)	69	Okrugljak
63., 64., 65., 66., 67., 68., 69., 70., 71.	*Lymnocardium riegeli* (M. Hörnes, 1862)	145	Okrugljak
88., 89., 90., 816., 817.	*Tauricardium baraci* (Brusina, 1884)	52	Okrugljak
715., 716.	*Lymnocardium inflatum* (Gorjanović-Kramberger, 1899)	13	Glogovnica
748.	*Lymnocardium diprosopum* (Brusina, 1884)	25	Glogovnica
682., 683.	*Prosodacnomya vutskitsi* (Brusina, 1902)	41	Glogovac
1168., 1169., 1170.	*Pseudocatillus simplex* (Fuchs, 1870)	23	Kindrovo

Table 1: List of the analyzed Late Miocene cockles from the CNHM collection. Grey shaded rows show specimens which were not included in the analysis.

All cockle shells were measured for their length (L), height (H) and width (W) using a digital caliper (**Figure 2**). Each shell was categorized according to its state of preservation, ranging from (1) best preserved (all shell elements are visible and in good condition allowing the determination), (2) partly preserved cockles (part of the valve missing, but still allowing measuring), and (3) poorly preserved cockles (could not be measured or determined because of the incomplete preservation of the shell). There are grades in between numbers, for example 1 to 2 if there is a small piece missing, but all of the essential parts for determination are present; or 2 to 3 for cockles that are filled with sediment and the inner side of the shell is not visible. The measurements were made on samples belonging to categories 1 and 2.
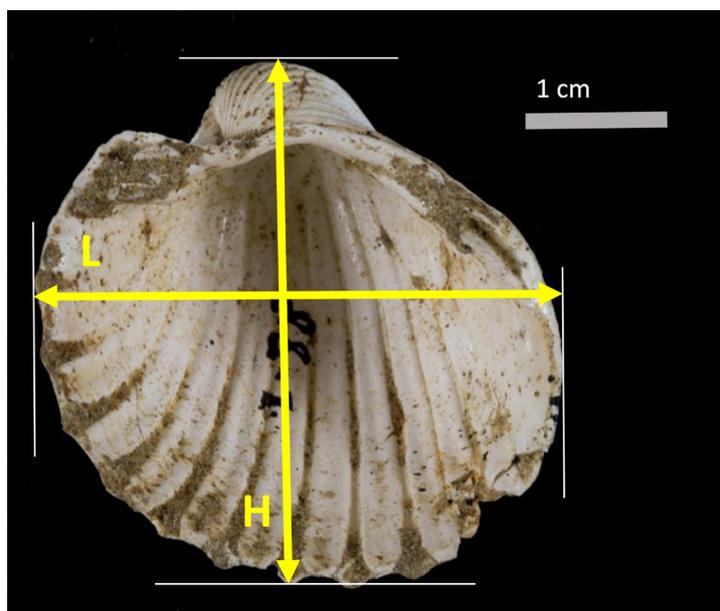

Figure 2: Measured elements on the analyzed cockles. L = shell length; H = shell height

From the measurements of shells, volume (V) was calculated by **Equation 1** and converted to dm^3 for better result visibility.

$$V = \frac{L * H * W}{1000}$$ (1),

Where are:
V = shell volume (dm³),
L = shell length (mm),
H = shell height (mm),
W = shell width (mm).

From all measured shell volumes, average and standard deviation were calculated using the standard formulas in the Microsoft Office Excel. The Normal distribution is calculated by (**Equation 2**).

=NORM.DIST(Ax,Cx,Dx,FALSE) (2),

Where are:
NORM.DIST. – normal distribution,
A, C, and D columns included in the equation,
x – row number in wich the calculation is performed.

The result is shown in the form of a Bell Curve which was constructed on the resulting calculations of the Volume and Normal distribution in Microsoft Office Excel. Shell surface was calculated in order to portray the situations where samples could not be measured by hand, but only from photographs without the lateral view and therefore width could not be measured. These calculations were made using the **Equation 3**, and the results are divided by 100 so they would be in in the same range as the volume.

$$S = \frac{L * H}{100}$$ (3),

Where are:
S = shell surface (cm²),
L = shell length (mm),
H = shell height (mm).

3. Results

The derived normal distribution of the shell volume and surface curves for measured cockles (**Table 1**) are shown in **Figures 3 and 4**. As it can be seen in **Figure 3**, shell volume bell curves have peaks in the middle or near the middle of the curve and a proper layout of the curve. This characteristic of the shell volume curve is present in species from all studied localities.

Looking at the normal distribution shell surface curve (**Figure 4**), there is a shift to the left in the bell curve of *Prosodacnomya vutskitsi*, and the species *Lymnocardium riegeli* is showing the better shaped bell curve than in the case of the shell volume curve (**Figure 3**). Other species are showing more or less similar shape of the shell surface curves (**Figure 4**), except the species *Tauricardium baraci* which is still shifted to the left.

Comparing the sampling locations by shell surface and volume curves, they cannot be linked (**Figures 1, 3 and 4**). In the Kalnik – Bilogora specimens these are slightly shifted to the right, but the curve itself has the same pattern of appearance. Specimens of *Lymnocardium diprosopum* and *Prosodacnomya vutskitsi* display a shift to the right, but *L. diprosopum* still kept the standard normal distribution curve appearance. Specimens of *L. inflatum* are similar to *L. rogenhoferi* resulting with a more prominent peak in the surface measurements. Okrugljak specimens have more diverse results than the Kalnik – Bilogora ones. Specimens of *Tauricardium baraci* are showing shell surface curve very similar to the volume, and for this purpose it can be considered as the same. Comparing shell surface results to volume, the Okrugljak samples of *Lymnocardium rogenhoferi* show a more prominent peak in the surface measurements, and *L. riegeli* shell surface has centered normal distribution curve (**Figures 3 and 4**).
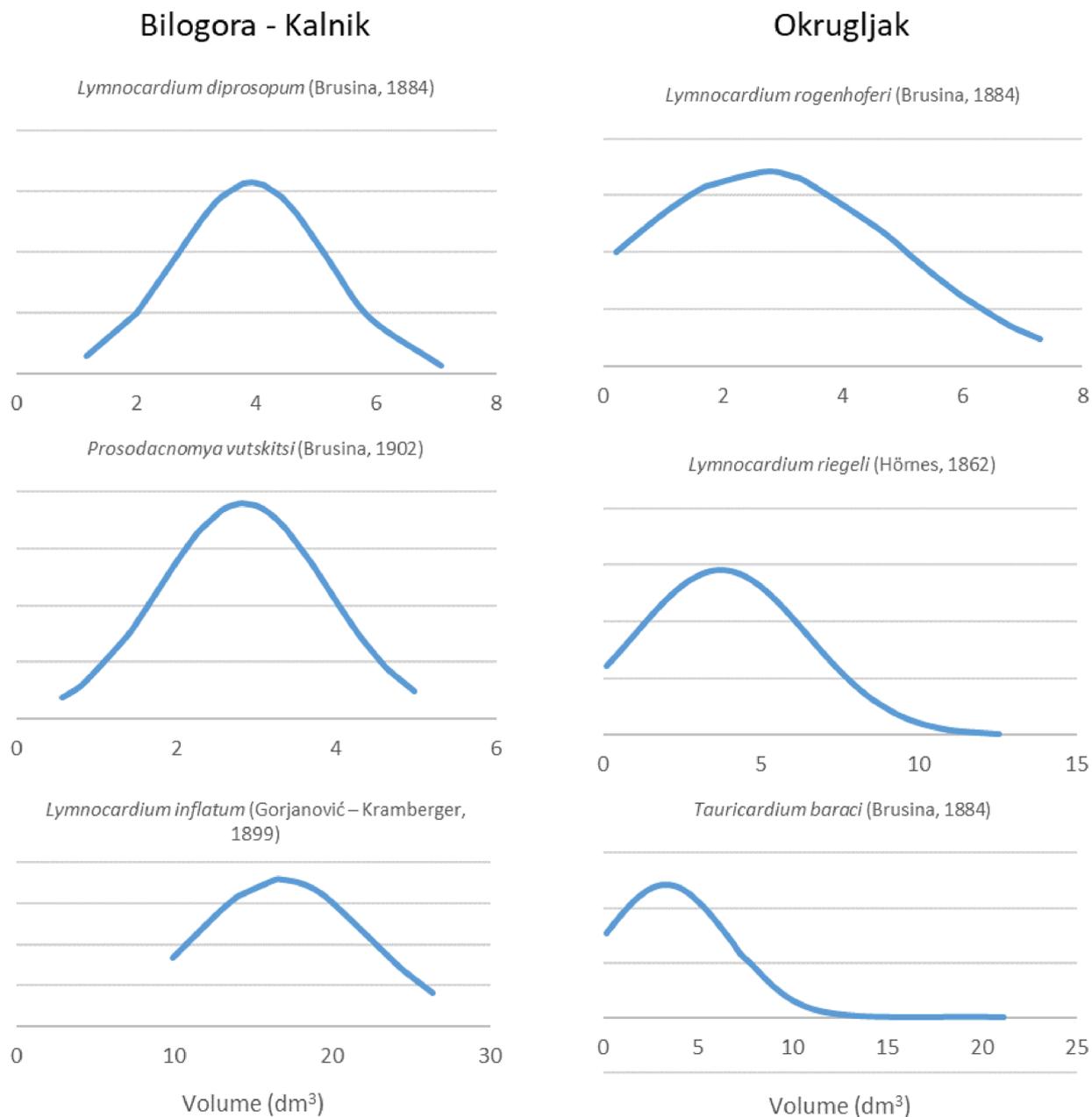
Bilogora - Kalnik

Okrugljak

Figure 3: Normal distribution shell volume curves of Lymnocardiinae after **Table 1**
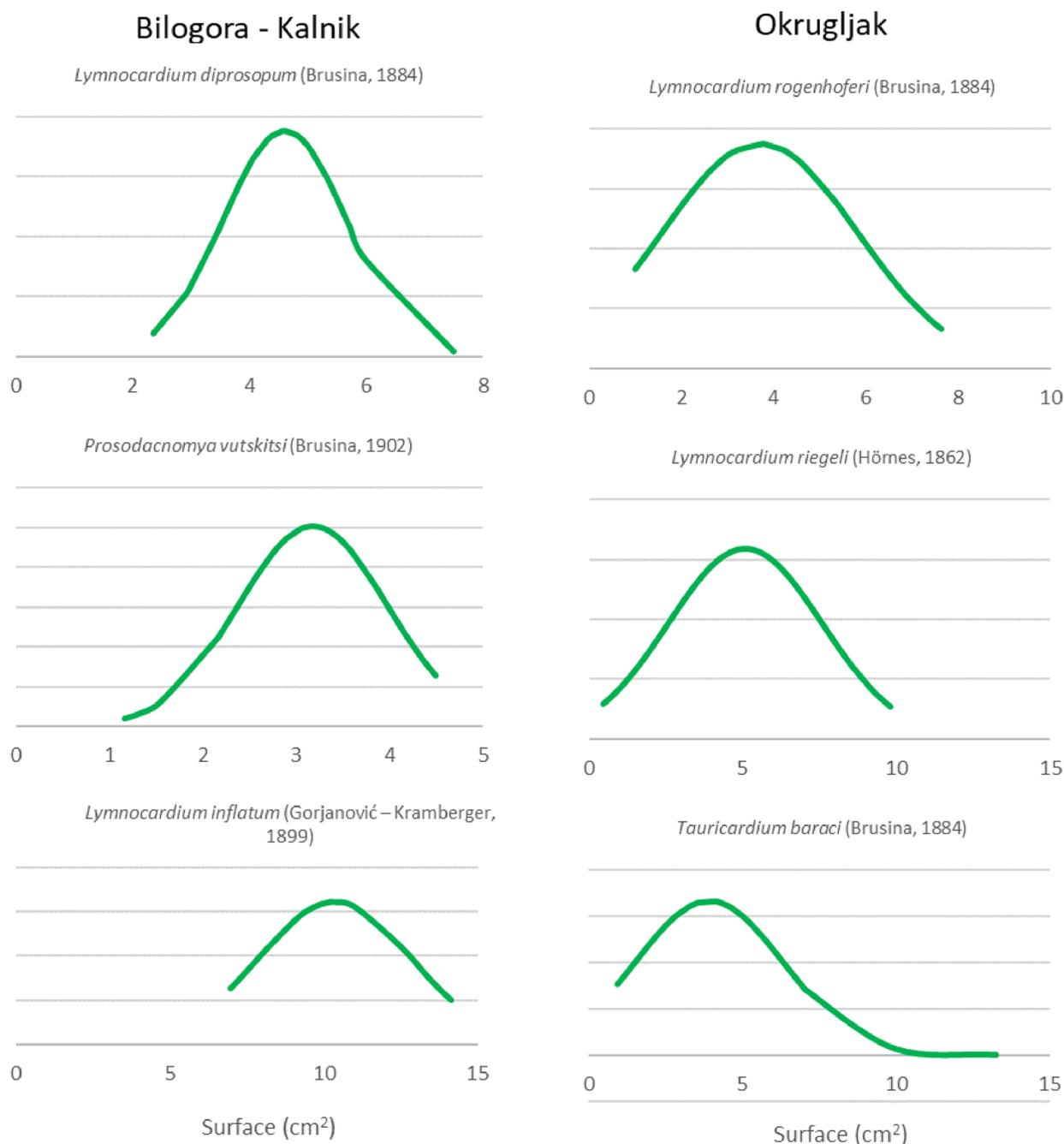
Figure 4: Normal distribution shell surface curves of Lymnocardiinae after **Table 1**

4. Discussion and conclusions

Lymnocardiinae bivalves belong to the Cardiidae family, named for rounded shells that are bilaterally symmetrical, and shaped like a heart when viewed laterally. There are numerous records of their findings in the Upper Miocene deposits (e.g. **Basch, 1990; Magyar et al., 1999; Müller et al., 2007; Sebe et al., 2020**). The Upper Miocene in the Croatian part of the Pannonian Basin is characterized by the isolation from the marine areas and by the formation of the long-lived brackish Lake Pannon (e.g., **Magyar et al., 1999; Pavelić and Kovačić, 2018**). The progradation of deltas from the north was the main force that was reducing the area of the Lake Pannon (e.g., **Magyar et al., 1999**). The youngest sediments deposited in the Lake Pannon are *Rhomboidea* beds, which can be found on elevated areas along the

mountain massifs of Northern Croatia (**Figure 5**), that emerged from the Lake Pannon during one or more time intervals (e.g., **Basch, 2009; Sebe et al., 2020**). *Rhomboidea beds* covered a great part of Northern Croatia and include the here analyzed Okrugljak and Bilogora-Kalnik localities (Glogovnica and Glogovac) which belonged to the margins of the Lake Pannon (**Figures 1** and **5**).
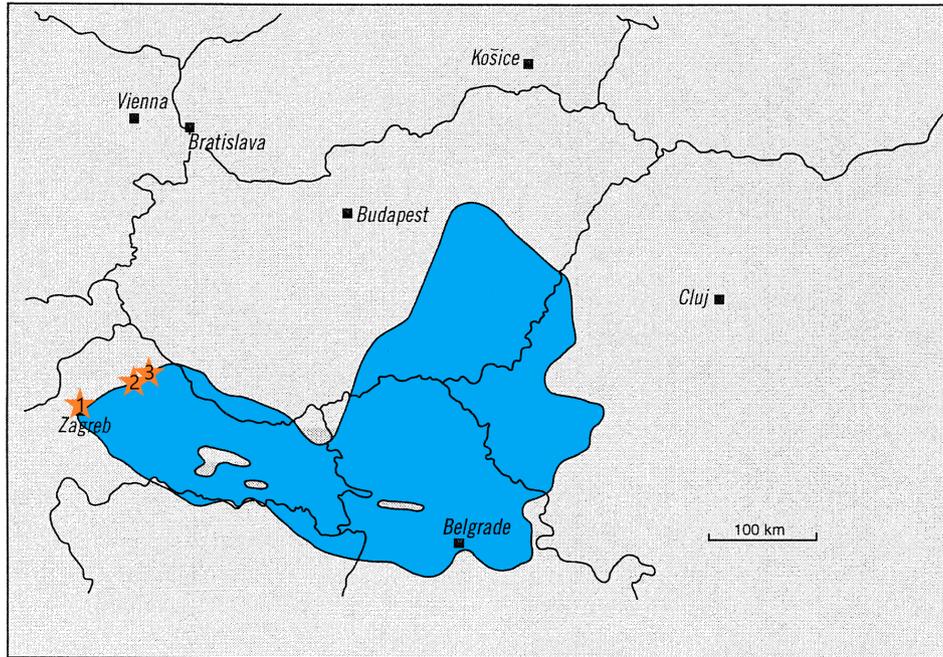

Figure 5: Distribution of the Lake Pannon deposits during the Upper Miocene – Rhomboidea beds, with marked localities presented in this paper (modifed after **Magyar et al., 1999**). Legend: 1 – Okrugljak locality; 2 - Glogovnica (Kalnik Mt.); 3 - Glogovac Bilogora Mt.).

In previous papers, Upper Miocene deposits of Northern Croatia were stratigraphically divided in the Pannonian and Pontian stages (**Figure 6**). After the study of **Mandic et al.** (**2015**), part of the Croatian geologists accepted the proposal to exclude the two-partite division (into the Pannonian and Pontian) and equalize the North Croatian Upper Miocene deposits with the single, Pannonian stage, keeping the division into the four fossiliferous horizons, including the here studied, youngest, *Rhomboidea* beds (e.g., **Mandic et al., 2015; Pavelić and Kovačić, 2018** and references therein), as shown in **Figure 6**.

Figure 6: Chronostratigraphic divison of the Upper Miocene deposits in Northern Croatia (modified after **Pavelić and Kovačić, 2018; Sebe et al., 2020**)

At the end of the Pannonian (**Figure 6**), frequent regressions took place in some parts of the basin (**Šimunić et al., 1990**). Shallowing caused the formation of wetlands, with accelerated vegetation growth under the favorable climatic conditions. After the repeated terrain sinking and the deposition of new layers of clay and sand, lignite was formed from plants and other organic material (**Šimunić et al., 1990**). Unlike Okrugljak locality, Bilogora-Kalnik samples are located in the area where coal layers occur (**Šuklje, 1933**). **Burdon et al.** (**2014**) recognized a number of reasons for cockle mortality. Oxygen depletion and organic loadings could be one of the reasons for mass mortalities in cockles. This can be also suggested to the environmental conditions on the Bilogora – Kalnik coast (**Figure 5**). Frequent and sudden changes in the environment of Bilogora – Kalnik area are possibly the reason for the normal distribution shell volume and surface curves to be positioned in the center of the population (**Figures 3 and 4**). The lack of young individuals could be explained through, e.g., (1) oxygen depletion and organic loadings that could possibly have a greater impact on smaller individuals, which caused their mortality, and (2) of predators. Okrugljak specimens have Bell curves that are leaning to the left (**Figures 3 and 4**), which indicates a larger number of younger members of the community. That would suggest a lack of predators (**Burdon et al., 2014**) that did not impact the young population of cockles and generally favorable conditions that prevailed during the late Pannonian for freshwater cockles. Answer to the question of the lack of young individuals requires further research.

In order to get a complete picture of the appearance of the Lymnocardiinae, it would be advisable to measure their shell length (L), height (H) and width (W). Based on the here presented analysis, samples that include L, H and W in shell volume have normal distribution curves showing two distinct groups matching two different sampling localities (**Figure 3**). The Okrugljak samples show a shift to the left on the distribution curve, while Bilogora – Kalnik samples have a centered normal distribution curve. Surface measurements are practical for situations when there is no possibility to measure specimens by hand, but only from the photographs. Sometimes there are available photographs with all necessary views for complete measurement (anterior, posterior and lateral view), but there can also be photographs showing only the anterior and posterior views, without the lateral view disabling the width measurement. Further research is needed to understand what caused the population differences in the studied locations, which were rather closely situated at the western coast of the Lake Pannon.

5. References

Allmon, W. D. (2005): The importance of museum collections in paleobiology. Paleobiology, 31, 1-5.

Basch, O. (1990): Cardiidae (Mollusca, Lamellibrachiata) pontijskog kata u Hrvatskoj (Cardiidae (Mollusca, Lamellibrachiata) of the Pontic Age in Croatia). Paleontologia Jugoslavica, 39, 1-158. (In Croatian and German)

Basch, O. (2009): Klastiti i ugljen (pont – M7) [Clastites and coal (Pontian – M7) – in Croatian]. - In: Velić, I. & Vlahović, I. (eds.): Tumač Geološke karte Republike Hrvatske 1:300.000 (Explanatory note of the Basic Geological Map of the Republic of Croatia 1:300000). Croatian Geological Survey, Zagreb, 141 p. (In Croatian)

Brusina, S. (1874): Fossile Binnen – Mollusken aus Dalmatien, Kroatien und Slavonien. Zagreb, Jugoslavenska akademija znanosti i umjetnosti, 138 p. (In German)

Brusina, S. (1897): Gragja za neogensku malakološku faunu Dalmacije, Hrvatske i Slavonije. Jugoslavenska akademija znanosti i umjetnosti, Zagreb, 38 p. (In Croatian and French)

Brusina, S. (1902): Iconographia Molluscorum Fossilium in Tellure Tertiaria Ungariae, Croatiae, Slavoniae, Dalmatiae, Bosniae, Hercegovinae, Serbiae Et Bulgariae Inventorum. Zagreb, 99 p. (In French)

Burdon, D., Callaway, R., Michael, E., Smith, T. and Wither, A. (2014): Mass mortalities in bivalve populations: A review of the edible cockle *Cerastoderma edule* (L.); Estuarine, Coastal and Shelf Science. 150, 5, 271-280.

Dominici S., Forli M., Bogi C., Guerrini A. and Benvenuti M. (2020): Paleobiology from Museum collections: comparing historical and novel data on Upper Miocene molluscs of the Livorno Hills. Riv. It. Paleontol. Strat., 126, 1, 65-109.

Kiseljak, I. (1889): Kongerijske okamine okolice Zagrebačke (Congeria fossils around Zagreb). Jugoslavenska akademija znanosti i umjetnosti 95, 52-78. (In Croatian)

Kochansky – Devidé, V. (1982): Prilozi povijesti geoloških znanosti u Hrvatskoj. VIII. Naši paleontolozi-amateri (Contributions to the history of geological sciences in Croatia. VIII. Our amateur paleontologists). Geološki vjesnik, 35, 209 – 215. (In Croatian)

Kovačić, M., Županić, J., Babić, L., Vrsaljko, D., Miknić, M., Bakrač, K., Hećimović, I., Avanić, R. and Brkić, M. (2004): Lacustrine basin to delta evolution in the Zagorje Basin, a Pannonian sub-basin (Late Miocene: Pontian, NW Croatia). Facies, 50, 19-33. https://doi.org/10.1007/s10347-003-0001-6

Lawrence D.R. (1971): The nature and structure of paleoecology. Journal of Paleontology, 45, 593-607.

Magyar, I. (2021): Chronostratigraphy of clinothem-filled non-marine basins: Dating the Pannonian Stage. Global and Planetary Change, 205, 1-10. https://doi.org/10.1016/j.gloplacha.2021.103609

Magyar, I., Geary, D.H. and Müller, P. (1999): Paleogeographic evolution of the Late Miocene Lake Pannon in central Europe. Palaeogeography Palaeoclimatology Palaeoecology, 147, 151-167.

Mandic, O., Kurečić, T., Neubauer, T.A. and Harzhauser, M. (2015): Stratigraphic and palaeogeographic significance of lacustrine molluscs from the Pliocene Viviparus beds in central Croatia. Geologia Croatica, 68, 3, 179-207. doi: 10.4154/gc.2015.15

Marshall C. (2018): Digitizing the vast 'dark data' in museum fossil collections. The Conversation, September 17, 2018: https://theconversation.com/ digitizing-the-vast-dark-data-in-museum-fossil-collections-102833

Müller, P., Geary, D. H. and Magyar, I. (2007): The endemic molluscs of the Late Miocene Lake Pannon: their origin, evolution, and family-level taxonomy. Lethaia, 32, 1, 47-60. https://doi.org/10.1111/j.1502-3931.1999.tb00580.x

Pavelić, D. and Kovačić, M. (2018): Sedimentology and stratigraphy of the Neogene rift-type North Croatian Basin (Pannonian Basin System, Croatia): A review. Marine and Petroleum Geology, 91, 455-469.

Poljak, J. and Šuklje, F. (1934): Pliocen Glogovnice i Osjeka u Hrvatskoj. Vesnik Geol. inst. 3, 3-26.

Sebe, K., Kovačić, M., Magyar, I., Krizmanić, K., Špelić, M., Bigunac, D., Sütő-Szentai, M., Kovács, A., Szuromi-Korecz, A., Bakrač, K., Hajek-Tadesse, V., Troskot-Čobić, T and Sztanó, O. (2020). Correlation of upper Miocene–Pliocene Lake Pannon deposits across the Drava Basin, Croatia and Hungary. Geologia Croatica, 73, 3, 177-195. https://doi.org/10.4154/gc.2020.12

Šimunić, A., Hećimović, I. & Avanić, R. (1990): Osnovna geološka karta SFRJ 1:100.000, Tumač za list Koprivnica L33–70 (Basic Geological Map of SFRY 1:100.000. Geology of Koprivnica sheet, L 33-70). Hrvatski geološki institut, Zagreb, 94 p.

Sremac, J., Bošnjak, M., Velić, J., Malvić, T and Bakrač, K. (2022): Nearshore Pelagic Influence at the SW Margin of the Paratethys Sea-Examples from the Miocene of Croatia. Geosciences, 12, 120, 1-30. https://doi.org/10.3390/geosciences12030120

Šuklje, F. (1933): Pontiska fauna Jagnjedovca i Glogovca u Hrvatskoj. Vesnik Geol. inst., 2, 57-82, Beograd.

Velić, I. and Velić, J. (1995): Geological Map of Croatia. In Proceedings of the First Croatian Geological Congress, Opatija, Croatia, 18-21.

Vrsaljko, D. (1999): The Pannonian Palaeoecology and Biostratigraphy of Molluscs from Kostanjek-Medvednica Mt., Croatia. Geologia Croatica, 52, 1, 9-27.

Vrsaljko, D., Pavelić, D. and Bajraktarević, Z. (2005): Stratigraphy and Palaeogeography of Miocene Deposits from the Marginal Area of Žumberak Mt. and the Samoborsko Gorje Mts. (Northwestern Croatia). Geologia Croatica, 58, 2, 133-150.

Internet sources:

URL: https://d-maps.com/carte.php?num_car=2242&lang=en

Sažetak

Testiranje valjanosti muzejskih podataka o gornjomiocenskim slatkovodnim srčankama iz fundusa HPM-a

Gornjomiocenske slatkovodne srčanke koje se čuvaju u fundusu Hrvatskoga prirodoslovnog muzeja (HPM) proučavane su kako bi se prepoznali uzorci veličine unutar populacije i otkrili mogući subjektivni pristupi procesu sakupljanja fosilnog materijala na terenu (preference veličine ili kvalitete očuvanja). Najbrojnije vrste, *Tauricardium baraci* (Brusina, 1884), *Lymnocardium diprosopum* (Brusina, 1884), *L. inflatum* (Gorjanović–Kramberger, 1889), *L. majeri* (M. Hörnes, 1862), *L. riegeli* (M. Hörnes, 1862), *L. rogenhoferi* (Brusina, 1884), *Prosodacnomya vutskitsi* (Brusina, 1902) i *Pseudocatillus simplex* (Fuchs, 1870), s lokaliteta: Okrugljak (JZ Medvednica), Glogovnica (J Kalnik), Glogovac (Bilogora) i Kindrovo, odabrani su za komparativnu analizu. Odnosi između vrijednosti duljine (L) i visine (H) (= površina) i duljine (L)/visine (H)/širine (W) (= volumen) izračunati su za svaku vrstu i uspoređeni unutar jedne vrste i unutar populacije srčanki s istog lokaliteta. Proračuni su dali sljedeće rezultate: (1) Volumen (D/H/W) u usporedbi s površinom (D/H) se pokazao kao bolji izbor u populacijskim analizama; (2) vrijednosti raspodjele veličine grupiraju se neovisno o dimenzijama vrste, ali mogu biti dobro povezane unutar nalazišta; (3) srčanke s Bilogorsko-Kalničkog područja pokazuju normalnu raspodjelu vrijednosti, dok sve vrste s lokaliteta Okrugljak imaju sličnu blagu asimetriju distribucije veličine; (4) takva raspodjela vjerojatno ukazuje na različite tafonomske procese u ova dva taložna bazena. Ovo istraživanje je pokazalo da se gornjomiocenske srčanke iz muzejskih zbirki mogu uspješno proučavati sa svih paleontoloških aspekata, čak i kada terenski izdanci više nisu dostupni, jer su fosili prikupljeni objektivno, uzimajući sve raspoložive primjerke s lokaliteta, bez obzira na njihovu veličinu ili kvalitetu očuvanosti.

Ključne riječi: Lymnocardiinae, zbirka HPM-a, biometrija, gornji miocen, Hrvatska

Author's contribution

Anja Jarić Matanović (PhD student) provided the shell measurements, suggested the first concept of the paper and prepared the manuscript and presentation of the results. **Marija Bošnjak (Dr.sc., senior curator, geology, paleontology, geomathematics)** prepared and provided the Lymnocardiinae specimens for measurement, contributed in conceptualization and participated in writing, reviewing and editing of manuscript. **Jasenka Sremac (Dr.sc., Full Professor, retired, geology, paleontology, paleoenvironment)** provided the conceptualization and methodology of the paper and participated in writing, reviewing and editing of manuscript.